nagra National Cooperative for the Disposal of Radioactive Waste

TECHNICAL REPORT 91-10

A natural analogue study of the Maqarin hyperalkaline groundwaters. I. Source term description and thermodynamic database testing.

December 1992

Maqarin Natural Analogue Site Study Group

Hardstrasse 73, CH-5430 Wettingen/Switzerland, Telephone +41-56-37 11 11

This report was prepared as an account of work sponsored by Nagra. The viewpoints presented and conclusions reached are those of the author(s) and do not necessarily represent those of Nagra.

AUTHOR LIST

C.M. LINKLATER and C.J. TWEED, AEA Technology (Decomm. and Radwaste), Harwell, UK

M. ALLEN, M. CAVE, J.M. COOK, S. GARDNER, E.K. HYSLOP, S. INCE, A.E. MILODOWSKI, J.M. PEARCE, B. SMITH and J.M. WEST, British Geological Survey, Keyworth, UK

G. HALL, Geological Survey of Canada, Ottawa, Canada

P. FRITZ, GSF-Institute of Hydrology, Neuherberg, Germany[1]

R. DAYAL and K. EAGLESON, Ontario Hydro (Civil Research), Toronto, Canada

R. BRUETSCH, C. DEGEULDRE, J. EIKENBERG and W. HUMMEL, Paul Scherrer Institute, Villigen, Switzerland

W.R. ALEXANDER, Rock-Water Interaction Group, Institute of Mineralogy and Petrology and Institute of Geology, University of Berne, Berne, Switzerland

H.N. KHOURY, Department of Geology and Mineralogy, University of Jordan, Amman, Jordan

E. SALAMEH, Water Resources and Study Centre, University of Jordan, Amman, Jordan

I.D. CLARK, Department of Geology. University of Ottawa, Ottawa, Canada

W. BAJJALI, Water Authority of Jordan, Amman, Jordan[2]

[1] Present address: Umweltforschungszentrum Leipzig-Halle, Germany

[2] Present address: Department of Geology, University of Ottawa, Ottawa, Canada

ABSTRACT

In several national radioactive waste management programmes, it is the intention to isolate low- and intermediate-level wastes (L/ILW) in cementitious matrices or in repositories backfilled with cementitious materials. In addition, some countries intend to dispose of long-lived, intermediate-level radioactive waste (so-called TRU) in a cement-dominated environment in a part of the high-level waste (HLW) repository. Cement and concrete are chosen predominantly for their favourable engineering properties, although the low solubilities of most radionuclides of concern in the hyperalkaline cement pore waters plus the high sorption characteristics of cementitious backfill are also important contributions to the safety case.

Models of the interaction of the host formation groundwater with cement/concrete suggest that KOH and NaOH leachates will be produced initially, followed by a longer period of $Ca(OH)_2$ buffered leachates. Such solutions will interact with the repository host formation and may well alter the rock properties, especially in the vicinity of the repository. This may result in local alteration of the original retardation qualities for which the repository site was originally chosen (including affecting the form of water-conducting fractures or the nature of sorbing minerals) and is therefore of considerable interest from a safety assessment viewpoint.

To date, some of these processes have been studied in the laboratory but, as always, the results remain somewhat ambiguous due to the necessarily short timescales over which the experiments are conducted. This is compounded by the fact that, to achieve results on a reasonable timescale, most experiments have to be conducted at unrealistically high temperatures, thus making extrapolation of the results to repository-relevant conditions even more problematic than usual.

An additional method of assessing models of repository behaviour does, however, exist: the study of appropriate natural systems which, in some way, are analogous to the processes or systems present in a repository. This approach (usually termed a natural analogue study) has the advantage of being able to study the processes of interest in action over more realistic timescales and, where the analogue site is carefully chosen, under more realistic conditions than can be produced in the laboratory. Although natural analogue studies now have a well established rôle in the safety assessment of radwaste repositories, it is only rarely that analogues have been examined in terms of a cementitious repository. One notable exception to date was the Nagra and UK Nirex joint funded Oman project, where geochemical thermodynamic codes were tested and the behaviour of microbes in a hyperalkaline system was assessed. The results of this study were encouraging enough to persuade Nagra and UK Nirex, this time in association with Ontario Hydro, of the value of continuing such natural analogue work; this led to the present study at Maqarin, in northwest Jordan.

This site differs from that in the Oman ophiolite in that the hyperalkaline groundwater chemistry is controlled by naturally occurring cement minerals and gels, thus making

the analogy with a cementitious repository even better. In addition, the site contains relatively high levels of U and other elements of interest to the safety assessment of a radioactive waste repository.

Nagra, Ontario Hydro and UK Nirex jointly funded a study of a range of processes of relevance to the performance of a cementitious repository, including:

- The interaction of hyperalkaline groundwaters with an unalterered host formation; this was the first study of its kind which focussed on a process directly analogous to the potential reaction of hyperalkaline leachates from a cementitious repository with the repository host rock

- The evaluation of the solubility and speciation of trace elements in hyperalkaline waters in order to test databases of thermodynamic geochemical codes, especially for those elements of interest to performance assessment (including U, Th, Ra, Pb, Se, Ni and Sn)

- The assessment of the significance of microbiological activity in hyperalkaline systems, thus establishing the likely impact of such activity in the near-field of a cementitious repository

- The measurement of colloid populations in hyperalkaline groundwaters as a guide to the rôle of colloids in and around the near-field of a cementitious repository, this being the first such study of its kind

- The evaluation of grout carbonation reactions of relevance to ^{14}C attenuation in cement engineered barriers of a HLW (spent fuel) repository.

In the case of the interaction of hyperalkaline groundwaters with the host formation, only preliminary data are presented due to the necessity to first fully characterise the cementitious source material in some detail. Nevertheless, initial data presented here and in an associated report (MILODOWSKI et al., 1992) indicate clear interaction of the hyperalkaline groundwater with the host rock. The full implications of the results are not yet clear, but a further study is currently underway on additional material from Maqarin.

The thermodynamic database testing exercise proved to be very successful, with several clear database inconsistencies being identified. Further testing was also carried out for Ni and Sn, following re-assessment of the databases, via comparison with well controlled laboratory experiments. In general, all of the databases behaved in a conservative manner (i.e. overestimating solubilities) even though the mineral phases included in the databases were a poor representation of reality. This, in itself, is reassuring from the safety assessment viewpoint, but perhaps more important is the fact that, in most cases, the modellers were able to explain precisely why the differences between the code predictions and reality occurred, thus further increasing confidence in the databases used. One significant failure was the case of U, where the

various databases disagree significantly on the U speciation and solubility and none predict the behaviour of U in the natural system particularly well.

The microbiological study indicates that nutrient availability, rather than the high pH conditions, appears to control microbial activity. This has important implications for those repository designs which cannot be specifically shown to have low microbial activity levels due to limited availability of nutrients.

Degradation of cement may enhance colloid populations in and around the near-field of a cementitious repository, although the potential of cement to produce colloids has actually been little studied. The data produced here are thus of great importance as they represent the only known results for colloids in aged hyperalkaline groundwaters. The data indicate low colloid populations in comparison with other sedimentary groundwaters, in spite of the fact that some types of colloids should be stable under hyperalkaline conditions and that the relatively open fractures at the Maqarin site would presumably offer little chance of significant colloid filtration.

Although little is known of the chemistry of the colloids, it is at least certain that there is little U associated with them. This is contrary to previous predictions (observations at Oman) of colloidal U under hyperalkaline conditions.

It should be noted, however, that the colloid populations measured here may be low due to precipitation during sample storage and that the data should therefore be treated as preliminary until the work can be repeated with an in-situ colloid sampling rig.

The grout carbonation study was carried out as a trial effort to evaluate the potential of studying natural systems to complement laboratory-based experiments. The results indicated that carbonation has been extensive in some areas at Maqarin and that the site could therefore be studied as an analogue to repository carbonation reactions and ^{14}C retardation.

Taken overall, the Maqarin natural analogue project has produced valuable (and, in some cases, unique) data on hyperalkaline leachate/repository host rock interaction, microbial and colloid populations in hyperalkaline groundwaters and on the applicability of current databases for thermodynamic geochemical codes used in assessing radionuclide releases from a cementitious repository. In some cases, the results of the study have already been included in repository safety assessment calculations and, as the project co-funders move towards constructing their own cementitious repositories, will probably be used even more so.

RESUME

Plusieurs programmes nationaux de stockage final de déchets de faible et moyenne activité (L/ILW) prévoient de les isoler dans une matrice à base de ciments ou de les placer dans des dépôts colmatés avec de tels matériaux. Par ailleurs quelques pays envisagent le stockage de déchets de moyenne activité à longue vie (dits TRU) dans une zone particulière d'un dépôt final pour déchets de haute activité (HLW) dans un environnement où prédominent les ciments. Le ciment et le béton sont essentiellement choisis pour leurs bonnes caractéristiques techniques mais de plus la faible solubilité dans l'eau intersticielle hyperalcaline du ciment de la plupart des radionucléides qui font problème ainsi que les propriétés de sorption remarquables des matériaux de colmatage à base de ciment, constituent d'importants facteurs de sécurité.

Les modèles d'interaction entre l'eau souterraine de la formation d'accueil et le ciment/béton suggèrent qu'initialement apparaîssent des fluides de lixiviation KOH et NaOH suivis d'une longue période de fluides de lessivage tamponnés au $Ca(OH)_2$. De telles solutions vont agir sur la formation d'accueil et pourraient bien altérer les propriétés de la roche, notamment à proximité du dépôt final. Cela peut conduire à une altération des propriétés retardatrices initiales (y compris la forme des fractures aquifères ou la nature des minéraux sorbants) qui au départ avaient conduit à la sélection du site de dépôt final, ce qui est du plus haut intérêt, du point de vue de l'évaluation de la sûreté.

Jusqu'ici quelques-uns de ces processus ont été étudiés en laboratoire, mais, comme toujours, les résultats sont quelque peu ambigus en raison de la durée nécessairement limitée des essais. Cela est encore compliqué par le fait que pour obtenir des résultats dans un délai raisonnable, la plupart des expériences doivent être exécutées à des températures élevées qui ne sont pas réalistes, ce qui rend l'extrapolation des résultats aux conditions en rapport avec celles d'un dépôt final encore plus problématique que d'ordinaire.

Une autre méthode pour juger les modèles de comportement d'un dépôt final existe toutefois: l'étude de systèmes naturels appropriés qui d'une certaine façon sont similaires aux processus ou aux systèmes rencontrés dans un dépôt final. Cette approche (ordinairement appelée étude d'analogies naturelles) présente l'avantage d'étudier des processus pertinents sur des échelles de temps plus réalistes et, lorsque le site de l'analogie est sélectionné avec soin, sous des conditions plus proches de la réalité que celles qui peuvent être reproduites en laboratoire. Bien qu'aujourd'hui les analogies naturelles jouent un rôle bien reconnu dans les analyses de sûreté de dépôts finals pour déchets radioactifs, ce n'est que très rarement que des analogies ont été examinées dans le cadre d'un dépôt final à base de ciments. Une exception notable à ce jour est représentée par le projet d'Oman, cofinancé par la Cédra et UK Nirex, où des codes thermodynamiques géochimiques ont été testés et le comportement de microbes dans un système hyperalcalin a été examiné. Les résultats de cette étude furent suffisamment encourageants pour persuader la Cédra et UK Nirex, cette fois en

association avec Ontario Hydro, de poursuivre de telles études d'analogies, ce qui a conduit à la présente étude à Maqarin, dans le nord-ouest de la Jordanie.

Ce site diffère de celui de l'ophiolite d'Oman par le fait que la chimie de l'eau souterraine hyperalcaline est contrôlée par des minéraux et gels de ciments naturels, ce qui constitue une analogie encore meilleure pour un dépôt final à base de ciments. De plus ce site présente un taux relativement élevé d'U et autres éléments intéressants pour l'évaluation de la sûreté d'un dépôt final de déchets radioactifs.

La Cédra, Ontario Hydro et UK Nirex cofinancèrent l'étude d'une série de processus pertinents pour le comportement d'un dépôt final à base de ciments, comprenant:

- L'interaction entre des eaux souterraines hyperalcalines et une formation d'accueil non-altérée; la première étude de ce type s'est concentrée sur un processus directement analogue à la réaction potentielle de fluides de lixiviation hyperalcalins provenant d'un dépôt final à base de ciments avec la roche d'accueil

- L'évaluation de la solubilité et de la spéciation d'éléments traces dans des eaux hyperalcalines en vue de tester les bases de données des codes thermodynamiques géochimiques, notamment pour les éléments intéressant l'évaluation du comportement d'un dépôt final (incluant U, Th, Ra, Pb, Se, Ni et Sn)

- L'estimation de la signification de l'activité microbienne dans des systèmes hyperalcalins, afin de déterminer l'impact probable de cette activité dans le champ proche d'un dépôt final à base de ciments

- La mesure des populations de colloïdes dans des eaux souterraines hyperalcalines à titre de guide pour le rôle des colloïdes dans et aux alentours du champ proche d'un dépôt final à base de ciments, la première étude de ce type

- L'évaluation de la réaction de carbonatation du mortier en relation avec l'atténuation du ^{14}C dans les barrières ouvragées en ciment d'un dépôt final pour HLW (combustible irradié).

Pour le cas de l'interaction entre des eaux souterraines hyperalcalines et la formation d'accueil, seules des données préliminaires sont présentées ici en raison de la nécessité de tout d'abord pleinement caractériser de façon détaillée le matériau source à base de ciments considéré. Néanmoins les données initiales présentées ici ainsi que celles d'un rapport associé (Milodowski et al., 1992) montrent une interaction évidente entre l'eau souterraine hyperalcaline et la roche d'accueil. La totalité des implications des résultats ne sont pas encore claires mais des études complémentaires sont actuellement en cours sur d'autres matériaux provenant de Maqarin.

Les essais relatifs aux bases de données se sont révélés être des succès, de nombreuses inconsistances ayant été clairement identifiées. D'autres tests ont

également été faits pour le Ni et le Sn suite à une réévaluation des bases de données par comparaison avec des essais en laboratoire soigneusement contrôlés. De façon générale toutes les bases de données se sont révélées situées du côté de la prudence (par ex. en surestimant les solubilités) bien que les phases minérales comprises dans ces bases de données ne constituaient qu'une piètre représentation de la réalité. Cela est en soit rassurant du point de vue de l'évaluation de la sûreté, mais plus important peut-être est le fait que dans la plupart des cas les concepteurs de modèles ont été à même d'expliquer de façon précise pourquoi des différences apparaissaient entre les pronostics des codes et la réalité, ce qui contribue à renforcer la confiance placée dans les bases de données utilisées. Un échec significatif est représenté par le cas de l'U pour lequel les bases de données sont en contradiction évidente en ce qui concerne les spéciations de l'U et leurs solubilités et aucune d'elles ne prédit particulièrement bien le comportement de l'U dans un système naturel.

Les études microbiologiques indiquent que c'est la disponibilité d'éléments nutritifs qui semble piloter l'activité microbienne plutôt que des conditions de pH élevé. Ceci a des implications importantes pour les concepts de dépôts finals pour lesquels on ne peut démontrer de façon spécifique l'existence d'une faible activité microbienne du fait de la pénurie d'éléments nutritifs.

La dégradation de ciments peut intensifier les populations de colloïdes dans et aux alentours du champ proche d'un dépôt final à base de ciments, bien que la propension du ciment à produire des colloïdes n'ait été que peu étudiée en fait. Les données élaborées ici sont par conséquent d'une grande importance car elles représentent les seuls résultats connus pour les colloïdes dans des eaux souterraines hyperalcalines agées. Les données indiquent de faibles populations de colloïdes par comparaison avec d'autres eaux souterraines sédimentaires, malgré le fait que certains types de colloïdes devraient être stables sous conditions hyperalcalines et que les fractures relativement ouvertes du site de Maqarin ne devraient probablement guère offrir beaucoup de possibilités significatives de filtration des colloïdes.

Bien que peu de choses soient connues au sujet de la chimie des colloïdes, il est au moins certain que seulement un peu d'U leur soit associé. Ceci est contraire aux prévisions antérieures (observations à Oman) relatives à l'U colloïdal sous conditions hyperalcalines.

Il y a toutefois lieu de relever que les populations de colloïdes mesurées ici sont peut-être faibles en raison de précipitations durant le stockage des échantillons et que ces données doivent par conséquent être considérées comme préliminaires jusqu'à ce que les travaux puissent être répétés avec un dispositif de collecte des colloïdes in-situ.

L'étude de carbonatation du mortier a été menée à titre d'effort modeste pour évaluer le potentiel d'études de systèmes naturels en vue de compléter des essais en laboratoire. Les résultats montrent que la carbonatation a été extensive dans quelques zones à Maqarin et que ce site pourrait par conséquent être étudié comme analogie pour les réactions de carbonatation de dépôts finals et de retardement par ^{14}C.

De façon générale le projet d'analogies naturelles de Maqarin a livré des données précieuses (uniques dans certains cas) relatives aux interactions entre fluides de lixiviation hyperalcalins et roche d'accueil, les populations microbiennes et colloïdales dans des eaux souterraines hyperalcalines ainsi qu'au sujet de l'applicabilité des bases de données actuelles pour les codes thermodynamiques géochimiques utilisés pour évaluer le relâchement de radionucléides d'un dépôt final à base de ciments. Dans quelques cas les résultats de l'étude ont déjà été introduits dans les calculs d'évaluation de sûreté de dépôts finals et ils seront probablement encore utilisés bien davantage, les co-participants au projet se dirigeant vers la réalisation de leurs propres dépôts finals à base de ciments.

ZUSAMMENFASSUNG

Bei mehreren nationalen Entsorgungsprogrammen für radioaktive Abfälle ist vorgesehen, die schwach- und mittelaktiven Abfälle (SMA) entweder in Zementmatrix oder in mit Zement verfüllten Endlagern einzuschliessen. Im weiteren planen einige Länder, die langlebigen mittelaktiven Abfälle (LMA) in einem räumlich abgetrennten Teil des Endlagers für hochaktive Abfälle (HAA) ebenfalls in einem zementdominierten Milieu zu lagern. Zemente und Beton werden vor allem aufgrund ihrer guten bautechnischen Eigenschaften eingesetzt. Diese Materialien zeigen aber auch in Bezug auf die Endlagersicherheit vorteilhafte Merkmale, da im allgemeinen für die meisten wichtigen Radionuklide in den hyperalkalischen Zementporenwässern niedrige Löslichkeiten und in der zementösen Verfüllung eine hohe Sorptionsfähigkeit resultieren.

Modellrechnungen über die Wechselwirkung zwischen Grundwasser und Zement/ Beton weisen darauf hin, dass vorerst KOH- und NaOH-haltige Lösungen entstehen. Nach dieser ersten Phase werden über einen längeren Zeitraum $Ca(OH)_2$-gepufferte Lösungen gebildet. Diese Lösungen treten in Wechselwirkung mit dem Endlager-Wirtgestein ein und vermögen dabei die Gesteinseigenschaften vor allem in unmittelbarer Nähe des Endlagers zu verändern. Das ursprüngliche Retardierungsvermögen des Gesteins, welches bei der Begründung der Standortwahl mitentscheidend war, könnte dabei lokal gerändert werden (diese Umwandlungsvorgänge können auch die Eigenschaften der wasserführenden Klüfte sowie der sorbierenden Mineralien beeinflussen). In Bezug auf die Sicherheitsanalyse des Endlagers ist dies von grosser Bedeutung.

Einige dieser Prozesse wurden bisher im Labor untersucht. Die Resultate sind aber mit einer gewissen Unsicherheit behaftet, weil die Dauer der Laborexperimente zeitlich begrenzt ist. Um Resultate innerhalb eines vernünftigen Zeitraums zu erhalten, müssten die meisten Experimente bei unrealistisch hohen Temperaturen durchgeführt werden; die Extrapolation der Resultate auf endlagerrelevante Bedingungen ist deshalb problematisch.

Es besteht aber eine weitere Möglichkeit, die Modelle des Endlagerverhaltens zu prüfen, indem geeignete natürliche Systeme, welche auf irgendeine Weise den in einem Endlager vorkommenden Prozessen oder Systemen analog sind, untersucht werden. Diese Methode der sogenannten Analogstudien bietet den Vorteil, dass dabei die relevanten Prozesse, die in der Natur über längere Zeiträume ablaufen, studiert werden können. Falls der Standort der Untersuchungen sorgfältig ausgewählt wird, dürfen gegenüber Laborversuchen realistischere Resultate für die effektiven Bedingungen in Endlagern erwarten werden. Obwohl natürliche Analogstudien bereits eine wohldefinierte Rolle in Analysen der Endlagersicherheit spielen, wurden diese bis anhin eher selten im Hinblick auf ein zementhaltiges Endlager angewendet. Eine bemerkenswerte Ausnahme ist das gemeinsame Nagra/UK Nirex Oman-Projekt. Im Rahmen dieses Projekts wurden geochemische-thermodynamische Rechenmodel (Codes) getestet sowie das Verhalten von Mikroorganismen in einem hyperalkalischen System untersucht. Die Ergebnisse dieser Studie waren derart vielversprechend, dass die Nagra

und UK Nirex (diesmal in Zusammenarbeit mit Ontario Hydro) sich entschieden haben, solche Analogstudien weiterzuführen. Dies führte zum gegenwärtigen Projekt in Maqarin, im Nordwesten von Jordanien.

Dieser Standort unterscheidet sich von den Ophioliten in Oman, in dem die Chemie des hyperalkalischen Grundwassers durch natürlich vorkommende Mineralien und Gele bestimmt wird, wie sie auch in Zement vorkommen. Damit ist die Analogie mit den Bedingungen in einem zementdominierten Endlager noch besser. In Maqarin wurden auch relativ hohe Konzentrationen von U und anderen sicherheitsrelevanten Elementen festgestellt.

In einem gemeinsam von der Nagra, Ontario Hydro und UK Nirex finanzierten Untersuchungsprogramm wurden unter anderem eine Reihe von Prozessen studiert, die relevant für die Entwicklung eines zementdominierten Endlagers sind:

- Die Wechselwirkung zwischen hyperalkalischen Grundwässern und einem noch nicht umgewandelten Umgebungsgestein. Dies war die erste Studie ihrer Art, die sich auf Prozesse konzentriert, die potentiell auch zwischen hyperalkalischen Lösungen aus einem zementdominierten Endlager und dem umgebenden Wirtgestein stattfinden können.
- Bestimmung der Löslichkeit und der Speziation von Spurenelementen in hyperalkalischen Grundwässern, um damit die Datenbasis, vor allem für sicherheitsrelevante Elemente (z.B. U, Th, Ra, Pb, Se, Ni und Sn), für thermodynamisch-geochemische Rechenmodelle prüfen zu können.
- Beurteilung der Bedeutung von mikrobiellen Prozessen in hyperalkalischen Systemen, um die möglichen Auswirkungen solcher Mikroben auf das Nahfeld eines zementhaltigen Endlagers festzustellen.
- Messung der Kolloidkonzentrationen in hyperalkalischen Grundwässern als Hinweis auf das Verhalten von Kolloiden im und um das Nahfeld eines zementhaltigen Endlagers (dies war die erste derartige Analogstudie).
- Beurteilung von Mörtel-Karbonatisierungsprozessen, die relevant sind für die mögliche Fixierung von ^{14}C Isotopen in den zementhaltigen technischen Barrieren eines Endlagers für hochaktive Abfälle oder abgebrannte Brennelemente.

Es werden nur vorläufige Daten über die Wechselwirkung zwischen den hyperalkalischen Grundwässern und der Wirtgesteinsformation präsentiert, weil die zementhaltigen Materialien für die Endlager noch nicht festgelegt sind. Trotzdem zeigen die hier, wie auch im Bericht von Milodowski et al. (1992) dargestellten Daten eine deutliche Wechselwirkung zwischen dem hyperalkalischen Grundwasser und dem Wirtgestein. Die Bedeutung der Resultate ist noch nicht vollständig klar; eine weitere Studie mit zusätzlichem Probematerial von Maqarin wird gegenwärtig durchgeführt.

Die Prüfung der thermodynamischen Databasis wurde mit grossem Erfolg durchgeführt und mehrere deutliche Widersprüche konnten identifiziert werden. Nach der Überarbeitung der Datenbasis wurden weitere Tests für Ni und Sn durchgeführt, in dem die Daten mit den Resultaten von sorgfältig kontrollierten Laborexperimenten verglichen wurden. Obwohl die Auswahl der in der Datenbanken enthaltenen Mineralphasen eher unrealistisch ist, führen die Parameter im allgemeinen zu konservativen Ergebnissen, d.h., die resultierenden Nuklidlöslichkeiten werden meistens überschätzt. Dies ist für die rechnerische Abschätzung der Endlagersicherheit beruhigend. Im weiteren ist zu bemerken, dass die meisten vorkommenden Diskrepanzen zwischen Modellvoraussagen und natürlichen Befunden genau erklärt werden konnten, was für die gute Belastbarkeit der verschiedenen Datenbasen spricht. Ein eigentlicher Fehlschlag muss jedoch im Falle von Uran festgestellt werden, wo die vorhandenen Datenbanken stark abweichende Hinweise auf die Speziation und Löslichkeiten ergeben; leider verhalfen keine der jeweiligen Angaben zu einer einigermassen befriedigenden Interpretation des natürlichen Verhaltens von Uran.

Die mikrobiologische Studie hat gezeigt, dass die mikrobielle Aktivität durch die Verfügbarkeit von Nährstoffen und nicht sosehr durch die hohen pH-Werte limitiert wird. Dieses Resultat ist wichtig für Endlagerauslegungen, bei denen nicht spezifisch gezeigt werden kann, dass die mikrobielle Aktivität wegen limitierter Verfügbarkeit von Nährstoffen begrenzt sein wird.

Die Umwandlung von Zement könnte möglicherweise die Kolloidkonzentrationen im und um das Nahfeld eines zementhaltigen Endlagers erhöhen. Solche Prozesse wurden aber bis jetzt nur wenig untersucht. Die in diesem Bericht präsentierten Daten sind daher von grosser Bedeutung, weil sie die einzigen Daten für Kolloide in alten hyperalkalischen Grundwässern darstellen. Im Vergleich mit anderen sedimentären Grundwässern weisen die Maqarin-Daten auf niedrige Kolloidkonzentrationen hin, obwohl eigentlich einige der erwarteten Kolloide unter hyperalkalischen Bedingungen stabil sein sollten und die relativ offenen Klüfte am Maqarin-Standort vermutlich nur wenige Kolloide auszufiltrieren vermögen.

Obwohl die Chemie der Kolloide nur wenig bekannt, ist offensichtlich, dass nur ein unbedeutender Anteil des gelösten Urans in Form von Kolloiden vorliegt - im Widerspruch zu früheren Veraussagen für hyperalkalische Bedingungen (Beobachtungen aus Oman). Es kann aber nicht ausgeschlossen werden, dass allenfalls Ausfällungen während der Probenlagerung vor der Bestimmung der Kolloidkonzentrationen zu künstlich tieferen Messwerten führen könnten. Die Kolloidresultate sind deshalb nur als vorläufig zu betrachten, bis die Resultate von gezielte Untersuchungen vor Ort vorliegen.

Mit der Studie der Mörtel-Karbonatisierung wurde eruiert, inwieweit Laborexperimente durch die Untersuchung natürlicher Systeme ergänzt werden können. Die Resultate zeigen, dass in einigen Gebieten von Maqarin die Karbonatisierung ziemlich bedeutend ist. Der Standort wäre also geeignet als Analogon für die im Endlager vorkommenden Karbonatisierungsprozesse, die potentiell auch zur Retardation von ^{14}C beitragen können.

Im allgemeinen hat das Maqarin-Analogprojekt wertvolle, und zum Teil einzigartige Daten geliefert über die Wechselwirkung zwischen hyperalkalischen Lösungen und Endlagergesteinen, über Mikroben und Kolloide in hyperalkalischen Grundwässern, sowie die Eignung der gegenwärtigen Datenbasis für thermodynamisch-geochemische Modelle, die zur rechnerischen Abschätzung der Nuklidfreisetzung aus einem zementhaltigen Endlager dienen. Die Resultate der Maqarin-Studie wurden schon zum Teil bereits in Endlager-Sicherheitsanalysen berücksichtigt. Da die Realisierung von Endlagern, die zementhaltige Materialien enthalten, auch in den Ländern der verschiedenen Co-Sponsoren des Maqarin-Projekts immer näher rückt, ist zu hoffen, dass die Ergebnisse dieser Studie in der Zukunft noch mehr Anwendung finden werden.

CONTENTS

FIGURES

TABLES

1 INTRODUCTION TO THE MAQARIN NATURAL ANALOGUE PROJECT

W. R. ALEXANDER

1.1 Background to the project

In most planned low and intermediate level radioactive waste (L/ILW) repositories (plus, potentially, several high level waste repositories), the near-field is dominated by cement based materials. These mainly consist of the waste immobilisation matrices and backfill but also include tunnel construction materials, grouts and seals and constitute by far the largest proportion of the material in the repository (in the Swiss concept, for example, some 1.5 million tonnes of cement will be utilised, approximately 87 % by weight of the total repository). Such a repository concept has been developed to maximise radionuclide retardation in the near-field through the presumed low solubility of most radionuclides of concern in hyperalkaline media allied to the seemingly large surface area afforded by the porous cement (HODGEKINSON and ROBINSON, 1987).

Conditions in such a repository are expected to be highly alkaline and models (e.g. BERNER, 1987, ATKINSON and GUPPY, 1988) suggest that interaction of the concrete with the groundwater will initially produce KOH and NaOH leachates followed by an extended period of high pH (12.5) leachates buffered by $Ca(OH)_2$ (portlandite). It is further predicted (eg. HAWORTH et al., 1987) that hyperalkaline pore waters will leach out of the near-field and interact with the repository host rock. This may significantly alter the original nature of the host formation in the vicinity of the repository, affecting the retardation qualities for which the formation was originally chosen, by changing the pre-existing geochemical and hydrological conditions. From a safety assessment point of view, the precise retardation properties of both the near-field and the potential alteration zone (in the far-field) must, therefore, be carefully assessed.

Repository safety assessment is supported by an integrated research programme of laboratory experiments, field measurements and modelling studies all of which aim to predict radionuclide retardation in and around the repository. To date, information already exists, in the form of model predictions (eg. BERNER, 1990) based on short term (a few years at the most), laboratory studies (eg. EWART et al., 1985; JEFFERIES et al., 1988; GLASSER et al., 1989), on the probable behaviour of several components of a cementitious repository. However, the models have not been validated on the time scales of concern to a repository safety assessment. An additional technique must then be employed, one which will allow validation of, at least, part of the predictive models currently employed and which, by investigating appropriate field examples, can test the applicability of the laboratory derived data to the repository environment: this approach is usually termed a natural analogue study

(see CHAPMAN et al., 1984 and CHAPMAN and McKINLEY, 1987, for detailed discussions on the use of natural analogues in radwaste disposal).

The role of the so called natural analogues in the safety assessment of a radwaste repository is well established, as is their place in the triunity of laboratory studies, models and field work supporting the safety case (eg. HSK, 1991), but it is interesting to note that analogues have only rarely been discussed in terms of a cementitious repository system (see the review of McKINLEY and ALEXANDER, 1992, for example). One notable exception to date is the Oman project where the behaviour of certain radionuclides of interest in a natural hyperalkaline groundwater was examined (BATH et al., 1987). Here, the laboratory produced values included in the databases of geochemical thermodynamic codes (such as PHREEQE) were tested by direct comparison with measured concentrations of trace elements in the groundwaters (see McKINLEY et al., 1988). In addition, alkalophilic sulphate reducing bacteria were shown to be viable in this unusual environment. The results of this study were encouraging enough to suggest that the natural analogue approach was worth pursuing further with regards to the rather complex hydrogeochemical system representing the near-field and immediate environs of a cementitious repository.

One of the major problems facing such a study of natural analogues of a cementitiuos repository, however, is that appropriate analogues are rare. It is not, of course, necessary to have a carbon copy of a repository system (and, in any case, no such perfect analogue actually exists) but, to minimise the inherent complexity of a natural system, it is useful to study an example which mimics the repository environment as closely as possible. The highly successful Oman study, for example, featured hyperalkaline groundwaters buffered by high temperature silicates in an ophiolite complex rather than with the low temperature cement minerals which would be required of a "better" analogue of a cementitious repository. Although this caused problems in that the solubility controlling phases identified in the groundwater system were often inappropriate to the study of low temperature, cement-dominated systems, the overall results were nevertheless extremely useful from a safety assessment viewpoint, indicating as they did those areas adequately covered by present thermodynamic databases and those requiring further effort.

The study described here is somewhat different in that the groundwater chemistry of the Maqarin area is controlled by naturally occurring cement minerals and gels (SAINES et al., 1980; BARNES et al., 1982; KHOURY and NASSIR, 1982a). Other features representative of cementitious repository designs are also present, including natural bitumen with associated U and the presence of other trace elements of interest to the safety assessment of a L/ILW repository (eg. Se and Ni) in relatively high concentrations in both the groundwater and host rock. This fortuitous combination of repository analogous features is a product of the spontaneous combustion of the bitumen-rich limestone host rock, forming lime in the absence of quartz. Subsequent groundwater flow hydrated the lime to form portlandite initially, followed by further reaction with the groundwater to produce ettringite, thaumasite and other cement

phases (KHOURY et al., 1992). Recarbonation also appears to have occurred and the temperature of the retrograde hydration and alteration was initially high enough to produce hydrothermal minerals such as apophyllite which are typically enriched in trace elements.

The attenuation of ^{14}C in the cementitious engineered barriers of a repository is likely to be associated with recarbonation reactions and so the site is also an useful test of the applicability of the laboratory produced data to an actual repository environment.

The main objective of studying the Maqarin hyperalkaline groundwater system was to test performance assessment models. In particular, the databases of geochemical thermodynamic codes were to be assessed, in the manner of the Oman study, by comparing the speciation and solubility of several trace elements predicted when using the databases with that actually measured. In addition, it was intended to test coupled (transport and geochemistry) codes, to provide data on recarbonation reactions (potentially, a significant ^{14}C retardation mechanism) in natural systems and to assess both the microbiological and colloidal populations of the hyperalkaline groundwaters.

The main method employed to achieve these ends was to describe the unique Maqarin groundwater system in as much detail as limited sampling and analysis time would reasonably allow. This was carried out in two ways: the groundwater chemistry (especially trace element chemistry) and stable isotope signatures were characterised in some detail (see KHOURY et al., 1992, for example) and the mineralogy and geochemistry of the host rock are described in great detail. This was necessary to provide enough data to test the various models under scrutiny in as unambiguous a manner as possible, something which had proven impossible in the earlier Oman hyperalkaline groundwater study due to a lack of data, especially on the mineralogy of the host rock (see McKINLEY et al., 1988, for details).

Overall, a large body of data already existed on the high temperature phases in the Maqarin system (and similar formations in other parts of Jordan and Israel) but little was known of the low temperature system which is of more relevance to L/ILW disposal concepts. Consequently, much effort has been expended in this current phase of the Maqarin project to detail the mineralogical relationships of the various low temperature phases and associated trace elements (although, because the high temperature minerals may also act as solubility controlling phases, they have not been completely ignored). The main result of this work then, has been that the speciation, solubility and solubility controlling phases of several trace elements of direct interest to a safety assessment of a cementitious repository have been defined in enough detail to allow rigorous testing of the predictive capabilities of that part of performance assessment models which is carried out via the thermodynamic codes. This phase of the project also included a predictive modelling component along the lines of the earlier Oman study (see BATH et al., 1987, for details). In this instance, the various modelling groups involved in the project were provided with the major element chemistry of the Maqarin groundwaters and then, on the basis of "reasonable" estimated concentrations

of a suite of trace elements of interest (to a repository safety assessment), proceeded to calculate (i.e.predict) the likely solubility, speciation and solubility controlling phases in the Maqarin system (full details in ALEXANDER et al., 1992). As well as providing a prediction which could then be compared with the subsequent analytical data (so testing the code databases), this allowed some focussing of the sample analyses on, for example, specific minerals in the rock.

Similarly, the flow system has also been studied in an attempt to define groundwater sources, residence times and zones of hyperalkaline groundwater/unaltered host rock interaction. The former part of this work, conducted via stable isotope analyses, has been successful but the latter part, to have been carried out by physically characterising alteration zones in the rock, has not worked so well. This was due in large part to extremely difficult field conditions but it is hoped that further sampling in the future will provide appropriate samples for detailed characterisation which will then produce enough information to allow thorough tests of the coupled codes as was originally intended.

This report thus contains much detailed information on the Maqarin hyperalkaline groundwater system but the data, and the effort involved in collecting the information, must be seen in the context of the main aim of the project, namely the rigorous testing of repository safety assessment models. It is only by taking such great care over work like this that the end users, the safety assessors themselves and the relevant regulatory bodies, will be convinced as to the integrity of the repository safety assessment as a whole.

1.2 Layout of the report

This report contains a particulary detailed and extensive description of all of the work carried out in the project. This approach has been taken because it is likely that the sampling site will be inundated, in the near future, by the construction of the Jordanian-Syrian Unity Dam. That such a unique site as the Maqarin Springs will be lost by such an action is regretable, but at least the information documented here will be detailed enough to allow further work to be carried out in the future, either by simply using the data included here or by re-examining existing rock and water samples.

The report thus includes an introduction to the sampling area (chapter 2) which details the most up-to-date information on the site geology and hydrology, followed by a thorough description of the sampling sites and field and analytical methodology (chapter 3). The next chapter (4) contains a summary of the investigations (including mineralogy and geochemistry) of the rock and groundwaters of the site. Full data (and a fuller discussion) are included in appendices A through C. Also included in chapter 4 are data on microbiology and colloids plus a study of stable isotopic behaviour in the rock-groundwater system (also discussed in appendices A and E).

Chapter 5 describes the main thrust of the current project, the validation of several databases utilised in thermodynamic geochemical codes which are used as part of a radwaste repository performance assessment. An additional description of a code intercomparison is included in appendix D. Finally, the report is closed with a summary chapter (6) which highlights the important findings of the project, details the relevance of these results to safety assessors and indicates areas requiring further study.

2 INTRODUCTION TO THE MAQARIN AREA OF NORTHERN JORDAN

E. SALAMEH

2.1 Geological Setting: regional geology

The stratigraphical history of Jordan is related mainly to the deposition of marine sediments, with repeated oscillations of the Tethys transgressions which invaded the land from the northwest and west. The land at that time compromised a small area of Precambrian granitic basement, outcropping in what is now the southwestern part of the country, which thickened and deepened to the north and east.

The most prominent structural feature that controlled the geomorphology and hydrogeology of the area is the Jordan Graben. It formed along a Cambrian weakness zone during the late Miocene, as a result of sinistral movements (QUENNEL, 1959; FREUND, 1965) or differential uplift movements (PICARD, 1943; BENDER, 1968).

2.2 Stratigraphy

Introduction

A complete succession from Permian through Quaternary sediments underlies the study area (figure 2.1). The regional lithostratigraphic correlation chart (table 2.1) shows the formation names and age relationships. The various rock formations which comprise the study area are given in figure 2.2 while the subsurface geology is illustrated in the geological cross-section of figure 2.3. The full succession is now detailed on a period by period (and era where applicable) basis.

Permian

Permian rocks (mainly sandstones) have been recovered from some recent oil and gas exploration wells (drilled to the south-east of the study area) with partial recovery in the Er-Al well (N208.8, E246.5, cf. figure 2.2) which was drilled to a total depth of 3500 m and full recovery of a 250 m thick section in the NM-2 well (N224.8, E245.9, cf. figure 2.2), also drilled to a depth of 3500 m (NRA, 1991).

Triassic

The Triassic is exposed along a narrow strip parallel to the Zarqa River, at the mouth of Wadi Al-Huni (figure 2.4). The rocks were first recognised by Cox (1932) and consist of a few metres of crystalline limestone alternating with thin bedded shales and a 20 - 30 m thick bed of massive gypsum. This is followed by an argillaceous marly limestone, shales and iron oolites and finally a varigated sandstone at the top of the succession at the contact with the overlying Jurassic sediments (BENDER, 1974). All facies belong to the Ma'in Formation.

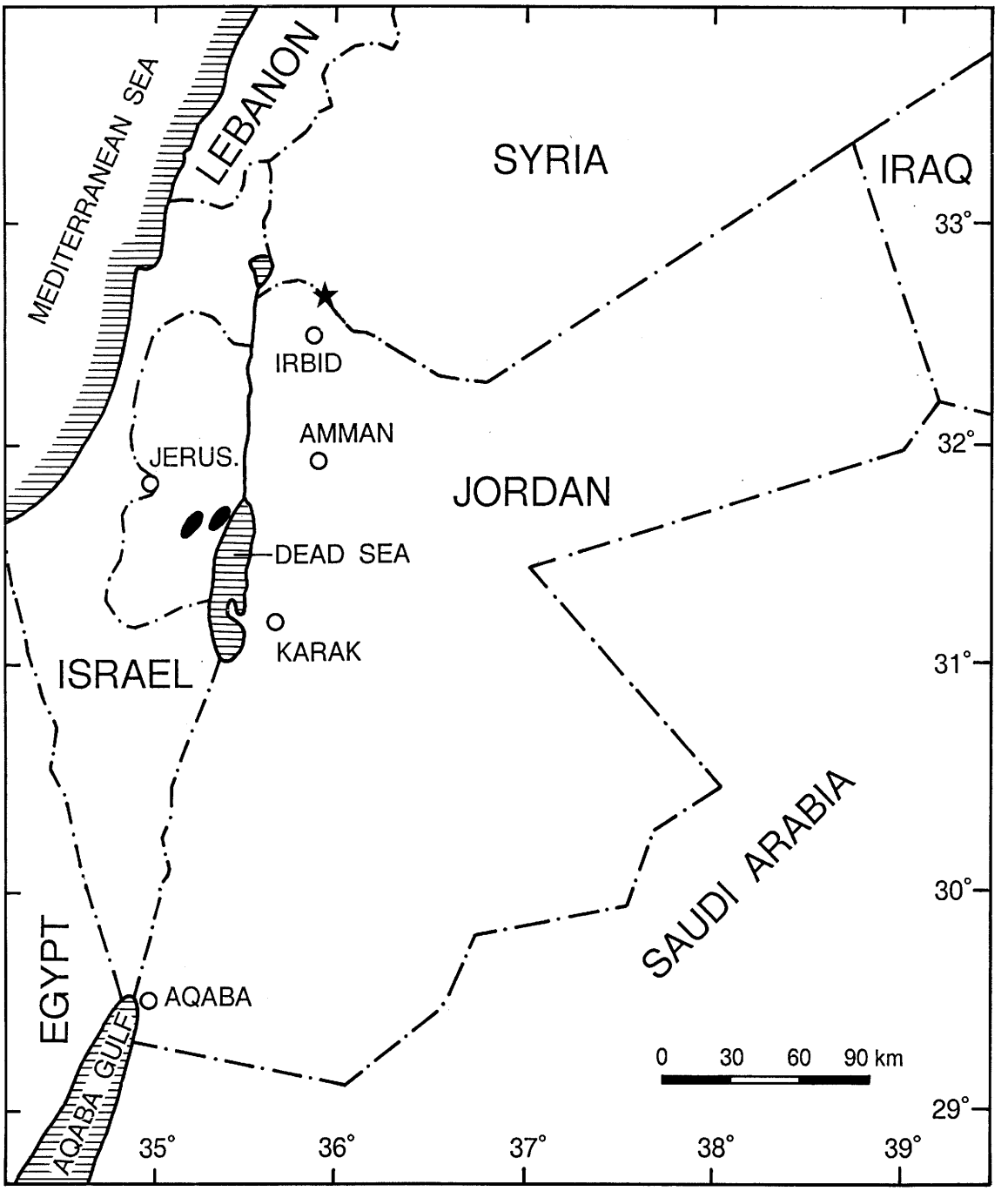

Figure 2.1 Maqarin natural analogue study site, northern Jordan.

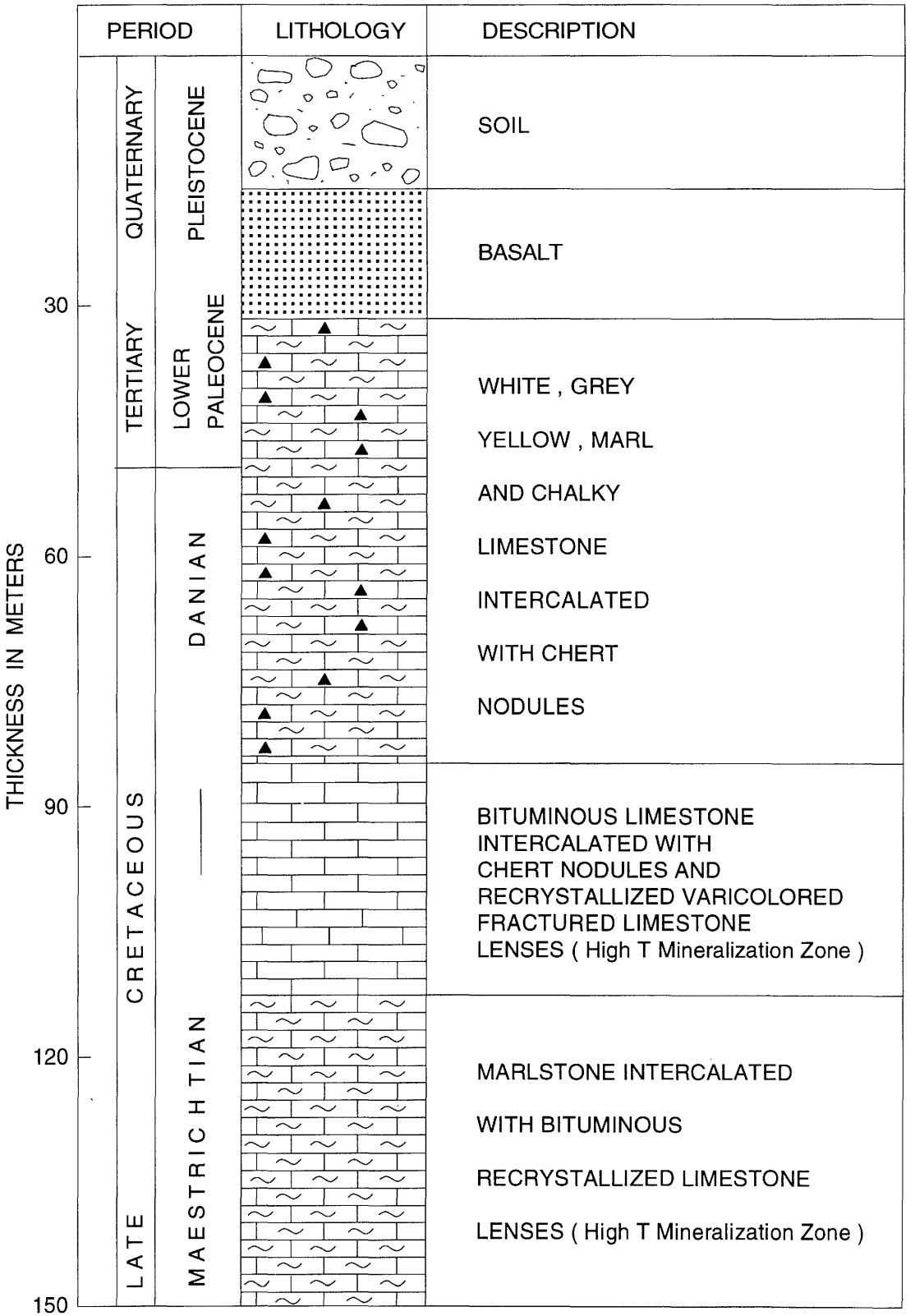

Table 2.1 Regional lithostratigraphic correlation chart of the different geologically relevent units and formations recognised by various authors.

Jurassic

A 220 m thick (WETZEL and MORTON, 1959) succession of Jurassic beds are exposed in Wadi Al-Huni on the northern side of the Zarqa River and at the Arda'a Road, south of the Zerka River. Dolomitic, massive, crystalline limestone with marl, clay and sandstones are common (BENDER, 1974). The Jurassic sequences are represented by the Azab Formation of table 2.1.

Lower Cretaceous

Barremian-Aptian-Albian

Lower Cretaceous rocks are exposed locally in some structurally elevated areas. The lower Cretaceous sandstones overlie the Jurassic sediments with a distinct erosional unconformity at the Zarqa River (BENDER, 1974).

In north Jordan (Zarqa River, Wadi Al-Huni and Ain Khuneizer; figure 2.4), the lower Cretaceous sandstones begin with basal conglomerates, or with sandstones intercalated with conglomeratic layers, up to 5 m in thickness and are followed by vari-coloured, alternating silty and marly, coarse to medium and fine grained sandstone with some shales and marls up to 140 m in thickness. Yellow - brown, reddish and greenish marls, partly sandy or glauconitic, are present within this sequence. It is then followed by vari-coloured, medium to coarse grained sandstones, alternating limey sandstones and dolomites, up to 100 m in thickness (BENDER, 1974).

The presence of glauconite, fossil fish, bedded limestone, and amber are taken as evidence of minor marine influence by BENDER (1974) and BANDEL and HADDADIN (1979).

Cenomanian to Early Campanian

Shallow and warm seas covered Jordan during this period and limestones, marls and dolomites were deposited throughout the Cenomanian to Early Campanian. These carbonates are refered to as the Ajlun Group (table 2.1).

The lower Cenomanian consists of the Nau'r and Fuheis Formations (Nodular Limestone Unit; BENDER, 1968). Two sub-units are recognized within the Nau'r Formation: a lower formation (A/1) consisting mainly of marls and ranging in thickness from 60 to 120 m and an upper formation (A/2) of 100 to 150 m in thickness (MacDONALD and HUNTING, 1965) consisting mainly of limestones and marly limestones. The Fuheis Formation (A/3) overlies the Nau'r Formation and consists of marls and very thin intercalations of marls and limestones (3 to 5 cm) and has a thickness of 70 to 90 m.

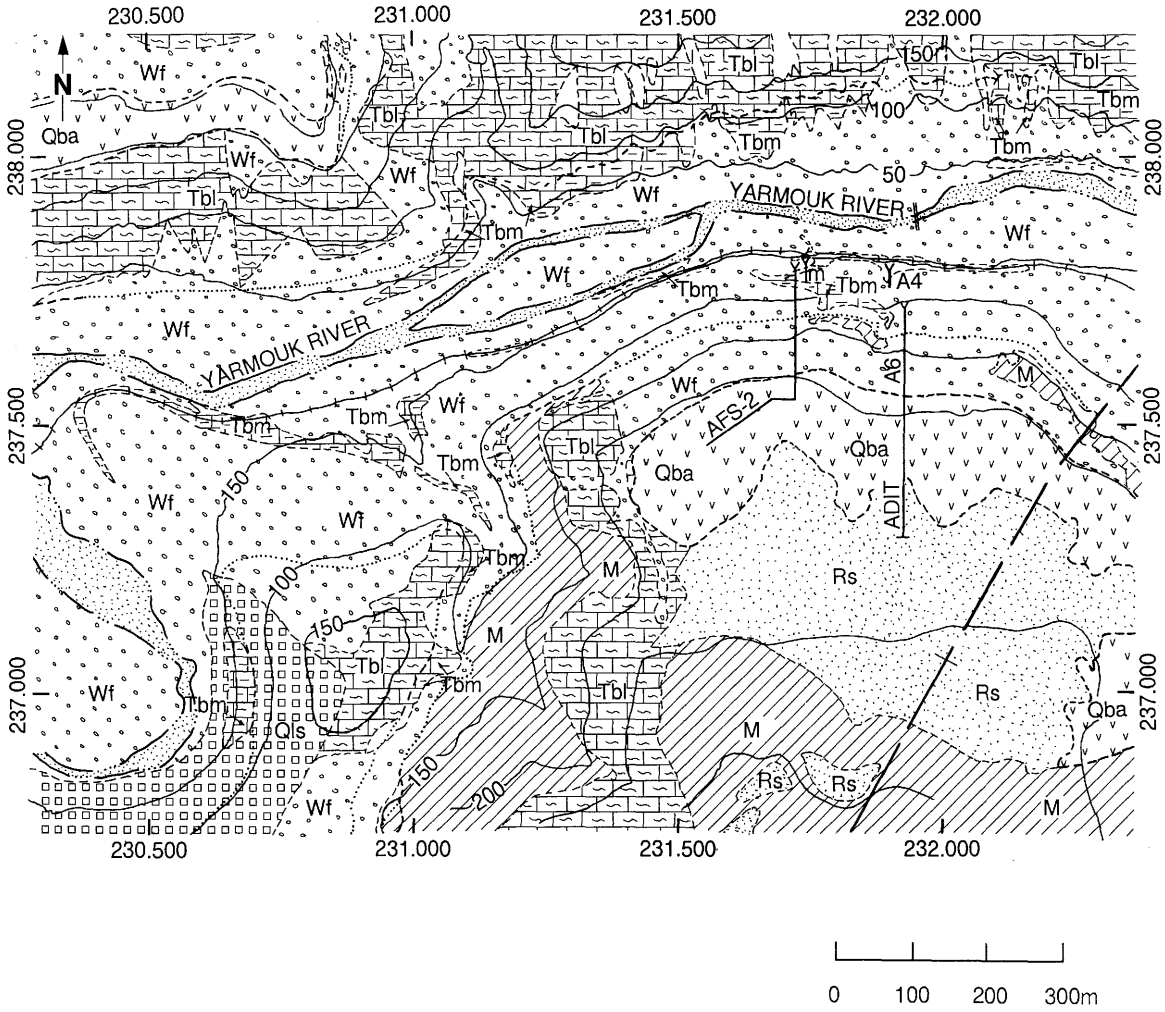

Figure 2.2 Superficial geology of the Maqarin area (after BENDER, 1968 and HARZA, 1987).

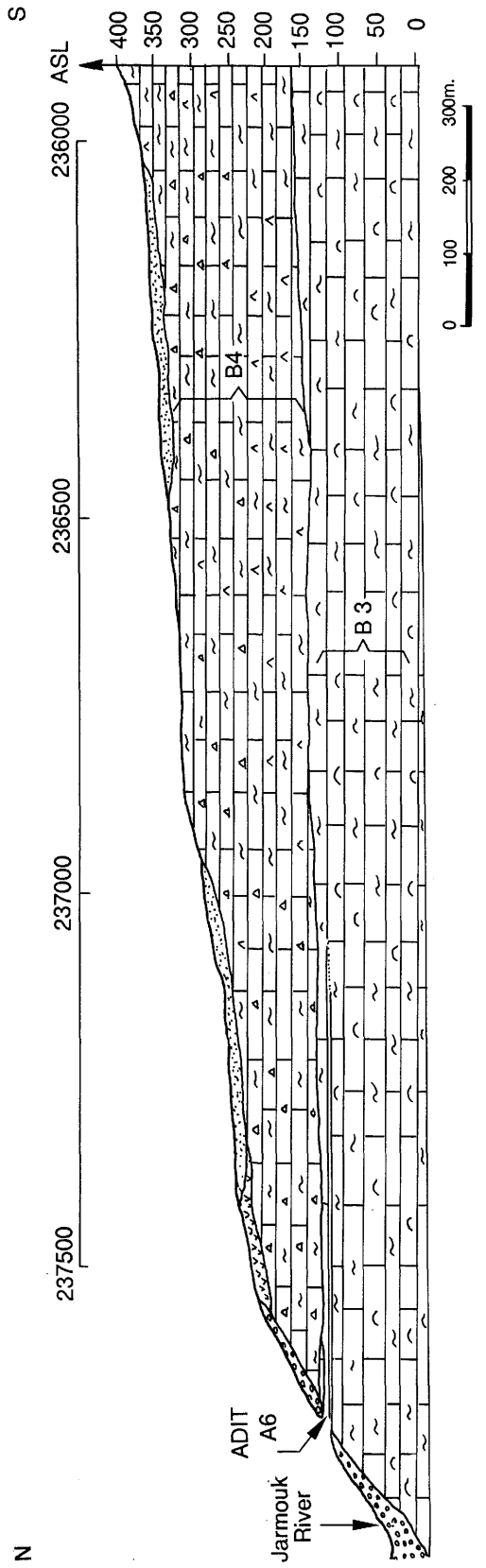

Figure 2.3 Geological cross-section N-S along the line of Adit A6 with an extension to the S.

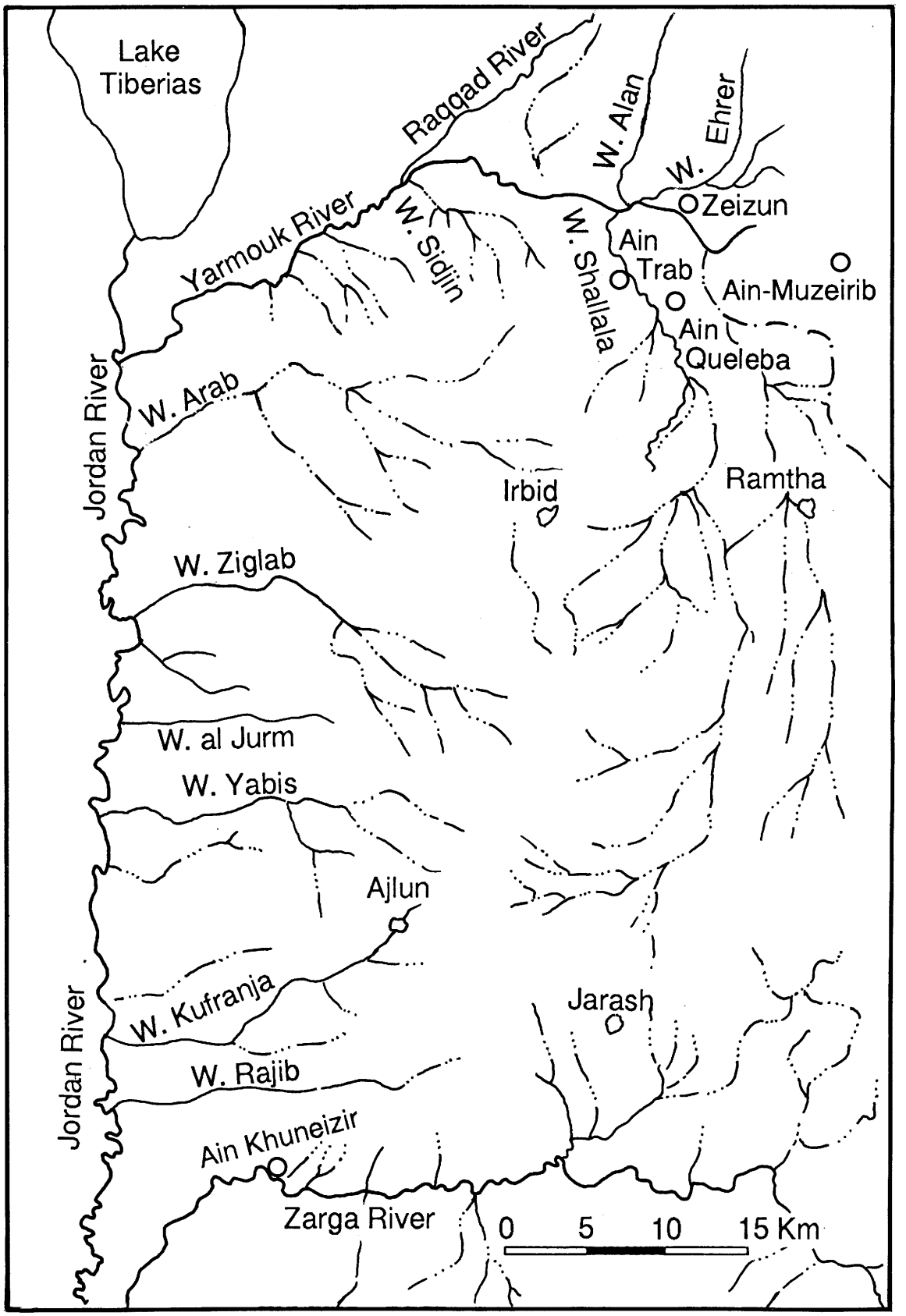

Figure 2.4 Regional drainage pattern, Maqarin, northern Jordan.

The Upper Cenomanian is represented by the Hummar and Shueib Fomations (Echinoidal Limestone Unit). The Hummar Formation (A/4) has a thickness of about 40 to 45 m, consisting mostly of karstified dolomitic limestone. The Shueib Formation overlies the Hummar Formation and was subdivided by MASRI (1963) and MacDONALD and HUNTING (1965) into two sub-units: A5, consisting of thin bedded limestone with marl intercalations and A6, consisting of crystalline, massive bedded limestone. The total thickness of both formations (A4 and A5-6) increases up to 170 m in the study area (observed in the Jordan River Valley, or JRV, borehole number 1; NRA, 1991).

The Turonian is represented by the Wadi Es-Sir Formation (A7) which forms the uppermost part of the Ajlun Group. (Massive Limestone Unit). Its thickness increases from 80 - 90 m in the central part of the country to about 200 m (JRV1 and JRV3b wells) in the northern part of the country.

The Santoian sediments (B1) consist of chalk and marl and directly overlie the Wadi Es-Sir Formation. Biostratigraphically, it belongs (according to BENDER, 1968) to the Massive Limestone Unit and represents the Wadi Ghudran Formation. The formation is only found in the study area, with a thickness of about 35 m in the Muhkheiba area, thining out towards the south and entirely missing in some places.

Upper Cretaceous

Late Campanian to Maestrichtian

The Amman Formation (B2) was deposited in the late Campanian. It consists predominantly of chert, marly limestone, tripoli (idiomorphic, fine grained, authigenic quartz) and some phosphate-bearing strata (phosphatic chert and phosphatic limestone) with a total thickness of about 60 m in the study area.

Maestrichtian to Lower Paleocene

Sedimentary rocks of this age (Muwaqqar Formation; B3) consist of an interbedded sequence of marls, chalks and chalky limestones. The sequence is generally rich in organic matter whose content can reach 18% of the total rock. The thickness in the Maqarian area is more than 300 m (HARZA, 1979).

Tertiary

Paleocene to Eocene

Marine sedimentation continued without a major lithological break into the Tertiary in Jordan. Sedimentary rocks of Paleocene to Middle Eocene (Rijam Formation; B4) and Upper Eocene (Wadi Shallala Formation; B5) consist of limestone and chalky limestone with chert layers. The Rijam and Wadi Shallala Formations have a thickness of about 300 and 45 m, respectively (U.N.D.P./F.A.O., 1970).

Quaternary

Pleistocene

Basalt flows occur in the northern and eastern parts of the Irbid district in the Yarmouk River catchment area. They consist of a sequence of flows, filling former river courses and forming wadi terraces. They consist mainly of alkali basalts and basanites (VAN DEN BOOM, 1968). VAN DEN BOOM and SAWWAN (1966) subdivided the basalts into six different flows with tuff horizons of Pleistocene age between the fifth and sixth flow. According to PICARD (1965), the basalts of the Yarmouk area are of Middle Pleistocene age. They are mainly related to the final (sixth) flow of Pleistocene volcanic activity which is separated from the others by clays and gravels (BENDER, 1974).

Holocene

These are alluvial fluviatile deposits, consisting of gravel, sand, silt and clay with pebbles and boulders of chert and limestone. The most important occurence of wadi deposits in the study area are found along the Yarmouk river and its tributaries.

Recent

Soils cover an extensive part of the study area and can be divided into two groups. MOORMAN (1959) recognised Red Mediterranean soils, which cover the Irbid area, and Yellow Mediterranean soils, covering the area along the Jordan Rift Valley. They are also present in the area east of Irbid where average precipitation falls below 250 mmy^{-1}.

2.3 Hydrology

The four aquifers found in the study area are discussed below;

Amman Formation (B2)

There is no outcrop of this formation in the study area but it lies some 100 m below the surface. It is composed of highly fractured cherts resulting in relatively high secondary porosity and permeability. The permeability, calculated from pumping tests of exploratory wells and from the artesian flow of boreholes, ranges from 10^{-5} cms^{-1} to more than 10^{-3} cms^{-1} (HARZA, 1978). The results of various pumping tests indicate an increase in permeability towards the Yarmouk river axis.

Bituminous Marl Formation (B3)

This formation consists of about 220 m of bituminous limestone with generally very low

permeability and is generally considered as a fairly good aquiclude. In the study area, however, the formation is partly fractured in places and forms an aquifer with measurable permeability (water pressure tests in this formation give a permeability of 1.0×10^{-5} cms^{-1}; HARZA, 1978).

The high pH waters are found as perched water within the upper part of the Bituminous Marl formation which is exposed on the south side of the river (figure 2.2) and they emerge as springs and seep down the slopes towards the Yarmouk river.

Chalky Limestone Formation (B4)

In the mapped area, this formation lies within the unsaturated zone and its hydrogeological importance as an aquifer is thus limited. It proved impossible to determine the formation permeability, although the nature of the rock suggests it is very low. Nevertheless, springs do issue along fractures in this formation in the surrounding areas of Ain Quelbe, Ain et Trab and the springs of Wadi Shallala.

Basalt Flows

The basalts in the study area are good aquifers, mainly due to their high porosity and permeability. Most of the Yarmouk river baseflow water is derived from this aquifer, mainly from the (Zeizon and Mezairib) springs on the Syrian side of the river. Ain El Quseir and Ain Ghazala which are located outside the study area also issue from this same unit. It is not possible, with the available information, to determine the precise permeability of the basalts, but the groundwater movement in this aquifer is known to be directed towards the river.

Ground Water Movement

Within the study area, waters from the Amman Formation, the Bituminous Marl Formation and from the vadose zone discharge towards the Yarmouk river. The water of the confined Amman Formation seeps upwards through the fractures and joints of the Bituminous Marl Formation to the Yarmouk river.

Groundwater isopachs have been constructed on the basis of measurements of the piezometric levels in the boreholes penetrating the Amman Formation (March, 1980) and figure 2.5 shows that the groundwater flow is directed towards the Yarmouk river. On the northern side, the water moves southwards toward the Yarmouk river with a gradient ranging between 0.022 and 0.029. On the southern side, the water moves northwards with a gradient of 0.085. Along the Yarmouk flood plain, the flow in this formation coincides with that of the river, mainly from east to west with a gradient ranging between 0.034. and 0.039.

The high pH water in the vadoze zone on the southern side of the Yarmouk river seeps down along slopes and fractures towards the River.

2.4. Hydrochemistry

Various waters, widely differing in their chemical and physical properties are found in the study area. Full details are provided in chapter 4 but, in brief, the groundwater is highly variable with the pH ranging from 6.5 to 12.9 and the electrical conductivity (EC) values ranging from 450 μScm^{-1} to more than 8000 μScm^{-1}. Generally, the water is very low in NO_3^- and has a weak to moderate H_2S odour.

The various types of water can be subdivided, by aquifer, into the following groups:

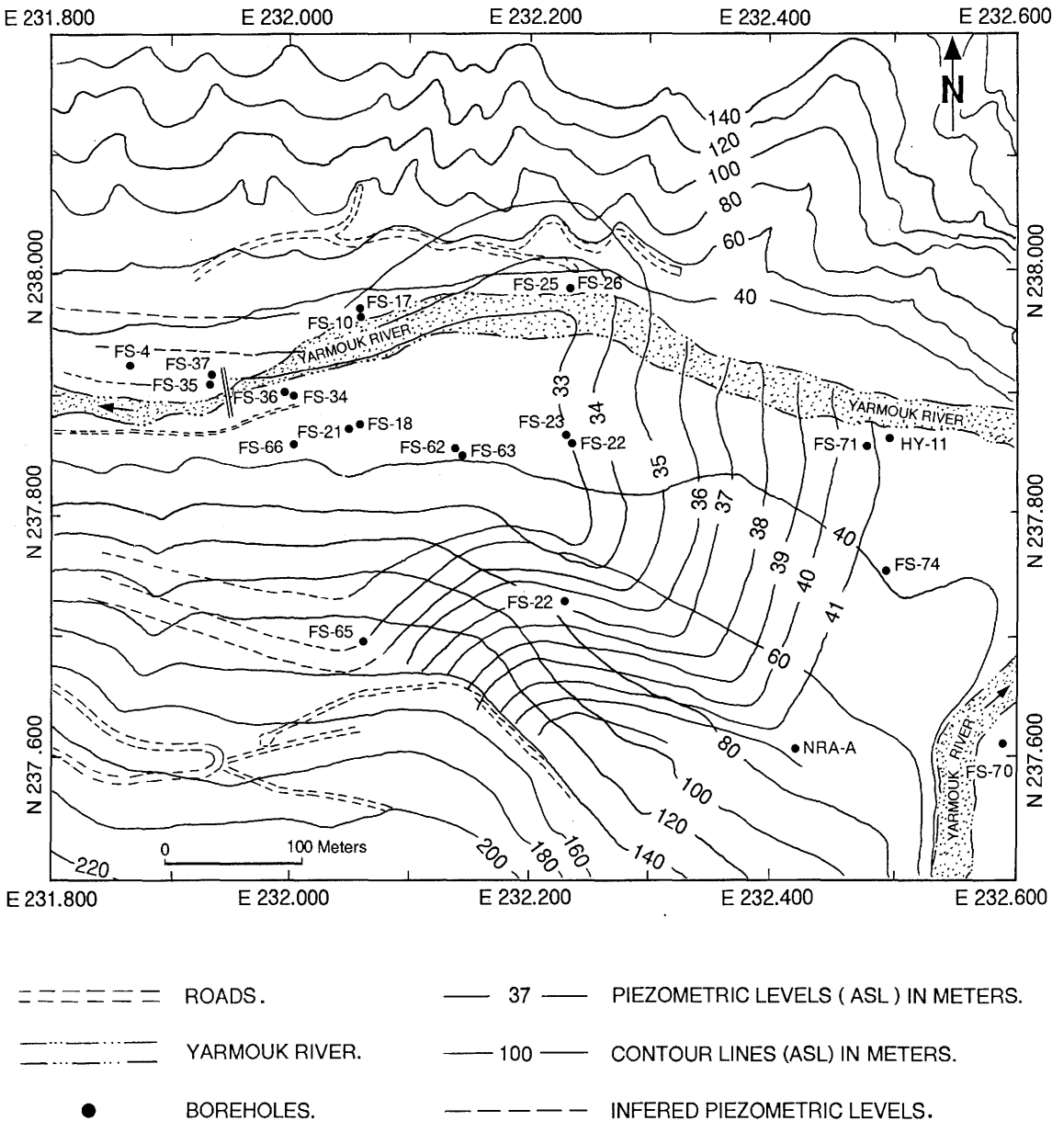

Figure 2.5 Amman Formation piezometric isopach map (March, 1980).

Yarmouk River Water

The main source of this water is the basalt aquifer covering the flanks of the Yarmouk river and extending far into Jordan and Syria. The chemical composition of the river baseflow is relatively stable with a total dissolved solid (TDS) load ranging between 400 and 500 mgl^{-1}.

The results of around 30 analyses show that Na > Ca ; Mg > K ; Ca + Mg > Na + K ; Cl > SO_4 ; Cl > Na and Ca + Mg > HCO_3 + CO_3. The water is saturated with O_2 and contains around 0·24mM NO_3^- (from non-anthropogenic sources).

During floods, the TDS becomes diluted to 250 to 300 mgl^{-1} but without major changes in the ionic ratios.

Amman Formation (B2) Water

The groundwater of the Amman Formation is confined and has no known (unmixed with other waters) surface seepages. Samples from this aquifer were obtained during 1980 and 1981 in the course of a sampling campaign (after drilling boreholes) to investigate the Maqarin dam site. The temperature of the water ranges from 24.5 to 29 C.

The chemical composition of the water varies widely between boreholes (table 2.2) but is consistent within any given borehole. This behaviour was attributed to differing flow paths and pressures within the aquifer, to differing flow paths in the overlying aquifers and to various mixing processes.

The water of the Amman Formation is recharged along its outcrops further to the south in the Ajlun-Irbid area and to the north in Syria. But even the water in the Amman Formation itself is a mixture of different sources seeping upwards from deeper lying aquifers whose piezometric heads go higher than that of the Amman Formation. The precise water chemistry in the Amman Formation therefore differs from one place to the other according to the presence of joints, fissures and other flow channels.

Muwaqqar Formation (B3)

Generally, the water in this formation has a strong H_2S odour and a neutral pH of around 7 (table 2.2), although the water in one well (S-8) has a pH of 12.9. In a few cases, the pH reaches 8, apparently, indicating mixing processes between the high and low pH water. The samples described here were collected from boreholes in the early 1980's and, in other samples collected from the same aquifer more recently, the water chemistry is seen to fluctuate widely depending on the time and place of sampling, possibly indicating complex mixing processes.

Rijam and Shallala Formations

Water from this aquifer has a neutral pH and a low TDS concentration (230-600 ppm). In contrast to the other groundwaters, the Rijam and Shallala Formations water contains relatively high amounts of nitrate (0·1-0·7 mM NO^-_3; table 2.2) indicating direct connection to surface waters.

The Rijam and Shallala Formations are directly recharged by precipitation along their outcrops at the flanks of Wadi Shallala, a side wadi of the Yarmouk river, lying about 2 km to the east of the Maqarin Dam site (figure 2.4).

High pH-Water

This type of water is encountered in the Rijam Formation and in the upper part of Muwaqqar Formation as it percolates through metamorphosed portions of these Formations.

The origin of the water is precipitation falling over the southern flank of the Yarmouk river. Generally, precipitation in the study area infiltrates directly (or via a thin soil horizon) into a thin basalt flow to the Rijam Formation or directly into the Rijam Formation. Samples collected from this formation also display rather large ranges in the concentration of defined species (table 2.2).

Parameter (mM unless otherwise stated)	Yarmouk river water	Amman Formation aquifer	Muwaqqar Formation aquifer	Rijam-Shallala aquifer	Hyperalkaline groundwaters[1)]
pH (units)	6.8-9.0	6.8-8.5	6.5-12.9	6.8-8.16	10.38-12.8
EC (μScm^{-1})[1)]	300-700	--	--	--	--
TDS (ppm)	--	240-685	--	--	--
Ca^{2+}	1.50-3.10	0.40-5.18	3.30-5.18	3.30-6.38	0.24-2.72
Mg^{2+}	1.56-2.72	<4.60	0.68-3.26	2.22-3.36	<0.12
Na^+	1.74-3.74	1.04-4.56	1.30-3.80	0.45-1.80	0.02-0.26
K^+	0.05-0.14	0.04-0.57	0.12-0.31	0.01-0.08	0.01-0.33
HCO_3^-	2.51-4.26	0.70-6.70	4.52-7.28	3.31-6.69	--
CO_3^{2-}	<0.8	<0.8	--	--	0.02-0.08
SO_4^{2-}	0.74-1.70	0.10-3.36	0.28-2.42	0.04-2.34	0.08-0.72
Cl^-	1.53-2.54	1.10-4.75	1.21-2.41	0.57-2.21	0.04-2.51
NO_3^-	0.18-0.44	<0.02	<0.17	0.10-0.73	<0.01

1) excluding analyses reported in chapter 4

-- not measured

Table 2.2 Range in groundwater chemistry observed in the Maqarin area

3 SAMPLING AND ANALYTICAL METHODS

I.D. CLARK, P. FRITZ, A.E. MILODOWSKI and H.N. KHOURY

3.1 Field Programme Objectives

The objectives for field sampling were the following:

(i) Measuring field parameters including pH, Eh, temperature, and electrical conductivity (E.C.) at the principal discharge points.

(ii) Obtaining geochemical and isotope samples from the principal discharge points for the hyperalkaline springs.

(iii) Collecting biological samples from all points sampled for aqueous geochemistry.

(iv) Taking carbonate precipitate samples forming at discharge points, for geochemical, mineralogical and isotopic analysis.

(v) Sampling the host rock in the altered brecciated zones and collecting samples of unaltered bituminous marl and limestone for source term geochemistry and for isotopic analysis.

3.2 Site Visit

This chapter describes the sampling sites in great detail because of the complex nature of the local hydrology. It is intended that the original sites can be unambiguously identified by future field workers unfamiliar with the area.

Field work was undertaken during the period of June 3 to 7, 1990. The Jordan-Syria border along the Yarmouk River is a highly restricted zone with border posts maintained by the military. Access to the site required Cabinet approval and was restricted to a minimum period. The Maqarin site was visited on June 4 and June 6, while the balance of the time was spent in the laboratories of the Water Research and Study Centre at the University of Jordan. Maximum time was spent during the site access periods measuring in situ parameters and collecting samples, while sample treatment was, where possible, undertaken in the geochemistry laboratory in the University of Jordan.

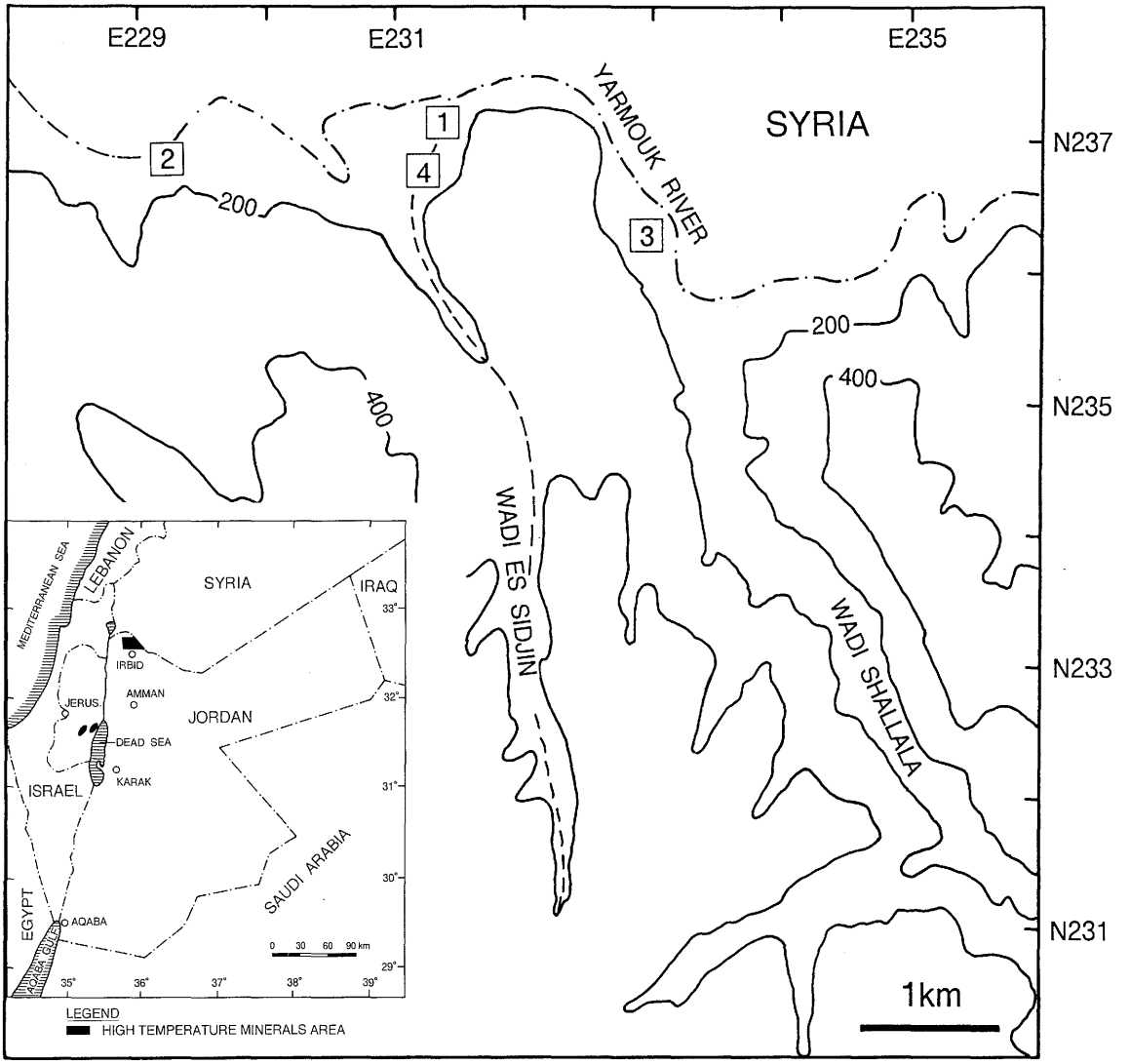

1 Adit A-6 (samples MQ1-MQ4) Collection points 200m from the entrance.

2 Western springs (samples MQ5 and MQ6)

3 Railway cutting (samples MQ7-MQ9)

4 Wadi Sijin springs

Figure 3.1 Sampling sites in the Yarmouk River valley, Jordan

3.3 Occurrence of Hyperalkaline Groundwater Discharge

The Maqarin hyperalkaline groundwater discharges are situated on the southern side in the Yarmouk River valley, 10 km upstream from the Jordan River. At this site, construction was in progress for the diversion tunnel for the future Jordan-Syria Unity Dam.

The Maqarin region hosts two areas where hyperalkaline discharges are found (figure 3.1). As will be shown below by geochemical and isotopic parameters, springs within each of these two areas are probably associated with circulation systems which are unrelated. The eastern discharges are aligned with the strike of the Yarmouk River, possible signifying structural control for a brecciated zone of altered host rock. The western group of hyperalkaine seeps discharge from colluvium along the bank of the Yarmouk River. No structural control or zone of brecciation has yet been identified.

3.3.1 Eastern Groundwater Flow System

ADIT A-6

Adit A-6, dug as an engineering test tunnel in 1979, originates about 50 m above the river level and has been driven 450 m horizontally into the valley wall. The principal seepage of hyperalkaline groundwater into the adit occurs in a several metre wide brecciated zone intersected by the adit between about 155 and 180 m (figure 3.2). A second zone is found at about 210 m and in a third location at about 300 m. However, minor seeps occur through fractures in the unaltered bituminous marl in many parts of the adit.

Samples MQ-1 to 4 were collected from the first principal seepage at about 155 to 165 m. The seepage in this area occurs mainly on the western wall of the adit with some drips from the roof. Calcitic flowstone on the wall characterises this site, with some stalactites up to 50 cm in length on the roof. The two principal seepage sites further back are characterised by stalactites and stalagmites up to 1 m in length.

MQ-1 Small clear pool on floor of adit, fed by seeps from base of wall

This site is a small pool situated close to the western flowstone wall, 25 to 30 cm diameter and 10 cm deep, developed in the deposits on the floor. The pool is fed by drips from the roof as well as seepage from the flowstone. The pool floor is covered by a soft, fine, pure white precipitate and has an accretionary rim of hard precipitate. No precipitate is apparent in suspension or on the surface of the pool.

MQ-2 Drips from several stalactites into plastic bag funnel

This sample represents water dripping from a series of stalactite "straws", on the west wall of Adit 6, 5 m north of MQ-1. Source of the water is behind a coating 10 to 30 cm thick of white calcite "flowstone" formed on the adit wall. Straws are mixed calcite and aragonite, formed by CO_2 diffusing from the adit atmosphere into the high pH water and remain saturated by water surface tension. Several drips were collectively sampled into a plastic bag funnel with Tygon tubing leading from the corner of a polythene bag to a sample bottle on the adit floor.

MQ-3 Small drip situated between MQ-1 and MQ-2

This sample comes from a small drip between MQ-1 and MQ-2 on flowstone wall. This drip was collected directly into a 60 ml Nalgene bottle.

MQ-4 Single drip situated 2m towards adit mouth from MQ-2

This was a single drip situated on flowstone wall 2 m down adit from MQ-2. It was sampled anaerobically by placing the end of a Tygon tube over the stalactite tip. This tube was connected to a Cu He sampling tube, through which at least 3 volumes were allowed to pass before sealing the Cu tube. This drip was then allowed to flow through the Tygon tube over the next two days into a 500 ml bulk sample.

RAILWAY CUTTING SEEPAGE FACE

This site is situated below Adit A6 at about 15 to 20 m above river level, upstream of the intake structure for the Wadi Yarmouk diversion tunnel near the Maqarin Railway Station. Original construction of a railway from Syria to Jordan in the early 1900's created two cuttings into the bedrock of the hillslope, with a total length of about 50 m. Discharge of hyperalkaline groundwater occurs along both faces over a 4 m high face, creating a spectacular curtain of flowstone with columns, stalactites and stalagmites. These deposits were principally creamy white in colour with some streaks of yellow. The tops of active stalagmites had irregular mammalated shapes and were frequently yellow with ettringite. All samples were collected from drips, using methods developed during the Adit A-6 sampling (figure 3.3).

MQ-7 Railway cutting 200 m downstream of railway station

Samples from two drip seepages at this site were collected into a bag funnel and fed via Tygon tubing to a 500 ml bottle. Flow was measured to be 0.01 l min^{-1}.

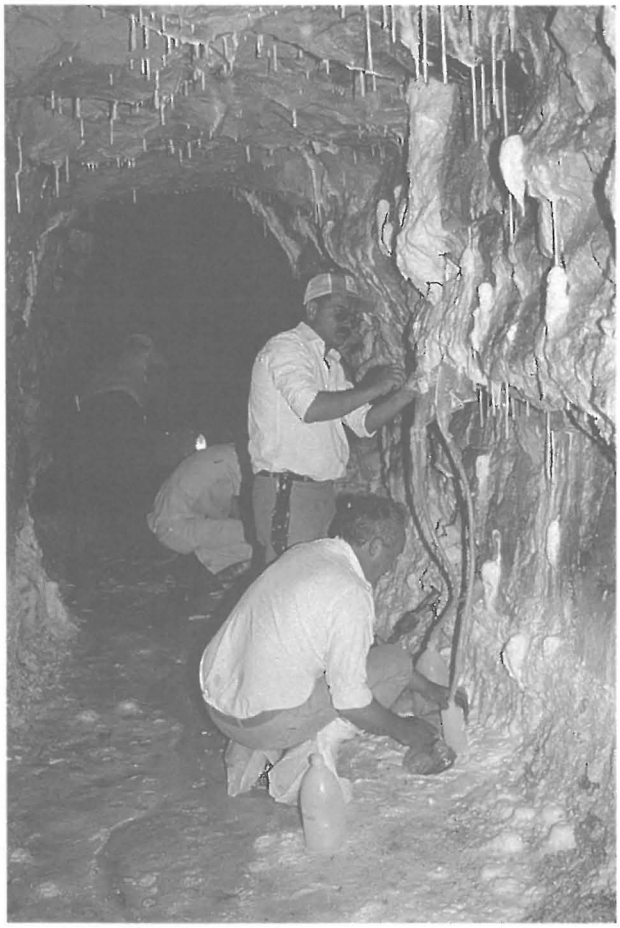

Figure 3.2 Principal sampling point in Adit A-6.

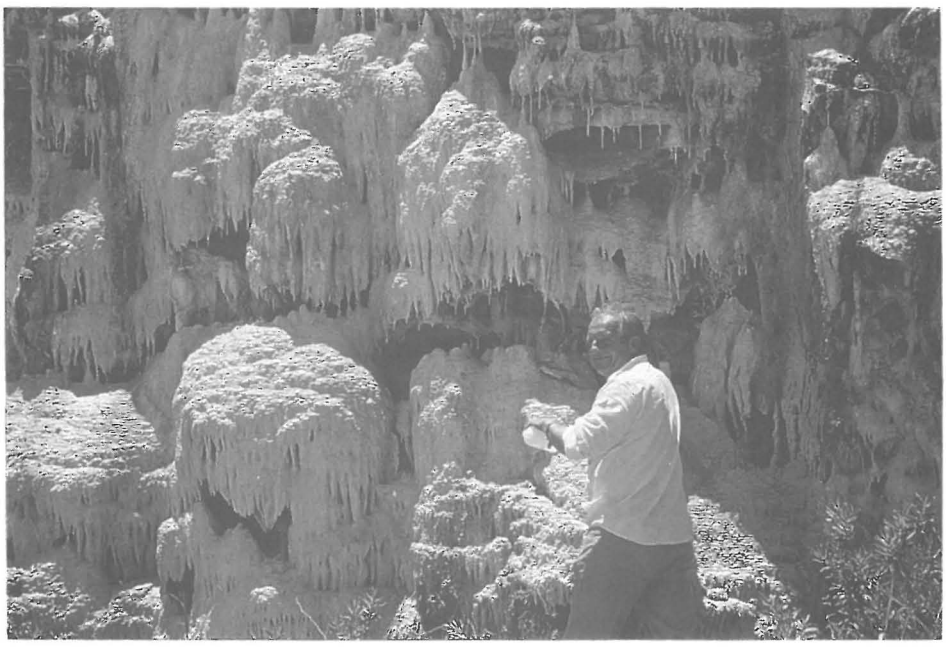

Figure 3.3 Railway cutting sampling area.

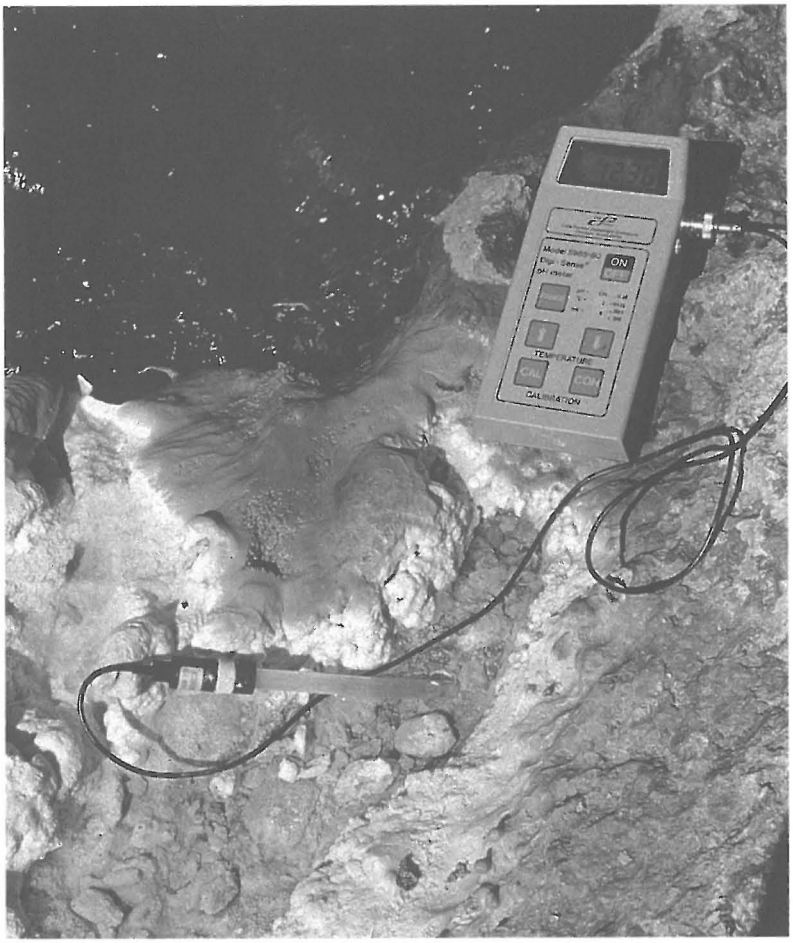

Figure 3.4 Site pH measurement at the bank seepage.

MQ-8 Railway cutting, 10 m downstream (west) from MQ-7

Discharge from a single drip site from a carbonate straw was collected by a funnel into a 500 ml bottle. No pH or Eh was measured at this site.

MQ-9 Railway cutting, 5 m downstream (west) from MQ-7

Discharge from this single drip site was collected by a syringe placed over the carbonate straw, flowing directly into a 500 ml bottle. Minimal contact with air occured in this sampling. No pH or Eh measurement was possible at this site.

WADI SIJIN AND BOREHOLE FW-1

Surface seepage and small pools found in one section of Wadi Sijin, a small tributary to the Yarmouk River, represents one of only two sites in the Maqarin region where hyperalkaline groundwaters discharge naturally at the surface. The second site is the MQ-5 and MQ-6 spring vents discussed below. These seeps have been sampled in the

past by KHOURY et al. (1985) and by KHOURY, FRITZ and CLARK (unpublished data). Total discharge at this site is less than 0·01 l min^{-1}. The site was not sampled during the June, 1990 field work due to extreme time constraints in this militarized zone.

A borehole, FW-1, was drilled upslope from the Wadi Sijin seepages which encountered hyperalkaline groundwater. The chemistry of this water has been presented by KHOURY et al. (1985). Deterioration of the casing and time constraints made it impossible to consider this borehole for sampling in the June, 1990 field programme.

3.3.2 Western Groundwater Flow System

WADI YARMOUK BANK SEEPAGE

On the Jordan side of Wadi Yarmouk, 1 km downstream from the dam site, hyperalkaline waters dicharge from colluvium, within about 1 m of river level (figure 3.4). Seepage occurs as either discrete points or diffuse discharges, which, in all cases, is forming extensive travertine along at least 100 m of river bank. Carbonate precipitation forms as either laminated crusts on the surface or as cemented alluvium. The seepage of this site was discovered and a preliminary sample collected by Khoury and Salameh in May, 1990 but it has not been previously described. An access road along Wadi Yarmouk is cut into cemented colluvium 5 m up slope from the seepage zone, although it is not apparent that this excavation has affected the springs in any manner. The valley wall continues steeply upwards for at least 100 m vertically.

Between springs MQ-5 and MQ-6, the river bank is covered with crusts of calcite precipitated from diffuse discharge throughout this area. Associated with the crusts are effluorescences of a yellow powdery mineral (ettringite) and a fresh pistachio green (Cr rich) mineral.

MQ-5 Spring on bank of Wadi Yarmouk, 10 cm above river

Site MQ-5 produced active localised discharge at about 10 cm above river level, flowing from a fissure, probably in bedrock.

Flow was visually estimated at about 0.2 to 0.4 lmin^{-1}. Direct sampling from this source was possible with no atmospheric contamination. Although having no suspended load, this water has a distinct and most unusual greenish-yellow tinge.

MQ-6 Spring on Wadi Yarmouk, 30 cm above river level

Similar greenish-yellow hyperalkaline water at this spring vent discharges from partially cemented colluvial material along the river bank. Localised discharge was pooled and sampled through a Tygon tube leading from the base of the pool. Atmospheric contact was minimal with this arrangement. Green mineralisation permeated the silty matrix at the spring vent.

3.4 Sampling Protocol

3.4.1 Field Measurements

The geochemical parameters measured in the field at the sampling points include temperature, pH, and Eh. table 3.1 summarizes all field measurements. A Cole-Palmer portable, hand-held meter and electrodes were used to measure T (± 0.1 C), pH (± 0.01 pH unit) and Eh (± 0.1 mV). The meter was calibrated for pH with commercially available buffer solutions at pH 7 and 11, and checked with a saturated $Ca(OH)_2$ solution, which has a pH of 12.51 at 25C. All field measurements were corrected by the difference between this calculated value and the value measured for this buffer in the field.

Eh was measured with a standard Pt - Ag/AgCl electrode and verified with Zobell's solution (Eh = 429 + 2.4(25-T) mV, where T is the temperature in Celsius). Due to the very low flow of these seeps, Eh measurement in a sealed flow-through cell was not possible. During measurement, Eh readings typically drifted slowly downward as the electrode apparently moved toward equilibrium with the aqueous redox couples, then would reverse and drift slowly upward, representing contamination by diffusion of atmospheric O_2. The most negative value observed during this period was recorded and must be considered as maximum values for the waters. All recorded measurements were corrected to the hydrogen electrode scale (Eh) by standard temperature correction factors for the Ag/AgCl redox electrode.

Alkalinity measurements, typically carried out in the field, were undertaken in the laboratory due to equipment problems. Methods included both micro-titration (with 0.16N H_2SO_4 and pH measurement, under an N_2 atmosphere) and by total dissolved carbonate measured as CO_2 (extracted under vacuum following acidification by 100 % H_3PO_4).

3.4.2 Geochemical Samples

In addition to total aqueous concentrations for major, minor and trace elements in the hyperalkaline waters, information on aqueous speciation and colloids was also sought. Thus, the geochemical sampling programme employed a variety of sampling, filtration and preservation methodologies.

Table 3.1 Summary of Field Measurements

Sample	Date	T °C	pH Measured	pH Corrected	Eh (mV)	CO_3^{2-} Titrated (mM)	CO_3^{2-} Extracted (mM)
MQ-1	90-6-4	24.2	12.33	12.32	192.1	0.07	0.033
MQ-2	90-6-4	--	12.35	12.34	308.0	0.41	--
MQ-4	90-6-4	--	--	--	--	--	0.035
MQ-5	90-6-4	26.9	12.36	12.52	121.0	0.26	--
MQ-6	90-6-4	26.3	12.51	12.56	127.4	0.41	0.020
MQ-7	90-6-6	26.5	12.50	12.58	243.0	--	0.036

Note: pH measurements corrected by difference between field measured value of saturated $Ca(OH)_2$ buffer and the calculated value of 12.51 (at 25 C) from thermodynamic data.

Eh data corrected to standard hydrogen electrode

3.4.2.1 Dissolved Cations and Anions

Water samples were collected from the seeps described above, with efforts to minimise atmospheric contact. All water was filtered through 0.45 µm pore diameter Acrodisc nylon filter disks into Nalgene bottles. One bottle was preserved with 1% vol. concentrated Aristar HNO_3 for major, minor and trace cations. Samples collected for selected trace element analysis and speciation were concentrated in the field by adsorption onto small SEPAK silica-gel ion-exchange columns. These are discussed more fully in section 3.4.6.

Samples collected for major anion, nutrient and total organic carbon (TOC) analysis, were filtered but not acidified. All filtering was carried out at the spring, with the exception of MQ-7 which was collected as a bulk sample and treated at the laboratory in Amman 15 hours later. Dissolved inorganic carbon (DIC) samples were collected separately in 60 ml sealed syringes and in 1 l glass bottles for measurement by micro-titration and by CO_2 extraction under vacuum by acidification respectively (discussed above). Major and minor element data for all samples was produced by BGS Keyworth, by ICP-OES and ion chromatography. All laboratory data are given in appendix A. Selected inorganic geochemistry for representative samples from this and previous field visits are presented in table 3.2.

Trace element data for Mo, Se, Sn, Pd, Ni, Th and U was carried out by GSC; analyst G. HALL. All elements were analysed direct by ICP-MS (Sciex/Perkin-Elmer Elan model 250 ICP mass spectometer) with the exception of Ni (graphite furnace, AAS), Se and Sn (Hydride generation, ICP-MS) and Pd (adsorbed onto activated charcoal, ashed, solubilized in aqua-regia, ICP-MS). These data are given in table 3.3.

3.4.3 Colloid Sampling and analytical techniques

3.4.3.1 Sampling

Initially it was intended to both sample colloids in the field for enumeration and identification as well as to collect bulk samples for colloid separation in the laboratory. An Amicon 10 ml ultrafiltration cell pressurised by prefiltered bottled nitrogen gas was taken into the field for this purpose. However, it proved impractical to carry out the necessary accurate sample volume measurement and ultrafiltration operations under both the very dusty conditions and time constraints prevailing in the field. Although a portable glove-bag and filtered nitrogen gas supply was taken into the field, it was impossible to prevent dust getting into the bag when introducing samples and apparatus. Consequently, field separation of colloid fractions was abandoned. As an alternative, unfiltered bulk samples were collected in 30 ml amber glass bottles and analysed in the laboratory.

The effect of colloid population on the bulk geochemistry of the groundwater was also investigated via ultrafiltration of groundwater samples. Although, again because of the adverse field conditions this was not carried out directly in the field, samples were prepared using the Amicon ultrafiltration cell within 24 hours of collection. Prior to ultrafiltration, the samples were filtered through 0.45 µm nylon Acrodisk filters. The collecting syringe was flushed with 0.45 µm filtered samples before collection of a sample for ultrafiltration. Ultrafiltration was performed sequentially through 0.2 µm, 15 nm and 3 nm Nuclepore filters (pre-soaked for 24 hours and rinsed in 0.45 µm Acrodisk-filtered double-distilled water). Splits stored in Sterylin plastic tubes for anion (5 ml unpreserved) and cation (10 ml, acidified with concentrated AristaR HNO_3) analysis were taken after each filtration stage.

3.4.3.2 Analytical techniques

The analytical methods used for colloid characterisation were a combination of micro/ultrafiltration techniques coupled with scanning electronic microscopy (SEM), energy dispersive spectroscopy (EDX) and ultraviolet/visible spectroscopy. Static light scattering tests were also used to empirically evaluate the colloid concentration.

Table 3.2 Major element composition of groundwaters from the Maqarin area, northern Jordan. Units are mM (except for pH, TDS and TOC). Complete results are given in appendix A.

	Eastern Zone						Western Zone	
	A-6[a]	Adit A6 MQ-1[b]	MQ-2[b]	Wadi Sidjin[a]	Rail cut MQ-7[b]	MQ-8[b]	MQ-5[b]	MQ-6[b]
pH[e]	12.5	12.32	12.34	12.5	12.58	12.64	12.52	12.56
Eh (mV)	-	< +192	<+308	-	-	+121	+127	
T (C)	-	24.2	24.2	29.8	-	26	26.3	
TDS	2222	1457	1391	1155	1612	1713	3825	4365
OH-	31.62	22.39	23.44	31.62	33.88	38.90	28.18	31.62
Cl-	2.15	1.77	1.59	2.59	1.93	2.04	1.44	1.29
F-	-	0.014	0.021	-	0.019	0.017	0.049	0.033
Br-	-	0.004	0.004	-	0.005	0.004	0.001	0.001
SO_4^{2-}	5.66	3.04	2.90	4.96	2.96	3.03	15.42	17.39
CO_3^{2-}	1	0.033d	0.15e	3.6	0.036d	0.31e	0.15e	0.020d
NO_3^-	0.05	0.03	0.08	0.14	0.12	0.12	0.62	0.62
TOC[f]	-	<0.05	<0.05	-	1.7	1.8	8.0	11.8
Ca^{2+}	24.30	16.29	14.72	-	15.52	15.57	26.20	27.94
Mg^{2+}	0	<0.008	<0.008	0	<0.004	<0.004	<0.016	<0.062
Na+	2.90	1.82	2.13	1.50	1.50	1.52	5.74	8.39
K+	0.66	0.45	0.30	0.42	0.42	0.48	15.68	19.72
Li+	-	0.006	0.003	-	0.006	0.007	0.081	0.108
Sr^{2+}	-	0.11	0.08	-	0.119	0.124	0.18	0.27
Ba^{2+}	-	0.00027	0.00025	-	0.00038	0.00035	0.00016	0.00017
Cr	-	0.011	0.014	-	0.012	0.012	0.105	0.135
Si	-	<0.001	<0.001	-	0.002	.0003	<0.002	<0.11

a Khoury et al. 1985

b Sampled June, 1990, this study

c Field measurement. pH calibrated to $Ca(OH)_2$-saturated buffer.

d Quantitatively measured by acidification and CO_2 extraction under vaccuum

e Titrated under N_2 atmosphere (error: ~ 50 % of measurement)

f Total Organic Carbon, as mg C l^{-1}

Table 3.3 Trace element composition of groundwater from the Maqarin area, northern Jordan. Units are in ppb, except Pd which is given in ppt.

	Mo[1]	Se[2]	Sn[2]	Pd[3] (ppt)	Ni[4]	Th[1]	U[1]
	<0.1	<1	1.5	<0.2	1.0	<0.02	<0.02
MQ-1·4[5]	82	136	1.0	<0.2	2.1	<0.02	<0.02
MQ-1·2[6]	84	137	1.1	<0.2	2.1	<0.02	<0.02
MQ-2[7]							
MQ-4[7]							
MQ-5·4	210	1480	0.9	<0.2	4.6	<0.02	0.13
MQ-5·2	244	1500	1.2	<0.2	3.6	<0.02	1.40
MQ-6·4	277	2080	1.0	<0.2	2.5	<0.02	0.09
MQ-6·2	302	2096	0.8	<0.2	4.3	<0.02	0.13
MQ-7·4	82	299	3.5	<0.2	1.4	<0.02	0.05
MQ-7·2	95	300	11.6	<0.2	1.1	<0.02	0.02

1. Direct analysis by ICP-MS
2. Hydride generation, ICP-MS
3. Adsorbed onto activated charcoal (1 l --> 5 ml)
   repeated on acid scrubbed bottle
4. Graphite furnace, AAS
5. filtered through 0.45 µm nominal pore size filtre then HNO_3 acidified
6. filtered through 0.22 µm nominal pore size filtre then HNO_3 acidified
7. not analysed

Ultrafiltration with polyacrylamide membranes (Amicon XM50) was performed using an Amicon cell under a 1 bar N_2 overpressure. These filters are resistant to high pH solutions up to pH12.5 and the microscopically thick active skin is not affected during filtration, unlike the normally used Nucleopore membranes. Preparation and solution transfer were carried out under controlled atmosphere conditions to avoid carbonation of the fluid samples, even though the period of sample storage may already have produced some carbonation. Optimal filtration volumes were evaluated from the colloid concentration deduced by light scattering laser test. All membranes were promptly

washed after filtration to remove precipitates formed during membrane drying. The prepared filters were then pasted onto an Al stub prior to coating with Au for SEM analysis using a Cambridge S4-10. The layer of Au is in the order of 20nm thick and, due to interference from Au, particles below 40nm in diameter cannot be resolved with any certainty. The samples were observed with primary magnifications of 500, 2000 and 10000. Each negative photomicrograph was developed with high contrast paper and enlarged to produce A4 sheets of magnification 1100, 4400 and 22000. These photomicrographs were then studied using a quantimeter (Cambridge Instruments Quantimet 920) which includes a video camera, an image analyser and a recorder. The Quantimet programme allows cutting of overlapping particles so that they are counted separately and dust particles or microbes can be erased manually. A size distribution is thus produced for each membrane with variable size ranges between 40 and 3200 nm.

Ultraviolet and visible spectroscopy was carried out with a Guided Wave model 260. The light sources were a deuterium lamp (D2) for the ultraviolet and a tungsten lamp for the visible near infra-red spectra. The detectors were a photomultiplier for the 200-400 nm range and a Si detector for the 400-1000 nm range. All samples were injected into a 1mm quartz flow-through cell which was fitted, on-line, to a filtration cell and connected to both lamps and to the spectrometer with a fibre optic cable. Spectra were recorded from 200 to 1000 nm although only the ultraviolet-blue region (200-600 nm) was of interest. Blanks were run to correct the background and fibre optic scatter. Spectra were analysed on an IBM PC model 30 286 with the Guided Wave programme.

3.4.4 Microbiological Sampling and analytical techniques

3.4.4.1 Sampling

All materials and media necessary for the microbiological field sampling component of programme were prepared asceptically in the BGS microbiology laboratory and immediately shipped to Jordan, by air, for use. All the media were prepared and sterilised at tenfold strength and reconstituted to normal strength by the addition of water or sediment/water inocula in the field following the method adopted by BATH et al. (1987). Details of the growth media used are given below. All inoculations were carried out in triplicate. In addition to the on-site inoculations of specific growth media for particular key microbial groups, a test using dip-slides (Millipore SPC tester) for aerobic heterotrophs was also performed. Water samples were also taken for epifluorescence microscopy.

Samples for microbiological investigations were taken from discharges at MQ1, MQ2, MQ5 and MQ6. The hyperalkaline seepages within the railway cutting to the east of the area were not considered suitable for microbiological sampling since the seepages were exposed to dusty atmospheric condiditons and therefore likely to be

contaminated. Site MQ1 was sampled directly from a pool collecting drips from roof stalactites in Adit A-6. Samples were taken using a sterile syringe and immediately placed into the sample tubes. The MQ2 sampling site was the tip of an actively dripping straw stalactite. In order to sample this, one end of an open ended plastic bag was tied to the stalactite, the other end being fastened to a length of Tygon tubing running directly into a Nalgene collecting bottle. The apparatus was not sterilised but was flushed with several litres of the flowing water prior to microbiological sampling. Sampling sites MQ5 and MQ6 were sampled on two occasions. On the first (June 4, 1990) bulk samples were taken in non-sterile, but well-flushed Nalgene bottles and microbiological sub-samples taken from these and processed two hours later. On the second occasion (June 6, 1990) the samples were taken in situ directly from the flowing discharge using sterile syringes and processed immediately.

3.4.4.2 Analysis

(i) Microbial enrichments

Enrichments were carried out in the field for the following groups of micro organisms:

Aerobic and anaerobic heterotrophic and oligotrophic bacteria

Nitrifying bacteria

Denitrifying bacteria

Sulphur oxidising bacteria

Alkalophilic photosynthetic bacteria

Sulphate reducing bacteria (SRB)

Algae

In addition, enrichments for fungi were also performed on samples returned to the UK.

All the media used are listed in section 3.4.4.2 (III)

(ii) Laboratory processing of samples

After inoculation and collection of samples, all materials were flown to the UK for further processing and analysis. Proposed methodologies were:

1. Aerobic/anaerobic heterothrophic bacteria (CPS medium) and Oligotrophic bacteria (1% CPS medium)

   Three dilutions (no dilution and 1:10, 1:100) of the enrichment was inoculated in triplicate onto CPS plates (full strength and 1% strength). Plates were incubated aerobically and anaerobically at 30 C in the dark for 48 hours and the numbers of colonies determined. Any dominant microbes were then picked off and isolated on CPS medium.

2. Nitrifying bacteria - ammonia oxidisers and nitrite-oxidising bacteria

   The disappearance of ammonium and nitrite in the enrichments using analytical chemical techniques was noted over a period of 4 weeks at weekly intervals.

3. Denitrifying bacteria

   The Durham tubes were examined for the presence of gas and where positive, 0.1ml of the enrichment was inoculated in triplicate onto solid CPSN medium (no dilution and 1:10, 1:100) and incubated anaerobically in the dark at 30 C for 48 hours. The numbers of colonies were then determined.

4. Sulphur oxidising bacteria - obligate chemolithotrophs and facultative chemolithotrophs

   The enrichment media were checked daily for a drop in pH by ~2.0 units.

5. Alkalophilic photosynthetic bacteria and Chu medium for algal growth

   The tubes were exposed to light at 30 C for one week. The bottles were then examined for signs of growth (green/blue green colouration).

6. Sulphate reducing bacteria

   The presence of lactate utilising bacteria is shown by blackening of the medium. The tubes were incubated in the dark at 30 C for 1 month or until blackening occured. Where positive, 0.1ml of the enrichment was inoculated in triplicate onto solid Postgate's E medium (no dilution and 1:10, 1:100) and incubated anaerobically and aerobically (no growth should occur) in the dark at 30 C for 48 hours. The numbers of colonies were then determined. Any dominant microbes were then picked off and isolated on Postgate's E medium.

7. Fungi

   0.1ml of unpreserved sample was inoculated in triplicate onto plates containing Sabourauds Dextrose Agar (Oxoid) in triplicate and incubated at 30 C for 48 hours.

8. Total microbial numbers using epifluorescence microscopy

   Water samples were processed and counted using the method of WEST et. al., (1988).

(III) Media Compositions

The following media were used for enrichment of different groups of micro- organisms. All the media are 10 times normal strength and were distributed into acid washed universals as 3ml aliquots. The normal strength of the media was restored upon

universals as 3ml aliquots. The normal strength of the media was restored upon inoculation with a total volume of 30ml. No attempt was made to control pH after inoculation. The media were sterilised by autoclaving at 15psi, 121 C for 15min.

a. Aerobic and anaerobic heterotrophs (CPS medium) (BATH et. al., 1987)

Peptone	0.5g
Casein hydrolysate	0.5g
Soluble starch	0.5g
K_2HPO_4	0.02g
$MgSO_4.7H_2O$	0.05g
Glycerol	1ml
$FeC1_3.6H_20$ (0.01% w/v)	4 drops
Distilled water	to 100ml

b. Oligotrophic bacteria (BATH et. al., 1987)

1% CPS medium (1ml of the above CPS medium in 100mls distilled water)

c. Nitrifying bacteria (BATH et. al., 1987)

i. Ammonia-oxidising bacteria

K_2HPO_4	0.05g
$FeSO_4.7H_2O$	0.05g
$MgSO_4.7H_2O$	0.1g
$CaCO_3$	1.0g
$(NH_4)2SO_4$	0.26g
Distilled water	to 100ml

ii. Nitrite oxidising bacteria

K_2HPO_4	0.05g
$FeSO_4.7H_2O$	0.05g
$MgSO_4.7H_2O$	0.1g
$CaCO_3$	1.0g
$NaNO_3$	0.1g
Distilled water	to 100ml

d. Denitrifying bacteria (BATH et. al., 1987)

CPS medium as for 1 with the addition of KNO3 (2.0g). A Durham tube was present in each enrichment bottle for gas evolution.

e. Sulphur oxidising bacteria (BATH et. al., 1987)

i. Obligate chemolithotrophs

$(NH_4)2SO_4$	0.1g
K_2HPO_4	0.4g
KH_2PO_4	0.4g
$MgSO_4.7H_2O$	0.1g
$CaCl_2$	0.1g
$FeCl_3.6H_2O$	0.02g
$MnSo_4.4H_2O$	0.02g
$Na_2S_2O_3.5H_2O$	10.0g
Distilled water	to 100ml

ii. Facultative chemolithotrophs

K_2HPO_4	0.4g
KH_2PO_4	0.15g
$(NH_4)2SO_4$	0.3g
$MgSO_4.7H_2O$	0.5g
Yeast extract	0.3g
$Na_2S_2O_3.5H_2O$	10g
Trace minerals soln	10ml
Distilled water	to 100ml

Trace minerals solution

$FeCl_2.4H_2O$	1.5g
H_3BO_3	60mg
$MnCl_2.4H_2O$	100mg
$CoCl2.6H_2O$)	120mg
$ZnCl_2$	70mg
$NiCl_2.6H_2O$	25mg
$CuCl_2.2H_2O$	15mg
$Na_2MoO4.2H_2O$	25mg
HCl (25%)	6.5ml
Distilled water	993ml

f. Alkalophilic photosynthetic bacteria (GRANT and TINDALL, 1980)

NH_4Cl	1.0g
NaCl	0.4g
$MgSO_4.7H_2O$	0.4g
$CaCl_2.2H_2O$	0.5g
KH_2PO_4	0.1g
Sodium acetate	1.0g
Trace element solution	1ml
Distilled water	to 100ml

Trace element solution

$ZnSo_4.7H_2O$	5.5g
$FeSO_4.7H_2O$	5.0g
$Na_2MoO4.2H_2O$	1.0g
$MnCl_2.2H_2O$	5.5g
$CuSO_4$	1.5g
$CoCl_2$	1.5g
Distilled water	to 1litre

g. Sulphate reducing bacteria

Postgates medium B (POSTGATE, 1984) was used for the enrichment of lactate utilising SRB.

h. Algae (Chu number 10) (BATH et. al., 1987)

$Ca(NO_3)_2$	0.04g
K_2HPO_4	0.01g
$MgSO_4.7H_2O$	0.025g
Na_2CO_3	0.02g
$Na_2S_2O_3$	0.025g
$FeSO_4.7H_2O$	13.6mg
Distilled water	to 100ml

i. Fungi (Sabouraud's Dextrose Agar - Oxoid Ltd)

Mycological peptone	10g
Dextrose	10g
Agar number 1 (Oxoid)	15g
Distilled water	to 1litre

This agar medium was inoculated in the laboratory.

3.4.5 Environmental Isotopes

Water samples were collected for stable isotope analyses in 50 ml Nalgene bottles. No filtration or specific preservation methodologies are required. Stable isotope ratios in water samples were determined at GSF (Institute for Hydrology) by standard methods involving measurement of CO_2 gas equilibrated with water samples at 25 C (for ^{18}O) and measurement of hydrogen gas evolved by the reduction of water by reaction on zinc at 430 C.

Water samples for dissolved SO_4 were collected into 500 ml bottles to which about 1 g of cadmium acetate was previously added. The Cd^{2+} dissolved by the sample water will immediately precipitate any dissolved sulphide in the sample and preclude its oxidation to sulphate which would distort the true sulphate isotope values. The CdS precipitate, if present, can then be collected for $\delta^{34}S$ determination. Following filtration of the sample to remove any CdS, barium chloride was added and sulphate then precipitated as $BaSO_4$. SO_4 was converted to SO_2 for mass spectrometric analysis by high temperature reaction in the presence of copper oxide (GSF and the University of Ottawa; UO).

Dissolved carbonate was sampled by filtration of the spring waters, under closed system conditions where possible, and preserved in glass bottles prior to analysis. Petrological samples for carbonate isotope analysis (^{18}O and ^{13}C) were collected from the unaltered and altered host rock as well as from spring precipitates. Isotope analyses of dissolved and solid carbonate samples were performed on CO_2, evolved by acidification with 100 % H_3PO_4, at UO.

Bitumen from samples of bituminous limestone were analysed by convertion to CO_2 for mass spectrometric analyses (UO) through oxidation under an O_2 atmosphere.

All stable isotope data for water and dissolved constituents are discussed in chapter 4.3.

3.4.6 Ion exchange analyses

The application of small portable SEPAK ion-exchange cartridges was intended to attempt to define the complex speciation of the trace elements in solution in the groundwater (table 3.4). Three types of column were used: CM-silica substrate bonded with carboxymethyl groups (for cation exchange); QMA-silica substrate bonded with quaternary methyl amine groups (for anion exchange); and C18-silica substrate bonded with non-polar straight-chain hydrocarbon groups for neutral species. These columns have previously been used with some success to help define the speciation of various trace elements (including U and REE) in moderate to neutral pH groundwaters from a number of natural

analogue studies (VICKERS, 1989; SMITH et al, 1989). Unfortunately, insufficient time was available to conduct laboratory studies to check the suitability of these columns under high pH conditions before the necessary commencement of the field programme. Groundwater samples were collected and analysed both before and after passing through the columns, as well as analysing elluents from the columns after leaching (details given in appendix A). Samples fom MQ1, MQ2, MQ5, MQ6 and MQ7 were examined.

No significant or consistent differences were noted for most of the trace element chemistry of the groundwaters before and after column extraction (see appendix A for results) and many of the variations are experimental as can be seen by comparison of results from duplicated 0.45 μm filtered samples collected for bulk geochmeistry, ultrafiltration and speciation. In both cases, many of the trace elements were below detection limits for routine ICP-OES and ICP-MS. A significant increase in TOC in all the samples after passaage through the column was seen, suggesting that the columns may be breaking down in these high pH conditions. This is supported by the very high Si content noted during analysis of column effluent (below detection in the normal groundwater samples).

Cr was noted to show significantly different behaviour after passage through the columns. The concentration of Cr in MQ1, MQ2, and MQ7 is significantly reduced (by up to 66 %) on passage through the QMA column but unaffected by CM or C-18 columns. The subsequent NaOH washes from the QMA columns (which leach the anionic QMA exchange sites) were also found to have elute Cr from the columns, whereas, no Cr was detectable in HNO_3 of either QMA (ellution of unbonded Si-O-cation exchange sites), CM and C18 columns (ellution of cationic sites). This implies that a highly significant proportion of the Cr present in solution is present as ionic species. In MQ5 and MQ6, no difference was noted between samples analysed before or after passage through the columns. However, the NaOH elluent of the QMA column (table A3.1, appendix A) did show that Cr had exchanged with anion exchange sites indicating the presence of anionic species. However, the amount of Cr exchanged is small in comparison to the total Cr concentration of the groundwaters. No Cr was detected in the HNO_3 washes from the column indicating that no exchanges with cationic Cr species had occured. In both eastern and western discharge areas therefore, it appears that Cr is present as anionic species. This is consistent with the observation in section 4.5.3 which detected the presence of chromate species and which are probably responsible for imparting the yellow-green colouration to the waters. Saturation of the available exchange sites on the QMA column by the very high concentrations of Cr present in MQ5 and MQ6 probably explains why only a small proportion of the total Cr was fixed on QMA columns from these sites.

Although close to ICP-OES detection limit in some cases, Mo was also detected before and after passage through the columns at most of the sites. However, it does not appear to have been influenced particularly by any of the exchange columns. This would suggest that Mo exhibits neither cationic or neutral speciation but may be anionic

in character but in the presence of such high concentrations of chromate, may be unable to compete effectively with Cr for anionic exchange sites. Mo might be expected to behave similarly to chromium in these waters (both are Group VI B elements) and may be present as molybdate species. The observations above may be used to infer this relationship.

Zn is detectable in the groundwater prior to passage through the ion-exchange columns at levels of about 0.03 to 0.06 ppm. However, the distribution of Zn is unlike many of the other trace elements possibly being slightly more enriched in the eastern discharge area, rather than in the western discharge area. Zn appears to be efficiently extracted by all three column types and is below detection (below blank values) in all column effluents. No Zn is present in the NaOH (anionic) ellutration of the QMA column but is released from the column on elution by HNO_3 which leaches the Si-O- cation sites. Similarly, Zn is present in the acid (cationic) washes from the Cm and C-18 columns. Mass balance caclulation shows that the acid wash from all columns can account for the bulk of the Zn in the groundwater sample and suggests that Zn is present as a cationic species.

In most of the groundwater samples, U and REE are below detection by ICP-MS. However, U, La and Ce are detectable above blank values in the HNO_3 wash through the ion-exchange columns used at most sites (table A3.2, appendix A). Taking the blank values into account and assuming that U, La and Ce uptake on the columns an their subseqent ellution is quantitative, a lower limit of concentration for these elements can be determined. This suggests that U and light REE behaviour is similar to many of the other trace elements, occuring in concentrations about an order of magnitude greater in the western discharge area. These elements are detected in the cationic (acid wash) fractions from the columns which implies that the elements are present in solution as cationic species.

3.4.7 Petrological Samples

A variety of rock samples were collected for both geochemical and isotopic analysis. The major lithologies sampled included the host bituminous limestone, the high temperature mineralogy suite in the brecciated metamorphic zone, the low temperature mineralogical suite where retrograde reactions have been important, and the spring precipitates forming around all the discharge points. The term "bitumen" is used here for the organic material found in certain limestone units within the region. The molecular weight and/or volatility of this material has not been evaluated analytically, and so the term bitumen is not applied sensu stricto.

Petrological and geochemical analysis of the specimens collected from the Maqarin area are discussed in section 4.1. The following presents the results of a selective dissolution of the unaltered bituminous limestone in an effort to identify the carrier phases for trace elements in the host rock.

Source Term Geochemistry

The geochemistry of the alteration products in this thermally metamorphosed precurser represent the initial control on the chemistry observed in these unusual groundwaters. Accordingly, it was undertaken to determine the major and trace element contents of the original unaltered bituminous marls and limestone. A series of selective leaches and digestions of the host rock was carried out in order to characterise the geochemistry of both the acid soluble (dominantly carbonate) phase and the bitumen phase. The latter can represent up to about 15 % by weight of the host rock.

Determination of the major, minor and trace element distribution between the calcite and bitumen phases of the unaltered Maqarin bituminous limestone was carried out for four samples.

Samples were crushed and dissolved in 5 % HCl for 5 days, then filtered with 0.45 μm pore diameter discs. The filtrant was analysed by ICP-OES and ICP-MS to determine the geochemistry of the carbonate fraction. Results were calculated as ppm (ICP-OES) and ppb (ICP-MS, except Ni) of total rock. The filtrate was then weighed into clean, fired COORS crucibles and thermally decomposed by gradual heating to 550 C and the residue reacted in 1 ml ULTREX HNO_3 followed by 3 ml ULTREX HCl. Samples were then filtered (0.45 μm) and the filtrant analysed by ICP-OES and ICP-MS. Results are calculated as ppm (ICP-OES) and ppb (ICP-MS, except Ni) of total rock for the bitumen fraction. The results are presented in appendix B.

4 RESULTS: SOURCE / SINK TERMS

4.1 Discussion of the mineralogy, petrography and geochemistry of the Maqarin source-term rocks and their secondary alteration products

A.E. MILODOWSKI, H.N. KHOURY, J.M. PEARCE and E.K. HYSLOP

4.1.1 Introduction

The hyperalkaline groundwaters in the Maqarin area are closely associated with the occurrence of high temperature-low pressure metamorphosed Upper Cretaceous to Lower Paleocene marls and limestones (KHOURY, 1985; KHOURY et al., 1985). Similar but larger areas of marble occur within marls and limestones at approximately the same stratigraphic level in the Daba-Siwaqa and Suweileh areas of central Jordan (HEIMBACH & ROSCH, 1980; NASSIR and KHOURY, 1982; KHOURY and NASSIR, 1982b; KHOURY and SALAMEH, 1986) and in the Hatrurim Formation (Mottled Zone) of Israel (BENTOR et al., 1963; GROSS et al., 1967; BENTOR et al., 1972; GROSS, 1977; KOLODNY, 1979). However, active hyperalkaline springs discharges have been reported only from the Maqarin area.

The metamorphic assemblage in these rocks belongs to the sanidinite and pyroxene hornfels facies (WINKLER, 1976; TREIMAN and ESSENE, 1983) and in many respects resembles that found in the contact metamorphic alteration of limestones and marls by igneous intrusions (eg TILLEY, 1929; 1947; TILLEY and ALDERMAN, 1934; BURMAN, 1959; AGRELL, 1965; SABINE, 1975; CRESSEY, 1987). However, the metamorphism of the marbles from Maqarin and elsewhere in central Jordan and Israel is spatially unrelated to igneous activity and has been interpreted as the result of thermal metamorphism arising from the in situ combustion of abundant organic matter (KOLODNY et al., 1972; KOLODNY and GROSS, 1974; MATTHEWS and KOLODNY, 1978; KOLODNY, 1979; HEIMBACH and ROSCH, 1980; GROSS, 1983; KHOURY and SALAMEH, 1986).

It is of note that much of the detailed trace mineralogy analyses were carried out subsequent to the predictive trace element modelling described in chapter 5. This focussed the analytical effort on those minerals indicated to be solubility controlling phases of, for example, Se, U and Ra and a spin-off of this effort was the description of several new minerals in addition to much data of direct use in constraining the predictions of the geochemical codes under scrutiny (discussed in chapter 5).

To maintain the flow of the discussion, the highly detailed mineralogical descriptions have been placed in appendix C while here only the main discussion is presented along with a list of the primary metamorphic minerals (table 4.1.1) and secondary minerals (table 4.1.2) in the field area.

4.1.2 Field relationship of the metamorphic zone and host rock enclave

The high temperature mineralisation zone occurs as an irregular lensoid mass within the bituminous limestone beds of Upper Cretaceous - Lower Paleocene age in the Maqarin area. The regional and local stratigraphic relationships of the area have been described earlier in chapter 2. The metamorphic zones occur principally within the Bituminous Marl Formation (B3) which reaches a thickness of 120 m to the west of the Maqarin railway station.

The unmetamorphosed rocks comprise micritic limestone and are highly bituminous. ABED and AMIREH (1983) described the bituminous rocks as biomicrites composed essentially of calcite containing accessory amounts of quartz, dolomite, apatite, pyrite and clay minerals (illite, kaolinite, mixed-layer illite-smectite). Organic matter composes between 15% and 20% of the rock and the sulphur content of this material may reach in excess of 12%. The upper part of the Bituminous Marl Formation is characterised by large limestone concretions. A massive bituminous limestone bed (2m thick) marks the top of the formation.

Overall, the Bituminous Marl Formation is slightly to moderately fractured and joints are filled with secondary calcite although the upper part is highly brecciated and thermally metamorphosed on the left flank of the Yarmouk River. The metamorphic rocks can be traced from Wadi-es-Sidjin eastwards to the dam site and then for about 1900m towards Wadi Shallala to the south east (figures 2.2 and 2.4). The rocks in the metamorphic zone are highly heterogenous in both texture and mineralogy. Although Pleistocene alkali flood-basalts (BENDER, 1968), reaching a maximum thickness of 120m, cap both sides of the Yarmouk Valley, there is no spatial relationship with the metamorphic rocks. Consequently, the metamorphic rocks are believed to have suffered metamorphism as a result of spontaneous in situ combustion of the bituminous rocks (KHOURY and NASSIR, 1982b).

Springs and groundwater discharges emanating from the metamorphic zones are associated with localised precipitation of travertine deposits, stalactites and stalagmites formed as a result of rapid reaction of the high pH waters with atmospheric CO_2.

Table 4.1.1 Primary metamorphic minerals in the Maqarin metamorphic zone.

Mineral species	**Ideal formula**	**Identified**
flourapatite	$Ca_{10}(PO_4)_6F_2$	**A + B**
francolite	$Ca_{10-x-y}(Na,K)_xMg_x(PO_4)_{6-z}(CO_3)_zF_{0.4z}F_2$	**A**
ellestadite	$Ca_{10}(SiO_4)_3(SO_4)_3O_{24}(Cl,OH,F)_2$	**B**
spurrite	$Ca_5(SiO_4)_2(CO_3)$	**A + B**
wollastonite	$CaSiO_3$	**A**
larnite	Ca_2SiO_4	**B**
diopside-hedenbergite	$Ca(Al,Fe)Si_2O_6$	**A**
anorthite	$CaAl_2Si_2O_8$	**A**
brownmillerite	$Ca_2(Al,Fe)_2O_5$	**A + B**
Ca-ferrite	$CaFe_2O_3$	**B**
(?)ferrites	undefined Ba,Cr,Al,Ti,Mg,Zn,Mn-bearing	**B**
hematite or ferric oxide	Fe_2O_3	**B**
Ca-aluminate	undefined	**B**
calcite	$CaCO_3$	**A + B**
graphite	C	**A**
lime	CaO	**B**
Ba,Ca,S-silicate	undefined	**B**
Ba,Ca,Zr,Mo,silicate	undefined	**B**
oldhamite	CaS to $CaS_{0.9}Se_{0.1}$	**B**
Cu,K,Na-selenide	$Cu_{10.2}K_3Na_{0.2}Se_{7.7}S_{2.3}$(approx)	**B**
UCa-oxycarbonate (?)	Ca : U = 2	**B**

A: reported by KHOURY and NASSIR (1982a)

B: this study

Table 4.1.2 Secondary minerals in the Maqarin metamorphic zone and spring discharges

Mineral species	Ideal formula	Identified
calcite	$CaCO_3$	A + B
aragonite	$CaCO_3$	B
vaterite	$CaCO_3$	A + B
kutnahorite	$Ca_{0.75}(Mn,Mg)_{0.26}CO_3$	A
strontianite	$SrCO_3$	B
hematite	$-Fe_2O_3$	A + B
maghemite	$-Fe_2O_3$	A
gibbsite	$-Al(OH)_3$	A + B
brucite	$Mg(OH)_2$	A
portlandite	$Ca(OH)_2$	A + B
quartz	SiO_2	A + B
opal-CT	SiO_2	A
opal-A	$SiO_2.nH_2O$	A
baryte	$BaSO_4$	A + B
barytocelestite	$(SrBa)SO_4$	B
calcian barytocelestite	$(SrBaCa)SO_4$	B
hashemite	$BaCrO_4$ to $BaSO_4$ complete solid solution	B
Cd-sulphate	undefined	B
Pb-sulphate	undefined	B
gypsum	$CaSO_4$	A + B
bassanite	$CaSO_4.0.5H_2O$	A
ettrinigte	$Ca_6Al_2(SO_4)_3(OH)_{12}.25H_2O$	A + B
thaumasite	$Ca_6Si_2(SO_4)_2(CO_3)_2(OH)_{12}.24H_2O$	A + B
Cu,Zn-sulphate	undefined	B
hydroxyapatite	$Ca_{10}(PO_4)_6(OH)_2$	A
flourapatite	$Ca_{10}(PO_4)_6F_2$	A + B
francolite	$Ca_{10-x-y}(Na,K)_xMg_x(PO_4)_{6-z}(CO_3)_zF_{0.4z}F_2$	A
ellestadite	$Ca_{10}(SiO_4)_3(SO_4)_3O_{24}(Cl,OH,F)_2$	A + B
afwillite	$Ca_3Si_2O_4(OH)_6$	A + B
tobermorites	$Ca_5Si_6O_{16}(OH)_2.2\text{-}8H_2O$	A + B
jennite	$Ca_9H_2Si_6O_{18}(OH)_8.6h_2O$	A + B
apophyllite	$KCa_4Si_8O_{20}(OH,F)8H_2O$	A + B
birunite	$Ca_{15}(CO_3)_{5.5}(SiO_3)_{8.5}SO_4.15H_2O$	B
CSH gel	amorphous, undefined	B
U,Ca-silicate	undefined	B

A: reported by KHOURY and NASSIR (1982a)
B: this study

4.1.3 Discussion

4.1.3.1 Diagenesis of the bituminous limestones

The bituminous limestones of the Maqarin area are strongly enriched in trace elements, particularly Sr, Ni, Cu, Zn, Co, Cr, V, U, F and Se. The trace element concentrations of these rocks far exceed levels expected for average limestone and shale (WEDEPOHL, 1978). The high trace metal contents are more typical of black shales (WEDEPOHL, 1978) and are suggestive of deposition in euxinic (oxygen-free) environments. A more extensive study by ABED and AMIREH (1983) suggested that the geochemical characteristics and the existence of trace fossils in these rocks were indicative of deposition and metal enrichment within an oxygenated "gyttja" environment (ie H_2O/O_2 interface is somewhere below the sediment-water interface) rather than a more euxinic environment characteristic of sapropelic deposits (cf ROSSLER et al., 1977). The more detailed petrographic observations of the present study further support this interpretation (see appendix C). Early authigenic framboidal pyrite and glauconite are normally considered to form close to the sediment-water interface. Their restricted occurrence within microfossil chambers indicates that the reducing conditions necessary for their formation were largely only achieved within these restricted microenvironments probably in relation to the decay of the organism. The absence of these phases in the surrounding sediment matrix supports the conclusion that the early near-surface porewaters were probably oxygenated.

Diagenesis of these metal-enriched sediments has produced a complex assemblage of authigenic minerals. However, most mineral authigenesis appears to have occurred relatively early during diagenesis. The earliest diagenetic phase recognised is glauconite which scavenged or coprecipitated elements such as Cr and V. Framboidal pyrite appears to accompany, or closely follow, glauconite authigenesis and is associated with the precipitation of native Se. The presence of Se in pyrite-mineralised fabrics resembling microbial membranes is consistent with authigenesis being related to early diagenetic microbial reduction. Ni, Zn, Cu, Pb, Cd, Mn, As and Se appear to have coprecipitated in significant concentrations, substituting within the framboidal pyrite or as discrete accessory sulphides such as sphalerite, Cu-Zn sulphides, Ni-Fe-selenides and sulphides. In some foram tests, fine microsparry calcite overgrowths on chamber walls appear to predate pyrite authigenesis. A later generation of pyrite authigenesis relates to deeper burial and, in some cases, appears to post-date minor compactional deformation. This later pyrite replaces early glauconite and was also formed by recrystallisation, or seeding, upon earlier fine-grained pyrite fabrics.

Calcite generally occurs as a relatively late diagenetic phase, infilling microfossil porosity post-dating pyrite formation and also infilling large fractures. This indicates that calcite mineralisation was related to, or post-dates, the tectonic episode that caused uplift and fracturing of the region.

Late stage oxidative weathering of these rocks has also produced a complex

assemblage of secondary phases related to sulphide oxidation which include gypsum, celestite, Ca selenate, mixed Sr-Ca selenates and sulphates and goethite.

4.1.3.2 Trace element source-terms

Phases potentially responsible as the source of many of the trace elements present in the hyperalkaline groundwaters (see also chapter 5) have been identified in both the metamorphic zone and its sedimentary enclave of bituminous limestone and marls. These are summarised below (see also tables 4.1.1. and 4.1.2. for mineral formulae):

U and Th

(a) Bituminous limestone and marl

The bulk of the U in the bituminous limestones and marls appears to be uniformly distributed throughout the matrix of the rock at levels between 10-20 ppm. The HCl-insoluble fraction accounts for between 44-56% of the total U content in the unaltered sample examined in this study. For partially combusted or altered limestones, this value may be as low as 4%. Since the acid insoluble fraction is dominated by organic material (tableC6, appendix C) and, in the general absence of radioactive resistate heavy detrital minerals such as zircon, monazite and xenotime, it would seem likely that most of this U is complexed with organic matter. However, not all organic matter is uraniferous and fission-track registration indicates that the coarser discrete organic particles are devoid of U. It is therefore concluded that U resides in significant amounts within finely-dispersed organic matter.

44-56% of the U is also present within the HCl-soluble fraction (up to 96% in altered rocks). This fraction largely comprises calcite but will also have been influenced by the dissolution of collophanic and apatitic material. Fission-track registration indicated that collophane and apatite contained up to 50ppm U. Assuming all P_2O_5 in the whole rock analyses is due to apatite (the only phosphate mineral identified), then calculation shows that this can account for 20-25% of the whole rock U content. Thus, up to 25-30% of the U content of the bituminous limestone appears to be present within the carbonate fraction (largely calcite). However, if account is taken of the presence of significant U (50-100ppm) in goethitic alteration products (which would also influence the acid-soluble fraction U content), then the U content of the carbonate fraction is probably lower.

Th concentrations in the bituminous limestones are very low (<1ppm Th) and no discrete Th minerals were identified. Low levels of Th are present in both HCl-soluble and insoluble fractions and it may therefore be present in trace quantities in both organic matter and in the carbonate fraction.

(b) Unaltered metamorphic rocks

In the present study, sampling of unaltered metamorphic rock was biased towards more phosphatic varieties. These appear to be more resistant to hydration and retrograde alteration than marbles derived from less phosphatic combusted limestone. However, relicts of less phosphatic marble were also examined. In the least altered material (phosphatic rock, M15P) fission-track registration revealed that U was present in apatite (silicosulphatic variety) at levels between 15-20ppm. This could account for about 20% of the total U. The bulk (up to 80%) of the U is probably present as a discrete but as yet undefined Ca-U mineral (Ca:U=2:1)(possibly an oxycarbonate).

Since Th contents are very low in the precursor limestones, the levels are also very low in their metamorphic equivalents. No discrete Th-bearing phases were identified and the sources of Th in the maltered metamorphic rocks have not been resolved.

Se

(a) Bituminous limestone and marl

Se is present in unaltered bituminous limestone as discrete minerals which include probable native Se and Ni-Fe-selenide. However, these are relatively minor phases and the bulk of the Se is probably present substituting for S in the ubiquitous pyrite. Semi-quantitative estimates suggest that pyrite may contain up to 5-10% Se. The limestone samples examined in the present study all contained secondary oxidation (weathering) products after sulphides and selenides. These comprise $CaSeO_4$ and solid-solutions of gypsum or bassanite with $CaSeO_4$ (often with significant Sr substitution for Ca). These may also be very significant and relatively soluble Se sources in the shallow Maqarin hyperalkaline groundwater system.

(b) Unaltered metamorphic rocks

In the primary metamorphic assemblage, trace amounts of a discrete Cu-K-selenide mineral (approximate composition $Cu_{10.2}K_3Na_{0.2}Se_{7.7}S_{2.3}$) are present. Se is also present in solid solution oldhamite (CaS) in concentrations up to 10 mole % CaSe. Both of these phases are reactive and are the first phases to be affected and dissolved during retrograde hydration.

Ni, Cu, Zn, Cd, As and Pb

(a) Bituminous limestones and marls

Zn, Ni and Cu are present as discrete traces in sphalerite and as Cu-Zn

sulphides and Ni-Fe-selenide. Cd and Pb are detectable (qualitatively estimated to be present at 1-2%) in sphalerite. However, quantitatively these phases are relatively minor and the significantly more abundant pyrite probably accounts for most of these elements as solid-solution substitutions, in addition to containing significant As and Se. Zn is also present in trace amounts (qualitative estimate c. 0.2-0.5% Zn) substituting for Ca in authigenic calcite.

(b) Unaltered metamorphic rocks

Cu is present in discrete Cu-K-selenide and in traces of CuS (covellite). The Cu-K-selenide is extremely soluble and is rapidly dissolved on hydration. Cu is also present in trace amounts in oldhamite (CaS). Zn is present as discrete complex Cr, Zn, Al, Mn, Mg, Fe oxides, probably ferrites, and as a trace element in spurrite (0-2500 ppm) and brownmillerite (up to 1.2 % ZnO). The ferrite and aluminate phases are relatively common, particularly as fine inclusions and may account for the bulk of the Zn. Ni, Cd, Pb and As do not occur as discrete minerals and, although below detection limits for EMPA, must be present as trace elements within other minerals.

Cr and V

(a) Bituminous limestones and marls

Authigenic glauconite appears to contain significant concentrations of both V and Cr and is probably the main source of these elements in the marls. Secondary goethite oxidation products of either pyrite or glauconite are also enriched in these elements and may represent a secondary source in the shallow aerobic groundwater system

(b) Unaltered metamorphic rocks

Cr is present in discrete Cr, Zn, Ti, Al, Mn, Mg, Fe oxide, Al, Cr, Ba, Fe oxide and Fe, Cr oxide phases. These are probably ferrite phases and occur largely as abundant but minute inclusions in apatites, ellestadite and other major minerals. Release of these particular elements would thus require dissolution of the host mineral before groundwaters could access the inclusions. Cr is also present as a trace element in brownmillerite (0-2000 ppm) and possibly in spurrite (0-600 ppm). All these phases are extensively altered during hydration. Although V can be attributed to a specific phase (ie glauconite) in the precursor limestones, no discrete V minerals are present in the metamorphic rock. V concentrations within other minerals are too low to detect by the analytical techniques used but it is likely to be largely present within the ferrite-like minerals.

Sr and Ba

(a) Bituminous limestones and marls

Sr and Ba are largely present within the HCl-soluble fraction of the limestones and are most likely to be present as trace elements in calcite and, to a lesser extent in apatite or collophane. Although no discrete primary Sr minerals are present, Sr is present in discrete secondary Ca-Sr-SO_4 and SeO_4 minerals formed by the reaction of acidic pyrite oxidation products with calcite. These secondary minerals are relatively soluble phases and could contribute significant Sr to percolating meteoric porewaters.

(b) Unaltered metamorphic rocks

In the primary metamorphic rocks, Ba is present in Ba-aluminoferrite inclusions in the groundmass. Ba is also present as a primary, high-temperature Ba-Ca sulphate-silicate phase. These two phases are relatively common and probably represent the bulk of Ba source-term. Calcite is also a potentially significant source of Ba with up to 1000 ppm Ba. Trace amounts of a complex Zr, Ba, Ca, Mo silicate phase were also identified but this phase is volumetrically insignificant with respect to other Ba phases. No discrete Sr mineral has been identified but Sr is present as a significant trace element in most Ca minerals: calcite (up to 3300 ppm); apatite and ellestadite (up to 4200 ppm); spurrite (up to 4200 ppm) and larnite (up to 850 ppm).

4.1.3.3 Trace element mobility and sites of secondary deposition

U and Th

There is considerable evidence from this study to indicate that U is mobilised and redistributed during hydration and alteration of the metamorphic rocks and by action of hyperalkaline fluids on the host-rock bituminous limestone. Fission-track registration reveals that the primary major U-bearing phases which include the Ca-U oxycarbonate phase and ellestadite-apatite are rapidly attacked and altered by groundwater. The U is partially redistributed within fine-grained secondary major minerals in the matrix. These include portlandite, calcite, ettringite, thaumasite and ferric oxides or hydroxides. U is significantly enriched along alteration or hydration fronts where it may be related to possible sorption on secondary Fe-oxides formed at the front or incorporated within secondary apatite formed just behind the front. Traces of an undefined secondary gel-like U-Ca-silicate phase are present but this is a volumetrically insignificant sink for U compared to the presence of U in the major secondary minerals. However, the fission track registration analyses show that the secondary products do not account for all the U liberated by alteration of primary phases, indicating an overall loss of U from the system. Leaching and loss of U is also inferred from natural decay series data (appendix C) and from comparison of bulk rock geochemistry of altered and unaltered lithologies.

Limited natural decay series data also suggests that, in some samples, there may be evidence for localised leaching of Th from the metamorphic rocks. However, unlike U, the location of Th in the alteration assemblage has not been identified (see also appendix C).

Se

No discrete secondary Se minerals have been found in the retrograde hydrated and altered metamorphic rocks. However, primary Se rich minerals such as oldhamite and Cu-K-selenide are rapidly dissolved during alteration. Qualitative XRF data suggests that traces of Se may be incorporated in secondary SO_4 minerals such as ettringite or birunite. Comparison of bulk rock geochemical data from altered and unaltered lithologies indicates that Se is leached during alteration.

Alteration of authigenic sulphides (mainly pyrite) in the bituminous limestone results in the precipitation of secondary Se-rich gypsum, $CaSeO_4$ and Ca-Sr-SeO_4. However, these phases are most probably the result of weathering oxidation rather than precipitation from the hyperalkaline groundwaters.

Ni, Cu, Zn, Cd, As and Pb

Trace amounts of Cu-, Zn-, Pb- and Cd - SO_4 and Zn- or Cu-Zn-CO_3 or OH phases have been identified as secondary phases within the altered metamorphic rocks. These minerals are very fine grained and their precise mineralogy remains undetermined. Traces of most of these elements are also incorporated in the major alteration products such as thaumasite, ettringite, vaterite and calcite.

Cr

Cr is present in significant quantities as a trace element incorporated in ettringite (up to 4000 ppm) and gypsum (>1400 ppm Cr recorded from one vein gypsum). In these sulphates it is most likely to be present as CrO_4 substituting for SO_4. Secondary baryte is present as a very common minor phase and is commonly Cr rich. A complete solid-solution between baryte and barium chromate (hashemite) has been identified in the altered rocks. Cr is probably responsible for the colouration of many of the secondary minerals imparting green, violet and yellow colours to ettringite and gypsum. In addition, green Cr-rich smectites (volchanskoite) have been previously identified from these rocks.

Sr and Ba

The principal secondary Ba minerals are baryte and hashemite and a complete solid-solution exists between these two end-member phases. Sr is present as minor amounts of secondary celestite and in solid-solutions between celestite, baryte and hashemite. However, Sr is also present as a trace element in major secondary phases

which include ettringite, thaumasite, calcite, gypsum and vaterite. Very high concentrations on Sr were identified in secondary apophyllite and vein apophyllite was found to be zoned with definite bands of strontian fluoroapophyllite. Strontian calcite and strontianite were identified as alteration products in bituminous limestone believed to have been affected by percolating hyperalkaline groundwaters.

Both Sr and Ba have similar geochemical behaviour to Ra and are good chemical-analogues for that element. Sr and Ba appear to relatively mobile during the alteration of the metamorphic assemblage and are clearly redistributed. Ra might be expected to behave similarly and evidence from natural decay series disequilibrium studies (appendix C) suggests that Ra is, in fact, concentrated in secondary carbonate and sulphate-rich alteration products.

4.2 Aqueous Geochemistry

I.D. CLARK, A.E. MILODOWSKI, P. FRITZ, H.N. KHOURY, G. HALL, M. CAVE, B. SMITH and J.M. COOK

4.2.1 Introduction

The unusual chemistry of some high pH seepages in the Maqarin area were described as early as 1978 (HARZA, 1978) during preliminary investigations for the Jordan-Syria Unity Dam project. KHOURY, et al. (1985) further characterised the seepages which occur in Wadi Sidjin as well as in drillholes and two adits constructed during engineering investigations. Some of these data are presented in table 3.2 along with new analyses undertaken for this study on samples from the Adit A-6 (MQ-1 and MQ-2), the railway cutting (MQ-7 and MQ-8), and the springs which discharge on the southern bank of the Yarmouk River, about 1 km further west (MQ-5 and MQ-6) (see figure 3.1, tables 3.2 and 3.3). The full data set is presented, for completeness, in appendix A.

Two distinctly different geochemical regimes exist in the Maqarin area. The eastern discharges, including seepages from the railway cutting, Adit A-6 and Wadi Sidjin (MQ-1,2,7,8) are characterized by high hydroxide alkalinity and total dissolved solids varying from 1100 to 1700 ppm. The western discharges (MQ-5 and MQ-6), also characterized by calcium-hydroxide saturation, are considerably more mineralised than the eastern discharges, with a total dissolved load of up to 4400 ppm (figure 4.2.1).

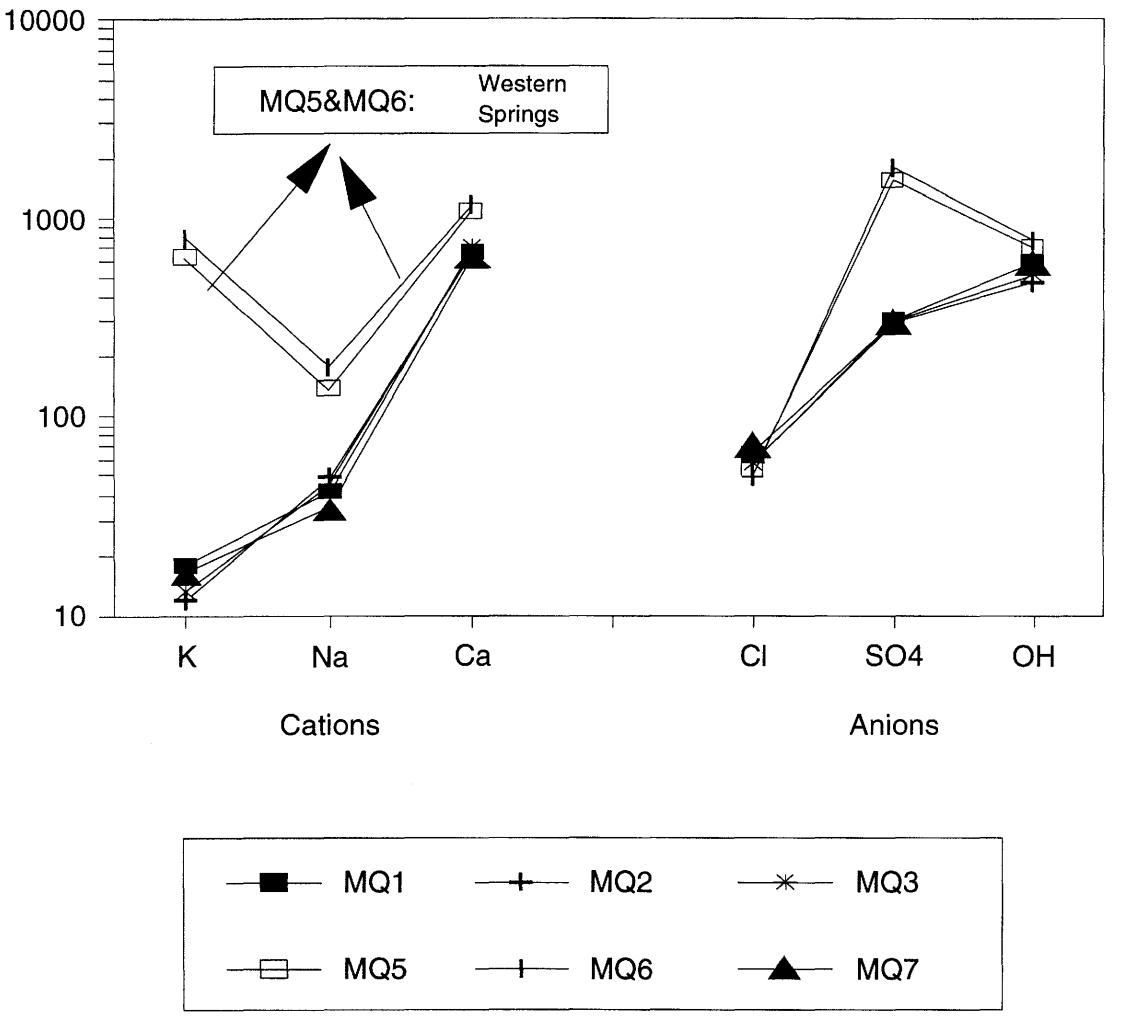

Figure 4.2.1 Two distinctly different geochemical regimes (Western and Eastern Zones) can be characterised by the major elements

4.2.2 Hydroxide Alkalinity

The differences in mineralisation of these two groundwater systems may relate to early and later stages of retrograde alteration, hydration and mineral dissolution subsequent to in situ combustion of the bituminous limestone. Hydration of CaO, which is still observed in the high temperature mineral suite, produces portlandite, $Ca(OH)_2$, the dissociation of which provides the high hydroxide alkalinity characteristic of spring waters from both discharge zones. The pH of a calcium-hydroxide saturated water ($K_{Ca(OH)2} = 10^{-5.02}$ at 25 C) is 12.51. Minor differences in measured pH (table 3.1) may be due to variations in the dissociation constant for water with temperature ($K_{H2O} = 10^{-13.83}$ at 20 C; $10^{-14.18}$ at 30 C), and slight undersaturation in portlandite. Tables D4 and D5 (appendix D) show that while MQ-5 (western springs) is very close to saturation with respect to portlandite, MQ-2 (eastern springs) is marginally undersaturated. As supported by additional geochemical and isotopic evidence, the eastern flow system is clearly at a more advanced stage of alteration-mineral dissolution in the brecciated zone than is the western flow system, whose mineralization is more characteristic of early discharge from a cementitious environment (BERNER, 1987; ATKINSON and GUPPY, 1988).

4.2.3 Source of Major Ions

High concentrations of major ions in groundwaters from semi-arid regions are often attributed to the accumulation of salts from marine aerosols in the recharge environments. Certainly, the Maqarin area is in close proximity to sources from both the Dead Sea and the Mediterranean Sea. However, such a process should preserve approximately the proportions of most major ions in the aerosols. The alkalies, which correlate poorly, and the exceedingly high SO_4^{2-} and K^+ concentrations, do not bear this out, demonstrating a subsurface origin for most of the dissolved constituents. Chloride and bromide alone, vary little between eastern and western springs, and with a proportionate fraction of sodium, may be largely attributed to a marine aerosol source.

The high temperature alteration of marine limestone and marl during in situ combustion leads to the formation of calcium and magnesium oxides. Further, under the high temperatures supposed to exist during the thermal event (800 to 1000 C; KOLODNY, 1979) the decomposition of clays or loss of poorly bound alkali cations would produce Na and K -oxides, hydroxides or other readily soluble salts. Oxidation and hydration of other metals found in the bituminous limestone host formation would similarly produce high solubility salts in the brecciated zone. The early chemistry of recirculating groundwaters would be controlled by the rapid dissolution of such products. Comparison of the chemistry of the highly mineralised western discharges (MQ-5 and MQ-6) with the eastern springs (MQ-1,2,7,8) in view of the mineralogical and whole rock geochemical analyses is instructive.

In the western springs, the alkali concentrations correlate well with TDS (figure 4.2.2). Further, the molar ratios of their aqueous to source rock concentrations are similar, (tables 3.1, C5, and C6) suggesting dominantly a subsurface origin by dissolution of altered and unaltered metamorphic minerals (e.g. francolite and Cu,K,Na-selenide; tables 4.1.1, 4.1.2). Their aqueous concentrations could be limited only by highly soluble salts, by ion exchange with the minor clay fraction, or by precipitation of secondary alkali-bearing minerals (e.g. apophyllite). In the lower TDS eastern springs, alkali concentrations are sharply reduced.

Silica levels in these waters are limited by formation of various calcium-silica-hydrate (CSH) phases observed in the suite of secondary minerals from the metamorphic zone (KHOURY and NASSIR, 1982a; chapter 4 and appendix C). In cement terminology "CSH" is normally retained for non-crystalline calcium silicate hydrate gels such as the tobermorite-structure series (CSH I type) and the jennite-structure series (CSH II type). Although tobermorite, afwillite and amorphous Ca-silicate have been recorded by KHOURY and NASSIR (1982a), material examined in this study suggests that volumetrically, thaumasite ($Ca_6H_4(SiO_4)_2(CO_3)_2 \cdot 2H_2O$) is the most significant Si-bearing phase. Thaumasite is not a CSH phase but sensu stricto is an ettringite-structured mineral showing solid-solution between silicate and carbonate in thaumasite and sulphate in ettringite. Hence, it is more likely that the Si-limiting phase is thaumasite and not sensu stricto CSH phases (chapter 4.1). This may affect to some extent the reactions outlined in chapter 4.3 as well. This contrasts with hydrated Portland cements in which CSH compounds are the major components.

The low Mg^{2+} concentrations can be accounted for in view of a water dominated by $Ca(OH)_2$ dissolution. The low solubility of $Mg(OH)_2$ ($K_{sp} = 10^{-11.0}$) at high pH values accounts for the absence of Mg^{2+} in these waters ($aMg^{2+} < 0.05$ M at pH 10).

4.2.4 Sulphate and Alkali-Earths

The exceedingly high SO_4^{2-} concentrations in the western discharge waters would suggest evaporite dissolution. However, none have been mapped in the region, nor does the geochemistry of local bicarbonate groundwaters indicate their occurence. Minor authigenic sulphates such as gypsum or anhydrite occur as accessory minerals within the unaltered limestone but are volumetrically insignificant. More likely, the sulphate originates in the bitumen, transformed during metamorphism into sulphates (including gypsum, SrBaCa-sulphates, ettringite-thaumasite solid solutions and pure end-members; table 4.1.2). The sulphur content of the unmetamorphosed bituminous limestone is high, ranging between 10 and 100 ppm in two samples. As discussed in 4.1.2, the sulphur content in this organic component can reach 12% or more. Corroborative evidence from $\delta^{34}S$ and $\delta^{18}O$ data is discussed below.

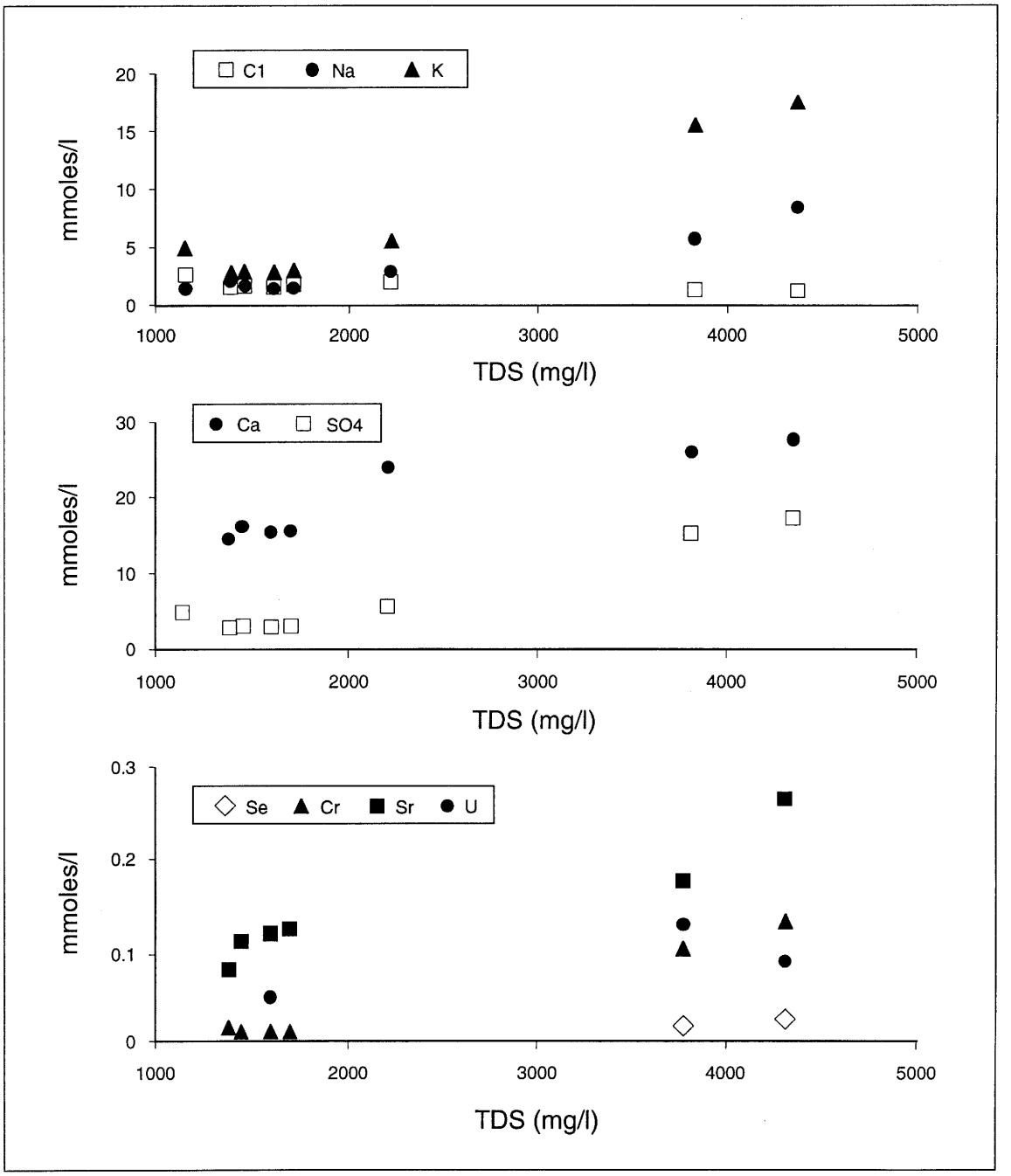

Figure 4.2.2 Alkali concentrations verses TDS.

The high sulphate concentration in the western springs is responsible for limiting the aqueous concentrations of all alkali-earths. Table D5 shows all the principal sulphate minerals to be at saturation in the MQ-5 water. In the eastern discharges (MQ-2), these minerals are marginally undersaturated (table D4). Ba and Sr are present in the secondary mineral suite as pure sulphates and as solid-solutions between baryte, celestite and hashemite (section 4.1.3.3)

Dissolved carbonate contents in these high pH waters are low, controlled by calcite solubility. The more precise DIC measurements (by acid extraction under vacuum; table 3.1) indicate only about 1 to 2 mgl^{-1} carbonate exists in solution, which suggests that carbonate complexing may not be a significant transport mechanism in these waters.

A comment is worthwhile on the TOC contents of these waters, which vary from over 11 mgl^{-1} in the western springs to near or less than detection (<0.5 mgl^{-1}) in the eastern springs. Although geochemical and isotopic characterization is yet to be done, the TOC in these waters likely originates as a product of the incomplete combustion of bitumen during metamorphism. Organic complexation may be a potential transport mechanism for radionuclides in such waters (although speciation calculations suggest this is not significant; chapter 5).

4.2.5 Trace Elements

The early and late stage dissolution scheme observed in the major element chemistry is strongly evident in trace element concentrations (figure 4.2.2). ICP-MS analyses (table 3.3) show that Mo, Se, Ni, and even U show a significant decrease in concentration from the western to the eastern springs. Only Th and Pd, present in the unaltered limestone at very low levels (1 ppm and <0.01 ppb respectively), were not detected in the spring waters.

Uranium is present in the MQ-5 and MQ-6 samples at concentrations up to at least 0.13 ppb, although one sample yielded a suspiciously high value of 1.40 ppb (table 3.3). Remobilization of uranium during hydration of the primary metamorphic suite is extensive, with incorporation into fine grained secondary oxides, hydroxides and sulphates, although these products do not account for all the U liberated from the primary phases (section 4.1.3.3). The strong variation in U concentrations measured in the hyperalkaline waters reflects this apparent loss of U from the solid phases by leaching. U contents decrease from the 0.13 ppb range in the highly mineralized MQ-5 and MQ-6 samples to the near detection in the lower TDS samples (MQ-7) and to less than detection in the lowest TDS samples (MQ-1 and MQ-2).

Selenium, present in the unaltered metamorphic rocks as a reactive Cu-K selenide, is found in the western springs in the ppm range. In the lower mineralised seepages, Se drops by over an order of magnitude, apparently due to advanced leaching of this

highly soluble secondary phase. A strong correlation exists between Se and K, consistent with the leaching of KCu-selenide, which has been observed in the alteration mineralogical suite (section 4.1.3.3, table 4.1.2). Se is also present in unusually high concentrations in the unaltered bituminous marls and limestones, often as native selenium and seleniferous sulphides (see section 4.1.3.2; table C6).

The presence of Re is also of interest as it is a chemical analogue for Tc. Both Re and Mo are chalcophyllic elements and, although not detected in the sulphide minerals (e.g. oldhamite) of the primary metamorphic rocks. Their relative concentrations in MQ-5 and MQ-6 waters would also be consistent with their release from highly reactive oldhamite (CaS) and K(Na)Cu-selenide. However, these elements may also correlate with Cr and could possibly be derived from the same oxide phases (ferrites or spinels) that are the source for Cr in the primary metamorphic rocks (chapter 4.1).

Chromium substituted in oxide phases of the unaltered metamorphic rocks is remobilised in the altered suite into a host of secondary chromate and sulphate solid-solution phases. Cr decreases in concentration by over an order of magnitude from several ppm in the western springs, tinted yellow-green by dissolved chromate, to less than 1 ppm in the low TDS Adit A-6 seeps.

4.2.6 Summary

The mineralisation of the western spring waters can be attributed to the dissolution of the soluble secondary alteration phases in the metamorphic zone. Portlandite, gypsum, celestite and baryte are at saturation, controlling the pH as well as SO_4^{2-} and alkali-earth concentrations. The eastern springs are marginally undersaturated for these phases, and are 70 percent less mineralised.

Overall, the higher mineralisation of the western springs relative to the eastern discharges parallels the evolution of pore fluid chemistry during the early stages of portland cement hydration (LEA, 1970; DOUBLE, 1983). Alkalis and sulphate concentrations rise rapidly during early hydration as a result of the dissolution of soluble sulphates and the release of K and Na from primary calc-silicates, and, in the Maqarin site, from K(Na)Cu-selenide. The sharp decrease in mineralisation and mineral saturation between the western and eastern spring waters is analogous to early and later stage leaching of the reactive secondary mineralisation in the metamorphic zone.

Trace elements and safety-relevant nuclides behave similarly to the alkalis and sulphate, suggesting that dissolution of highly soluble phases rather than equilibrium with discrete minerals, is controlling their concentrations in these hyperalkaline waters.

4.3 Isotopic composition of the hyperalkaline waters

P. FRITZ, I.D. CLARK, W. BAJJALI and H.N. KHOURY

4.3.1. Stable Isotopes in Precipitation

In humid climates, the isotopic composition of groundwaters closely reflects the average annual composition of rainfall in the recharge area. The stable isotope composition of rainfall has been monitored at the meteorological station at Irbid, 20 km to the south of the study area (BAJJALI, 1990 a). These data have been used to define the local meteoric water line (LML) given in figure 4.3.1, for which:

$$\delta 2H = (6.5 +/- 0.8)\ \delta 18O + (14.2 +/- 5.7) \quad r2 = 0.75$$

Also shown is the weighted average for precipitation collected at Irbid, and the eastern Mediterranean line (EML) as defined by GAT and CARMI (1970).

4.3.2. Hyperalkaline Groundwaters

The results obtained for the Maqarin alkaline springs and seeps (figure 4.3.2) show that these isotope data fall below both the local meteoric water line (LML) and the eastern meteoric water line (EML). This demonstrates that either evaporation occurs prior to or during recharge (BAJJALI, 1989) or that other secondary subsurface processes are important.

The effects of evaporation on groundwater recharge in a similar arid region are well documented (eg CLARK et al., 1988) and are also observed in shallow groundwaters in potential recharge areas between the city of Irbid and the Yarmouk river valley (BAJJALI, 1990 b). However, in the case of the highly alkaline groundwaters, other reactions also may be important. In a series of simple experiments and observations made on cemented observation wells, DAKIN et al. (1983) noted an ^{18}O enrichment of 1 to 2 permil in the waters that hydrated the cement. These waters aquired pH values > 10 in the process. No significant deuterium shift was noted. The controlling reactions and the reasons for this shift were not investigated but warrant further study. A similar process might be envisaged for the hyperalkaline waters discussed here, and could explain in part the observed displacement from the Local and Eastern Mediterranean meteoric water lines. At present it is not possible to assess the importance of these reactions for the alkaline waters especially since the effects cannot easily be distinguished from evaporation effects. The very narrow range in δ^2H values seen in the hyperalkaline spring data suggests that the flow systems are relatively well mixed, and do not show any strong seasonal variations. Variations in $\delta^{18}O$, which are less than about 1 permil, support this, as do the tritium data which are discussed below.

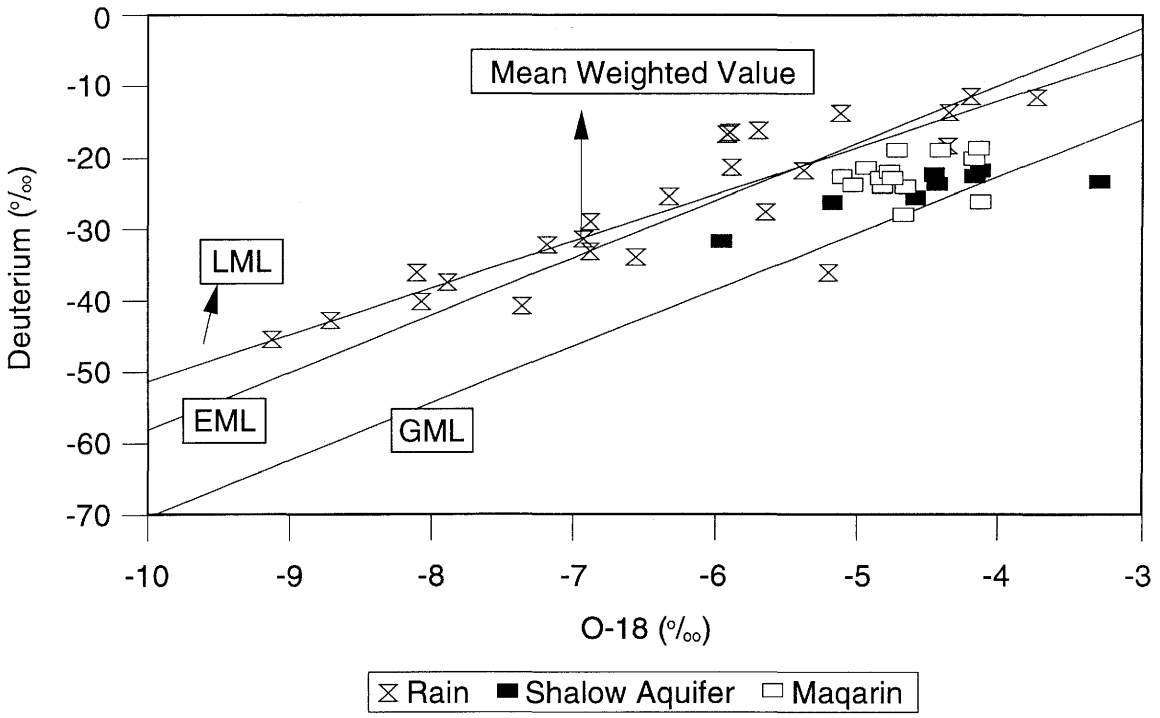

Figure 4.3.1 Plot of the δ^{D} vs $\delta^{18}O$ data for rain and groundwater in the Maqarin area with respect to the local meteoric water line (LML), the eastern Mediterranean line (EML) and the global mean line (GML).

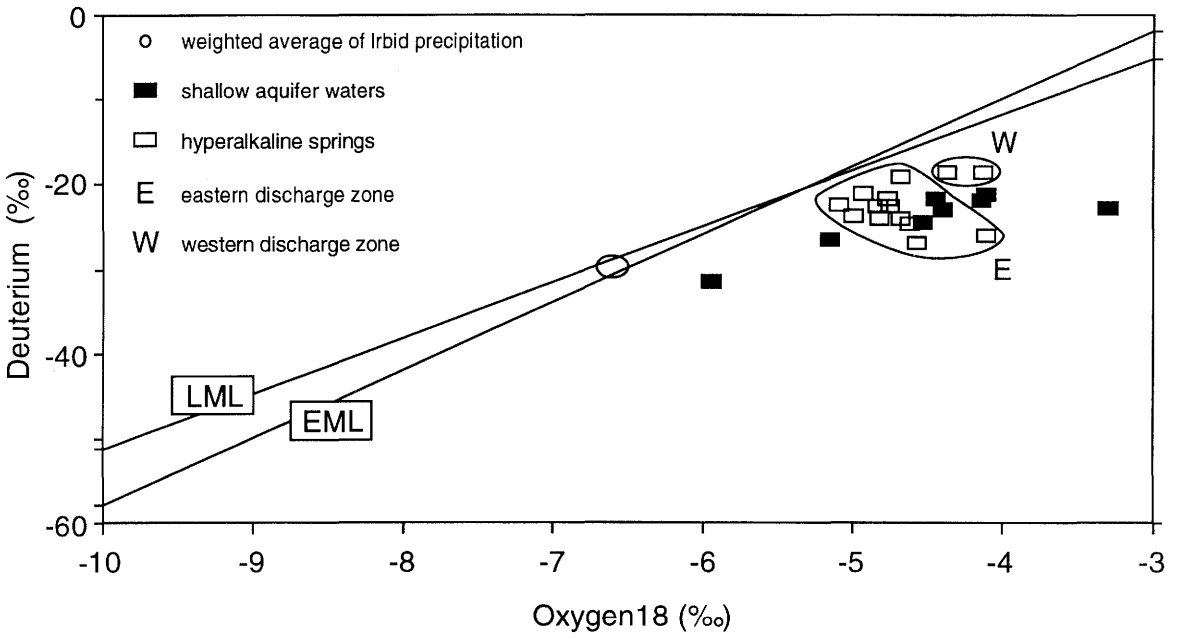

Figure 4.3.2 Plot of the δ^{D} vs $\delta^{18}O$ data for the Western and Eastern zones, Maqarin. The eastern Mediterranean line (EML) and the local meteoric Water (LML) lines are also plotted.

A third observation emerges from the isotope data, which supports the geochemical data in suggesting two separate hyperalkaline flow systems. A clear distinction is observed in figure 4.3.2 between the samples collected from the eastern discharges (Adit A-6, Railway Cut and Wadi Sadjin) versus the western discharges along the Yarmouk River (MQ-5 and MQ-6). This is strong evidence that the two hyperalkaline spring and seep areas discharge from quite separate flow systems, possibly with variations in evaporation during infiltration.

4.3.3. Sulphate Isotopes

In addition to the differences in the SO_4^{2-} concentration in the groundwaters from the eastern and western zones (table 3.2), there exists a significant difference in the $\delta^{34}S$ and $\delta^{18}O$ values of the dissolved SO_4^{2-} (table 4.3.1 and figure 4.3.3). Nevertheless, the isotopic data concur with a subsurface origin for the SO_4^{2-}, probably within the bituminous material in the formation. As can be seen from figure 4.3.3, the dissolved SO_4^{2-} isotopic signature lies within the $\delta^{34}S$ field reported for Mesozoic petroleum and bitumen (KROUSE, 1980). The higher $\delta^{18}O$ values of the groundwater SO_4^{2-} are consistent with such an origin as they are typical for SO_4^{2-} formed by the oxidation of reduced S with atmospheric O_2.

However, the processes associated with the high pH generating reactions should be considered in more detail before a clear statement on the environment and mode of formation of the groundwater SO_4^{2-} is possible.

4.3.4 Tritium

Lastly, it has to be noted that the alkaline groundwaters are essentially free of tritium, with the possible exception of MQ-6, which discharges from consolidated river gravels about 1 m above the water level in the Yarmouk River. Resampling would be necessary to verify either contamination by surface water or the real presence of tritium in this groundwater. If the measured tritium contents of MQ-6 are not local contamination, this represents a significant component of modern recharge to the hyperalkaline groundwater system. This is consistent with the high mineralisation in these western discharges, suggesting that they are much younger than the geochemically more "mature" groundwaters in the Eastern Discharge Zone. The absence of tritium in the other groundwaters shows that they have mean residence times exceeding about 40 years. Despite this, it must be assumed that groundwater flows are local rather than regional given the evidence from the stable isotope data for water and dissolved SO_4^{2-}.

Table 4.3.1 Isotopic composition of water and sulphate for the hyperalkaline groundwater discharges from the Maqarin area.

Locality	Date	Water $\delta^{18}O$	Water $\delta^{2}H$	Tritium TU	Sulfate[a] $\delta^{18}O$	Sulfate[a] $\delta^{34}S$	CO_3^{2-} $\delta^{13}C$
ADIT 6							
RUNOFF	03.11.88	-4.11	-26.0	-0.19			
	24.11.88	-4.67	-24.1				
DRIP	03.11.88	-4.62	-26.9				
	24.11.88	-4.60	-24.7				
	24.01.90	-4.41	-20.8				
MQ1	04.06.90	-4.74	-22.6		12.2	-1.7/1.6	-23.94
MQ2	04.06.90	-4.67	-21.7	0.6±0.4	12.7	-0.8	
MQ3	06.06.90	-4.83	-22.6				
WESTERN-SPRINGS							
MQ5	04.06.90	-4.36	-18.6	0.0±0.4	9.7[b] 9.1[c]	-2.6/0.5[b] -2.6/0.7[c]	
MQ6	05.06.90	-4.13	-18.6	3.0±0.4	9.6[c]	-2.5/1.2[c]	-19.86[d] -25.53[e]
RAILWAY CUT							
MQ7	07.06.90	-4.81	-23.9	0.7±4.1		-- /0.3	-23.66
MQ8	07.06.90	-4.99	-23.8			-- /0.1	
YARMK RIV.	24.11.88	-5.65	-32.2	1.5			
	24.01.89	-5.85	-27.4	1.3			
	20.07.89	-5.6	-30.3	1.0			
	06.06.90	-5.68	-28.8				
DIVERSION TUNNEL	24.01.90 06.04.89	-4.34 -4.90	-19.2 -20.2	4.0			

a Duplicate analyses for $\delta^{34}S$ given with the GSF value on the left, University of Ottawa on the right
b Sulphate samples collected without prior addition of cadmium acetate
c Sulphate samples collected following addition of cadmium acetate and filtering, for precipitation of aqueous sulphide
d Sample filtered through 0.45 µm nominal pore size filter
e Sample not filtered

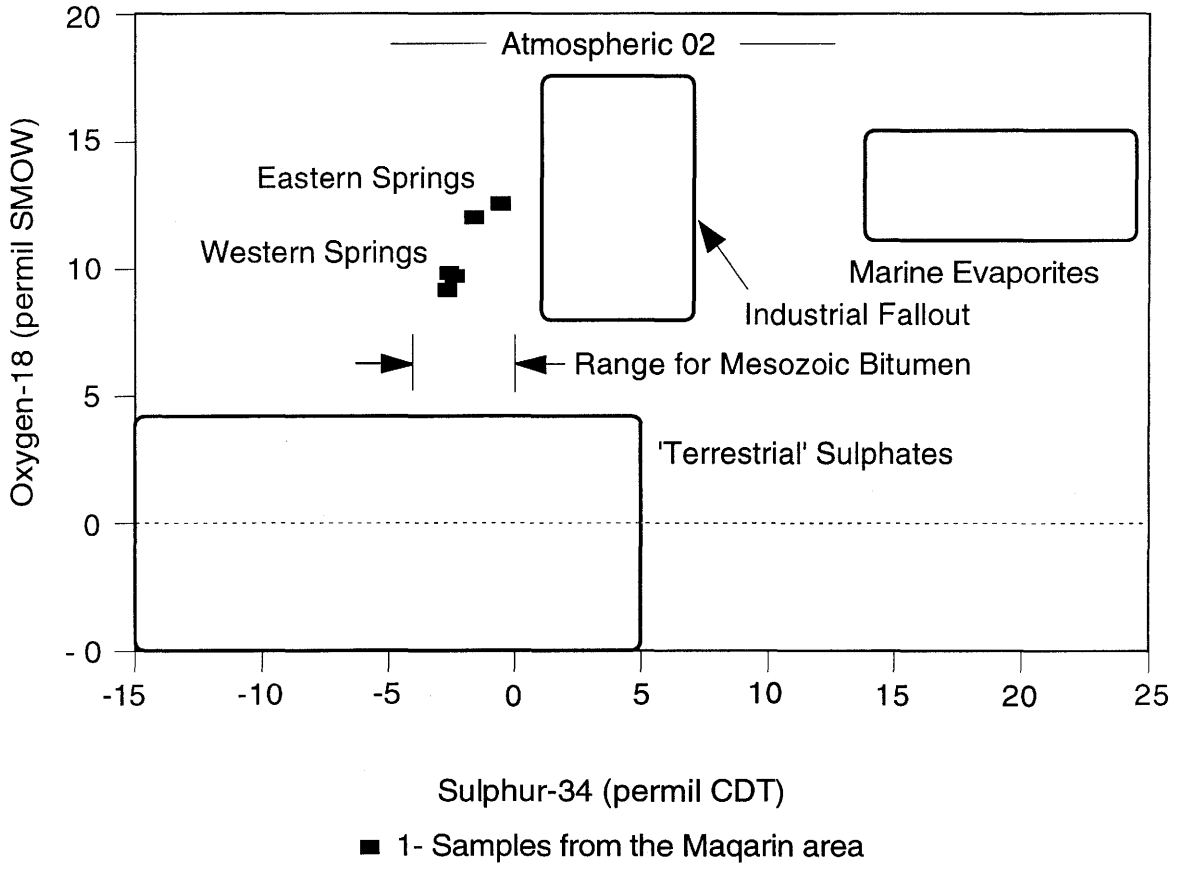

Figure 4.3.3 Plot of the $\delta^{34}S$ vs $\delta^{18}O$ data for the Maqarin area. Fields of interest for a variety of sources are also shown for comparison.

4.4 Stable Isotopes in the Carbonate Phases

I.D. CLARK, P. FRITZ, R. DAYAL, H.N. KHOURY and A.E. MILODOWSKI

The reactions of recarbonation of cementitious grouts have been examined by several workers (e.g. DAYAL and KLEIN, 1988; REARDON et al., 1989). Such studies are relevant to the attenuation of $^{14}CO_2$ by grout backfill materials. The Maqarin site is of particular interest as a field scale analogue where the cement reactions of interest occur naturally. Evidence from the work presented here suggests that recarbonation by CO_2 during retrograde reactions following combustion have been substantial.

4.4.1 Stable Isotopes in the Carbonate Phases

An evaluation of the stable isotope content of the host carbonate rocks and the calcite precipitates was made in order to understand the decarbonation/recarbonation reactions taking place during thermal metamorphism and retrograde alteration. The CO_2 attenuating properties of the cement-type minerals has implications for the uptake of ^{14}C in certain radioactive waste repositories.

Samples of the host carbonate rock units were collected both during this study and during earlier mineralogical evaluations in the Maqarin area (KHOURY and NASSIR, 1982a). Samples were collected from both the unmetamorphosed and metamorphosed limestones and marls, and from the brecciated zones where hydration and retrograde alteration of thermally altered carbonate strata have occured. Mineralogical determinations were carried out by KHOURY and NASSIR (1982a) and by BGS (discussed above). Stable isotope analyses for samples collected during this study were carried out at the University of Ottawa (UO) whereas samples collected earlier were analysed by the USGS (KHOURY, unpublished data). Most samples were collected from Adit A-6 (this study) and other engineering adits constructed over the past ten years. The MQ.10P series of samples were collected from a dump of bituminous limestone waste rock excavated during construction of the Yarmouk River diversion tunnel for the Unity Dam project. This waste rock was burning during the 1990 field work and presented a unique opportunity to observe combustion of these rock types.

Various aspects of the behaviour of stable isotopes during decarbonation reactions, and during subsequent recarbonation and rehydration reactions have been investigated by a variety of studies. The Maqarin study is interesting in that it combines most of these processes together at one site. Further, each process imparts diagnostic stable isotope signatures onto the phases involved.

4.4.1.1. Decarbonation Reactions

High temperature (>600 C) metamorphism of limestone results in calcination of calcite to CaO with loss of CO_2. In the presence of sufficient Si, the reaction can proceed at a considerably lower temperature with the production of CO_2 and wollastonite ($CaSiO_3$). Such decarbonation reactions are accompanied by strong isotope effects, enriching the evolved CO_2 gas phase by up to $3^o/_{oo}$ for ^{13}C and between 6 and $9^o/_{oo}$ for ^{18}O under equilibrium conditions (BOTTINGA, 1968). If decarbonation proceeds towards quantitative conversion of $CaCO_3$ to CaO under open system conditions (continual removal of the CO_2 gas), the ^{13}C and ^{18}O in the residual $CaCO_3$ can evolve to considerably depleted values (figure 4.4.1). This evolution in isotope values is represented by the arrow in figure 4.4.1. These trends have been observed in areas of contact metamorphism (e.g. SHIEH and TAYLOR, 1969) and in geothermal areas were decarbonation of limestone is shown to occur at depth (e.g. VALLEY, 1986; CLARK et al. 1989).

Stable isotope analyses of samples taken from the burning waste rock dump provide an indication of the this trend for partial high-temperature decomposition of carbonate under open system conditions (figure 4.4.1). Also shown on this diagram are data for thermally altered limestones sampled near the brecciated zones. These data show that a negative shift occurs for both $\delta^{13}C$ and $\delta^{18}O$ of the $CaCO_3$, similar to the calculated trend represented by the arrow in figure 4.4.1. However, the maximum departure from initial values is no more than about 5 to 7 $^o/_{oo}$ for either isotope.

Stable isotope data for samples of unaltered limestone and altered carbonates from the brecciated zones at Maqarin also are shown in figure 4.4.1. The carbonate in these rocks, however, have ^{13}C contents which are much more depleted than expected for simple prograde decarbonation. Further, these data do not fall on the calculated trend line for decarbonation, indicating that high-temperature decarbonation may not be responsible for such significant heavy-isotope depletions. All these rocks contain minerals characteristic of retrograde reactions including hydration, recarbonation and sulphatisation (e.g. thaumasite, ettringite, portlandite and CSH phases), suggesting that these reactions are responsible for the strong depletions observed.

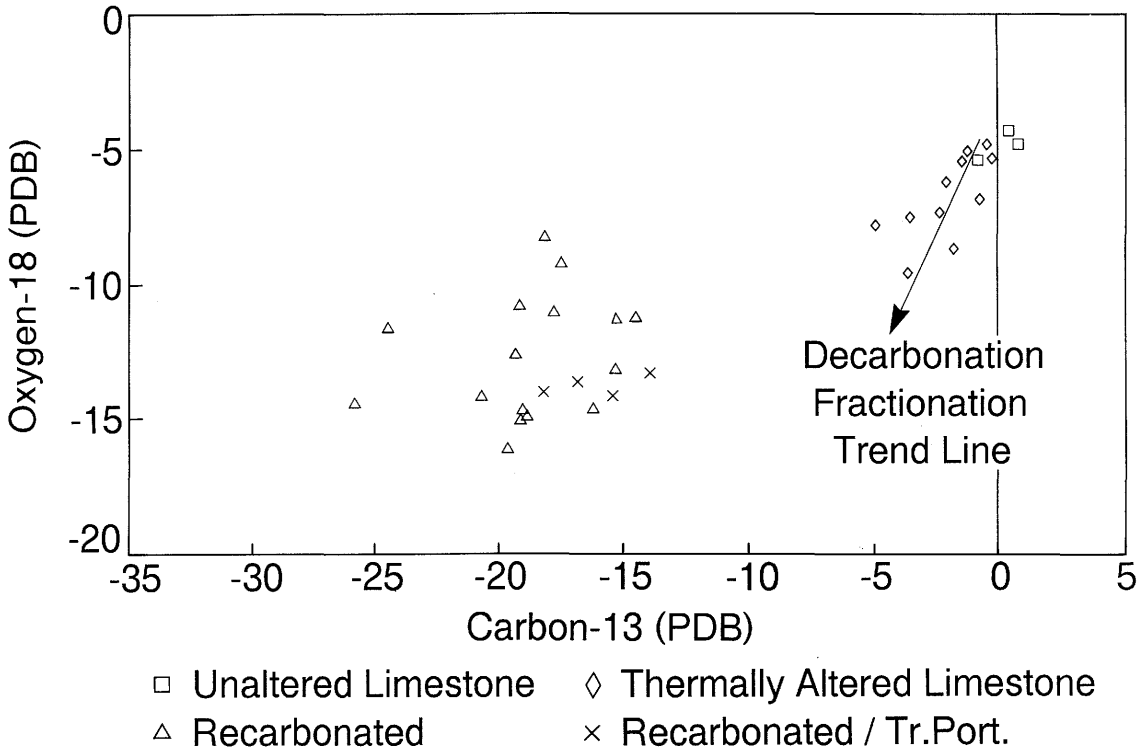

Figure 4.4.1 Stable isotope contents of unaltered limestone and altered carbonates from the brecciated zone in Adit A-6 at Maqarin. The altered suite includes samples from the retrograde alteration zone, including recarbonated and hydrated phases.

4.4.1.2 Hydration and Recarbonation Reactions

Following thermal metamorphism and decarbonation of the original marls and limestones, low temperature retrograde alteration takes place (discussed above, chapters 2 and 4.1). Secondary mineral phases include portlandite which maintains high hydroxide alkalinity in the pore waters for considerable periods of time. Carbonation of these CSH phases then acts as a sink for dissolved carbonate or CO_2 entering the system. Calcite saturation is exceeded at very low concentrations of dissolved carbonate (< 2 mgl^{-1}) in these high pH waters. DIC contributions from mixing with bicarbonate groundwaters, oxidation of organics or uptake of other sources of CO_2 are immediately precipited as $CaCO_3$. This is observed in the discharge areas of the Maqarin hyperalkaline groundwaters where travertine forms around spring vents. Such travertines form by the uptake of atmospheric CO_2 and are accompanied by large isotope effects due to non-equilibrium (kinetic) processes during $CaCO_3$ precipitation (CLARK et al., 1992).

Stable isotope values are given in figure 4.4.2 for calcite travertines forming around spring vents and for carbonates collected from the brecciated zones where rehydration and recarbonation reaction products are found. The travertines forming around spring vents are indeed highly depleted in ^{13}C and ^{18}O giving a characteristic isotopic signature. The "retrograde" carbonates found in the brecciated zone, however, have $\delta^{13}C$ and $\delta^{18}O$ values which are intermediary between the kinetically-depleted vent travertines, and the thermally altered carbonates. These retrograde carbonates can be shown to be a product of recarbonation reactions in the brecciated zone following the spontaneous combustion event. This is of considerable importance, in that it demonstrates that a considerable amount of the material in the brecciated zone could be calcite precipitated from recirculating CO_2 reacting with portlandite and CSH phases.

REARDON et al. (1989) discuss the important recarbonation reactions which occur during the uptake of CO_2 by hydrated portlandite cement:

$$CSH_{(s)} + CO_{2(g)} \rightarrow CaCO_{3(s)} + \text{silica} + H_2O$$

$$Ca(OH)_{2(s)} + CO_{2(g)} \rightarrow CaCO_{3(s)} + H_2O$$

In these reactions, Reardon notes the important role played by moisture in the sample for catalyzing the reaction. However, when the sample reached saturated conditions, CO_2 transport became diffusion dominated, and the reaction was slowed considerably.

Alternatively, recarbonation could proceed under saturated conditions according to the following reactions:

$$CSH_{(s)} + CO_3^{2-} \rightarrow CaCO_{3(s)} + \text{silica} + OH^-$$

$$Ca(OH)_{2(s)} + CO_3^{2-} \rightarrow CaCO_{3(s)} + 2OH^-$$

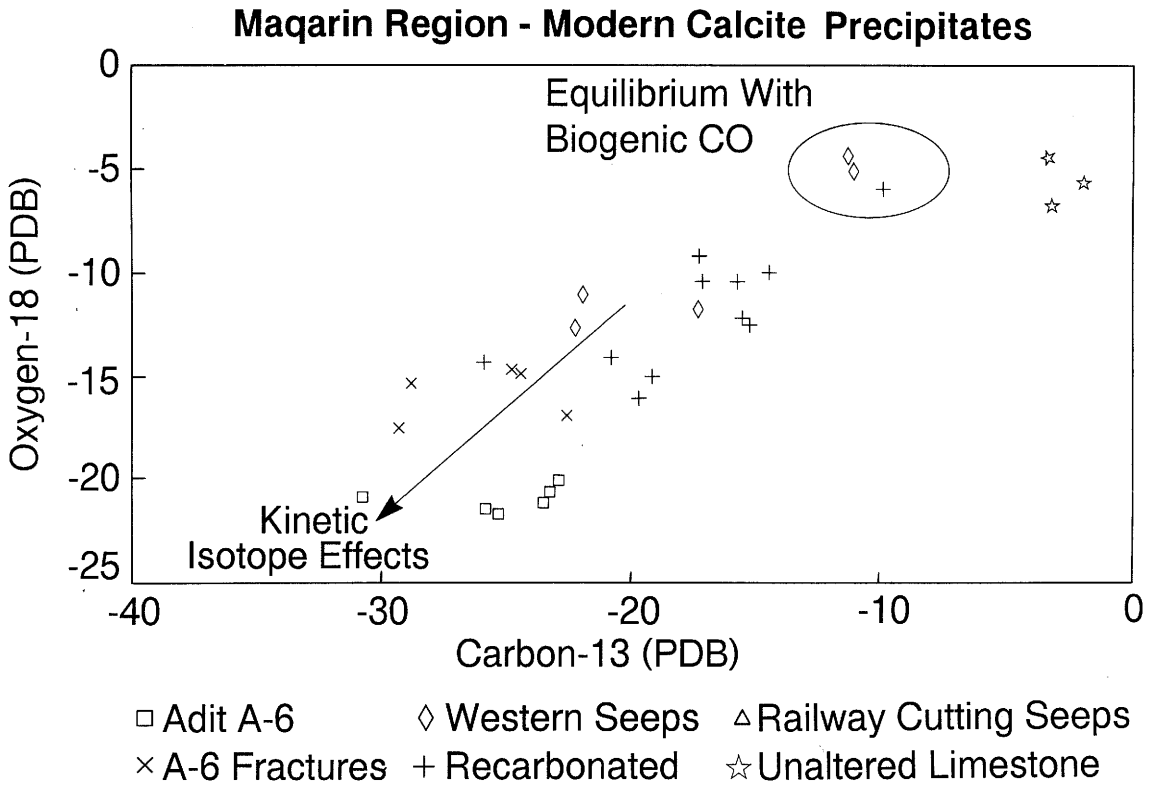

Figure 4.4.2 Plot of the $\delta^{18}O$ vs $\delta^{13}C$ data for modern calcite precipitates, Maqarin area.

At Maqarin, it is unclear whether recarbonation took place according to these reactions, under non-saturated conditions following combustion in the brecciated zones, or at a later stage under saturated conditions by dissolved carbonate reaction with CSH and $Ca(OH)_{2(s)}$. However, $\delta^{13}C$ values which would be anticipated for calcite produced by these recarbonation reactions would be a function of the carbon precurser. Two sources can be considered for the Maqarin area:

(i) Biogenic CO_2 dissolved in the soil zone during groundwater recharge prior to infiltration into the brecciated zone. Such DIC would be expected to have a $\delta^{13}C$ value in the order of -5 to -15 $^{o}/_{oo}$, depending on the degree of dissolution of carbonate material in the soil zone.

(ii) CO_2 generated by the combustion of bitumen in adjacent bedrock zones, if such combustion was contemporaneous with recarbonation reactions in other nearby zones. The $\delta^{13}C$ values for bitumen in these strata are all in the range of -26 $^{o}/_{oo}$ PDB. This source of carbon would impart a significant depletion on the $\delta^{13}C$ of the secondary carbonate.

The low $\delta^{13}C$ values for these secondary carbonates from the brecciated zone (figure 4.4.1) suggests that CO_2 from combustion of bitumen was the primary source of carbon during recarbonation. CO_2 transport throughout the brecciated zone may have taken place, at least initially, by diffusive/advective transport as gas under non-saturated conditions following combustion. Condensed water vapour in the reaction zone would have been important in catalyzing the recarbonation reactions.

The $\delta^{18}O$ data suggest the carbonates in the brecciated zone formed at elevated temperatures, consistent with $\delta^{13}C$ data suggesting extensive recarbonation immediately following combustion. Oxygen-18 fractionation between calcite and water, which is in the order of 29 $^{o}/_{oo}$ at ambient temperatures reduces to about 15 $^{o}/_{oo}$ at 100C. This reduced fractionation at higher temperatures would impart a strong $\delta^{18}O$ depletion on the secondary carbonate. Samples showing extensive recarbonation (figure 4.4.1) fall in the range of -10 to -15 $^{o}/_{oo}$, suggesting formation at temperatures approaching 100 C. This assumes that the waters involved in the reaction were similar to local Maqarin groundwaters ($\delta^{18}O$ =5 $^{o}/_{oo}$ SMOW).

4.4.2 Radiocarbon Evidence

To date, only one sample of these characteristically depleted carbonates from the brecciated zone has been analysed for ^{14}C. Sample A6.5p, a sample of massive,fine grained, buff-white calcite from the brecciated zone at 160 m in Adit A-6 has a measured ^{14}C activity of 3.73 % modern ±1.33 %. Although too little is known about the source of carbon in this sample to calculate an age for the material, it is evident that a modern component is present. This is supporting evidence that much of the carbonate found in the brecciated zones may have formed after the thermal alteration event by recarbonation during the hydration process.

4.5 Microbial and Colloidal Populations in the Maqarin Groundwaters

J.M. WEST, C. DEGUELDRE, M. ALLEN, R. BRUETSCH, S. GARDNER, S. INCE and A.E. MILODOWSKI

4.5.1 Introduction

The natural microbial and colloidal populations indigenous to the Maqarin alkaline springs provide an indication of the potential rôle of microbes and colloids in the cement dominated environment of a repository. Microbial degredation of cements could be enhanced by the sulpher oxidising bacteria and the sulphate reducing bacteria (SRB). The SRB are of particular interest as they participate in steel corrosion, may affect concrete integrity by hydrogen sulphide production and are known to withstand high pH (BATH et al., 1987).

Colloids are present in all groundwaters and radionuclides may sorb onto them, thus enhancing nuclide mobilisation or retardation (McCARTHY and ZACHARA, 1989). The stability of colloids in high pH environments is well documented (eg STUMM and MORGAN, 1981), but little is known of colloid behaviour under such conditions in the field.

4.5.2 Results of the microbiology study

Alkalotolerant and alkalophilic microbes belong to a number of different genera and a review of these groups is given in BATH et al., (1987). In this study, samples were taken from various hyperalkaline seepages in the Maqarin area in order to isolate and identify the bacterial populations with, as far as possible, particular emphasis on the sulphate reducing bacteria. Details of the field sampling programme and analytical techniques are given in section 3.4.4.

The enrichments for the denitrifying and sulphur oxidising bacteria, alkalophilic photosynthetic bacteria, algae and also fungi were all negative. Tests for heterotrophs and oligotrophs (aerobic and anaerobic) were all negative. However, the on-site test with the Millipore filters did reveal the presence of low numbers of heterotrophs in samples from all the sites although this did vary with sampling methodology (table 4.5.1a and b). Higher numbers were obtained from the epifluorescence microscopy counts (figure 4.5.1), although numbers were still very low. Sulphate reducing bacteria were detected in all samples using the qualitative Postgate's B medium, but the isolation of these bacteria onto Postgate's E medium proved impossible using this methodology. Thus it was not possible to estimate the numbers of this group present in the samples. It was also not possible to determine their pH tolerance, as this requires isolates to be plated onto a pH gradient with a subsequent determination of their growth. The sulphate reducing bacteria are, however, lactate oxidisers because of their

growth of Postgate's B medium (possibly of the genera Desulphovibrio or Desulphotomaculum).

These results are not surprising in the light of the hydrochemistry of the samples (table 3.2) which reveals an oligotrophic environment for microbial activity. The major nutrients for microbial growth and metabolism are carbon, phosphorus, sulphur and nitrogen in an aqueous environment. Electron donors and acceptors are also required for energy generation. Carbon levels are low (less than $1.8mgl^{-1}$ for Total Organic Carbon) except for the MQ5 and MQ6 samples where the results vary from 8.0 to $11.8mgl^{-1}$. These lower carbon concentrations could support only a low heterotrophic population. Low levels of phosphorus (0.01 mM maximum as HPO_4; appendix A2) are also available. Nitrate has a range of values from less than 0.03mM to 0.62mM. Sulphate concentrations vary from less than 3mM to greater than 17mM. The higher values for phosphate, nitrate and sulphate are from the same samples (MQ5 and MQ6) which also tallies with the higher organic carbon results. MQ6 has the highest total microbial counts which could be attributed to these higher nutrient values with carbon possibly acting as the limiting factor on microbial growth. It is also interesting to note that Se levels are high, as it is an analogue of sulphate and is used by microbes preferentially. Selenium thus acts as an inhibitor for sulphate reduction which could have implications for this system.

The environment of a cementitious, radwaste repository produces constraints on microbial growth which may influence their capacity to compromise repository integrity (WEST et al, 1988). The results of this study follow on from the microbiological study carried out in Oman (BATH et. al., 1987) where a variety of microbial groups were found and isolated. These included heterotrophs (thought to be introduced from animal sources) and sulphate reducing bacteria. This study again demonstrates the presence of sulphate reducing bacteria (and some unknown heterotrophs which cannot be isolated in pure culture) thus confirming that they can readily adapt to this pH. Their growth is likely to be controlled by the availability of organic carbon rather than the extreme pH of the environment. It is unfortunate that the pH range cannot be investigated further using current methodologies.

4.5.3 Results of the colloid study

This work reports the characterisation of the colloidal population of the Maqarin hyperalkaline groundwaters, providing information on colloid concentration, size distribution and composition. Details of the field sampling programme and analytical techniques are presented in section 3.4.4.

Colloid concentrations ([coll]) and size (Ø) distribution ($\delta[coll].\delta Ø^{-1}$) were assessed with the PSI size distribution calculation method which assumes that all colloids are spherical. These parameters were calculated on the basis of the filtered volume (V, ml), number of counted particles per size class ($\Sigma N(Ø+\delta Ø)\cdot\delta Ø^{-1}$), magnification (defining the area(s) of each photomicrograph studied) and active surface of the filter (S).

Table 4.5.1a Results from Milipore SPC dip stick sampling carried out on June 4 1990

Sample no	Sample Date	Sample site	Exam date	No. colonies ml^{-1}
MQ1A	June 4 1990	Pool MQ1 Adit 6	June 8 1990	2
	June 8 1990			2
	June 11 1990			2
MQ1B	June 4 1990	Pool MQ1 Adit 6	June 8 1990	2
	June 8 1990			3
	June 11	1990		3
MQ2A	June 4 1990	Straw stalactite	June 8 1990	2
	MQ2 Adit 6	June 8 1990		3
	June 11 1990			4
MQ2B	June 4 1990	Straw stalactite	June 8 1990	1
	MQ2 Adit 6	June 8 1990		2
	June 11 1990			1
MQ5A	June 4 1990	Seeps 10cm above	June 8 1990	0
	river active	June 8 1990		0
	discharge 1km	June 11 1990		0
	downstream of adit 6			
MQ5B	June 4 1990	Seeps 10cm above	June 8 1990	?2
	river active	June 8 1990		0
	discharge 1km	June 11 1990		0
	downstream of adit 6			
MQ6A	June 4 1990	10m upstream of MQ5	June 8 1990	0
	June 8 1990			0
	June 11 1990			1
MQ6B	June 4 1990	10m upstream of MQ5	June 8 1990	0
	June 8 1990			1
	June 11 1990			1

Table 4.5.1b Results from Milipore SPC dip stick sampling carried out on June 6 1990

Sample no	Sample Date	Sample site	Exam date	No. colonies ml^{-1}
MQ51A	June 6 1990	Seeps 10cm above	June 8 1990	0
	river active	June 8 1990		0
	discharge 1km	June 11 1990		0
	downstream of adit 6			
	Sampled in situ			
MQ51B	June 6 1990	Seeps 10cm above	June 8 1990	0
	river active	June 8 1990		0
	discharge 1km	June 11 1990		0
	downstream of adit 6			
	Sampled in situ			
MQ51C	June 6 1990	Seeps 10cm above	June 8 1990	0
	river active	June 8 1990		0
	discharge 1km	June 11 1990		0
	downstream of adit 6			
	Sampled in situ			
MQ61A	June 6 1990	10m upstream of	June 8 1990	0
	MQ5	June 8 1990		0
	Sampled in situ	June 11 1990		0
MQ61B	June 6 1990	10m upstream of	June 8 1990	0
	MQ5	June 8 1990		0
	Sampled in situ	June 11 1990		0
MQ61B	June 6 1990	10m upstream of June 8 1990		0
	MQ5	June 8 1990		0
	Sampled in situ	June 11 1990		0

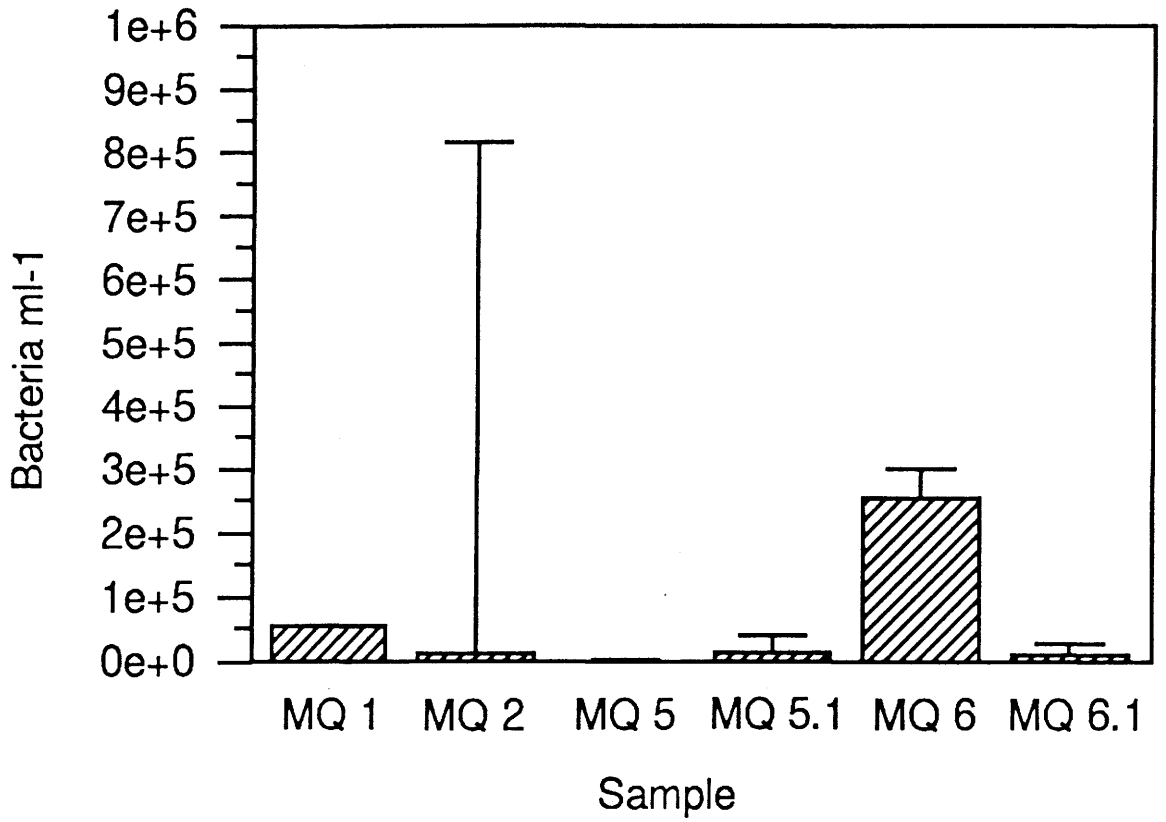

Figure 4.5.1 Direct counts of microbes ml^{-1} in Maqarin samples (MQ1, 2, 5, 5.1, 6 and 6.1) by means of epifluorescence microscopy.

The full formula is thus

$$\frac{\delta\,[coll]}{\delta Ø} = \frac{\Sigma N\,(Ø, Ø + \delta Ø) \cdot \delta Ø^{-1}}{\Sigma s} \cdot S \cdot \frac{1000}{V} \qquad -(4.1)$$

and the data are presented in two ways, linear/linear barcharts and log/log distributions.

The so produced size distribution can (eg. BUFFLE, 1988) be analysed as a normalised distribution (independent of the range of size) and the linear plot of $\delta[coll]\cdot\delta Ø^{-1}$ vs Ø shows that, for a natural system, it follows Pareto's law where:

$$\frac{\delta\,[coll]}{\delta Ø} = A.Ø^{-b} \quad \text{for } Ø = Ø_{(m)} + n.5\ \delta Ø \tag{4.2}$$

where n is an integer and A and b are constants

for $\delta Ø \rightarrow 0 (\delta Ø < Ø)$ it becomes:

$$\frac{\delta\,[coll]}{\delta Ø} = A.Ø^{-b} \tag{4.3}$$

This becomes:

$$\log \{\delta[coll] \cdot \delta Ø^{-1}\} = \log A - b.\log Ø \tag{4.4}$$

When the log-log plot is linear, the Pareto law applies and determination of A and b is simple. From this plot various parameters, such as the total concentration of colloids or the way they behave in the system (aggregation/filtration), can be evaluated on the basis of A and b. The concentration of colloids from a minimum size ($Ø_{(m)}$) to a maximum size ($Ø_{(M)}$) can be calculated by integrating $\delta[coll].\delta Ø^{-1}$ over the size range. However, prior to integration, the [coll] should be expressed in units of mass (i.e. ppb). If it is assumed that the colloids are spherical, then the colloid mass,

$$m = {}^1/_6\, \rho\, \Pi\, Ø^3 \tag{4.5}$$

where ρ is the colloid density.

Multiplying equation 4.5 by $\delta[coll].\delta Ø^{-1}$ thus converts the size distribution ito units of mass.

The data on colloidal size distribution and colloidal concentration (derived from a combination of ultrafiltration and SEM) is presented in figures 4.5.2 to 4.5.6. Here, assuming a colloid density of 2 gcm^{-3} (equation 4.5), the data has been converted to a mass basis. In this case, the slope coefficient of the cumulative size distribution plots equals b+1 and, for the log normal plots, equals b (equations 4.2 to 4.4). According to BUFFLE (1988), when b=4, the size distribution corresponds to a constant mass per class unit, suggesting neither aggregation nor filtration/sedimentation of colloids in the particular groundwater system under study. Aggregation occurs when b<4 and filtration when b>4.

The log-normalised plots in figures 4.5.2 to 4.5.6 all have values for b of around 4, suggesting a stable colloid population in this system. This is presumably due to the previously described high pH effect (STUMM and MORGAN, 1981). Table 4.5.2 summarises the colloid concentration data, with all waters examined containing less than 1ppm colloids and the more weakly mineralised groundwaters of the eastern site as little as 0.1 ppm colloids..

Spectral analysis of the solution was also carried out (in a flow-through cell) before and after filtration. The spectra of the filtered phase was the same as the parent groundwater and direct observations showed that the absorption spectra was not due to the presence of humic acids (a 1-5 ppm humic solution precipitated in the $Ca(OH)_2$ buffer solution) but rather to chromate colouring the groundwaters.

An attempt was also made to establish the U content of the colloidal population as this had some bearing on the results of the U modelling in chapter 5. U was thought to be associated with colloids in the Oman hyperalkaline groundwaters (BATH et al., 1987), but a cursory examination of colloids from the MQ6 site (by direct counting of a filter membrane) indicated that less than 0.2 % of the total dissolved U was associated with colloids.

Further, groundwaters samples from sites MQ1, MQ2, MQ5 and MQ6 were analysed for a suite of elements both before and after ultrafiltration. Although the data are not presented here, there are no detectable diffrences between the two samples sets, implying that colloidal population has an insignificant effect on the bulk geochemistry of the groundwaters.

Table 4.5.2 Groundwater and colloid analysis

Sample	Remarks	pH	Ø(nm)	Laser test (ppb)	SEM (ppb)
MQ1	Uncoloured	12.50	40-3200	200-500	
MQ2	Yellow	12.45	40-3200	100	87
MQ5	Yellow	12.58	40-2800	1000	189
MQ6	Yellow	12.63	40-3200	1000	270
MQ7	Uncoloured	12.53	40-3200	500	346

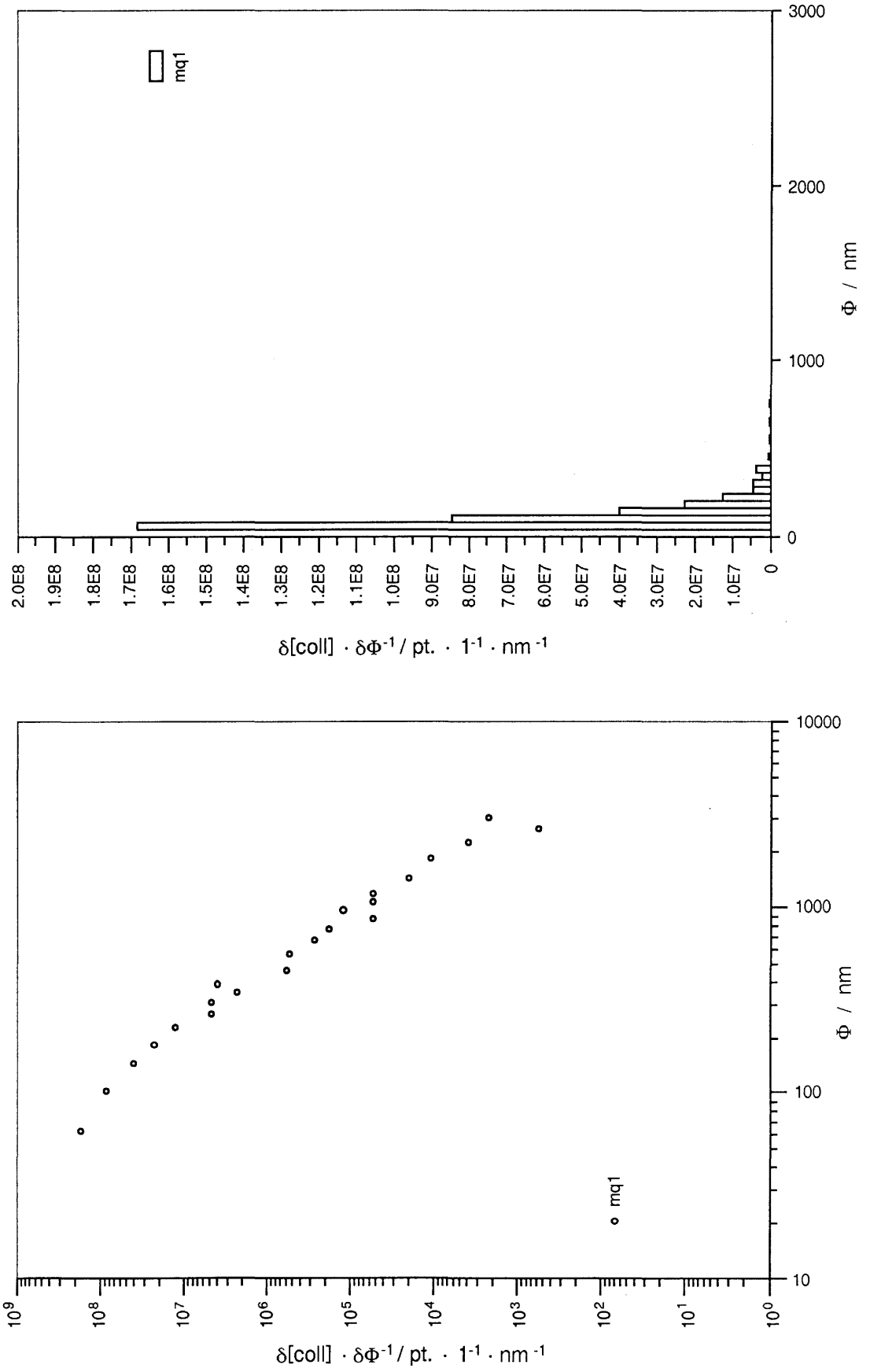

Figure 4.5.2 Colloidal size distribution in sample MQ1.

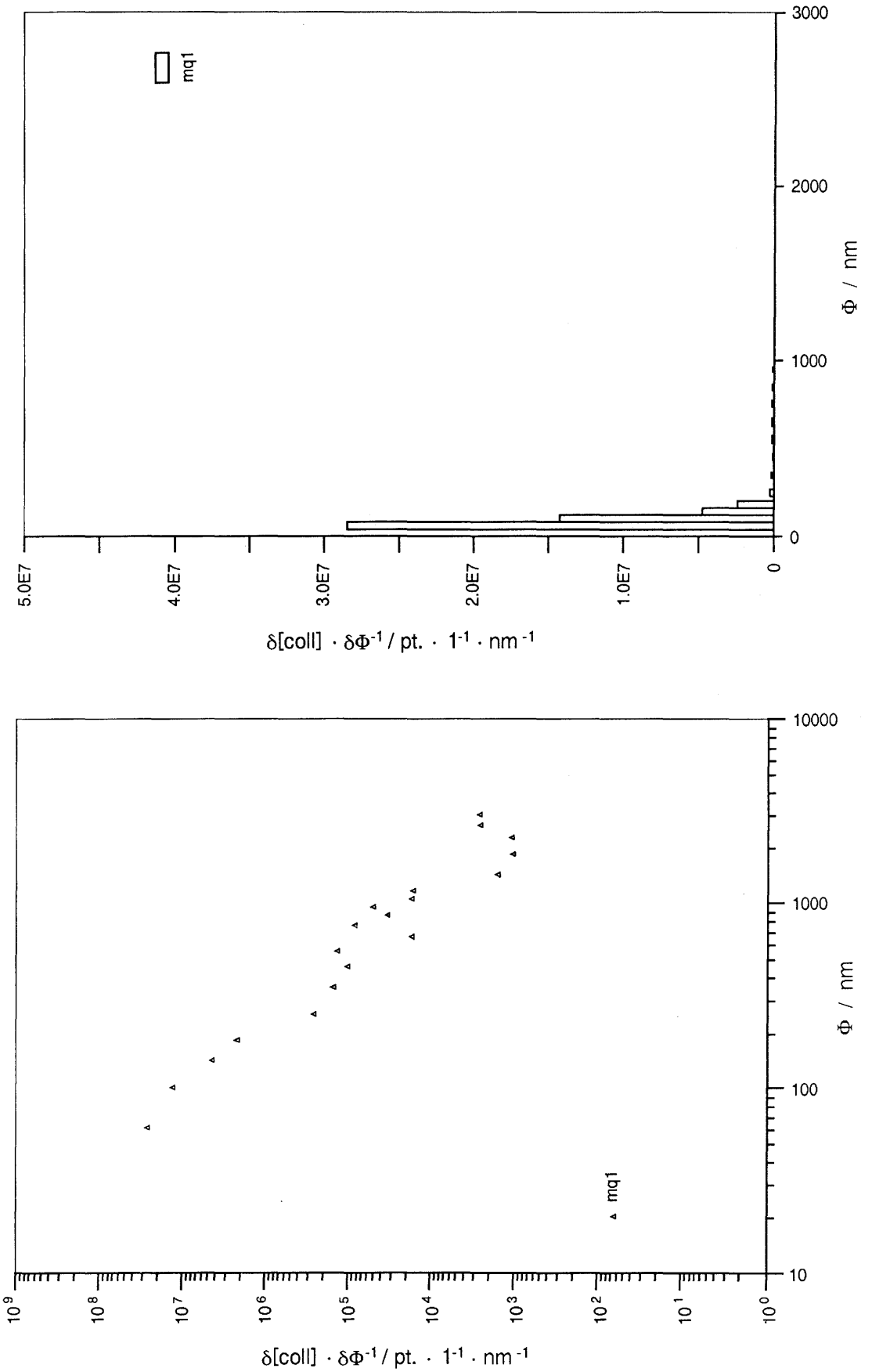

Figure 4.5.3 Colloidal size distribution in sample MQ2.

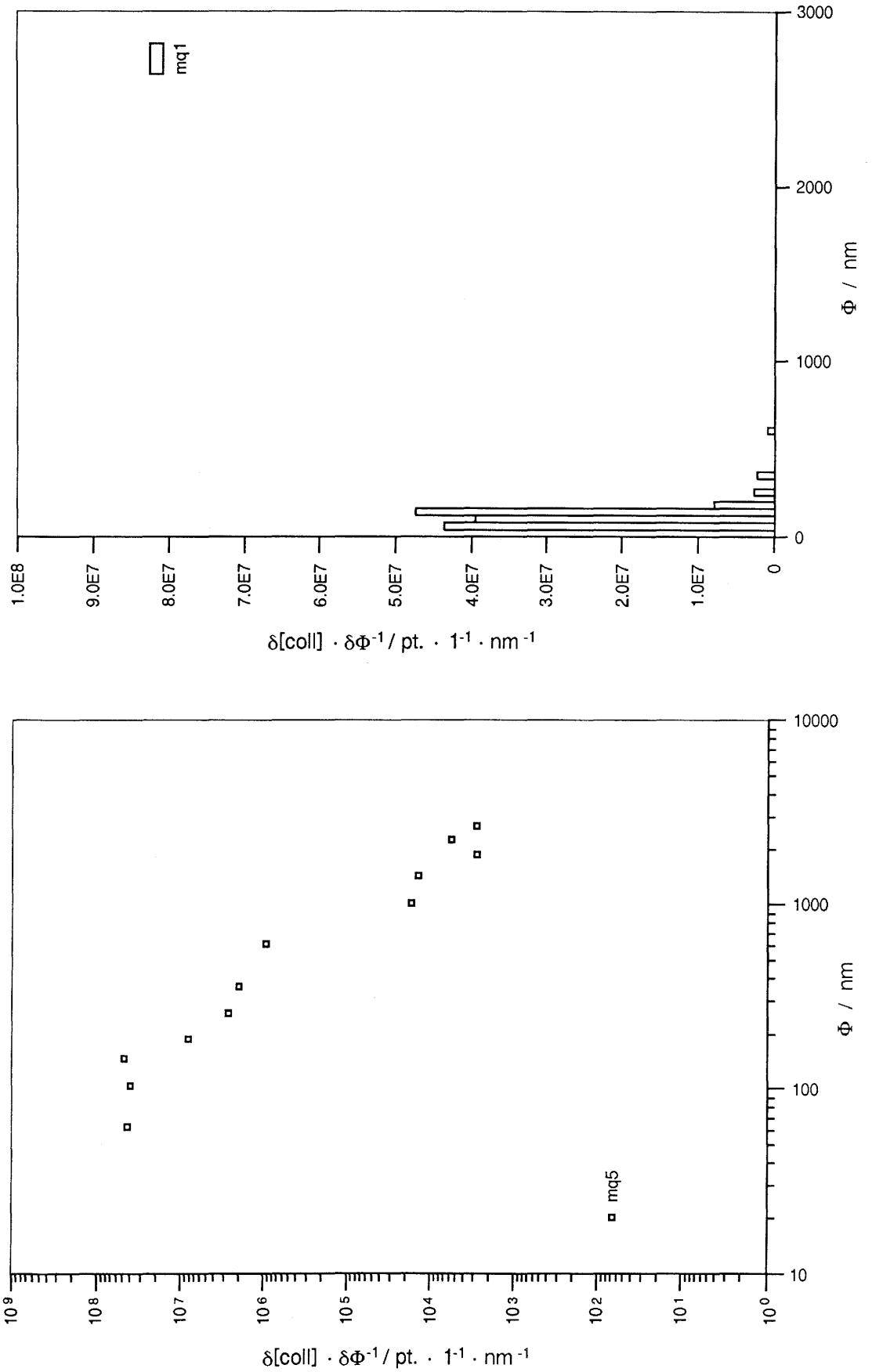

Figure 4.5.4 Colloidal size distribution in sample MQ5.

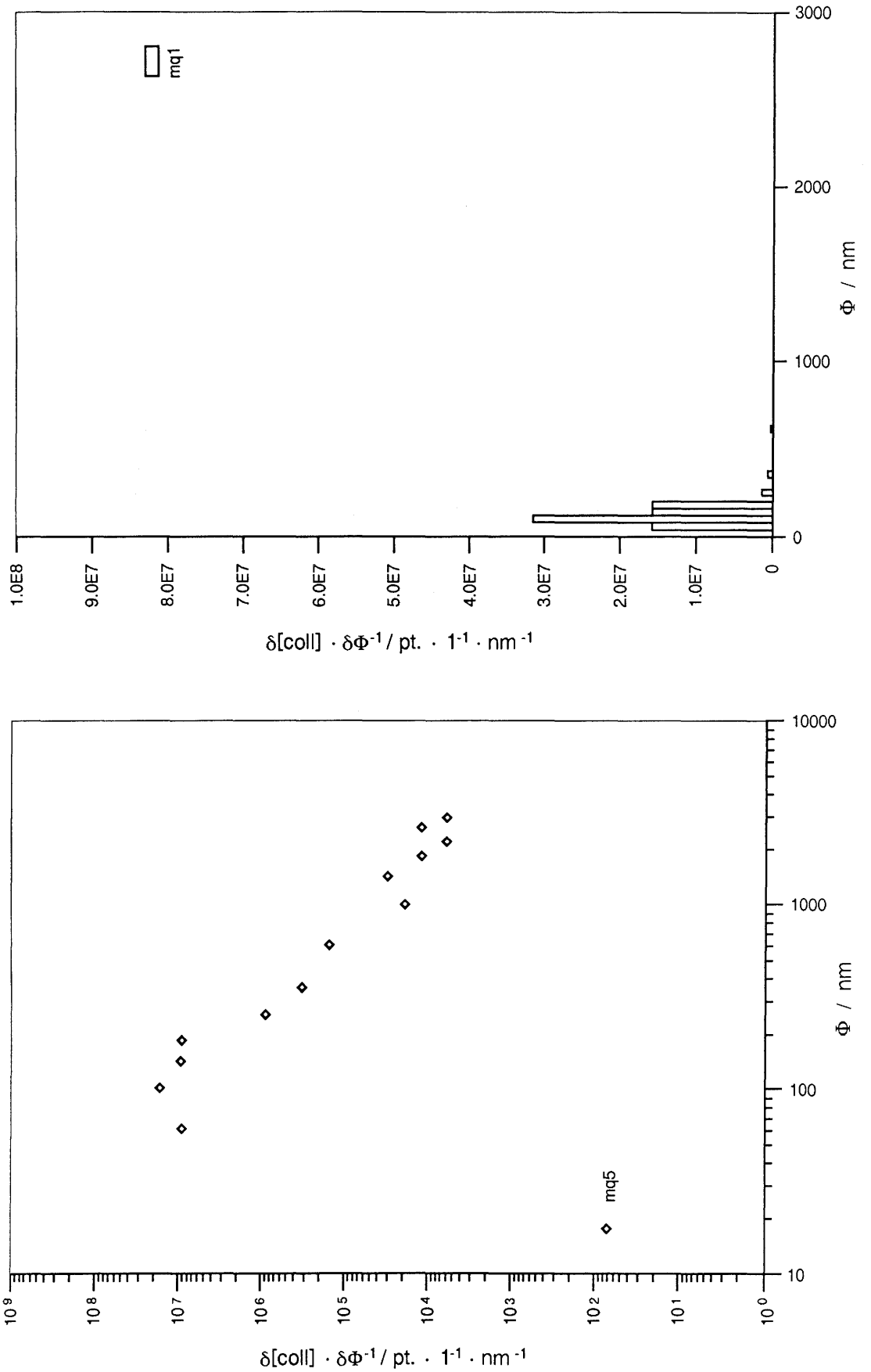

Figure 4.5.5 Colloidal size distribution in sample MQ6.

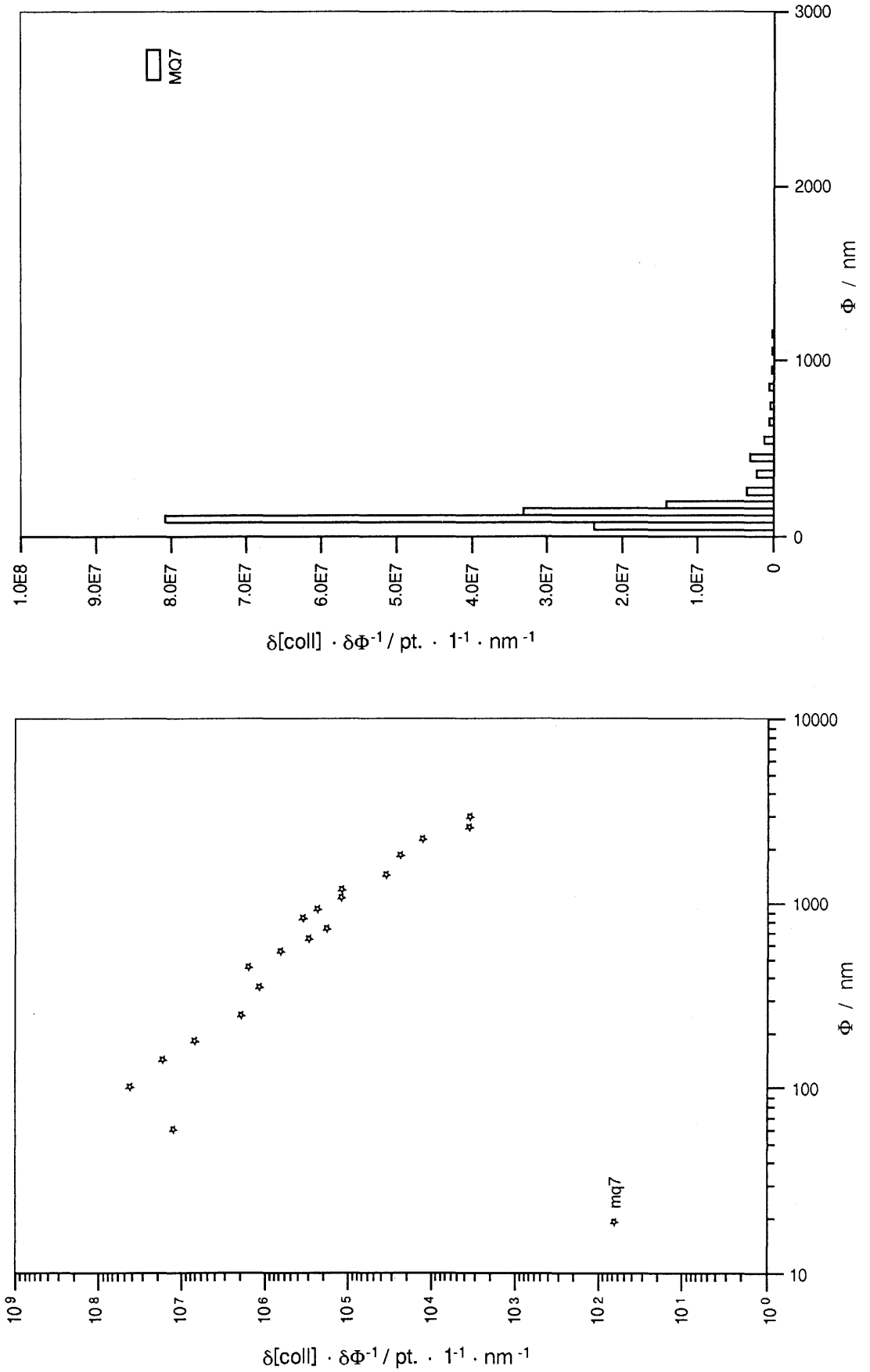

Figure 4.5.6 Colloidal size distribution in sample MQ7.

4.5.4 Summary

Both microbes and colloids are present in the Maqarin groundwaters. Microbial enrichment tests for denitrifying and sulphur oxidising bacteria, alkalophilic photosynthetic bacteria, algae, fungi were all negative. Tests for heterotrophs and oligotrophs (aerobic and anaerobic) were also negative but on-site tests did reveal the presence of low numbers of heterotrophs in samples from all the sites. Sulphate reducing bacteria were detected in all samples but their isolation proved impossible. These results are not surprising in this oligotrophic environment and it appears that low concentrations of nutrients control microbial growth rather than the alkaline pH of the environment. Colloid concentrations were less than 1ppm. EDS analysis indicates that they are composed mainly of Ca (probably $Ca(OH)_2$) and Fe (probably $Fe(OH)_3$). The colloid particles do not agglomerate (because of the high pH) and the size distribution follows Pareto's power law with constant mass per size class. Humic acids are not detected and are assumed to have precipitated in this alkaline water, probably as Ca-humates under the prevailing conditions of high ionic strength.

5 GEOCHEMICAL MODELLING OF HIGH PH CEMENT PORE WATERS FROM THE MAQARIN AREA OF NORTHERN JORDAN

C.J. TWEED, C.M. LINKLATER, J. EIKENBERG, W.R. ALEXANDER, R. DAYAL and K. EAGLESON

5.1 Introduction

Geochemical modelling of data produced in natural analogue studies forms an important part of repository performance assessment procedure as it can demonstrate the applicability of a thermodynamic approach to predicting trace element solubility and speciation in systems which have evolved over geological timescales. They thus provide data for interpretive modelling to improve understanding of the physical and chemical processes that are likely to occur as the repository environment evolves with time and, potentially, also an useful validation of both the models and the supporting thermodynamic data.

Geochemical codes utilise thermodynamic databases which are usually compiled from the best available experimental values measured in laboratory studies. Although thermodynamic data for the major elements are fairly well known, data for most radionuclides of interest to a repository safety assessment are sparse, especially at the high pH (12-13) expected in the vicinity of a cementitious repository. It is therefore necessary to check the existing databases by direct comparison of code predictions with analytical results. The following sections, after briefly outlining the methodology, record the results of predictive and interpretive geochemical modelling of the Maqarin hyperalkaline groundwaters.

Four groups of geochemical modellers are involved in the exercise: AEA Technology, Harwell (U.K.); Nationale Genossenschaft für die Lagerung radioaktiver Abfälle (NAGRA), Wettingen (Switzerland), the Paul Scherrer Institute (PSI), Villigen (Switzerland); and the Civil Research Division of Ontario Hydro (ONHY), Toronto (Canada).

5.2 Methods

5.2.1 Work Programme

Geochemical modelling exercises were carried out in several stages during this analogue study, as described below.

i) In the initial planning stages of the project, prior to the field trip, a preliminary scoping exercise was performed using a typical groundwater analysis from the

Maqarin area obtained from a previous study by KHOURY et al., 1985 (site referred to as Adit A-6 in chapter 3). The temperature was assumed to be 25 C, the pH was measured at 12.5 and, in the absence of measurements, redox was varied with pe values of 0 (oxidising), -4 (intermediate), and -8 (reducing).

The trace elements studied were U, Th, Ra, Pb, Se, Ni and Sn. For convenience, the concentration of these elements was estimated at 1.0×10^{-6} g l^{-1}, a level considered reasonable in the light of previous studies of high pH groundwaters (eg. McKINLEY et al., 1988).

This scoping exercise allowed identification of those elements/species and minerals which would be worth extra attention during the analytical phase of the project. Potential problem areas were highlighted, such as those elements with particularly low solubilty which might then prove difficult to detect in solution. In addition, the petrologists involved in the description of the solid phase could focus on the trace level minerals most likely to be controlling the solubility of the elements of interest.

ii) In Autumn 1990, when field data from the major element chemistry were available, the predictive modelling exercise was repeated using the measured groundwater chemistry from samples MQ2 and MQ5 and assuming the trace element concentrations as before. The major difference between these two studies was that field measurements indicated that the groundwaters in the area were oxidising. The measured Eh values were in the range +310mV to +120mV (pe values between 5.2 and 2.1) and this affected the predicted solubilities and speciation of those elements which are redox sensitive over the range of conditions of interest. This exercise immediately indicated several problem areas in the databases, with notable differences seen between the Se and U predictions of the various groups (see ALEXANDER et al., 1992 for details). This exercise also acted as a useful code verification, through the direct comparison of major element chemistry as predicted by the four modelling groups.

iii) The final stage of the modelling exercise was performed in March 1991, following the completion of the laboratory analyses. Four groundwaters were selected this time; MQ2 and MQ5 were retained, and a further two, MQ6 and MQ7 were included so that comparison between prediction and observation could then be made as measured values for major and trace element concentrations in these groundwaters were available together with detailed mineralogical data.

For this stage, in addition to the groundwater chemistry, there were detailed supporting mineralogical data (chapter 4). Thus the predicted solubility limiting phases could be directly compared with the minerals identified from the field samples. This stage therefore represented a validation exercise, testing how well the databases performed in predicting the trace element behavior in the groundwaters modelled.

Nagra and ONHY made no changes to their databases during the project. AEA carried out a programme of ongoing database development. HATCHES version 2.1 (CROSS and EWART, 1991) was used for the first two stages of the modelling programme. HATCHES version 3.0 was used for the final stage as it included an expanded minerals database. Minor changes were also made to the aqueous databases between the two releases and these are highlighted in the following text. PSI updated the NAI0289 database for the final modelling stage by including the NEA (1990) recommended data for U. This means that it is not really possible to compare the predicted U results with the final stage data and, as such, the PSI data are only fleetingly mentioned in the discussion of the interpretive U results.

5.2.2 Modelling Procedure

The procedure followed in the modelling exercise was to simulate equilibration of the selected groundwater chemistries, at the measured pH and pe (or range of pe) values. Following the equilibration, the aqueous speciation of the trace elements of interest were recorded, along with the identities of possible solubility limiting phases. No attempt was made to equilibrate the groundwaters with solid phases and the degree of saturation was quantified by a saturation index (SI) defined as the ratio of the logarithm of the ion activity product to the solubility product. This procedure ensured that the speciations were carried out at the same concentrations for all codes.

During the modelling exercise, five speciation codes were used and reference was made to six associated databases. The details of these are given in table 5.1. The main code employed was PHREEQE (PARKHURST et al., 1985) and variants thereof. PSI also utilised the MINEQL code (WESTALL et al., 1976) and, independently, also carried out a PHREEQE/MINEQL intercomparison which is presented in appendix D. The groundwater compositions used during the the modelling exercise are given in tables 5.2 and 5.3. Table 5.2 shows the compositions used in stages i and ii, and table 5.3 shows the compositions used during stage iii. The main differences between the compositions used in the initial stages and the final stage are that the final groundwater compositions are more complete, including some major elements not considered in the intial stages e.g. Si, Al and Fe. This allowed the role of silicate and Fe-bearing minerals to be assessed.

In stage iii, the concentration of some of the elements of interest were below the detection limits of the analytical technique employed. For these elements, assumed values were selected for the modelling exercise which were less than or equal to the detection limits. The reasoning behind the choice of values for trace elements present at such low levels is given in the relevant section in the following discussion. Some comments on the choice of major element data are given below.

Table 5.1 Summary of the geochemical speciation codes and associated databases used during the modelling study

Organisation	Code	Database
AEA	HARPHRQ (extended PHREEQE BROWN et al., 1990)	HATCHES (version 2.1) (CROSS and EWART, 1991) HATCHES (version 3.0)
NAGRA	RIPP2 (modified PHREEQE) (YUSAF and HAMILTON, 1992)	NEWTHERM (YUSAF and HAMILTON, 1992)
PSI	MINEQL/PSI (WESTALL et al., 1976) PHREEQE (original code, PARKHURST et al., 1980, 1985)	MINEQL (SCHWEINGRUBER, 1983; BERNER, 1992) NAI0289 (PEARSON et al., 1989)
ONHY	PHREEQE (original PARKHURST et al., 1980 version modified to accept a larger database)	MINTEQAI (PETERSON et al., 1987) CHEMVAL/MIRAGE project database produced by WS Atkins Engineering Science Ltd. (UK) for Th

Table 5.2 Major element compositions of three groundwaters used during predictive modelling

Parameter	Adit A-6	MQ2	MQ5
pH	12.5	12.26	12.44
pe	0,-4,-8	5.22	2.05
Ca (mgl^{-1})	481	590	1050
Na	67.4	49	132
K	25.3	11.7	613
Mg	-	<0.2	<0.4
TIC	30	<0.5	-
Cl	76.3	56.4	51.0
SO4	272	278	1480
NO3	3.1	5.1	38.2

Table 5.3 Major and trace element chemistry of four groundwaters used during the interpretive modelling

	MQ2	MQ5	MQ6(3828)	MQ7
pH*	12.53	12.6	12.71	12.67
pe	5.2	2.05	2.17	2.0
	-4	-4	-4	-4
	-8	-8	-8	-8
Major Elements (mgl^{-1})				
Ca	590	1050	1110	662
Na	49	132	173	34.4
K	11.7	613	785	16.4
Cl	56.4	51.0	47.8	68.5
SO_4	278	1480	1700	284
NO_3	5.1	38.2	40.5	7.55
TIC**	0.5(<0.5)	0.5(<0.5)	0.5(2.9)	0.5(2.7)
Mg**	0.1(<0.2)	0.1(<0.4)	0.1(<1.5)	0.1(<0.1)
Fe**	0.01(<0.02)	0.01(<0.02)	0.01(<0.15)	0.01(<0.01)
Al**	0.01(<0.05)	0.01(<0.05)	0.01(<0.05)	0.01(<0.05)
Si**	0.01(<0.03)	0.01(<0.06)	0.01(<3.0)	0.06
Trace elements (μgl^{-1})				
U	0.03	0.15	0.18	0.03
Se	500	1500	2100	300
Cr	720	5530	7040	600
Th**	0.1(<0.2)	0.1(<0.2)	0.1(<0.2)	0.1(<0.2)
Pb**	5(<5)	5(<5)	5(<5)	5(<5)
Sn	1	1.05	0.9	7.5
Ni	1	4.1	3.4	1.2
Ra***	0.03	<0.01	<0.01	0.01

* Note that the pH values quoted here are laboratory values whereas those of table 5.2 are field values. NAGRA used the field values in the interpretive modelling phase too and later tables are annotated when a significant difference arose in the results.

** Values given are reasonable estimates of the concentration levels present and the limits of detection are given in the brackets.

*** Data for MQ5 and MQ6 represent the detection limit (of around 1.1×10^{-2} μgl^{-1}). MQ7 value is for a MQ1 water analysis (appendix A5).

The carbon was input as total inorganic carbon rather than alkalinity during the modelling. The concentration used ($0.5 mgl^{-1}$) is assumed and may not accurately represent the amount of total inorganic carbon (TIC) in the system. Data for TOC (table 3.2) became available after the completion of the modelling exercise and these values range up to 11.8 mgl^{-1}. However, even if TIC is assumed to be present at similar levels, scoping calculations indicate that the solubilities and speciation of the trace elements of interest are insensitive to carbon at the high pH levels considered. The concentrations used for Mg, Fe, Si and Al were values which are less than or equal to the limits of detection (see table 5.3). There is a measured value for Si in MQ7 of 0.06 mgl^{-1}.

5.3 Results

The first part of this section describes the results of the predictive modelling of stages i and ii. These stages were principally verification exercises; highlighting possible weaknesses in databases etc. These results have been published elsewhere (ALEXANDER et al., 1992) and a summary is included here only for completeness.

The second part of this section describes the results of the interpretive modelling (stage iii) and discusses comparisons of predictions with data collected from the field (summarised in TWEED and MILODOWSKI, 1992).

Within each of the following sections, the results are discussed on an element by element basis.

5.3.1. Results of the initial intercomparison (stage i and ii)

Using different databases can affect predictions of the aqueous speciation and solubilities of the elements of interest. As will be seen in the following sections, for some of the elements, agreement between the different modelling groups is very good, reflecting the use of similar or identical databases. For other elements, however, predictions of solubilities varied by many orders of magnitude between the calculations of different modellers. The following paragraphs describe only the obvious differences in the results of the four participating groups. The full reasons for the differences are not discussed at this stage in order to avoid repetition in the discussion in the next section.

Nickel

The results of modelling at AEA, Nagra, and ONHY show close agreement (table 5.4) whereas those from PSI differ slightly. The main aqueous species is predicted to be $Ni(OH)_3^-$ by all four groups and, with the exception of PSI, the controlling solid is identified as $Ni(OH)_2$. The PSI results differ due to the inclusion of an extra aqueous

species, $Ni(OH)_4^{2-}$, and an extra solid, NiO, in the PHREEQE NAI0289 database (amended to include the data of BAEYENS and McKINLEY, 1989). BAES and MESMER (1976) indicate that $Ni(OH)_4^{2-}$ may well be important at higher pH values and so, in this respect, the PSI predictions may be more representative of Ni in the Maqarin groundwaters. $NiO_{(s)}$ was included by BAEYENS and McKINLEY (1989) due to the rather uncertain solubility of $Ni(OH)_{2(s)}$ as included in the other databases used here.

Table 5.4 Predicted nickel speciation: comparison of 4 calculations

NICKEL MQ2 pH=12.26, pe=5.2

	AEA	**Nagra**	**ONHY**	**PSI**
Aqueous species (%)				
$Ni(OH)_3^-$	96	96	96	97
$Ni(OH)_2^o$	4	4	4	-
$Ni(OH)_4^{2-}$	-	-	-	3
Solubility controlling solid (saturation index)				
$Ni(OH)_2$	-0.9	-0.9	-0.9	-
NiO, bunsenite	-	-	-	-2.6

NICKEL MQ5 pH=12.44, pe=2.05

	AEA	**Nagra**	**ONHY**	**PSI**
Aqueous species (%)				
$Ni(OH)_3^-$	98	98	97	91
$Ni(OH)_2^o$	2	2	3	-
$Ni(OH)_4^{2-}$	-	-	-	9
Solubility controlling solid (saturation index)				
$Ni(OH)_2$	-1.1	-1.1	-1.1	-
NiO, bunsenite	-	-	-	-2.8

NICKEL ADIT A-6 pH=12.5, pe=0

	AEA	**Nagra**	**ONHY**	**PSI**
Aqueous species (%)				
$Ni(OH)_3^-$	97	98	97	92
$Ni(OH)_2^o$	3	2	2	-
$Ni(OH)_4^{2-}$	-	-	-	8
Solubility controlling solid (saturation index)				
$Ni(OH)_2$	-1.2	-1.2	-1.2	-
NiO, bunsenite	-	-	-	-2.8

No change from above for pe=-4, -8

Lead

The results of AEA, Nagra and PSI calculations are identical with $Pb(OH)_3^-$ being the sole (100%) aqueous species and $Pb(OH)_2$ (S.I. -5.2 to -5.6), the controlling solid. In the PSI calculations for Adit A-6, the speciation changes at lower pe values (-4 and -8) to $Pb(OH)_3^-$ (94%) along with $Pb(OH)_2^0$ (6%). PbS_2 takes over as the controlling solid phase (S.I. -5.4) at pe = -8. The ONHY results, although also indicating $Pb(OH)_2$ as the controlling solid phase predict a higher solubility (S.I. -1.7 at pe = 5.2, dropping to -2.1 at pe = 0). ONHY results are significantly different in the predicted speciation with $Pb(OH)_4^{2-}$ playing the dominant role (87% at pe = 5.2, 93% at pe = 2.1 and lower) and $Pb(OH)_3^-$ comprising the remainder of the aqueous Pb.

Radium

Only AEA and Nagra carried out modelling on Ra speciation. Both groups obtained the same results i.e. Ra^{2+} (97-98%) as the main aqueous species along with $RaOH^+$ (2-3%), and $RaSO_4$ as the controlling solid (S.I. -1.3). It should be noted, however, that these databases were limited (Ra^{2+}, $RaOH^+$ and $RaSO_4^0$ as the only aqueous species and only the solids $RaCO_3$ and $RaSO_4$). More data on Ra chemistry are available and some further calculations were carried out at AEA with additional data from BENSON and TEAGUE (1980) and LANGMUIR and RIESE (1985). These data included a modified constant for $RaSO_4^0$, extra aqueous species ($RaCO_3^0$ and $RaCl^+$) and additional solids (pure Ra and $RaCl_2.2H_2O$) as well as modified constants for the previously considered solids. These simulations showed different speciation, predicting 75% Ra^{2+}, 20% $RaSO_4^0$ and 4% $RaOH^+$. The identity of the solubility controlling phase remained the same.

Thorium

Th speciation was calculated by all four groups and in all cases $Th(OH)_4^0$ was found to be the sole aqueous species (100%) and ThO_2 the solubility controlling phase. The solid phase was oversaturated (S.I. +1.2) in the Nagra, PSI and ONHY results and the degree of oversaturation increased (to +5.7) in the AEA results. This is due to the inclusion of a more crystalline ThO_2 solid in the HATCHES database (cf. discussion of the effects of ThO_2 crystallinity on solubility in LANGMUIR and HERMAN, 1980).

Selenium

The results of Se speciation calculations are rather complex (table 5.5). In the MQ2 water, $CaSeO_4$ is predicted to be the controlling phase with SeO_4^{2-} or SeO_3^{2-} the dominant species. Decreasing the pe to 2.1 (MQ5 water) introduces $CaSeO_3$ as the solid phase in the case of all groups apart from ONHY.

Further decreases in pe indicate the dominance of SeO_3^{2-} in solution in the AEA, Nagra and PSI results and introduce Se_2^{2-} as the dominant species in the ONHY calculations. At the lowest pe (-8), HSe^- dominates the AEA, Nagra and PSI data while the ONHY calculations continue to indicate Se_2^{2-}. The controlling solid also changes frequently and it is only at the lowest pe that agreement is once more reached, with elemental Se as the dominant phase. The ONHY results predict massive oversaturation with respect to elemental Se under all redox conditions. The numerical values of the saturation indices calculated by ONHY should not be taken at face value; indices greater than about 10-15 simply represent negligible solubility.

Tin

Sn modelling was carried out by AEA and Nagra. AEA predict the aqueous species to be dominated by $Sn(OH)_6^{2-}$, whereas Nagra predict $Sn(OH)_3^-$ to be dominant (table 5.6). In both simulations the controlling solid was predicted to be SnO_2, but the solubilities were different. AEA predict a considerably higher solubility with undersaturation of the solid phase, whereas Nagra predict a low solubility and oversaturation. The differences are due to the inclusion in the HATCHES (AEA) database of Sn(IV) hydrolysis products.

The predicted solubility of Sn is heavily dependent on the database used, the two organisations calculate solubilities varying by over 25 orders of magnitude! The AEA Sn database has been tested against in-house Sn experimental work (BAYLISS et al., 1989) and found to correctly predict Sn solubility over a range of pH conditions including the very high pH values being modelled for the Maqarin site. This additional experimental evidence supports the inclusion of Sn(IV) hydrolysis products in the database and the AEA database is therefore probably more appropriate in this instance.

Uranium

There is little consensus between the four participating groups with respect to the predictions of U speciation and controlling solid phase (table 5.7) and a similar situation was also evident in the Oman study (BATH et al., 1987; McKINLEY et al., 1988). In general, however, the results of this study are a little more consistent, with $CaUO_4$ predicted as the predominant controlling solid, in agreement with the conclusions of LEMIRE (1988) for U in high pH solutions. That work, however, also reported UO_2 as the likely controlling solid under strongly reducing conditions, in agreement with the ONHY predictions at lower pe (which consistently differ from the other three groups here). It should be noted, however, that $CaUO_4$ is absent from the ONHY database.

Table 5.5 Predicted selenium speciation: comparison of 4 calculations

SELENIUM MQ2 pH=12.26, pe=5.2	**AEA**	**Nagra**	**ONHY**	**PSI**
Aqueous species (%)				
SeO_4^{2-}	100	100	3	100
SeO_3^{2-}			97	
Solubility controlling solid (saturation index)				
$CaSeO_4$	-7.6	-7.5	-	-7.6
Se			+163.7	

SELENIUM MQ5 pH=12.44, pe=2.05	**AEA**	**Nagra**	**ONHY**	**PSI**
Aqueous species (%)				
SeO_4^{2-}	49	49	-	53
SeO_3^{2-}	51	51	100	47
Solubility controlling solid (saturation index)				
$CaSeO_3$	-5.5	-5.5	-	-5.6
Se			+152.4	

SELENIUM ADIT A-6 pH=12.5, pe=0	**AEA**	**Nagra**	**ONHY**	**PSI**
Aqueous species (%)				
SeO_3^{2-}	100	100	18	100
Se^{2-}			82	
Solubility controlling solid (saturation index)				
$CaSeO_3$	-5.3	-5.5	-	-5.3
Se			+145.3	

pe=-4	**AEA**	**Nagra**	**ONHY**	**PSI**
Aqueous species (%)				
SeO_3^{2-}	100	100		100
Se^{2-}			100	
Solubility controlling solid (saturation index)				
$CaSeO_3$	-5.3	-5.5	-	-5.3
Se	-	-	+137.3	-

pe=-8	**AEA**	**Nagra**	**ONHY**	**PSI**
Aqueous species (%)				
HSe^-	99	99		99
Se^{2-}	1	1	100	1
Solubility controlling solid (saturation index)				
Se	-3.9	-4.0	+129.3	-4.0

Table 5.6 Predicted tin speciation: comparison of 2 calculations

TIN MQ2 pH=12.26, pe=5.2

	AEA	**Nagra**
Aqueous species (%)		
$Sn(OH)_6^{2-}$	76	
$Sn(OH)_5^-$	24	
$Sn(OH)_3^-$		100
Solubility controlling solid (saturation index)		
SnO_2	-3.3	+34.7

TIN MQ5 pH=12.44, pe=2.05

	AEA	**Nagra**
Aqueous species (%)		
$Sn(OH)_6^{2-}$	84	
$Sn(OH)_5^-$	15	
$Sn(OH)_3^-$		100
Solubility controlling solid (saturation index)		
SnO_2	-3.7	+28.5

TIN ADIT A-6 pH=12.5, pe=0

	AEA	**Nagra**
Aqueous species (%)		
$Sn(OH)_6^{2-}$	84	
$Sn(OH)_5^-$	15	
$Sn(OH)_3^-$		100
Solubility controlling solid (saturation index)		
SnO_2	-3.8	+21.6

NAGRA predict that as the pe is reduced to -4 and -8, SnO_2 becomes slightly more soluble with the saturation index changing from +13.6 to 5.6. The aqueous speciation remains the same. Harwell predict no change with pe.

Table 5.7 Predicted uranium speciation: comparison of 4 calculations

URANIUM MQ2 pH=12.26, pe=5.2

	AEA	Nagra	ONHY	PSI
Aqueous species (%)				
$UO_2(OH)_4^{2-}$	67	-	100	-
$UO_2(OH)_2^{o}$	33	-	-	14
$UO_2(OH)_3^{-}$	-	100	-	81
$(UO_2)_3(OH)_7^{-}$	-	-	-	4
Solubility controlling solid (saturation index)				
$CaUO_4$	+10.3	+7.5	-	+10.4
$UO_2(OH)_2$	-	-	-33.7	-

URANIUM MQ5 pH=12.44, pe=2.05

	AEA	Nagra	ONHY	PSI
Aqueous species (%)				
$UO_2(OH)_4^{2-}$	86	-	100	4
$UO_2(OH)_2^{o}$	14	-	-	10
$UO_2(OH)_3^{-}$		100	-	86
Solubility controlling solid (saturation index)				
$CaUO_4$	+10.4	+7.8	-	+10.3
$UO_2(OH)_2$	-	-	-34.1	-

URANIUM ADIT A-6 pH=12.5, pe=0

	AEA	Nagra	ONHY	PSI
Aqueous species (%)				
$UO_2(OH)_4^{2-}$	87	-	100	-
$UO_2(OH)_2^{o}$	13	-	-	-
$UO_2(OH)_3^{-}$	-	100	-	100
Solubility controlling solid (saturation index)				
$CaUO_4$	+10.2	+4.5	-	+7.4
$UO_2(OH)_2$	-	-	-34.1	-

Table 5.7 cont.

pe=-4

	AEA	**Nagra**	**ONHY**	**PSI**
Aqueous species (%)				
$UO_2(OH)_4^{2-}$	85	-	100	-
$UO_2(OH)_2^{o}$	13	-	-	-
$UO_2(OH)_3^{-}$	-	100	-	100
$UO_2(OH)_4^{?}$	2	-	-	-
Solubility controlling solid (saturation index)				
$CaUO_4$	+10.2	+4.5	-	+7.4
UO_2, uraninite	-	-	-31.7	-

pe=-8

	AEA	**Nagra**	**ONHY**	**PSI**
Aqueous species (%)				
$UO_2(OH)_4^{2-}$	-	-	100	-
$UO_2(OH)_3^{-}$	-	64	-	-
$UO_2(OH)_2^{-}$	2	32	-	-
$U(OH)_5^{-}$	7	2	-	100
$U(OH)_4^{o}$	91	-	-	-
$UO_2(CO_3)_3^{5-}$	-	2	-	-
Solubility controlling solid (saturation index)				
$CaUO_4$	-	+4.3	-	+1.5
$UO_2(OH)_2$	-	-	-	-
UO_2, uraninite	-	-	-23.7	-
U_4O_9	+7.9	-	-	-

It is interesting to note the predicted presence of $U(OH)_5^-$ by some groups at pe = -8. There is still considerable doubt as to the actual existence of $U(OH)_5^-$ (see discussion in BRUNO et al., 1987 and NEA, 1990).

5.3.2 Results of the interpretive modelling

In this part of the study, measured trace element concentrations were used in the modelling. Equilibrations were carried out to assess how saturated the groundwaters were with respect to the elements of interest, and to identify a range of possible

solubility limiting phases. The results of these equilibrations were then compared to the analytical data and it was possible to assess how well the codes were performing under the very high pH conditions being modelled. It was also possible to identify possible weaknesses in the solids databases which it might be possible to follow up in future work. Because of difficulties in measuring Eh values in the field, modelling was carried out at pe values of -4 and -8 as well as the measured values. It was thought that, in doing so, the range of likely redox conditions would be covered. Most of the elements considered are insensitive to redox variation over this range of pe values but Se and U did show significant variation.

For certain elements, comparison between modelling groups may show some minor differences to those described in the previous section. This is because the databases used by AEA for some of the elements were updated between stages ii) and iii) of the modelling study.

A major benefit to this modelling study of Maqarin was that, in addition to the groundwater chemistry there were detailled supporting mineralogical data. Thus the predicted solubility limiting phases could be directly compared with the minerals identified from field samples. The minerals identified from Maqarin were classified into primary and secondary mineral assemblages. The primary assemblage is believed to have formed by combustion of a limestone. Interaction of this primary mineral assamblage with groundwater has resulted in the formation of the secondary mineral assemblage. The concentrations of the elements in solution at any one time are controlled by all or some of the following: dissolution/precipitation, the solubility limit, the amount of contact between the groundwater and the mineral grains. In simplistic terms, the primary mineral assemblage may be regarded as the dominant source of the major and trace elements in solution whereas the secondary mineral assemblage is a sink for these elements.

There was very good agreement between the minerals predicted by the models to control major element chemistry in the groundwaters and those observed in the field samples. Some of the important minerals as indicated by the models were portlandite ($CA(OH)_2$), gypsum ($CaSO_4$), calcite ($CaCO_3$) and brucite ($Mg(OH)_2$), among others. These minerals, or close equivalents, were all observed in the field, either within the primary or the secondary mineral assemblages. The major element chemistry would appear therefore to be controlled locally and not by some "distant" lithology through which the water has passed prior to arrival at the sampling site. The trace element chemistry is likely also to be controlled locally, confirming that this area is appropriate to test models of trace element behaviour in hyperalkaline conditions.

For clarity, the results of the trace element modelling are discussed in the following text on an element by element basis.

Nickel

The Ni concentrations used in the modelling were all analytical data except for MQ2 which was an estimate based on the measured value for the chemically similar MQ7 groundwater. The results of the modelling are shown in table 5.8. NAGRA and ONHY both predict that the aqueous species $Ni(OH)_3^-$ dominates the solution (>98%) in all cases with a minor contribution from $Ni(OH)_2^o$. As in section 5.3.1, PSI predict $Ni(OH)_3^-$ to be less dominant (around 90%), with the species $Ni(OH)_4^{2-}$ making most of the remainder and a very minor contribution from $Ni(OH)_2^o$. The results differ due to the inclusion of the extra aqueous species $Ni(OH)_4^{2-}$ and an extra solid, NiO, in the PHREEQE NAI0289 database (amended to include the data of BAEYENS and McKINLEY, 1989). AEA similarly amended the HATCHES database (ie version 2.1 to version 3.0) between the earlier work and the present and so also report the same results. Interestingly, HATCHES (version 3.0) had previously predicted experimental Ni solubility data reasonably well (PILKINGTON and STONE, 1990).

BAES and MESMER (1976) indicate that $Ni(OH)_4^{2-}$ may well be important at higher pH values and so, in this respect, the AEA and PSI predictions , may be more representative of Ni in the Maqarin groundwaters. $NIO_{(s)}$ was included by BAYENS and McKINLEY (1989) due to the rather uncertain solubility of $Ni(OH)_{2(s)}$ as included in the other databases mentioned here.

In table 5.8, the saturation indices for a number of possible Ni solids are given. With the exeption of ONHY, the calculations predict that the groundwaters are undersaturated with respect to NiO (bunsenite) and $Ni(OH)_2$. OHNY predict only very minor oversaturation with respect to bunsenite. The discrepancies in the degree of over or under saturation predicted by the different orangisations is probably related to uncertainty regarding the assumed degree of crystallinity of these phases.

The Ni-bearing silicate and oxide minerals are generally oversaturated. Ni silicate minerals such as olivine and pyroxene occur in high pressure/temperature geological situations and are not present at Maqarin. It is unlikely, therefore, that these phases will be important source or sink phases for Ni. A further low solubility phase is the Ni-bearing spinel, $NiFe_2O_4$. Although, this phase does not form by precipitation in low temperature systems (as confirmed in the Poços de Caldas study, BRUNO et al., 1991), it is present in the (metamorphosed) source rock here at Maqarin.

Mineralogical descriptions of the Maqarin rocks (chapter 4 and appendix C) record the presence of other spinel phases such as the Fe end member, magnetite, in the primary mineral assemblages. It is possible that nickel might be present in trace quantities in this magnetite. The solutions are undersaturated with respect to magnetite. It is possible that a mixed spinel phase, between the two end-members mentioned above, might be the phase controlling Ni solubility in the system.

As stated above, the mineralogical descriptions also indicate an abundance of another Fe-bearing spinel, ferrite, in the primary mineral assemblage. This ferrite contains relatively high concentrations of various trace elements and may act as a source phase for Ni. If this is the case, coprecipitation of Ni with ferrite may be a more important control on Ni levels in solution than dissolution of the primary mineral, magnetite.

Table 5.8 Results of interpretive modelling: NICKEL

NICKEL MQ2 pH=12.53
pe=5.2

	AEA	Nagra	ONHY	PSI
Aqueous species (%)				
$Ni(OH)_3^-$	92	98	98	94
$Ni(OH)_4^{2-}$	6	-	-	6
$Ni(OH)_2o$	2	2	2	-
Solubility controlling solid (saturation index)				
NiO, bunsenite	-2.9	-	0.1	-2.9
$Ni(OH)_2$	-1.2	-1.2	-	-3.2
Ni_2SiO_4	-5.4	-	0.3	-
$NiFe_2O_4$, trevorite	4.3	-		8.7
$NiSiO_3$	-	-		2.9

No change from above for pe=-4, -8

NICKEL MQ5 pH=12.60
pe=2.05

	AEA	Nagra	ONHY	PSI
Aqueous species (%)				
$Ni(OH)_3^-$	91	98	98	92
$Ni(OH)_4^{2-}$	7	-	-	8
$Ni(OH)_2^o$	2	2	2	-
Solubility controlling solid (saturation index)				
NiO, bunsenite	-2.3	-	0.7	-2.3
$Ni(OH)_2$	-0.7	-0.3	-	-2.6
Ni_2SiO_4	-4.6	-	1.1	-
$NiFe_2O_4$, trevorite	4.7	-		7.1
$NiSiO_3$	-	-		0.5

No change from above for pe=-4, -8

Table 5.8 cont.

NICKEL MQ6 pH=12.71
pe=2.17

	AEA	**Nagra**	**ONHY**	**PSI**
Aqueous species (%)				
$Ni(OH)_3^-$	89	99	99	90
$Ni(OH)_4^{2-}$	10	-	-	10
$Ni(OH)_2^o$	1	1	1	-
Solubility controlling solid (saturation index)				
NiO, bunsenite	-2.6	-	0.5	-2.5
$Ni(OH)_2$	-0.9	-0.9	-	-
Ni_2SiO_4	-5.2	-	0.5	-
$NiFe_2O_4$, trevorite	4.3	-		-
$NiSiO_3$	-	-		-

No change from above for pe=-4, -8

NICKEL MQ7 pH=12.67
pe=2.0

	AEA	**Nagra**	**ONHY**	**PSI**
Aqueous species (%)				
$Ni(OH)_3^-$	90	98	98	92
$Ni(OH)_4^{2-}$	8	-	-	8
$Ni(OH)_2^o$	2	2	2	-
Solubility controlling solid (saturation index)				
NiO, bunsenite	-2.9	-	0.1	-2.9
$Ni(OH)_2$	-1.3	-1.3	-	-3.2
Ni_2SiO_4	-5.9	-	0.7	-
$NiFe_2O_4$, trevorite	4.0	-		-
$NiSiO_3$	-	-		-

No change from above for pe=-4, -8

Lead

The Pb concentrations used in the modelling corresponded to the limits of detection of the analytical technique used (table 5.3). AEA and NAGRA results are identical with $Pb(OH)_3^-$ being the sole aqueous species (table 5.9). PSI also predicts this species to be dominant (93-94%) along with $Pb(OH)_2^0$ as a minor species. ONHY predict that the species $Pb(OH)_4^{2-}$ plays the dominant role (94-96%) with the remainder of aqueous Pb being present as $Pb(OH)_3^-$.

All four organisations predict that $Pb(OH)_2$ is the controlling solid. However, there are differences in the predicted solubility of this phase. AEA, NAGRA and PSI predict undersaturation (negative saturation indices in the range -4.8 to -5.0) in all the groundwaters, whereas ONHY calculates oversaturation (saturation indices of +1.0 to +1.4). The main reason for this difference is the use of different solubility products for $Pb(OH)_2$. The solubility product used by AEA and Nagra has been used to predict with accuracy experimental results under similar conditions (CROSS et al., 1987) and is therefore more likely to be correct in this instance. It is worth noting that the difference between the ONHY predicted solubilty and the results would be greater were it not for the presence on an extra species, $Pb(OH)_4^{2-}$, in the ONHY database. This should, of course, decrease the ONHY saturation indices.

Generally, the predicted high solubility of Pb under hyperalkaline conditions is compatible with the analyses by BAES and MESMER (1976) and the experimental studies of BAYLISS et al. (1988). Both BAES and MESMER (1976) and BROOKINGS (1988) indicate the presence of plumbate ($Pb(OH)_6^{2-}$) at high pH, a species that is also absent from the databases considered here.

At low pe values (<-8) the solubility of PbS_2 is reduced and it was noted that this phase may become important as a Pb solubility controlling phase.

Mineralogical descriptions of the Maqarin rock solid phases indicate that Pb is associated with a primary Cu.K selenide phase, sphalerite, pyrite and ferrites but that no $Pb(OH)_2$ was recorded. This implies that, regardless of the solubility results, the databases are a poor reflection of the (admittedly complex) field mineralogy.

Radium

The Ra concentrations used in the modelling were all analytical data except for MQ7 which used the Ra value for the chemically similar MQ1 groundwater. AEA and Nagra carried out modelling on radium speciation. Nagra predicts Ra^{2+} (94-95 %) as the main aqueous species along with $RaOH^+$ (5-6 %), and $RaSO_4$ as the controlling solid (table 5.10). It should be noted however that this Nagra database was limited (Ra^{2+}, $RaOH^+$ and $RaSO_4^0$ were the only aqueous species, and only the solid $RaCO_3$ and $RaSO_4$ were included). Calculations carried out at AEA included additional data from BENSON

Table 5.9 Results of interpretive modelling: LEAD

LEAD MQ2 pH=12.53
pe=5.2

	AEA	Nagra	ONHY	PSI
Aqueous species (%)				
$Pb(OH)_3^-$	100	100	6	96
$Pb(OH)_2^o$	-	-	-	4
$Pb(OH)_4^{2-}$	-	-	94	-
Solubility controlling solid (saturation index)				
$Pb(OH)_2^o$	-4.8	-4.8	1.4	-4.8
PbO	-5.7	-	-	-

No change from above for pe=-4, -8

LEAD MQ5 pH=12.60
pe=2.05

	AEA	Nagra	ONHY	PSI
Aqueous species (%)				
$Pb(OH)_3^-$	100	100	4	97
$Pb(OH)_2^o$	-	-	-	3
$Pb(OH)_4^{2-}$	-	-	96	-
Solubility controlling solid (saturation index)				
$Pb(OH)_2^o$	-4.9	-4.9	1.2	-5.0
PbO	-5.7			

No change from above for pe=-4, -8

LEAD MQ6 pH=12.71
pe=2.17

	AEA	Nagra	ONHY	PSI
Aqueous species (%)				
$Pb(OH)_3^-$	100	100	3	97
$Pb(OH)_2^o$	-	-	-	3
$Pb(OH)_4^{2-}$	-	-	97	-

Table 5.9 cont.

	AEA	Nagra	ONHY	PSI
Solubility controlling solid (saturation index)				
$Pb(OH)_2^0$	-5.0	-5.0	1.0	-5.0
PbO	-5.9	-	-	-

No change from above for pe=-4, -8

LEAD MQ7 pH=12.67

pe=2.00

	AEA	Nagra	ONHY	PSI
Aqueous species (%)				
$Pb(OH)_3^-$	100	100	4	97
$Pb(OH)_2^0$	-	-	-	3
$Pb(OH)_4^{2-}$	-	-	96	-
Solubility controlling solid (saturation index)				
$Pb(OH)_2^0$	-5.0	-5.0	1.2	-4.8
PbO	-5.8	-	-	-

No change from above for pe=-4, -8

and TEAGUE (1980) and LANGMUIR and RIESE (1985). These data included a modified constant for $RaSO_4^0$, extra aqueous species ($RaCO_3^0$ and $RaCl^+$) and additional solids (Ra and $RaCl_2$, $2H_2O$) as well as modified constants for the previously considered solids. These simulations showed different speciation, predicting 75 % Ra^{2+}, 20 % $RaSO_4^0$ and 4 % $RaOH^+$. The identity of the solubilty controlling phase remained the same, but it became slightly more soluble with the addition of the extra species. The aqueous speciation of Ra is influenced by the major element chemistry of the groundwaters. The presence of high concentrations of SO_4^{2-} in MQ5 and MQ6 is reflected by the increased level of $RaSO_4^0$ (to almost 50% according to AEA modelling). Ra is however generally present as Ra^{2+}, with minor contribution from $RaOH^+$.

The solubility controlling solid is predicted to be $RaSO_4$ by both modelling organisations. In each case it is slightly undersaturated with saturation indices in the range -2.8 to -3.6 (as a consequence of the differences in calculated aqueous speciation).

Table 5.10 Results of interpretive modelling: RADIUM

RADIUM MQ2 pH=12.53
pe=5.2

	AEA	Nagra
Aqueous species (%)		
Ra^{2+}	77	95
$RaSO_4^o$	19	-
$Ra(OH)^+$	4	5
Solubility controlling solid (saturation index)		
$RaSO_4$	-3.1	-2.8
No change from above for pe=-4, -8		

RADIUM MQ5 pH=12.60
pe=2.05

	AEA	Nagra
Aqueous species (%)		
Ra^{2+}	53	95
$RaSO_4^o$	44	-
$Ra(OH)^+$	3	5.0
Solubility controlling solid (saturation index)		
$RaSO_4$	-3.2	-2.8
No change from above for pe=-4, -8		

RADIUM MQ6 pH=12.76
pe=2.17

	AEA	Nagra
Aqueous species (%)		
Ra^{2+}	50	94
$RaSO_4^o$	46	-
$Ra(OH)^+$	4	6
Solubility controlling solid (saturation index)		
$RaSO_4$	-3.2	-2.8
No change from above for pe=-4, -8		

RADIUM MQ7 pH=12.67
pe=2.0

	AEA	Nagra
Aqueous species (%)		
Ra^{2+}	76	94
$RaSO_4^o$	18	-
$Ra(OH)^+$	6	6
Solubility controlling solid (saturation index)		
$RaSO_4$	-3.6	-3.4
No change from above for pe=-4, -8		

Pure Ra solids are rarely observed in natural systems and Ra is normally incorporated in co-precipitates or solid solutions with other alkaline earth elements. Mineralogical data indicates the presence of abundant gypsum, $CaSO_4$, and baryte, $BaSO_4$, in the secondary mineral assemblages at Maqarin. It is thus possible that these minerals are controlling the Ra solubility. The presence of Ra in calcite and primary ferrites, in analogy to Ba, should also not be ruled out. The predicted solubilities should thus be overestimates.

Thorium

The Th concentrations used in the modelling ($0.1\mu gl^{-1}$, table 5.3) were assumed values which were less than the limits of detection ($0.2\mu gl^{-1}$) of the analytical technique employed to measure Th levels. $Th(OH)_4^o$ is the sole aqueous species predicted by all four organisations in all four groundwaters (table 5.11).

ThO_2 is calculated to be the solubility controlling phase in all cases. All the solutions are oversaturated with respect to this solid. The degree of oversaturation is related to whether or not amorphous or crystalline ThO_2 is selected and it is more likely that the amorphous phase will be present at these low temperatures. So far, mineralogical studies of the rocks have recorded neither the presence of ThO_2 nor the presence of Th as a discrete phase within any of the other minerals present. It is tempting to suggest, for such a simple system, that further work be carried out to define the actual Th concentration in these waters, but it is possible that Th is source term limited and hence such evaluation is pointless.

Selenium

The Se concentrations used in the modelling (table 5.3) are all analytical data, except for the value for the MQ2 water. The MQ2 value was estimated based on the data for the chemically similar MQ7 water. The results of Se speciation calculation are rather complex as predicted Se speciation shows strong variation with Eh at this pH (table 5.12). The AEA, NAGRA and PSI results are identical, reflecting the use of the same source of Se data. The source of the Se data in the MINTEQA1 database used by ONHY is not known and it lacks certain solution species which are predicted to be important, such as HSe-. The constant for the reaction between SeO_4^{2-} and $HSeO_3^{2-}$ also differs by eight orders of magnitude between the two compilations.

Table 5.11 Results of interptretive modelling: THORIUM

THORIUM MQ2 pH=12.53
pe=5.2

	AEA	Nagra	ONHY	PSI
Aqueous species (%)				
$Th(OH)_4^o$	100	100	100	100
Solubility controlling solid (saturation index)				
$Th(OH)_2$ (amorphous)	0.2	0.2	3.2	0.2
$Th(OH)_2$ (crystalline)	4.7	-	3.2	-
No change from above for pe=-4, -8				

THORIUM MQ5 pH=12.60
pe=2.05

	AEA	Nagra	ONHY	PSI
Aqueous species (%)				
$Th(OH)_4^o$	100	100	100	100
Solubility controlling solid (saturation index)				
$Th(OH)_2$ (am)	0.2	0.2	3.3	0.2
$Th(OH)_2$ (cr)	4.7	-	3.3	-
No change from above for pe=-4, -8				

THORIUM MQ6 pH=12.71
pe=2.17

	AEA	Nagra	ONHY	PSI
Aqueous species (%)				
$Th(OH)_4^o$	100	100	100	100
Solubility controlling solid (saturation index)				
$Th(OH)_2$ (am)	0.2	0.2	3.3	0.2
$Th(OH)_2$ (cr)	4.7	-	3.3	-
No change from above for pe=-4, -8				

THORIUM MQ7 pH=12.67
pe=2.0

	AEA	Nagra	ONHY	PSI
Aqueous species (%)				
$Th(OH)_4^o$	100	100	100	100
Solubility controlling solid (saturation index)				
$Th(OH)_2$ (am)	0.2	0.2	3.3	0.2
$Th(OH)_2$ (cr)	4.7	-	3.3	-
No change from above for pe=-4, -8				

At higher pe values, the species SeO_4^{2-} and SeO_3^{2-} are dominant. AEA, NAGRA and PSI predict approximately 60 - 85 % of Se will be present as SeO_4^{2-} in most of the groundwaters at the measured pe values. MQ2 is predicted to be 100% SeO_4^{2-}. This is because of the higher pe value associated with this groundwater. In contrast, ONHY predict that 95 - 100 % of Se at these pe values is present as SeO_3^{2-} with the remainder as Se^{2-}.

At pe = -4 AEA, NAGRA and PSI predict SeO_3^{2-} as the sole aqueous species. ONHY predict Se^{2-} as the sole species. At pe = -8 AEA, NAGRA and PSI predict HSe^- as the dominant aqueous species with only a very minor contribution from Se^{2-}. ONHY, however, predict that Se^{2-} is still the sole aqueous species. When the predicted solubility-limiting phases are compared, again there are differences between the predictions of ONHY and the other modelling groups. The calculations of NAGRA, AEA and PSI predict that the identity of the controlling phases changes as the redox conditions change. At high pe values, $CaSeO_3$ and $CaSeO_4$ are the predicted solubility controlling phases. The solutions are undersaturated with respect to the phases.

As the pe is reduced, Fe selenide phases become important and are oversaturated in solution. The Fe content of the groundwaters has been estimated so the saturation index of pure Se has also been given in the tables. These data clearly indicate how important it is obtain the Fe content of the solutions when predicting Se solubility.

The ONHY results predict massive oversaturation with respect to elemental Se under all redox conditions. The numerical values of the saturation indices calculated by ONHY should not be taken at face value; S.I. numbers greater than 10 or 15 simply represent negligible solubility. This prediction conflicts with the field observation suggesting that the compilation of BAEYENS and McKINLEY (1989) is a more appropriate source of thermodynamic data for these conditions.

Mineralogical data (table 4.1.1.) indicate the presence of oldhamite (CaS) containing high Se levels and also a Cu, K selenide mineral in the primary mineral assemblage of the Maqarin rocks. An analogue of the latter, K_2Se, has a saturation index of >-70 at pe values of 2 and above according to AEA modelling. The saturation index increases to around -20 at lower pe values but is still very undersaturated. This implies that such a mineral would be extremely soluble in these solutions. This is consistent with the observation that it disappears immediately on contact with the circulating groundwaters of the area. This mineral is probably not present in large enough quantities to saturate the groundwater, explaining the large degrees of undersaturation.

$CaSeO_4$ has been identified in the secondary mineral assemblages, confirming that it may be an important control on subsequent Se solubility at Maqarin.

Table 5.12 Results of interpretive modelling: SELENIUM

SELENIUM MQ2 pH=12.53
pe=5.2

	AEA	**Nagra**	**ONHY**	**PSI**
Aqueous species (%)				
SeO_4^{2-}	100	100	9	100
SeO_3^{2-}			91	
Solubility controlling solid (saturation index)				
$CaSeO_3$	-9.0		-2.4	
$CaSeO_4$	-5.0	-5.0	27.3	-5.0
K_2Se	-99.9			
Se				
Fe_3Se_4				
$FeSe_2$				

pe=-4

	AEA	**Nagra**	**ONHY**	**PSI**
Aqueous species (%)				
SeO_4^{2-}				
SeO_3^{2-}	100	100		100
Se^{2-}			100	
Solubility controlling solid (saturation index)				
$CaSeO_3$	-2.6	-2.5		-2.6
$CaSeO_4$	-16.9	-17.4	-2.7	
K_2Se	-38.2			
Se	-5.1	-3.5	134.6	
Fe_3Se_4				
$FeSe_2$				

pe=-8

	AEA	**Nagra**	**ONHY**	**PSI**
Aqueous species (%)				
SeO_4^{2-}				
SeO_3^{2-}				
HSe^-	99	99		99
Se^{2-}	1	1	100	1
Solubility controlling solid (saturation index)				
$CaSeO_3$	-14.7	-16.6		
$CaSeO_4$	-37.0			
K_2Se	-26.4			
Se	-1.2	-1.6	126.6	-1.3
Fe_3Se_4	-3.1	-0.8		
$FeSe_2$	2.2			2.3

SELENIUM MQ5 pH=12.60

pe=2.05

	AEA	Nagra	ONHY	PSI
Aqueous species (%)				
SeO_4^{2-}	67	56		66
SeO_3^{2-}	33	44	95	34
Se^{2-}			5	
Solubility controlling solid (saturation index)				
$CaSeO_3$	-2.5		-2.0	-3.8
$CaSeO_4$	-4.6	-4.7		
K_2Se	-71.7			
Se			147.2	
Fe_3Se_4				
$FeSe_2$				

pe=-4

	AEA	Nagra	ONHY	PSI
Aqueous species (%)				
SeO_4^{2-}				
SeO_3^{2-}	100	100		100
Se^{2-}			100	
Solubility controlling solid (saturation index)				
$CaSeO_3$	-2.0	-2.1		-2.1
$CaSeO_4$	-16.2		-2.1	
K_2Se	-34.9			
Se	-5.1		134.6	
Fe_3Se_4				
$FeSe_2$				

pe=-8

	AEA	Nagra	ONHY	PSI
Aqueous species (%)				
SeO_4^{2-}				
SeO_3^{2-}				
HSe^-	99	99		99
Se^{2-}	1	1	100	1
Solubility controlling solid (saturation index)				
$CaSeO_3$	-13.6			
$CaSeO_4$	-35.8			
K_2Se	-22.5			
Se	-0.7	-0.8	126.6	-0.8
Fe_3Se_4	-1.8	-1.7*		
$FeSe_2$	3.0			2.0

* Changes to -0.4 when the field pH is used.

SELENIUM MQ6 pH=12.71

pe=2.17

	AEA	Nagra	ONHY	PSI
Aqueous species (%)				
SeO_4^{2-}	85	77		84
SeO_3^{2-}	15	23	99	16
Se^{2-}				
Solubility controlling solid (saturation index)				
$CaSeO_3$	-2.8		-1.9	-2.8
$CaSeO_4$	-4.4	-4.4		
K_2Se	-73.1			
Se			148.2	
Fe_3Se_4				
$FeSe_2$				

pe=-4

	AEA	Nagra	ONHY	PSI
Aqueous species (%)				
SeO_4^{2-}				
SeO_3^{2-}	100	100		100
Se^{2-}			100	
Solubility controlling solid (saturation index)				
$CaSeO_3$	-1.9	-2.0	-	-2.0
$CaSeO_4$	-15.9		-1.5	
K_2Se	-35.2			
Se	-5.6		134.9	
Fe_3Se_4				
$FeSe_2$				

pe=-8

	AEA	Nagra	ONHY	PSI
Aqueous species (%)				
SeO_4^{2-}				
SeO_3^{2-}				
HSe^-	99	98		99
Se^{2-}	1	2	100	1
Solubility controlling solid (saturation index)				
$CaSeO_3$	-12.8			
$CaSeO_4$	-34.7			
K_2Se	-22.0			
Se	-0.4	-0.5	126.9	-0.5
Fe_3Se_4	-2.1	-2.0		
$FeSe_2$	3.0			3.1

SELENIUM MQ7 pH=12.67

pe=2.0

	AEA	Nagra	ONHY	PSI
Aqueous species (%)				
SeO_4^{2-}	67	63		67
SeO_3^{2-}	31	37	98	33
Se^{2-}			2	
Solubility controlling solid (saturation index)				
$CaSeO_3$	-3.3		-2.6	-3.4
$CaSeO_4$	-5.4	-5.4		
K_2Se	-75.5			
Se			147.8	
Fe_3Se_4				
$FeSe_2$				

pe=-4

	AEA	Nagra	ONHY	PSI
Aqueous species (%)				
SeO_4^{2-}				
SeO_3^{2-}	100	100		100
Se^{2-}			100	
Solubility controlling solid (saturation index)				
$CaSeO_3$	-2.8	-2.9	-	-2.9
$CaSeO_4$	-16.9		-2.1	
K_2Se	-39.0			
Se	-6.2		135.1	
Fe_3Se_4				
$FeSe_2$				

pe=-8

	AEA	Nagra	ONHY	PSI
Aqueous species (%)				
SeO_4^{2-}				
SeO_3^{2-}				
HSe^-	99	99		99
Se^{2-}	1	1	100	1
Solubility controlling solid (saturation index)				
$CaSeO_3$	-14.0			
$CaSeO_4$	-36.0			
K_2Se	-26.2			
Se	-1.3	-1.4	127.1	-1.4
Fe_3Se_4	-5.1			
$FeSe_2$	1.5			1.5

The significance of elemental Se should not, however, be overlooked. Elemental Se has been identified in the (unaltered), bituminous limestone and in pyrite at Maqarin (section 4.1.) Not only is Se seen to be the predicted solubility limiting solid at intermediate pe values, but has also been indicated as the probable solubility controlling solid in another, similar, study of Se in hyperalkaline groundwaters (McKINLEY et al., 1988). This study did, however, question the validity of the equilibrium thermodynamic approach used here, partly due to the expected kinetic constraints on redox equilibrium in the Se system. Nevertheless, elemental Se is known to form under reducing conditions (often in association with microbial SO_4^{2-} reduction; GRANGER and WARREN, 1969; WERES et al., 1989) and has been suggested as the Se solubilty controlling phase in a range of reducing groundwaters (BAEYENS and McKINLEY, 1989). Certainly, Se may be involved in the microbiological cycle in the Maqarin groundwaters (see section 4.5).

Tin

The Sn concentrations used in the modelling (table 5.3) were all measured values apart from the data for MQ2, the value for which was estimated based on the measured value for the chemically similar MQ7 groundwater. Sn modelling was carried out by AEA and NAGRA (table 5.13). AEA predict that $Sn(OH)_6^{2-}$ dominates speciation (85% or more) in all solutions at all pe values. NAGRA predict that $Sn(OH)_3^-$ is the sole aqueous species. The difference in the results is due to the inclusion in the HATCHES database of data for Sn(IV) hydrolysis products. Under high pH conditions, these have been shown to be important at temperatures above 100C (KURIL'CHIKOVA and BARSUKOV, 1970). The solubility of SnO_2 (cassiterite) has been shown to increase at high pH associated with the appearance of the Sn(IV) species $Sn(OH)_5^-$ (BARSUKOV and KLINTSOVA, 1970).

Both AEA and NAGRA predict SnO_2 as the controlling solid: AEA predict a considerably higher solubility and undersaturation of the solid phase (saturation indices from -3 to -4). NAGRA predict a very low solubility and oversaturation (saturation indices in excess of +25) and also predict that solubility is redox sensitive with the saturation indices decreasing to less than +9 over the pe range modelled.The AEA Sn database has been tested against Sn experimental work performed at Harwell (BAYLISS et al., 1989) and found to predict correctly Sn solubility over a range of pH conditions, including the very high pH values being modelled at Maqarin. This additional experimental evidence supports the inclusion of Sn(IV) hydrolysis products in the database so the AEA database is therefore probably more appropriate in this instance (and is certainly more conservative).

Mineralogical data on the Maqarin rocks do not indicate the presence of discrete Sn in any of the solids analysed. The predicted solubility limiting phase, cassiterite, is more usually found associated with high temperature hydrothermal mineralisation and igneous activity (CRAIG and VAUGHAN, 1981), not limestone environments.

Table 5.13 Results of interpretive modelling: TIN

TIN MQ2 pH=12.53
pe=5.2

	AEA	**Nagra**
Aqueous species (%)		
$Sn(OH)_6^{2-}$	85	
$Sn(OH)_5^-$	14	
SnO_3^{2-}	1	
$Sn(OH)_3^-$		100
Solubility controlling solid (saturation index)		
SnO_2	-3.8	29.6
$Sn(OH)_4$	-11.3	-

NAGRA predict that as the pe is reduced to -4 and -8, SnO_2 becomes more soluble with the saturation index changing from 16.6 to 8.6. The aqueous speciation remains the same. Harwell predict no change with pe.

TIN MQ5 pH=12.60
pe=2.05

	AEA	**Nagra**
Aqueous species (%)		
$Sn(OH)_6^{2-}$	88	
$Sn(OH)_5^-$	11	
SnO_3^{2-}	1	
$Sn(OH)_3^-$		100
Solubility controlling solid (saturation index)		
SnO_2	-4.0	28.6
$Sn(OH)_4$	-11.4	-

NAGRA predict that as the pe is reduced to -4 and -8, SnO_2 becomes more soluble with the saturation index changing from 16.6 to 8.6. The aqueous speciation remains the same. Harwell predict no change with pe.

TIN MQ6 pH=12.71
pe=2.17

	AEA	**Nagra**
Aqueous species (%)		
$Sn(OH)_6^{2-}$	91	
$Sn(OH)_5^-$	8	
SnO_3^{2-}	1	
$Sn(OH)_3^-$		100
Solubility controlling solid (saturation index)		
SnO_2	-4.3	28.9
$Sn(OH)_4$	-11.7	-

NAGRA predict that as the pe is reduced to -4 and -8, SnO_2 becomes more soluble with the saturation index changing from 16.6 to 8.7. The aqueous speciation remains the same. Harwell predict no change with pe.

TIN MQ7 pH=12.67
pe=2.0

	AEA	Nagra
Aqueous species (%)		
$Sn(OH)_6^{2-}$	89	
$Sn(OH)_5^-$	10	
SnO_3^{2-}	1	
$Sn(OH)_3^-$		100
Solubility controlling solid (saturation index)		
SnO_2	-3.2	29.6
$Sn(OH)_4$	-10.7	-

NAGRA predict that as the pe is reduced to -4 and -8, SnO_2 becomes more soluble with the saturation index changing from 17.6 to 9.6. The aqueous speciation remains the same. Harwell predict no change with pe.

Uranium

The U concentrations used in the modelling were all measured. At high pe values (-4 and greater) the aqueous speciation is dominated by U(VI) hydrolysis products (see table 5.14). ONHY predict the presence of only $UO_2(OH)_4^{2-}$ whereas NAGRA predicts only $UO_2(OH)_3^-$. NAGRA is similar to ONHY with $UO_2(OH)_4^{2-}$ dominating the speciation but up to 11 % of the U speciation is predicted to be $UO_2(OH)_2^0$.

At pe = -8, the three groups predict a dominance of U(VI) species: NAGRA predicts $UO_2(OH)_2^-$ (~25 %) and $UO_2(OH)_3$ (~75 %) while AEA indicate a different dominant hydrolysis product, $UO_2(OH)_4^{2-}$ (75 - 90 %) with the remainder as the U(IV) species $U(OH)_4^0$. ONHY continues to predict the presence of only $UO_2(OH)_4^{2-}$.

Such discrepancies in the predictions of various databases are common in the high pH regime where anionic hydrolysis products are predicted to dominate the speciation.

Thermodynamic data for these complexes are estimated (CRAIG and VAUGHAN, 1981) and there is considerable debate as to the importance of this form of U species. An attempt was made to establish the U speciation in the Maqarin hyperalkaline groundwaters. Unfortunately the exchange columns used in the experiment degraded on contact with the hyperalkaline waters but, as the approach is nevertheless valid, this work will be repeated with more appropriate columns in the future when new samples are collected at Maqarin. Such work, even when successful, must be backed up with laboratory based studies of U speciation under appropriate conditions before the problems (inherent on utilising databases based on estimates, not measurements) with U databases can be fully addressed.

With the exception of ONHY, all the modelling organisations predict $CaUO_4$ as the solubility limiting phase over most of the pe range studied ($CaUO_4$ is not included in the MINTEQA1 database used by ONHY). This phase, although being the most stable thermodynamically, is rarely observed in nature, the formation of U-oxides being more common (LEMIRE, 1988). The groundwaters are predicted to be oversaturated with respect to this phase and there are a number of explanations for this oversaturation. The $CaUO_4$ phase represented in the database is a crystalline variety, if a less crystalline form was included which represented the observed phase more closely, a more realistic estimate of U concentrations could be calculated. An unidentified Ca-U phase, an oxide or a carbonate, has been identified in the primary mineral assemblage and may be acting as a source for U. U is widely observed within the secondary assemblage, generally incorporated as a trace component in hydrated silicate phases and ferric hydroxides. These phases, acting as sinks for U, may be a more important control on the U concentrations in solution.

Another explanation for the calculated oversaturation with respect to $CaUO_4$ is that U is present in colloidal form as was suggested in a previous study of hyperalkaline groundwaters (BATH et al., 1987) therefore causing overestimation of the

concentration of U in solution. However, study of the Maqarin groundwaters contradicts this, indicating that the colloids present do not contain significant quantities of U (section 4.5).

The data in table 5.14 indicate that the Maqarin waters are generally undersaturated with respect to uranium oxide phases. Thus, selection of an oxide or hydroxide as the solubility-limiting phase, as suggested by LEMIRE (1988) for a natural system, and in line with the choices for the other trace elements investigated during this project, would lead to a conservative prediction of uranium solubility, with the possible exception of the simulation at pe = -8 (≡ Eh~ -500 mV). However, the Eh values measured at the site are in the range +100 to +200 mV (verses Standard Hydrogen Electrode). It should be noted that the redox state of natural waters is notoriously difficult to specify (eg. LINDBERG and RUNNELS, 1984) and hyperalkaline groundwaters are even more problematic. The reaction of dominant redox buffers, such as the iron system, may by very slow under hyperalkaline conditions (GRAUER, 1988). Even in the "very reducing waters" of the Oman natural analogue study, where hydrogen gas bubbled from the groundwaters, the nitrogen and sulphur redox couples were out of equlibrium with each other and with electrode measured pe values.

Nevertheless, it seems unlikely that a swing of up to 700 mV, from the "measured" Eh to the calculated Eh will have occurred and so the simulations for U at p = -8 are probably unrealistic and the resultant predictions should be treated with extreme care.

Finally, it is worth noting that the complete change of the PSI U database between the predictive and interpretive phases of the work showed one thing: the new database is generally more conservative than the original with the degree of oversaturation of U dropping by four or five orders of magnitude more than can be explained by the change in the dissolved U concentration input to the codes.

Chromium

Calculations were carried out by AEA and ONHY (tables 5.15 and 5.16). This element was not studied as part of the predictive modelling work and was only included during the interpretive component as the very high concentrations observed in the groundwaters made it worthy of brief investigation.

Both organisations predict no change in the speciation with changing redox conditions (table 5.15). AEA predict that $Cr(OH)_4^-$ is the sole species present in all the groundwaters. In contrast, ONHY predict that the main species is CrO_4^{2-}, with minor contribution from $KCrO_4^-$ and $NaCrO_4^-$ depending on the chemistry of the groundwater concerned.

Table 5.14 Results of interpretive modelling: URANIUM

URANIUM MQ2 pH=12.53
pe=5.2

	AEA	Nagra	ONHY	PSI
Aqueous species (%)				
$UO_2(OH)_4^{2-}$	89	-	100	5
$UO_2(OH)_2^{o}$	11	-	-	-
$UO_2(OH)_3^{-}$		100	-	95
Solubility controlling solid (saturation index)				
$CaUO_4$	8.8	6.2		3.6
$UO_2(OH)_2$	-4.6		-32.7	

pe=-4

	AEA	Nagra	ONHY	PSI
Aqueous species (%)				
$UO_2(OH)_4^{2-}$	89	-	100	5
$UO_2(OH)_2^{o}$	11	-	-	-
$UO_2(OH)_3^{-}$		100	-	95
Solubility controlling solid (saturation index)				
$CaUO_4$	8.8	6.2	-	3.6
$UO_2(OH)_2$, schoepite	-4.6	-	-	-
UO_2, uraninite	-	-	-30.4	-

pe=-8

	AEA	Nagra*	ONHY	PSI
Aqueous species (%)				
$UO_2(OH)_4^{2-}$	79	-	100	-
$UO_2(OH)_2^{o}$	10	-	-	-
$UO_2(OH)_3^{-}$	-	67	-	-
$UO_2(OH)_2^{-}$		31	-	-
$U(OH)_5^{-}$	-	2	-	69
$U(OH)_4^{o}$	11	-	-	31
Solubility controlling solid (saturation index)				
$CaUO_4$	8.7	6.0	-	0.3
$UO_2(OH)_2$	-4.7	-	-	-
UO_2, uraninite	-	3.0	-22.4	-
U_4O_9	-	6.3	-	-

* U speciation changes slightly ($UO_2(OH)_3^{-}$ = 51%, $UO_2(OH)_2^{-}$ = 44% at the field pH.

URANIUM MQ5 pH=12.60
pe=2.05

	AEA	Nagra	ONHY	PSI
Aqueous species (%)				
$UO_2(OH)_4^{2-}$	93	-	100	9
$UO_2(OH)_2^{o}$	7	-	-	-
$UO_2(OH)_3^{-}$		100	-	91
Solubility controlling solid (saturation index)				
$CaUO_4$	9.5	7.0		4.1
$UO_2(OH)_2$	-4.1		-32.2	

pe=-4

	AEA	Nagra	ONHY	PSI
Aqueous species (%)				
$UO_2(OH)_4^{2-}$	93	-	100	9
$UO_2(OH)_2^{o}$	7	-	-	-
$UO_2(OH)_3^{-}$	-	100	-	91
Solubility controlling solid (saturation index)				
$CaUO_4$	9.5	7.0	-	4.1
$UO_2(OH)_2$, schoepite	-4.1	-	-	-
UO_2, uraninite	-	-	-30.1	-

pe=-8

	AEA	Nagra	ONHY	PSI
Aqueous species (%)				
$UO_2(OH)_4^{2-}$	88	-	100	-
$UO_2(OH)_2^{o}$	7	-	-	-
$UO_2(OH)_3^{-}$	-	70	-	-
$UO_2(OH)_2^{-}$		28	-	-
$U(OH)_5^{-}$	-	2	-	78
$U(OH)_4^{o}$	5	-	-	22
Solubility controlling solid (saturation index)				
$CaUO_4$	9.5	6.9	-	1.2
$UO_2(OH)_2$	-4.2	-	-	-
UO_2, uraninite	-	3.5	-22.1	-0.4
U_4O_9	-	8.4	-	-

URANIUM MQ6 pH=12.71
pe=2.17

	AEA	Nagra	ONHY	PSI
Aqueous species (%)				
$UO_2(OH)_4^{2-}$	96	-	100	9
$UO_2(OH)_2^{o}$	4	-	-	-
$UO_2(OH)_3^{-}$		100	-	91
Solubility controlling solid (saturation index)				
$CaUO_4$	9.5	7.2		4.2
$UO_2(OH)_2$	-4.3		-32.4	

pe=-4

	AEA	Nagra	ONHY	PSI
Aqueous species (%)				
$UO_2(OH)_4^{2-}$	96	-	100	9
$UO_2(OH)_2^{o}$	4	-	-	-
$UO_2(OH)_3^{-}$	-	100	-	91
Solubility controlling solid (saturation index)				
$CaUO_4$	9.5	7.2	-	4.2
$UO_2(OH)_2$, schoepite	-4.3	-	-	-
UO_2, uraninite	-	-	-30.5	-

pe=-8

	AEA	Nagra	ONHY	PSI
Aqueous species (%)				
$UO_2(OH)_4^{2-}$	94	-	100	-
$UO_2(OH)_2^{o}$	4	-	-	-
$UO_2(OH)_3^{-}$	-	76	-	-
$UO_2(OH)_2^{-}$	-	23	-	-
$U(OH)_5^{-}$	-	1	-	79
$U(OH)_4^{o}$	2	-	-	21
Solubility controlling solid (saturation index)				
$CaUO_4$	9.5	7.1	-	1.4
$UO_2(OH)_2$	-4.3	-	-	-
UO_2, uraninite	-	-	-22.5	-0.3
U_4O_9	-	7.7	-	-

URANIUM MQ7 pH=12.67
pe=2.0

	AEA	Nagra	ONHY	PSI
Aqueous species (%)				
$UO_2(OH)_4^{2-}$	94	-	100	5
$UO_2(OH)_2^{o}$	6	-	-	-
$UO_2(OH)_3^{-}$		100	-	95
Solubility controlling solid (saturation index)				
$CaUO_4$	8.7	6.3		3.6
$UO_2(OH)_2$	-4.9		-33.0	

pe=-4

	AEA	Nagra	ONHY	PSI
Aqueous species (%)				
$UO_2(OH)_4^{2-}$	94	-	100	5
$UO_2(OH)_2^{o}$	6	-	-	-
$UO_2(OH)_3^{-}$	-	100	-	95
Solubility controlling solid (saturation index)				
$CaUO_4$	8.7	6.3	-	3.6
$UO_2(OH)_2$, schoepite	-4.9	-	-	-
UO_2, uraninite	-	-	-31.0	-

pe=-8

	AEA	Nagra	ONHY	PSI
Aqueous species (%)				
$UO_2(OH)_4^{2-}$	91	-	100	-
$UO_2(OH)_2^{o}$	6	-	-	-
$UO_2(OH)_3^{-}$	-	74	-	-
$UO_2(OH)_2^{-}$		25	-	-
$U(OH)_5^{-}$		1		71
$U(OH)_4^{o}$	3			29
Solubility controlling solid (saturation index)				
$CaUO_4$	8.7	6.2	-	0.4
$UO_2(OH)_2$, schoepite	-4.9	-	-	-
UO_2, uraninite	-	2.7	-23.0	-0.8
U_4O_9		5.0		

The major difference in predicted speciations by the two organisations are related to the Cr databases used. The ONHY database contains only Cr(VI) species and the HATCHES (version 3.0) database contains only Cr(III) species. Additionally, Cr-ettringite is absent from both databases, ie neither database is therefore complete.

As a result of this comparison, thermodynamic data for Cr(VI) species were included in the AEA database and the calculations were repeated (table 5.16). Both organisations now predict that, under more oxidising conditions, the Cr(VI) species CrO_4^{2-} dominates in all the groundwaters studied. As the conditions become more reducing, AEA predict the appearance of Cr(III) species.

Using the AEA amended data, both organisations predict that chromate solid phases are solubility limiting. Both organisations also predict that the groundwaters are undersaturated with respect to these solids. According to ONHY the saturation indices range from -2.8 to -5.0, whereas AEA calculate saturation indices less than -13.0. The AEA values imply a solubility limit of 10^{-12}M for chromium in these groundwaters which is obviously unrealistic. It would appear, therefore, that the ONHY predictions are more appropriate in this instance.

In the presence of Ba, Cr(VI) solubility is thought to be controlled by the formation of $Ba(S,CrO_4)$ solid solution (RAI et al., 1988). This is confirmed by the identification of hashemite ($BaSO_4$-$BaCrO_4$ solid-solution) in the secondary mineral assemblage at Maqarin (chapter 4). Cr is also observed to form solid solution with gypsum at Maqarin ($CaSO_4$-$CaCrO_4$). Incorporation of solid solution into the geochemical codes may allow better estimation of Cr solubilities in these groundwaters. Overall, the ONHY database is conservative while the amended AEA database is generally non-conservative.

Table 5.15 Results of interpretive modelling: CHROMIUM

CHROMIUM MQ2 pH=12.53
pe=5.2

	AEA	**ONHY**
Aqueous species (%)		
$Cr(OH)_4^-$	100	
CrO_4^{2-}		100
Solubility controlling solid (saturation index)		
$MgCr_2O_4$	16.9	
$FeCr_2O_4$	2.4	
Cr_2O_3	12.4	
K_2CrO_4	8.4	
Na_2CrO_4		-4.6

ONHY predict no change with pe. Harwell predict no change in speciation but do predict differences in the degree of saturation of the minerals $FeCr_2O_4$ and K_2CrO_4.

pe	5.2	-4	-8
$FeCr_2O_4$	2.4	11.6	15.6
K_2CrO_4	8.4	-19.2	-31.2

CHROMIUM MQ5 pH=12.60
pe=2.05

	AEA	**ONHY**
Aqueous species (%)		
$Cr(OH)_4^-$	100	
CrO_4^{2-}		97
$KCrO_4^-$		2
Solubility controlling solid (saturation index)		
$MgCr_2O_4$	18.5	
$FeCr_2O_4$	7.1	
Cr_2O_3	14.0	
K_2CrO_4	3.5	
Na_2CrO_4		-3.1

ONHY predict no change with pe. Harwell predict no change in speciation but do predict differences in the degree of saturation of the minerals $FeCr_2O_4$ and K_2CrO_4.

pe	2.05	-4	-8
$FeCr_2O_4$	7.1	13.1	17.0
K_2CrO_4	3.5	-14.7	-26.7

CHROMIUM MQ6 pH=12.71

pe=2.17

	AEA	**ONHY**
Aqueous species (%)		
$Cr(OH)_4^-$	100	
CrO_4^{2-}		97
$KCrO_4^-$		2
$NaCrO_4^-$		1
Solubility controlling solid (saturation index)		
$MgCr_2O_4$	18.7	
$FeCr_2O_4$	6.7	
Cr_2O_3	14.0	
K_2CrO_4	4.6	
Na_2CrO_4		-2.8

ONHY predict no change with pe. Harwell predict no change in speciation but do predict differences in the degree of saturation of the minerals $FeCr_2O_4$ and K_2CrO_4.

pe	2.17	-4	-8
$FeCr_2O_4$	6.7	12.8	16.8
K_2CrO_4	4.6	-13.9	-25.9

CHROMIUM MQ7 pH=12.67

pe=2.0

	AEA	**ONHY**
Aqueous species (%)		
$Cr(OH)_4^-$	100	
CrO_4^{2-}		100
Solubility controlling solid (saturation index)		
$MgCr_2O_4$	16.6	
$FeCr_2O_4$	4.9	
Cr_2O_3	12.0	
K_2CrO_4	-0.4	
Na_2CrO_4		-5.0

ONHY predict no change with pe. Harwell predict no change in speciation but do predict differences in the degree of saturation of the minerals $FeCr_2O_4$ and K_2CrO_4.

pe	2.0	-4	-8
$FeCr_2O_4$	4.9	10.9	14.9
K_2CrO_4	-0.4	-18.4	-30.4

Table 5.16 Results of interpretive modelling: CHROMIUM

CHROMIUM MQ2 pH=12.53
pe=5.2

	AEA	**ONHY**
Aqueous species (%)		
$Cr(OH)_4^-$		--
CrO_4^{2-}	100	100
Solubility controlling solid (saturation index)		
$MgCr_2O_4$	-34.5	
$FeCr_2O_4$	-48.7	
Cr_2O_3	-39.0	
K_2CrO_4	-17.9	
Na_2CrO_4	19.5	-4.6

CHROMIUM MQ5 pH=12.60
pe=2.05

	AEA	**ONHY**
Aqueous species (%)		
$Cr(OH)_4^-$	--	
CrO_4^{2-}	100	97
$KCrO_4^-$		2
Solubility controlling solid (saturation index)		
$MgCr_2O_4$	-15.8	
$FeCr_2O_4$	-27.3	
Cr_2O_3	-20.4	
K_2CrO_4	-13.7	
Na_2CrO_4	-17.8	-3.1

CHROMIUM MQ6 pH=12.71

pe=2.17

	AEA	**ONHY**
Aqueous species (%)		
$Cr(OH)_4^-$	--	--
CrO_4^{2-}	100	97
$KCrO_4^-$		2
$NaCrO_4^-$		1
Solubility controlling solid (saturation index)		
$MgCr_2O_4$	-17.3	
$FeCr_2O_4$	-29.3	
Cr_2O_3	-22.0	
K_2CrO_4	-13.4	
Na_2CrO_4	-17.5	-2.8

CHROMIUM MQ7 pH=12.67

pe=2.0

	AEA	**ONHY**
Aqueous species (%)		
$Cr(OH)_4^-$	--	--
CrO_4^{2-}	100	100
Solubility controlling solid (saturation index)		
$MgCr_2O_4$	-17.9	
$FeCr_2O_4$	-29.6	
Cr_2O_3	-22.6	
K_2CrO_4	-17.7	
Na_2CrO_4	-19.9	-5.0

5.4 Conclusions

5.4.1 Predictive Modelling

An important conclusion from the preceding discussion is that differences in the results of modelling by the four different modelling groups can be directly ascribed to the choice of data for inclusion in the databases. Often, problems are related to either a lack of appropriate experimental data or to conflicting literature values. An important point to be borne in mind also, is that close agreement between the four different modelling groups with respect to chemical predictions does not necessarily indicate that the predictions are correct. The use of chemical speciation codes is entirely reliant on the quality of the data available on which to base the calculations and it must be remembered at all times that reliable data are essential for the use of these models. Studies of this type can help focus analytical study on areas of particular interest, or certain elements which are particularly problematical, as well as effectively testing the predictive capabilities of the particular codes and databases utilised.

5.4.2 Interpretive Modelling

The main finding from the interpretive modelling study was that, with the exception of U, the observed solution concentrations of the trace elements in these groundwaters was two or three orders of magnitude less than would have been predicted assuming that the concentrations were controlled by the solubility of simple stoichiometric oxide or hydroxide phases listed in the current databases. Thus, although the databases do not contain solid phases of direct relevance to either a cementitiuos repository or a likely repository host rock, they are clearly providing conservative results (from the safety assessment viewpoint). The oversaturation of U was with respect to $CaUO_4$, a phase which is not observed in nature. Choice of an oxide as the solubility limiting phase, as recommended by LEMIRE (1988) for a natural system, would lead to a conservative prediction of U solubility.

The main limitation of these geochemical codes in predicting element solubilities was the representation of the solid phase. Most of the solids contained in the databases are pure end-members and these are not generally observed in nature or a repository. Furthermore, mineralogical study of the secondary mineral assemblages at Maqarin showed that many of the trace elements were incorporated in major-element solid phases such as CSH phases (hydrated calcium silicates) and sulphate minerals. For instance, high concentration of U have been observed in thaumasite. Co-precipitation of trace elements with these major minerals is of paramount importance in dictating the concentrations of these elements in the groundwaters.

Such problems also exist in the Se databases, with the predicted solubility controlling phases generally not observed in the rock-water-system (the exception being

$CaSeO_4$). Further complications include a potential microbiological rôle in the Se cycle plus the presence of Se in solid-solution with S in some minerals (such as oldhamite; CaS). It remains unclear how the former problem can be addressed in such geochemical codes, but the latter is in hand with inclusion of solid-solution in the newly revised HARPHRQ code.

The value of comparing laboratory based results with data from the field (such as provided here) is clearly indicated in the results of the Sn and Ni modelling. In the case of Sn, the major differences between the Nagra and AEA predictions are the inclusion of Sn(IV) hydrolysis products in the HATCHES database. Comparison of this database with experimental Sn solubility data indicated good agreement, suggesting that the HATCHES Sn database was more appropriate than the NEWTHERM database. In contrast, the original HATCHES Ni database, which had also been shown to produce a reasonable fit to experimental Ni solubility data, was amended following the initial predictive phase of the project. The addition of an extra aqueous species and an extra solid (to conform with the PSI NAIO289 database) produced more conservative results when the field data was modelled. It should, however, be emphasised that the lack of relevant minerals in all of the Sn and Ni databases mean that none can be said to have been truly validated here.

Th and Pb (and sometimes Ra) were all below the detection limits of the analytical techniques employed in this study so it is difficult to formulate hard conclusions. One point which is clear is that none of the databases accurately reflect the mineralogy of interest: it seems likely that Ra is involved in solid-solutions in several minerals and this cannot yet be addressed rigorously; Pb is present as a minor component in a wide range of minerals whereas Th was not recorded as a discrete phase at all. The problems with Ra and Pb can be addressed by further code development, making the geochemical codes more closely reflect natural systems. In the Maqarin system, at least, it is possible that Th is source term limited and, as such, further effort would be pointless.

One particular area which is worthy of further study is the actual definition of the in situ speciation of the trace elements of interest. Clearly this can have a significant effect on (predicted and real) solubilities but, in studies of this type to date, little effort has been expended in this area. Admittedly, this is not on easy task (cf. the U work here), especially in the hyperalkaline conditions prevalent in the Maqarin groundwaters, but such data would be of enormous value for clarifying the current problems with U databases (for example).

Overall, however, the intercomparison has been successful. The opportunity to test databases which will be utilised in the performance assessment of a radioactive waste repository design against data for natural systems, that have evolved over geological timescales, increases confidence in the applicability of these databases to the disposal scenario. The comparison between the predictions of various organisations is also useful in directing database development. In cases where the predictions from one

organisation conflict with observation e.g. NAGRA prediction for Sn, ONHY prediction for Se, the sources of these data and their applicability should be reconsidered. Indeed, the results of this study have already led to NAGRA rejecting the particular database employed here in favour of a more appropriate version and has allowed ONHY to quickly establish the inapplicability of their Se database. It should be remembered, however, that agreement between the various databases does not automatically imply that they are correct: this can only really be ascertained by detailed examination of the information contained in the database and comparison with natural systems and laboratory data (as attempted here). Also, if the particular geochemical model being applied is inappropriate, then the predictions will be incorrect even using the correct database. The modelling performed to date does not include all factors which may influence observed concentrations. The effect of organic complexation, colloid formation and kinetics of mineral reactions have not been included in this modelling study.

It may, of course, be argued that it is not entirely necessary for such codes and databases, when used in safety assessment studies, to describe the groundwater system in such detail, but this is only acceptable when the codes and databases can be shown, by rigorous testing such as carried out here, to behave always in a conservative manner.

6 CONCLUSIONS

W.R. ALEXANDER

6.1 Introduction

The main objective of the Maqarin natural analogue project was to test performance assessment models for a cementitious radioactive waste repository, in particular to:

- test databases of thermodynamic geochemical codes, especially those pertaining to radionuclides of concern in a L/ILW repository.

- examine microbiological activity in hyperalkaline groundwaters as an aid to establishing the likely impact of microbes in the near-field of a cementitious repository.

- define the significance of colloidal material in hyperalkaline groundwaters as a guide to the significance of colloid formation in and around the near-field of a cementitious repository.

- study the interaction of hyperalkaline groundwaters with an unaltered sedimentary host rock, a process analogous to the potential reaction of hyperalkaline leachates from a cementitious repository with the surrounding host formation.

In order to fulfill these objectives, it proved necessary to characterise the site in some detail. Only when the various source terms were described was it possible to pursue the project aims further. A significant amount of data exists on the regional and local geology and also on the major element chemistry of the hyperalkaline groundwaters. It was, however, necessary to expend efford in careful trace and ultra-trace element analyses for the thermodynamic database testing. Similarly, much work has gone into defining the source and sink term mineralogy of the elements of interest.

Uranium, for example, was shown to be present in fine-grained organics, carbonates, geothite alteration products and in an as yet undefined Ca-U mineral (possibly an oxycarbonate). Fission-track registration revealed that this phase (along with U in ellastadite-apatite) is rapidly attacked and altered by groundwater and U is partially redistributed within fine-grained secondary major phases in the matrix (including portlandite, calcite, ettringite and iron oxyhydroxides). Leaching and overall U loss from the system was inferred from natural decay series data.

An interesting spin-off from the detailed mineralogical investigations includes discovery of a previously unrecorded natural uranium mineral, the first observation of calcium selenium sulphide in terrestrial rocks, the first description of natural calcium selenates and calcium-strontium selenates and a newly discovered calcium-potassium selenide-

sulphide. All clear indicators of the very high quality of the supporting studies.

An attempt has also been made to investigate further the overall groundwater evolution (via stable isotope studies) as an aid to understanding the differing water chemistries in the area (the western sampling sites are characterised by $Ca(OH)_2$ saturation and much greater mineralisation than the eastern sites). The additional isotopic and geochemical evidence collected here suggests that the higher mineralisation of the western springs relative to the eastern discharges parallels the evolution of hyperalkaline leachates of a cementitious repository. The marked differences in both mineralisation and mineral saturation between the western and eastern spring waters is analogous to early (NaOH/KOH dominated) and later ($Ca(OH)_2$ dominated) stage leaching of the cement phases in a repository. Recent re-sampling of the western site revealed a groundwater pH of up to 12·9 (MILODOWSKI, pers. comm.), in keeping with the above model.

6.2 Performance assessment model testing

6.2.1 Thermodynamic databases

This work was carried out in three phases:

- an initial scoping study, using previously published groundwater analyses, to assess the relevance of the Maqarin groundwater chemistry to a cementitious repository.

- a predictive modelling exercise, using newly measured major element data and reasonable, assumed values for the trace elements of interest.

- finally, following completion of the full groundwater analyses, the actual measured values for the trace elements of interest were included in the calculations.

The first phase is an obvious precaution before beginning a major project of this nature. Phases two and three are an important part in increasing confidence in the databases (and codes) which will be an integral part of a repository performance assessment. The procedure is simple: the major element chemistry of the groundwater is provided and a prediction is made on the solubility, speciation and solubility controlling solid of the trace elements of interest. After this is documented, the measured concentrations of the trace elements (and speciation, where possible), along with information on the controlling solid phase, are provided and differences between predictions and observations are examined.

Good agreement between observation and prediction is useful in building confidence in the applicability of the tested databases to natural systems, but this should not be over-interpreted. Agreement between prediction and observation does not conclusively

prove that the databases are correct, although glaring inconsistencies can often unambiguously identify problems in particular databases (eg missing or incorrect data).

This particular series of tests has produced several clear conclusions. The main limitation of all databases tested here was in the representation of the controlling solid phases. Most of the predicted solids were non-representative of the natural system, the databases containing mainly pure end-members whereas the actual mineralogical data indicated that many trace elements (eg U) were incorporated in major element solid phases such as CSH gels. Further complications include the presence of many of the trace elements (eg Se, Ra) in solid solution with major mineral phases or involvement in the microbiological cycle.

Regardless of the above problems, the databases generally behaved in a conservative manner (ie the solubilities of the trace elements of interest were over-predicted). In the case of the non-conservative prediction of U oversaturation, the effect has been indentified, again, as related to a non-realistic representation of the solubility controlling mineralogy. The predicted phase, $CaUO_4$, is not commonly observed in nature and use of an arguably more realistic solid phase (an U oxide) would lead to a conservative prediction of U solubility.

In the case of Se, the non-conservative behaviour of one database is less easy to explain, partly because, in effect, only two different databases were tested. Both databases contain non-representative minerals yet both also contain other solid phases observed in the field. It would be tempting to simply discard the database which predicted the meaningless, high levels of Se oversaturation, but this would ignore the fact that the predicted controlling phase, native Se, has been observed in the Maqarin rock and has also been suggested as the Se solubility controlling phase in other groundwaters.

It has been suggested that the equilibrium thermodynamic approach used here is, in fact, questionable due to the expected kinetic constraints on redox equilibrium in the Se system. This, along with a possible involvement in the microbiological cycle in the Maqarin groundwaters and clear evidence of Se solid-solution with major phases implies that a more sophisticated approach to Se database testing is required.

Finally, it should be emphasised that agreement between the various databases does not automatically imply that they are correct, it is only through the detailed examination of the database, and the type of comparison with laboratory experiments and the natural system carried out here, that this can be shown to be so.

6.2.2 Microbiology

The results of the microbiology investigations indicate that nutrient availability, not the groundwater pH, controls microbial activity in these hyperalkaline groundwaters. A similar result was reported in the Oman study but there were noticably more groups which appeared to be viable in those groundwaters than were seen in the Maqarin system. Here, tests indicate that denitrifying, sulpher oxidising and alkalophilic photosynthetic bacteria were all absent. Similarly, heterotrophs, aerobic and anaerobic oligotrophs, algae and fungi were also not detected. On-site tests did, however, indicate the presence of small populations of heterotrophs and sulphate reducing bacteria (SRB) were noted in all samples, although it proved impssible to isolate them. In addition, no dissolved sulphide was observed in the groundwaters, despite the use of highly sensitive analytical methods, indicating that the SRB were probably dormant. The presence of high levels of Se in the groundwater may be partly responsible for the inactivity of the SRB. Se, being an excellent chemical analogue of S, may be poisoning the SRB so reducing their activity to very low levels.

However, such poisoning is unlikely to occur in and around the near-field of a cementitious repository. Further, it is probable that nutrient availability will not be such an important factor as here, suggesting that substantial, viable populations of at least some species of bacteria is a possibility in the hyperalkaline near-field. It is of note that, in the non-nutrient limited groundwaters studied in Oman, many more species of bacteria were observed than in this study. Although, as stated previously, the Oman system is a much poorer analogue of a cementitious repository than the Maqarin site, it is recommended that the Oman results are used over the present Maqarin data in this case. Thus, unless a cementitious near-field can be shown to be nutrient limiting, the Oman data would at least be conservative from a safety assessment viewpoint.

6.2.3 Colloids

It has been stated that the degredation of cement may enhance colloid populations in and around the near-field of a cementitious repository, so potentially enhancing radionuclide transport. If the colloid populations were high enough and the colloids sorbed radionuclides, this process could negate the benefit of low radionuclide solubility bestowed by the hyperalkaline environment. However, the potential of cement to produce colloids upon leaching has been little studied to date.

The data produced here indicate low colloid populations in comparison with other sedimentary systems. This is in spite of the fact that colloids would be expected to be stable in hyperalkaline groundwaters and that the relatively open fracture systems at Maqarin offer little possibility of colloid filtration. This suggests that, at least for the natural cement minerals and gels present at this particular site, colloid production during groundwater leaching is minimal.

Of course, the long storage period of the groundwater samples before colloid filtration may have reduced colloid levels due to precipitation reactions so the data should be assumed to be non-conservative for the time being. Improved in situ or on-site sampling methods should clarify this question without a great additional expenditure of effort. The colloids predominantly consist of Ca and Fe (presumably as hydroxides?) and specific analysis for humic acids indicate not only no organo-colloid association in this system but also that the dissolved humic acid content was below detection. It was suggested in the Oman study that some form of colloidal U might exist under hyperalkaline conditions but scoping measurements of the Maqarin waters indicate that this is not a significant U reservoir here.

6.2.4 Hyperalkaline water / host rock interaction

Due to the highly complex nature of the mineralogical relationships in the Maqarin system, much effort had to be expended on the initial characterisation of both the primary mineral assemblage and the (prograde and retrograde) metamorphic mineral assemblage. Consequently, little has been done yet on the low temperature interaction between the hyperalkaline groundwaters and the pristine host formation. However, it should be noted that the in depth petrological analyses carried out to date were necessary to characterise fully the host rock and to disentangle secondary and primary alteration effects. Only with this detailed background information will it now be possible to test rigorously the coupled (geochemistry and transport) codes in the second phase of the project.

Indeed, a recent, small-scale scoping study (MILODOWSKI et al., 1992) on the hyperalkaline groundwater-rock interaction at the Maqarin site has already provided useful information for future work on the problem and has shown the worth of the backing data produced here in disentagling the recent interactions from earlier metamorphic signatures.

6.3 Recommendations for further work

Several areas worthy of additional investigation have been highlighted by this particular study:

- an expansion of the type of iterative thermodynamic database testing shown here for Ni and Sn is clearly worthwhile. It is only by the repeated testing of databases against differing field and laboratory data that the robustness of the databases can be demonstrated.

- an attempt to define the in situ speciation of the trace elements of interest would be valuable, especially in the case of U where large differences still exist between the databases.

- an obvious weakness of the databases tested here was the representation of the solid phases as pure end members, mainly because of a lack of approprate thermodynamic data for more complex, mixed phases. It is, however, debatable whether including such mixed phases is of use as slight changes in the phase composition could change predicted solubility enormously. Rather, it is recommended that more complex codes be developed, allowing treatment of, for example, solid solution effects.

- although not intended as a part of the original Maqarin project, the vast body of detailed mineralogical data may conceivably be used to investigate trace element sorption on cements under in situ conditions. Study of the U-portlandite (and other cement phases) relationship may shed light on U retardation by cementitious materials. This would be especially apt where U association with secondary portlandite, formed well away from the U source rocks, could be studied, so minimising confusion with U uptake during the carbonation phase of the site.

- numerous models of cement leaching predict that the leachates will initially be dominated by NaOH/KOH and only later by $Ca(OH)_2$. Nevertheless, little laboratory work and no field studies to date have examined this phenomena and so only sparse data exist on the form of the NaOH/KOH altered repository host-rock before interaction with the later $Ca(OH)_2$ leachates. This may well be a significant omission and it is therefore recommended that the western springs be considered for further work on the NaOH/KOH dominated system.

- the colloid data produced here represent the first such field information for a cementitious system. It is important then that the data not be overinterpreted but be treated rather as an indicator for future work. Certainly more appropriate field sampling apparatus should be employed to avoid sampling and storage artefacts. In addition, the high levels of a host of safety relevant trace elements in the Maqarin system suggest this to be an excellent site to further study the potential of colloids to sorb and transport radionuclides in the vicinity of a cementitious repository.

- the microbiological data presented here are a significant addition to the existing information on the potential influence of microbiology in a cementitious repository. However, it is recommended that further development work be carried out on the laboratory handling of microbes (eg incubation) under hyperalkaline conditions before further field work is considered.

- short-term laboratory studies of metal corrosion under hyperalkaline conditions indicate very low rates of corrosion. It would be useful to compare such short term data with samples of steel from Maqarin which have been in contact with hyperalkaline waters for ten (nails in Adit 6) to eighty (rails) years.

- the particular geochemical features of the Maqarin site make it a potentially useful natural analogue for the evaluation of grout carbonation reactions relevant to ^{14}C attenuation in cement-based engineered barriers. Of particular significance to the ^{14}C problem is the observation of "retrograde carbonates" in the brecciated zone. Further work should be aimed at identifying the sources of CO_2 and elucidating recarbonation mechanisms at the field scale.

7 ACKNOWLEDGEMENTS

The authors would like to express their thanks to numerous colleagues who have contributed in many ways to the success of this study, especially M.N. INGHAM, A.G. SCOTHERN and P.H. MILES of BGS for some of the XRF analyses; M.T. STYLES and D.J. BLAND of BGS for help with the electron microprobe; A.B. MacKENZIE (SURRC), S.A. SHORT (ANSTO) and their colleagues for the natural decay series nuclides; M. MOHOS (PSI for SEM data; J.E. BERRY (AEA), B. BAEYENS (PSI), E. HAMILTON and R. YUSAF (Edinburgh Polytechnic, UK), A.H. BATH and I.R. BASHAM (BGS) and I.G. McKINLEY (Nagra) for useful discussions during the course of this project.

We would also like to thank the government and armed forces of Jordan for invaluable assistance during the field phase of the study and, finally, Nagra, UK Nirex and Ontario Hydro for jointly funding this project and encouraging the publication of the results of our work (already begun with KHOURY et al., (1992), ALEXANDER et al., (1991), TWEED and MILODOWSKI (1992).

The editor would also like to add a word of thanks to all the authors for their strenuous efforts in writing the work up so professionally and to I.G. McKINLEY for a searching review of the report.

8 REFERENCES

ABED, A. and AMIREH, B. 1983. Petrography and geochemistry of some Jordanian oil shales from north Jordan. J. Petrol. Geol. **5**, 261-274.

AGRELL, S.O. 1965. Polythermal metamorphism of limestones at Kilchoan, Ardnamurchan. Mineral. Mag. **34**, 1-15.

ALEXANDER, W.R., MacKENZIE, A.B., SCOTT, R.D. and McKINLEY, I.G. 1990. Natural analogue studies in crystalline rock: the influence of water bearing fractures on radionuclide immobilisation in a granitic rock repository. Nagra Technical Report Series NTB 87-08, Nagra, Baden, Switzerland.

ALEXANDER, W.R., DAYAL, R., EAGLESON, K., EIKENBERG, J., HAMILTON, E., LINKLATER, C.M., McKINLEY, I.G. and TWEEd, C.J. 1992. A natural analogue of high pH cement pore waters from the Maqarin area of northern Jordan II: results of predictive geochemical calculations. J. Geochem. Explor 46, 133-146.

ATKINSON, A. and GUPPY, R.M. 1988. Evolution of pH in a radwaste respository. UKAEA Technical Report R126961, AEA Tech., Harwell, UK.

BAES C.F. and MESMER R.E. 1976. The hydrolysis of cations. John Wiley and Sons, New York.

BAEYENS B. and McKINLEY I.G. 1989. A PHREEQE database for Pd, Ni and Se. Nagra Technical Report Series NTB 88-28 Nagra, Baden, Switzerland.

BAJJALI, W. 1989. Isotopic composition of alkaline water in Maqarin area, a preliminary study. Jordanian Ministry of Water and Irrigation, unpublished Internal Report, Amman, Jordan.

BAJJALI, W. 1990a. Isotopic and hydrochemical characteristics of precipitation in Jordan. Unpubl. MSc Thesis, University of Jordan, Amman, Jordan, 99 pp.

BAJJALI, W. 1990b. Unpubl. Internal Report, Water Authority of Jordan, Amman, Jordan.

BANDEL, K. and HADDADIN, A.A. 1979. The depositional environment of amber bearing rocks in Jordan, Dirasat, **6**, 39-62.

BARBIN, V., RAMSEYER, K., DEBENAY, J.P., SCEIN, E., ROUX, M. and DECROUEZ, D. 1991. Cathodoluminescence of Recent biogenic carbonates: an environmental and ontogenetic fingerprint. Geol. Mag., **128**, 1-26.

BARNES, I., PRESSER, T.S., SAINES, M., DICKSON, P. and KOSTER VAN GROOS, A.F. 1982. Geochemistry of highly basic calcium hydroxide groundwater in Jordan. Chem. 35, 147-154.

BARSUKOV, V.L. and KLINTSOVA, A.P. 1970. Solubility of cassiterite in water and aqueous NaOH at 25C. Geochem. Int., 849-852.

BASHAM, I.R., MILODOWSKI, A.E., HYSLOP, E.K. and PEARCE, J.M. 1989. The location of uranium in source rocks and sites of secondary deposition at the Needle's Eye natural analogue site, Dumfries and Galloway. Report British Geological Survey, Technical Report, **WE/89/56**, 56 pp.

BATH, A.H., CHRISTOFI, N., NEAL, C., PHILIP, J.C., CAVE, M., McKINLEY, I.G. and BERNER, U. 1987. Trace element and microbiological studies of alkaline groundwaters in Oman, Arabian Gulf - A natural analogue for cement porewaters. British Geological Survey, Fluid Processes Group Technical Report. FLPU 87-2/NAGRA Technical Report Series NTB 87-16. NAGRA, Baden , Switzerland.

BAYLISS S., EWART F.T., HOWSE, R.M., LANE S.A., PILKINGTON N.J., SMITH-BRIGGS S.J. and WILLIAMS S.J. 1989. The solubility and sorption of Ra and Sn in a cementitious near-field environment. Sci Basis Nucl. Waste Manag. XII, 879-888.

BAYLISS S., EWART F.T., HOWSE, R.M., SMITH-BRIGGS J.L., THOMASON, H.P. and WILLMOTT, H.A. 1988. The solubility and sorption of ^{210}Pb and ^{14}C in a near-field environment. Sci Basis Nucl. Waste Manag. XI, 33-42.

BENDER, F. 1968. Geologie von Jordanien - Beiträge zur Regionalen Geologie der Erde. Gebrüder Borntraeger, Stuttgart, 230 pp.

BENDER, F. 1974. Geology of Jordan, Gebrüder Bornträger, Berlin, 196 pp.

BENSON, L.V. and TEAGUE, L.S. 1980. A tabulation of thermodynamic data for chemical reactions involving 58 elements common to radioactive waste package systems. Lawrence Berkeley Report LBL-11448, California, USA.

BENTOR, Y.K., GROSS, S. and HELLER I. 1963. Some unusual minerals from the "Mottled Zone" complex, Israel. Amer. Mineral. **48**, 924-930.

BENTOR, Y.K., GROSS, S. and KOLODNY, Y. 1972. New evidence on the origin of high temperature assemblage of the "Mottled Zone" Israel. 24th International Geological Congress (Montreal, Canada), **Section 2**, 265-275.

BERNER, U.R. 1987. Modelling porewater chemistry in hydrated Portland cement. Sci. Basis Nucl. Waste Manag., X, 319-325.

BERNER, U.R. 1990. A thermodynamic description of the evolution of pore water chemistry and uranium speciation during the degredation of cement. Nagra Technical Report NTB 90-12, Nagra, Baden, Switzerland.

BERNER, U.R. 1992. Revision of the MINEQL/EIR database. PSI Report (in prep.) Paul Scherrer Institute, Villigen, Switzerland.

BEVERIDGE, T.J., MELOCHE, J.D., FYFE, W.S. and MURRAY, R.G.E. 1983. Diagenesis of metals chemically complexed to bacteria: laboratory formation of metal phosphates, sulphides and organic conensates in artificial sediments. Appl. Environ. Microbiol. **45**, 1094-1108.

BLANDER, M. 1971. The constrained equilibrium theory: sulphide phases in meteorites, Geochim. Cosmochim. Acta **35**, 61-76.

BOTTINGA 1968. Calculation of fractionation factors for carbon and oxygen exchange in the system calcite - carbon dioxide - water. Jour. Phys. Chem. **72**, 800-808.

BROOKINGS, D.G. 1988. Eh-pH diagrams for geochemistry. Springer-Verlag, Berlin, Germany.

BROWN P.L., HAWORTH A., SHARLAND S.M. and TWEED C.J. 1990. HARPHRQ: An extended version of the geochemical code PHREEQE. NSS-R.188, UK Nirex Ltd., Chilton, UK.

BRUNO J., CASA, I., LAGERMAN, B. and MUNOZ, M. 1987. The determination of the solubility of amorphous UO2(s) and the mononuclear hydrolysis constants of uranium (IV) at 25C. Sci. Basis Nucl. Waste Manag. X; 153-160.

BRUNO J., CROSS, J.E., EIKENBERG, J., McKINLEY, I.G., READ, D., SANDINO, A. and SELLIN, P. 1991. Testing of geochemical models in the Pocos de Caldas analogue study. Pocos Tech. Rep. 11, NAGRA NTB 90-29/ SKB TR 90-20/ UKDOE RW 90-051. NAGRA, Wettingen, Switzerland.

BUFFLE, J. 1988. Complexation reactions in aquatic systems: an analytic approach. Ellis Horwood Ltd., Chichister, UK.

BURMAN, C.W. 1959. Contact metamorphism of magnesian limestones at Crestmore, California. Bull. Geol. Soc. Amer. **70**, 879-920.

BUTLER, B.C.M. 1977. Al-rich pyroxene and melilite in a blast-furnace slag and a comparison with the Allende meteorite. Mineralogical Magazine, **41**, 493-499.

CAVE, M.R. and GREEN, K.A. 1988. Determination of reduced sulfur content of groundwaters by hydrogen sulphide generation-inductively coupled plasma optical emission spectrometry. Atom. Spectros. **9**, 149-153.

CHAPMAN, N.A., McKINLEY, I.G. and SMELLIE, J.A.T. 1984. The potential of natural analogues in assessing systems for deep disposal of high level radioactive waste. Nagra Technical Report NTB 84-41. Nagra, Baden, Switzerland.

CHAPMAN, N.A. and McKINLEY, I.G. 1987. The geological disposal of nuclear waste. John Wiley and Sons, London, UK.

CHEMVAL PROJECT 1989 (ed. D. READ and T. BROYD). Report on Stage 1: Verifications of Speciation Models., CEC-Report, EUR 12237, Brussels, Belgium.

CHEMVAL PROJECT 1990. Report on Stage 2: Application of Speciation Models to Laboratory and Field Datasets. CEC-Report, EUR 13124, Brussels, Belgium.

CHERDYNSTEV, V.V. 1955. Trans. Proc. 3RD Session Comm. on absolute age determinations of geological formations. Moscow, 1954, 175.

CLARK, I.D., RAVENSCROFT, P. and FRITZ, P. 1988. Origin and age of coastal groundwaters in Northern Oman. in Proceedings, 10th Salt Water Intrusion Meeting, Ghent, Belgium. W. De Breuck and L. Walschot, eds.

CLARK, I.D., FRITZ, P. and SOUTHER, J.G. 1989. Geochemistry and isotope hydrogeology of the Mount Edziza - Mess Creek geothermal area. Can. J. Earth Sci. **26**, 1160-1171.

CLARK, I.D., KHOURY, H.N., SALAMEH, E., FRITZ, P., GÖKSU, H.Y., WIESSER, A., CAUSSE, C. and FONTES, J-Ch. 1991. Travertines in central Jordan: implications for palaeohydrology and dating. Proceedings, Int. Atom. Energy Agency, Symposium SM-312.

CLARKE, D.B. 1979. Experimental technique for synthesising alkali element - transition metal sulphides. Progress in Experimental Petrology, N.E.R.C., **4**, 131-132.

CRAIG, J.R. and VAUGHAN, D.J. 1981. Ore microscopy and ore petrography. John Wiley and Sons, London, UK.

CRESSEY, G. 1987. Skarn formation between metachalk and agglomerate in the Central Ring Complex, Isle of Arran, Scotland. Mineral. Mag. **51**, 231-246.

CROSS, J.E., EWART, F.T. and TWEED, C.J. 1987. Thermochemical modelling with application to nuclear waste processing and disposal. AERE R12324, Harwell, UK.

CROSS, J.E. and EWART, F.T. 1991. HATCHES - a thermodynamic database management system. Radiochim. Acta **52/53**, 421-422.

CZAMASKE, G.K, LANPHERE, M.A., ERD, R.C. and BLAKE, M.C. 1978. Age determination of potassium-bearing sulphide minerals by the $^{40}Ar/^{39}Ar$ technique. Earth Planet. Sci. Lett. **40**, 107-110.

DAKIN, R.A., FARVOLDEN, R.N., CHERRY, J.A. and FRITZ, P. 1983. Origin of dissolved solids in groundwaters of Mayne Island, British Columbia, Canada. J. Hydrology **63**, 233-270.

DAYAL, R., JOHNSTON, H. and ZHOU, Z. 1989. Reactor operating waste disposal program, 1989 progress report. Ontario Hydro Internal Report No. 89-226-K, Toronto, Canada.

DAYAL, R. and KLEIN, R. 1988. CO_2/grout interaction an their relevance to ^{14}C attenuation in cementitious backfill. Radiochimica Acta **44/45**, 263-270.

DAYAL, R. and KLEIN, R. 1987. Evaluation of cement-based backfill material. Ontario Hydro Internal Report No. 87-223-K, Toronto, Canada.

DEER, W.A., HOWIE, R.A. and ZUSSMAN, J. 1966. An Introduction to the rock-forming minerals. Longman, 528 pp.

DEGANS, E.T. and VENUGOPALEN, I. 1982. In-situ metal-staining of biological membranes in sediments. Nature, **298**, 262-264.

DEGUELDRE, C., LONGWORTH, G., MOULIN, V. and VILKS, P. 1991. The Grimsel colloid exercise. Nagra Technical Report Series, NTB90-01, Nagra, Wettingen, Switzerland.

DOUBLE, D.D. 1983. New developments in understanding the chemistry of cement hydration. Phil. Trans. Roy. Soc. Lond., A310, 53-66.

EWART, F.T., SHARLAND, S.M. and TASKER, P.W. 1985. The chemistry of the near-field environment. Sci. Basis Nucl. Waste Manag. IX, 539-546.

FINCHAM, C.J.B. and RICHARDSON, F.D. 1954. Proceedings of the Royal Society, London, **A223**, 40-62.

FREUND, R. 1965. A Model of the Structural Development of Israel and Adjacent Areas Since Upper Cretaceous Times. - Geol.Mag. **102, 3**; 189-205.

FUCHS, L.H. 1966. Djerfisherite, alkali copper-iron sulphide: a new mineral from enstatite chrondrites. Science, **153**, 166-167.

GAT, J. and CARMI, I. 1970. Evaluation of the isotopic composition of atmospheric waters in the Mediterranean Sea area. J. Geophys. Res. **75**, 3039-3078.

GLASSER, F.P., MacPHEE, D., ATKINS, M., POINTER, C., COWIE, J., WILDING, C.R., MATTINGLEY, N.J. and EVANS, P.A. 1989. Immobilisation of radwaste in cement-based matrices. UK-DoE Report DOE/RW/89/058, UK-DoE, London, UK.

GOLDSTEIN, J.I., NEWBURY, D.E., ECHLIN, P., JOY, D.C., FIORI, C. and LIFSHIN, E. 1981. Scanning Electron Microscopy and X-Ray Microanalysis. Plenum Press, New York.

GRAHAM, A.L., EASTON, A.J. and HUTCHISON, R. 1977. The Mayo Belwa meteorite: a new enstatite achondrite fall. Mineral. Mag. **41**, 487-492.

GRENTHE, I. and WANNER, H. 1989. Guide lines for the extrapolation to zero ionic strength. OECD/NEA Nucelar Energy Agency, Gif-sur-Guette, France.

GROSS, S. 1977. The mineralogy of Hatrurim Formation, Israel. Geol. Surv. of Israel Bull. **70**, 80 pp.

GROSS, S. 1983. Occurrence of ye'elimite and ellestadite in an unusual cobble from the "Pseudo-Conglomerate" of the Hatrurim Basin, Israel. Geol. Surv. of Israel, Current Research 1983-84, 1-4.

GROSS, S., MAZOR, E., SAAS, S. and ZAK, I. 1967. The "Mottled Zone" complex of Nahal Ayalon (central Israel). Israel Earth Sci. **16**, 84-96.

HARZA ENGINEERING COMPANY. 1978. Hydrological Investigation at Maqarin Damsite - Inter. Rep. Arch. Jordan Valley Authority, Amman.

HARZA ENGINEERING COMPANY 1978. Maqarin project: hydrogeological investigation at Maqarin Damsite. Intern. Rep., Harza Engineeering, Chicago, USA.

HARZA OVERSEAS ENGINEERING COMPANY. 1979. Maqarin Damsite Geological Investigations. Jordan Valley Irrigation Project-Stage 11. April and September 1979.- Intern. Rep. Arch. Jordan Valley Authority, Amman.

HAWORTH, A., SHARLAND, S.M., TASKER, P.W. and TWEED, C.J. 1987. Evolution of the groundwater chemistry around a nuclear waste repostitory Sci. Basis Nucl. Waste Manag. XI, 425 - 434.

HEIMBACH, W. and ROSCH, H. 1980. Die Mottled Zone in Zentral-Jordanien. Geologisches Jahrbuch, **B40**, 3-17.

HELZ, G.R. and WYLLIE, P.J. 1979. Liquidous relationships in the system $CaCO_3$-$Ca(OH_2$-CaS and the solubility of sulphur in carbonatite magmas. Geochim. Cosmochim. Acta **43**, 259-265.

HENDERSON, P. 1984. General geochemical properties and abundances of the rare earth elements. In: Henderson (editor). Rare Earth Element Geochemistry. Developments in Geochemistry Series, **2**, Elsevier, 1-32.

HOEFS, J. 1987. Stable Isotope Geochemistry Third Ed., Springer-Verlag, 241 pp.

HODGEKINSON, D.P. and ROBINSON, P.C. 1987. Nirex near-surface respository project. Preliminary radiological assessment: Summary. NSS-R. A100, UK Nirex Ltd., Chilton, UK.

HSK 1991. Regulatory guidance for radioactive waste disposal: an advisory document. Swiss Nuclear Safety Inspectorate, Würenlingen, Switzerland.

IVANOVICH, M. and HARMON, R.S. (eds.) 1982. Uranium series disequilibrium: applications to envrionmental problems. Oxford University Press, Oxford.

JARVIS, I. 1980. Geochemistry of phosphatic chalks and hardgrounds from the Santonian to early Campanian (Cretaceous) of northern France. J. Geol. Soc. Lond. 137, 705-721.

JCPDS. 1985. Powder diffraction file: inorganic phases,; alphabetical index (chemical and mineral name), JCPDS Internationl Centre for Diffraction Data, Swarthmore, USA.

KEIL, K. 1968. Mineralogical and chemical relationships among enstatite chondrites. J. Geophys. Res. **73**, 6945-6976.

KHOURY, H.N. 1985. The origin of highly alkaline waters from the Maqarin area, north Jordan. Dirasat, **12**, 125-131.

KHOURY, H.N. and NASSIR, S. 1982a. A discussion on the origin of Daba-Siwaqa marble. Dirasat, **9**, 55-66.

KHOURY, H.N. and NASSIR, S. 1982b. High temperature mineralisation in the bituminous limestone in Maqarin area - Northern Jordan. N. Jb. Miner. Abh. v. **144:2**, 197-213.

KHOURY, H.N. and SALAMEH, E. 1986. The origin of high temperature minerals from Sweileh area, Jordan. Dirasat, **13**, 261-269.

KHOURY, H.N., SALAMEH, E. and ABDUL-JABER, Q. 1985. Characterisation of an unusual highly alkaline water from the Maqarin area, northern Jordan. J. Hydrol. **81**, 79-91.

KHOURY, H.N., SALAMEH, E. CLARK, I.D., FRITZ, P., BAJJALI, W., MILDOWSKI, A.E., CAVE, M.R. and ALEXANDER, W.R. 1992. A natural analogue of high pH waters from the Maqarin area of northern Jordan I: introduction to the site. J. Geochem. Explor. 46, 117-132.

KLEEMAN, J.D. and LOVERING, J.F. 1967. Uranium distriubtion in rocks by fission track registration in Lexan plastic prints. Atomic Energy Australia, **10**, No. 4, 3-8.

KOLODNY, Y. 1979. Natural cement factory: a geological story. In: Skalny, J. (editor). Cement Production and Use: Engineering Foundation Conference, Rindge, New Hampshire, 24-29 June 1979. 203-216.

KOLODNY, Y. BAR, M. and SASS, E. 1971. Fission track age of the "Mottled Zone event" in Israel. Earth Planet. Sci. Lett. **11**, 269-272.

KOLODNY, Y. and GROSS, S. 1974. Thermal metamorphism by combustion of organic matter; isotopic and petrological evidence. J. Geol. **82**, 489-506.

KROUSE, H.R. 1980. Sulphur isotopes in our environment. in: Handbook of Evironmental Isotope Geochemistry, Volume 1, The Terrestrial Environment, A, P. Fritz and J-Ch. Fontes eds.

KURIL'CHIKOVA, G.E. and BARSUKOV, V.L. 1970. Stability of hydroxystannate complexes and experimental crystallisation of cassiterite under hydrothermal conditions. Geochem. Int. 31-37.

LAFLAMME, B.D. and MURRAY, J.W. 1987. Solid/solution interaction: the effect of carbonate alkalinity on adsorbed thorium. Geochim. Cosmochim. Acta 51, 243-250.

LANGMUIR, D. and HERMAN, J.G. 1980. The mobility of thorium in natural waters at low temperatures. Geochim. Cosmochim. Acta. **44**, 1753-1766.

LANGMUIR, D. and RIESE, A.C. 1985. The thermodynamic properties of radium. Geochim. Cosmochim. Acta **49**, 1593-1601.

LARIMER, J.W. 1968. An experimental investigation of oldhamite, CaS, and the petrologic significance of oldhamite in meteorites. Geochim. Cosmochim. Acta **32**, 965-982.

LEA, F.M. 1970. The Chemistry of Cement and Concrete. Edward Arnold (Publ.) Ltd., 727 pp.

LEMIRE, R.J. 1988. Effects of high ionic strength groundwaters on calculated equilibrium concentrations in the uranium-water system. AECL-9549, Atomic Energy of Canada, Ltd., Pinawa, Canada.

MACDONALD, M. and HUNTING TECHNICAL SERVICES LTD. 1965. East Bank Jordan Water Resources, Summary Report.-Publ. Rep. for the groundwater of Jordan. Arch. Natural Resources. Authority, London, UK.

MARRINER, G.F., TARNEY, J. and LANGFORD, J.I. 1991. Apophyllite group: effects of chemical substitutions on dehydration behaviour, recrystallisation products and cell parameters. Mineral. Mag. **54**, 567-577.

MARSHALL, J.D. 1987. Cathodoluminescenece of Geological Materials, Unwyn Hyman, London, UK.

MASON, B. 1962. Meteorites, John Wiley.

MASRI, M. 1963. Report on the Geology of the Amman Zarka area.-Publ. Rep., Central Water Authority, Amman, 92 pp.

MATTHEWS, A. and KOLODNY, Y. 1978. Oxygen isotope fraction in decarbonation metamorphism; the Mottled Zone event. Earth Planet. Sci. Lett. **39**, 179-192.

McCARTHY, J. and ZACHARA, J. 1989. Subsurface transport of contaminants. Environ. Sci. Technol. 23. 496-502.

McCLELLAN, G.H. 1980. Mineralogy of carbonate fluorapatites. J. Geol. Soc., Lond. **137**, 675-681.

McKINLEY, I., BATH, A.H., BERNER, U., CAVE, M. and NEAL, C. 1988. Results of the Oman Analogue Study. Radiochim. Acta. **44/45**, 311-316.

McKINLEY, I.G. 1990. Applying natural analogues in predictive performance assessment. In Risk Analysis in Nuclear Waste Management, 357-396, Klewer Academic Publications, Netherlands.

McKINLEY, I.G. and ALEXANDER, W.R. 1992. Use of natural analogues to test performance assessment models of a cementitious near-field. Waste Manag. 12, 253-259.

McRAE, S.G. 1972. Glauconite. Earth Sci. Rev. **8**, 397-440.

MILODOWSKI, A.E., BASHAM, I.R. HYSLOP, E.K. and PEARCE, J.M. 1989. The uranium source-term mineralogy and geochemistry at the Broubster natural analogue site, Caithness. British Geol. Surv. Technical Report, **WE/89/50**, 50 pp.

MILODOWSKI, A.E., WEST, J.M., PEARCE J.M., HYSLOP, E.K., BASHAM, I.R. and HOOKER, P.J. 1990. Uranium-mineralised micro-organisms associated with uraniferous hydrocarbons in southwest Scotland. Nature, **347**, 465-467.

MOORMAN, F. 1959. Report on the Soils of East Jordan, FAO-Report No. 1132, Rome.

NASSIR, S.G. and KHOURY, H.N. 1982. Geology, mineralogy and petrology of Daba Marble, Jordan. Dirasat, **9**, 107-130.

NEA 1990. Chemical thermodynamics of uranium (final draft, March 1990) OECD-NEA, Nuclear Energy Agency, Gif-sur-Guette, France.

NICKEL, E. 1978. The present status of cathode luminescence as a tool in sedimentology. Min. Sci. Engin. **10**, 73-100.

NRA 1991. Unpubl. files of the Natural Resources Authority of Jordan, Amman, Jordan.

PARKHURST, D.L., THORSTENSON, D.C., PLUMMER, L.N. 1985. PHREEQE - a computer programme for geochemical calculations. U.S.Geol.Survey, Water Resource Investigations 80-96, 216, Nat. Tech. Info. Serv. Tech. Rep. PB81-167801, 1980, revised 1985.

PEARSON, F.J., COLCAMA, J.L and SCHOLTIS, A. 1989. Chemistry of the waters in Böttstein, Weiach, Riniken, Schafisheim, Kaisten and Leuggern borehole. NAGRA Technical Report NTB 86-19, Nagra, Baden, Switzerland.

PETERSON, S.R., HOSTETLER, C.J., DEUTSCH, W.J. and COWAN, C.E. 1987. MINTEQ user's manual. Pacific Northwest Laboratory, NUREG/CR-4808 PNL-6106, Richland, USA.

PICARD, L. 1943. Geological Evolution of the Quaternar in the Central-Northern Jordan Graben, Israel. Geol. Soc. America Spec. Paper **84**, 337-366.

PILKINGTON, N.J. and STONE, N.S. 1990. The solubility of Ni and Nb under high pH conditions. NSS-R. 186, UK Nirex Ltd., Chilton, UK.

POSTGATE, J.R. 1984. The sulphate reducing bacteria. Cambridge University Press, Cambridge, UK.

QUENNELL: in BURDON, D.J. 1959. Handbook of the Geology of Jordan.-Clochester.

RAI, D., EARY, L.E. and ZACHARA, J.M. 1989. Environmental chemistry of chromium. Sci. Total Environ. **86**, 15-23.

REARDON, E.J., JAMES, B.R. and ABOUCHAR, J. 1987. Geochemical aspects of the carbonation of grout: 1. High pressure carbonation of cementitious grout. Unpubl. contractors rep. to Ontario Hydro, University of Waterloo Research Institute, Ontario, Canada.

REARDON, E.J., JAMES, B.R. and ABOUCHAR, J. 1989. High pressure carbonation of cementitious grout. Cem. Conc. Res. **19**, 385-399.

ROSSLER, H.J., BEUGE, P., ADAMSKI, B. and FREIBERG, S. 1977. Das Verhalten chemischer Elemental beider diagenese und metamorphose. Zeitschrift für angewdte Geologie, **23**, 53-56.

SABINE, P.A. 1975. Metamorphic processes at high temperature and low pressure: the petrogenesis of the metasomatised and assimilated rocks of Carneal, Co. Antrim. Phil. Trans. Royal Soc. Lond. **280(A)**, 225-265.

SABINE, P.A., STYLES, M.T. and YOUNG, B.R. 1985. The nature and paragenesis of natural bredigite and associated minerals from Carneal and Scawt Hill, Co. Antrim. Mineral. Mag. **49**, 663-670.

SAINES, M., DICKSON, P. and LAMBERT, P. 1980. An occurrence of calcium hydroxide ground water in Jordan. GroundWater 18, 503.

SCHWEINGRUBER, M. 1981. Löslichkeits-und Speziationsberechnungen für U, Pu, Np und Th in natürlichen Gewässern - Theorie, thermodynamische Dateien und erste Anwendungen. EIR-Report No. 449, Paul Scherrer Institute, Villigen, Switzerland.

SCHWEINGRUBER, M. 1982. User's Guide for Extended MINEQL (EIR version) EIR Internal Report, Paul Scherrer Institute, Villigen, Switzerland.

SCOTT, P.W., CRITCHLEY, S.R. and WILKINSON, F.C.F. 1986. The chemistry and mineralogy of some granulated and pelletized blastfurnace slags. Mineral. Mag. **50**, 141-147.

SCOTT, R.D., MacKENZIE, A.B. and ALEXANDER, W.R. 1992. The interpretation of natual decay series disequilibrium in non-ideal systems: an example from Poços de Caldos, Brazil. J. Geochem. Explor. 46, 323-343.

SHIEH, Y.N. and TAYLOR, H.P. 1969. Oxygen and carbon isotope studies of contact metamorphism of carbonate rocks. J. Petrol. **10**, 307-331.

SKINNER, I.J. and LUCE, F.D. 1971. Solid solutions of the type (Ca, Mg, Mn, Fe)S and their use as geothermometers for the enstatite chrondrites. Amer. Mineral. **56**, 1269-1296.

SMITH, B., STUART, M.E., VICKERS, B.P. and PEACHEY, D. 1989. The characterisation of organics from the natural analogue site at Broubster, Caithness, Scotland, British Geological Survey Technical Report WE/89/33.

SMITH, R.M. and MARTELL, A.E. 1976. Critical Stability Comstants, Vol. 4, Inorganic complexes. Plenum Press, New York, USA, 256 pp.

STUMM W. and MORGAN, J. 1981. Aquatic Chemistry (2^{nd} Edit.) J. Wiley and Sons, London, UK

TAYLOR, H.P. 1986. J. Am. Ceram. Soc. **69**, 464.

TILLEY, C.E. 1929. On larnite (calcium orthosilicate, a new mineral) and its associated minerals from the limestone contact-zone of Scawt Hill, Co Antrim. Mineral. Mag. **22**, 77-86.

TILLEY, C.E. 1947. The gabbro-limestone contact zone of Camus Mor, Muck, Invernesshire. Bull. Comm. Geol. Fin. **140**, 97-105.

TILLEY, C.E. and ALDERMAN, A.R. 1934. Progressive metasomatism in flint nodules of the Scawt Hill contact-zone. Mineral. Mag. **23**, 513-518.

TREIMAN, A.H. and ESSENE, E.J. 1983. Phase equilibria in the system CaO-SiO_2-CO_2. Amer. J. Sci. **283A**, 97-120.

TWEED, C.J. and MILODOWSKI, A.E. 1992. An overview of the Maqarin Natural analogue project - a natural analogue study of a hyperalkaline cement groundwater system. Presented at the 5^{th} CEC-NAWG Workshop. Toledo, Spain. September 1992. CEC-EUR report series (in press).

UNDP/FAO 1970. Investigation of the Sandstone Aquifer of East Jordan, FAO, AGL. SF/Jor. a. Rome **286**.

VALLEY, J.W. 1986. Stable isotope geochemistry of metamorphic rocks. in Stable Isotopes in High Temperature Geologic Processes, ed Paul H. Ribbe, Min. Soc. Amer. Reviews in Mineral. **16**, 445-487.

VAN DEN BOOM, G. 1968. Zur Petrogenese der Plateaubasalte. Nordost Jordaniens Geol. Jb., Vol. 85, 489-496.

VAN DEN BOOM, G. and SUWWAN, O. 1966. Geological and Petrographical Studies of the Plateau Basalts, Arch. BRG, Hannover.

VICKERs, B.P. 1989. The use of portable speciation equipment in groundwater studies at the Poços de Caldas field site (Brazil). British Geological Survey Technical Report WI/89/9.

WALSH, J.N., BUCKLEY, F. and BARKER, J. 1981. The simultaneous determination of the rare-earth elements in rocks using inductively coupled plasma source spectroscopy. Chem.Geol. **33**, 141-153.

WEDEPOHL, K.H. (editor). 1978. Handbook of Geochemistry; part II, Volumes 2-5.. Springer Verlag, Berlin, Germany.

WEST, J.M., ROWE, E.J., WEALTHALL, G.P. and ALLEN, M.R. 1988. The geomicrobiology of the Drigg Research Site. Rep. Brit. Geol. Surv. WE/88//????

WESTALL, J.C., ZACKANY, J.L. and MOREL, F.M.M. 1976. MINEQL - a computer programme for the calculation of chemical equilibrium composition of aqueous systems. Tech. Note 18, Dept. Civil Eng., MIT, Cambridge, Mass., USA.

WETZEL, R. and MORTEN, D.M. 1959. Contribution a La Geologie de La Trans Jordanie, Notes, Mem.Moyen-Orient, 7:95-191 Museum Nat.d'Hist.Natrue., Paris.

WINKLER, H.G.F. 1976. Petrogenesis of Metamorphic Rocks. 4th ed. Springer-Verlag, Berlin, Germany.

YUSAF, R. and HAMILTON, E. 1992. Ripp 2 User Manual. NAGRA Technical Report Series NTB (in prep.), NAGRA, Baden, Switzerland.

A AQUEOUS GEOCHEMISTRY DATA SET

A1 GROUNDWATER ANALYTICAL TECHNIQUES

Bulk Groundwater and Ultrafiltered Samples

On return to the BGS laboratories, the groundwater samples were subject to a comprehensive suite of analysis precedures. Major cation and trace element analysis was carried out by inductively-coupled plasma - optical emmision spectroscopy (ICP-OES). The ICP-OES used was a Perkin-Elmer Plasma II sequential scanning system with twin 1 m vacuum monochromators. Monochromator A with a 3600 line/mm grating and wavelength range of 160-400 nm, and the second (B) with an 1800 line/mm grating and wavelength range of 160-800 nm.

The ICP-OES analysis was carried out on the sample acidified in the field to 1 % with AristaR HNO_3. Samples were prepared for analysis by the addition of 0.4. ml of 1000 mg/l Sc internal standard to 15 ml of sample. Samples were standardised every 10 samples and quality control check samples were run every 20 samples.

Ultra-trace elements were determined by inductively-coupled-mass spectrometry (ICP-MS) using a VG Instrument PlasmaQuad II ICP-MS system. ICP-MS analyses were made on the sample acidified in the field to 1 % with AristaR HNO_3. Samples had to be diluted tenfold in order to prevent fouling of the ICP nebuliser. The instrument was used in the scanning mode.

pH was re-measured in the laboratory by pH glass electrode. The reduced sulphur content was determined by the hydrogen sulphide generation ICP-OES method (CAVE and GREEN, 1989). Anions were determined by a combination of titrimetric and ion-chromatography techniques. A Dionex 2000i ion-chromatography system was used (Cl^-, SO_4^{2-}, NO_3^-, Br^-,NO_2^-, HPO_4^{2-}). IC analyses were carried out on filtered and diluted unacidified samples. No further sample preparation was made prior to analysis. Standards and quality control checks were run every 11 samples. The bicarbonate content was determined on a Radiometer autotitrator system by titration with 0.01M sulphric acid and end-point detection with glass pH electrode.

Ion-Exchange Column Experiment

The QMA ion-exchange columns were leached initially with 1.0M sodium hydroxice to remove anionic species. The eluent was then preserved by acidification with nitric acid. The QMA columns were subsequently leached with 1M nitric acid to elute the cationic components. CM and C_{18} columns were leached only by 1M nitric acid. Eluents from the columns were then analysed by ICP-OES and ICP-MS techniques.

Rn/Ra analyses of groundwater

Rn and Ra were determined on bulk unfiltered groundwater samples collected in 200 ml glass bottles with tight-sealing metal caps. Analyses were performed using a RDA Radon Degassing Unit (EDA INSTRUMENTS INC.) and RDA-200 Portable Radon Detector (EDA INSTRUMENTS INC.). The time and date of collection of the samples was carefully noted and the time elapsed between collection and analysis taken into account in calculating original Rn content. After flushing the apparatus with clean air, 130 ml of groundwater were degassed with air and the air stream passed into a ZnS scintillation cell. Cell backgrounds were determined prior to degassing. When degassing was complete, the number of counts were recorded over 5 minutes after an initial 2 minute waiting period.

Measurement of Rn

Rn content was calculated as follows:

(a) measured cpm/l at time of analysis = counts x 1000/(130 x 5)

(b) corrected cpm/l at time of sampling (as) = am $x1/e^{-\lambda(ts-tm)}$ where:
ts = sampling time
tm = measuring time
am = count rate at tm
as = counts at sampling time
$\lambda = 0.693/t1/2$
t1/2 = half-life of ^{222}Rn in minutes

(c) corrected cpm/l to ^{222}Rn "concentration"
cpm/l x cell factor = pCi/l or Bq/l where 27 pCi = 1Bq (=1.76 x 10^{-5} ppm^{222}Rn)

The cell factor is based on measurements taken using a standard solution of Ra. ^{222}Ra results have an average error of ± 6 % one sigma.

Measurement of Ra

Ra was determined leaving the degassed samples in metal-capped glass bottles for over 1 month in order to allow residual ^{222}Rn to decay and for ^{226}Ra to reach equilibrium with alpha-emmitting ^{222}Rn. The Rn was then remeasured as outlined above and the Ra content calculated.

^{226}Rn results are quoted with detection limits of 0.5 Bq/l which was based on an integrated sample count one sigma above an average integrated background count. Counting errors associated with these measurements result in an error of approximately ± 20 % 1 sigma.

A2 DATA RELEASE COVER NOTE

Database Title: AEM 3823-3831

Version Number: 6

Database Status: FQCV

Requesting Officer: A.E. Milodowski
Sample Origin: Maqarin, Jordan
Project Code: 81AG
Sample Description: Groundwaters
Total Number of Samples: 9
Date Received: 20/06/90

Comment on Analysis and Results:

Due to turbidity interferences ammonium could not be determined on all of the samples.

Higher than normal detection limits are quoted for a number of species due to matrix interference effects and the necessity to dilute the samples prior to analysis.

Gd failed QC checks but all results are below detection limit so have not been rerun. Ion balances in some cases are higher than usually accepted, this is believed to be due to the unusual matrix.
HPO4 results are quoted as ranges as previously discussed.

This version is issued as FQCV and all results have been checked for errors and analytical validity. This version supersedes all previous versions.

Approved

M.R. Cave

12/12/90

AEM 3823-3831 Version 6 7.2.91

BGS Code	Sample Code	pH	Ca	Mg	Na	K	HCO3	CH	Cl
			mg/l	mg/l	mg/l	mg/l	mg/l	mg/l	mg/l
3823	MQ1 4-6-90	12.64	653.00	<0.20	41.80	17.70	<5.0	559.0	62.60
3824	MQ2 4-6-90	12.53	590.00	<0.20	49.00	11.70	<5.0	445.0	56.40
3825	MQ3 5-6-90	12.48	673.00	<0.40	46.20	13.10	<5.0	491.0	55.00
3826	MQ5 4-6-90	12.60	1'050.00	<0.40	132.00	613.00	<5.0	677.0	51.00
3827	MQ6 6-6-90	12.95	1'120.00	<1.50	193.00	771.00	<5.0	693.0	45.70
3828	MQ6 7-6-90	12.71	1'110.00	<1.50	173.00	785.00	<5.0	729.0	47.80
3829	MQ7 7-6-90	12.67	622.00	<0.10	34.40	16.40	<5.0	558.0	68.50
3830	MQ8 7-6-90	12.64	624.00	<0.10	34.90	18.80	<5.0	569.0	71.40
3831	MQB1 5-6-90	4.59	0.70	<0.10	0.04	<0.50	18.8	<0.5	<2.00

BGS Code	SO4	NO3	Cation Total	Anion Total	Balance	S Balance	Br	NO2	HPO4
	mg/l	mg/l	meq/l	meq/l	%	%	mg/l	mg/l	mg/l
3823	292.00	2.15	35.08	40.80	-7.54	-6.98	0.32	1.67	0.04-0.20
3824	278.00	5.10	32.04	33.68	-2.50	-2.26	0.30	1.40	0.12-0.28
3825	279.00	2.37	36.10	36.33	-0.32	-0.75	0.27	1.58	<0.04
3826	1'480.00	38.20	74.26	72.73	1.04	0.67	<0.05	<0.04	<0.20
3827	1'670.00	38.60	84.55	77.64	4.26	3.49	<0.05	8.24	0.20-1.00
3828	1'700.00	40.50	83.53	80.48	1.86	2.79	<0.05	8.43	<0.20
3829	284.00	7.55	33.20	40.83	-10.31	-9.86	0.37	1.41	<0.04
3830	291.00	7.65	33.39	41.71	-11.07	-11.02	0.30	1.64	0.32-0.48
3831	<2.00	<0.10	0.04	0.31	-76.71	-78.51	<0.05	<0.01	0.23

BGS Code	F	TOC	TIC	C Diff	Total P	Total S	Reduced S	S Diff	NH4
	mg/l	mg/l	mg/l	%	mg/l	mg/l	mg/l		mg/l
3823	0.270	<0.5	<0.5	-96.08	<0.20	90.00	<0.005	-8.15	n/d
3824	0.408	<0.5	<0.5	-96.08	<0.20	90.10	<0.005	-2.85	n/d
3825	0.345	<0.5	<0.5	-96.08	<0.40	98.00	<0.005	5.10	n/d
3826	0.931	8.0	<0.5	-96.08	<0.40	502.00	0.024	1.73	4.90
3827	0.633	11.8	<0.5	-96.08	<1.50	576.00	0.008	3.36	6.90
3828	0.633	11.0	2.9	133.81	<1.50	543.00	0.019	-4.36	7.10
3829	0.355	1.7	2.7	136.31	<0.10	88.80	<0.005	-6.61	n/d
3830	0.322	1.8	3.7	126.50	<0.10	96.30	<0.005	-0.73	n/d
3831	0.003	<0.5	<0.5	837.25	<0.10	<0.20	<0.005	-233.33	n/d

BGS Code	Si	Ba	Sr	Mn	Total Fe	Al	Co	Ni	Cu
	mg/l	mg/l	mg/l	mg/l	mg/l	mg/l	mg/l	mg/l	mg/l
3823	<0.03	0.037	9.650	<0.002	<0.02	<0.50	<0.03	<0.03	<0.01
3824	<0.03	0.035	7.120	<0.002	<0.02	<0.50	<0.03	<0.03	<0.01
3825	<0.06	0.042	7.210	<0.004	<0.04	<0.50	<0.06	<0.06	<0.02
3826	<0.06	0.022	15.700	<0.004	<0.04	<0.50	<0.03	<0.06	<0.02
3827	<3.00	0.024	18.800	<0.015	<0.15	<0.50	<0.30	<0.300	0.09
3828	<3.00	0.026	18.800	<0.015	<0.15	<0.50	<0.30	<0.300	0.07
3829	0.06	0.052	10.400	<0.001	<0.01	<0.50	<0.02	<0.02	<0.01
3830	0.09	0.048	10.900	<0.001	<0.01	<0.50	<0.02	<0.02	<0.01
3831	0.02	0.150	0.008	<0.001	<0.01	<0.50	<0.02	<0.02	0.03

BGS Code	Zn	Cr	Zr	Mo	Cd	Pb	V	Li	B
	mg/l	mg/l	mg/l	mg/l	mg/l	mg/l	mg/l	mg/l	mg/l
3823	0.046	0.55	<0.02	0.05	<0.01	<0.20	<0.02	0.04	<0.10
3824	0.045	0.72	<0.02	0.06	<0.01	<0.20	<0.02	0.02	<0.10
3825	<0.015	0.77	<0.04	<0.06	<0.02	<0.40	<0.04	0.02	<0.15
3826	0.031	5.53	<0.04	0.19	<0.02	<0.40	<0.04	0.56	0.11
3827	0.045	7.03	<0.15	<0.30	<0.100	<1.50	<0.15	0.75	<1.00
3828	0.040	7.04	<0.15	<0.30	<0.100	<1.50	<0.15	0.72	<1.00
3829	0.062	0.60	<0.01	0.07	<0.005	<0.10	<0.01	0.04	<0.05
3830	0.051	0.61	<0.01	0.07	0.011	<0.10	<0.01	0.05	<0.05
3831	0.021	<0.01	<0.01	<0.02	<0.005	<0.10	<0.01	<0.01	<0.05

BGS Code	Y	La	Ce	Pr	Nd	Sm	Eu	Gd	Tb
	µg/l	µg/l	µg/l	µg/l	µg/l	µg/l	µg/l	µg/l	µg/l
3823	n/d	0.2	<0.1	<0.1	<0.20	<0.20	<0.10	<0.20	<0.10
3824	n/d	0.2	<0.1	<0.1	<0.20	<0.20	<0.10	<0.20	<0.10
3825	n/d	<0.1	<0.1	<0.1	<0.20	<0.20	<0.10	<0.20	<0.10
3826	n/d	0.1	<0.1	<0.1	<0.20	<0.20	<0.10	<0.20	<0.10
3827	n/d	0.2	<0.1	<0.1	<0.20	<0.20	<0.10	<0.20	<0.10
3828	n/d	0.1	<0.1	<0.1	<0.20	<0.20	<0.10	<0.20	<0.10
3829	n/d	0.4	<0.1	<0.1	<0.20	<0.20	<0.10	<0.20	<0.10
3830	n/d	<0.1	<0.1	<0.1	<0.20	<0.20	<0.10	<0.20	<0.10
3831	n/d	0.1	<0.01	<0.01	<0.02	0.04	0.03	<0.02	<0.01

A3 RESULTS OF EXPERIMENTS WITH ION-EXCHANGE COLUMNS (CARRIED OUT BY BGS)

Table A3.1 SEP-PAK ion exchange column results determined by ICP-OES & ICP-MS

Sample:	MQ1	MQ2	MQ5	MQ6	MQ7	BLANK
0.45µm filtered (pre column)						
Cr(mg/l)	0.72	0.74	5.70	6.88	0.66	<0.01
Mo(mg/l)	0.06	0.07	0.22	0.32	<0.06	<0.02
Zn(mg/l)	0.054	0.040	0.030	0.030	0.060	0.021
U(µg/l)	<0.3	<0.3	<0.3	<0.3	<0.3	<0.02
La(µg/l)	0.2	0.3	0.2	0.2	0.4	0.1
Ce(µg/l)	<0.06	<0.06	<0.06	<0.06	<0.06	<0.01
CM effluent						
Cr(mg/l)	0.57	0.75	5.75	6.81	0.66	nd
Mo(mg/l)	<0.01	0.07	0.24	0.32	0.07	nd
Zn(mg/l)	<0.03	<0.01	<0.02	<0.02	<0.02	nd
U(µg/l)	<0.3	<0.3	<0.3	<0.3	<0.3	nd
La(µg/l)	<0.1	0.4	0.1	0.2	0.6	nd
Ce(µg/l)	<0.06	<0.06	<0.07	<0.06	0.06	nd
CM HNO_3 **wash**						
Cr(mg/l)	<0.05	<0.05	<0.15	<0.15	<0.05	<0.01
Mo(mg/l)	<0.10	<0.10	<0.30	<0.30	<0.10	<0.02
Zn(mg/l)	0.215	0.241	0.152	0.149	0.217	0.075
U(µg/l)	0.08	<0.05	0.32	0.40	0.08	0.07
La(µg/l)	0.67	0.78	0.89	0.66	0.64	0.69
Ce(µg/l)	0.70	0.68	0.71	0.67	0.62	0.72
QMA effluent						
Cr(mg/l)	0.29	0.26	5.76	6.77	0.37	nd
Mo(mg/l)	0.04	0.04	0.21	0.29	<0.06	nd
Zn(mg/l)	<0.01	<0.01	<0.02	<0.02	<0.02	nd
U(µg/l)	<0.3	<0.3	<0.3	<0.3	<0.3	nd
La(µg/l)	0.2	<0.1	0.2	0.2	0.4	nd
Ce(µg/l)	<0.06	<0.06	<0.06	<0.06	<0.06	nd

Table A3.1 (continued)

Sample:	MQ1	MQ2	MQ5	MQ6	MQ7	BLANK
QMA NaOH wash						
Cr(mg/l)	0.40	0.64	1.00	1.00	0.50	0.04
Mo(mg/l)	<0.10	<0.10	<0.30	<0.30	<0.10	<0.02
Zn(mg/l)	<0.025	<0.025	<0.075	<0.075	0.031	0.075
U(µg/l)	<0.50	<0.50	<0.50	<0.50	<0.50	<1.00
La(µg/l)	0.10	<0.10	<0.10	0.10	<0.10	<0.20
Ce(µg/l)	<0.10	<0.10	<0.10	<0.10	0.10	<0.20
QMA HNO_3 wash						
Cr(mg/l)	<0.05	<0.05	<0.15	<0.15	<0.05	<0.01
Mo(mg/l)	<0.10	<0.10	<0.30	<0.30	<0.10	<0.02
Zn(mg/l)	0.204	0.182	0.150	0.139	0.202	0.039
U(µg/l)	<0.05	0.08	0.30	0.28	0.05	<0.05
La(µg/l)	0.72	2.26	0.87	0.73	0.72	0.79
Ce(µg/l)	1.31	1.41	1.39	1.25	1.28	1.08
C-18 effluent						
Cr(mg/l)	0.54	0.74	5.71	6.78	0.65	nd
Mo(mg/l)	0.06	0.06	0.21	0.30	<0.06	nd
Zn(mg/l)	0.01	0.01	<0.02	<0.02	<0.02	nd
U(µg/l)	<0.3	<0.3	<0.3	<0.3	<0.3	nd
La(µg/l)	0.4	0.4	0.2	0.2	0.3	nd
Ce(µg/l)	<0.06	<0.06	<0.06	0.06	<0.06	nd
C-18 HNO_3 wash						
Cr(mg/l)	<0.05	<0.05	<0.15	<0.15	<0.05	<0.01
Mo(mg/l)	<0.10	<0.10	<0.30	<0.30	<0.10	<0.02
Zn(mg/l)	0.187	0.183	0.194	0.207	0.223	0.020
U(µg/l)	<0.05	<0.05	0.34	0.43	0.06	<0.05
La(µg/l)	0.15	0.19	0.15	0.17	0.13	0.04
Ce(µg/l)	0.19	0.25	0.13	0.13	0.10	0.07

Table A3.2 U, La and Ce concentration in groundwater recalculated from ion-exchange column experiments (after subtraction blank values).

Sample	U µg/l	La µg/l	Ce µg/l
MQ1(QMA)	<0.03	0.03*	0.12
MQ1(CM)	0.005*	<0.3	0.01*
MQ1(C-18)	<0.03	0.06	0.06
MQ2(QMA)	0.04	0.74	0.17
MQ2(CM)	<0.03	0.05*	<0.35
MQ2(C-18)	<0.03	0.08	0.09
MQ5(QMA)	0.15	0.08*	0.16
MQ5(CM)	0.13	0.10	<.035
MQ5(C-18)	0.17	0.06	0.03
MQ6(QMA)	0.14	0.02*	0.09
MQ6(CM)	0.17	<0.30	<0.35
MQ6(C-18)	0.22	0.07	0.03
MQ7(QMA)	0.03	<0.40	0.15
MQ7(CM)	0.005*	<0.30	<0.35
MQ7(C-18)	0.03	0.05	0.02*

note: * denotes value close to or only just above blank values.

A4 STABLE ISOTOPE DATA

Isotopic analyses

Stable isotope ratios in water samples were determined at the Institute of Hydrology/GSF by standard methods involving measurement of CO_2 gas equilibrated with water samples at 25 C (for ^{18}O) and measurement of hydrogen gas evolved by the reduction of water by reaction on zinc at 430 C. SO_4 was precipitated as $BaSO_4$ from filtered samples in the field and converted to SO_2 for mass spectrometric analysis by high temperature reaction in the presence of copper oxide (Institute for Hydrology/GSF and the University of Ottawa. CO_2 evolved from carbonate samples by acidification with 100 % H_3PO_4 were analysed at the University of Ottawa. Bitumen samples were converted to CO_2 for mass spectrometric analyses (University of Ottawa) by oxidation under an O_2 atmosphere.

MAQARIN BITUMEN SAMPLES

	Carbon-13
A6-3a (89-6-3)	-27.25
A6-2P (210 m)	-25.25
A6-7P (105 m)	-25.93
MQ-10.1P	-26.84

MAQARIN SULPHATE SAMPLES

		Sulphur-34 PDB	Oxygen-18 SMOW
GSF			
MQ-1	(BaSO4-A, no AC)	-1.7	12.2
MQ-2	(BaSO4, no AC)	-0.8	12.7
MQ-5	(BaSO4-A, no ZnAC)	-2.6	
MQ-5	(BaSO4-A, no ZnAC)	-2.6	
MQ-6	(BaSO4-A, no ZnAC)	-2.5	
Ottawa			
MQ-1	(BaSO4-B, no AC)	1.6	
MQ-5	(BaSO4-B, no ZnAC)	0.5	
MQ-5	(BaSO4-B, with ZnAC)	0.7	
MQ-6	(BaSO4-B, with ZnAC)	1.2	
MQ-7	(BaSO4, no AC)	0.3	
MQ-8	(BaSO4, no AC)	0.1	

MAQARIN WATER SAMPLES

	Oxygen-18 SMOW	Deuterium SMOW
MQ-1	-4.74	-22.6
MQ-2	-4.76	-21.7
MQ-3	-4.83	-22.6
MQ-4	-4.36	-18.6
MQ-5	-4.13	-18.6
MQ-6	-4.81	-23.9
MQ-7	-4.99	-23.8
MQ-8	-5.68	-28.8

MAQARIN CARBONATE SAMPLES (Sampled June/90, Analysed Aug/90)

Precipitates from hyperalkaline waters			Oxgen-18 PDB	Carbon-13 PDB
MQ-1.1P	Pool sediment	ap	-20.02	-22.92
MQ-1.2P	Pool rim	ap	-20.60	-23.29
MQ-2.1P	Drip straws	as	-21.62	-25.37
MQ-4P	Crust by He sample	aw	-21.40	-25.73
MQ-5P	Vent at river	mq5	-05.15	-11.05
MQ-5/6.1P	Seepage crust	mq5	-11.00	-21.92
MQ-5/6.2P	Seepage crust	mq5	-12.63	-22.23
MQ-5/6.4P	Colluvium Matrix	mq5	-11.76	-17.30
MQ-6.1P	Vent crust	mq6	-04.46	-11.26
A6-2 (89)	Stalactite	as	-20.87	-30.75
A6-12 (89)	White wall crust	aw	-21.08	-23.54
RS-3 (i)	Railway cut stalagmite/tites	rs	-16.86	-30.08
RS-3 (iii)		rs	-18.32	-28.32
RS-3 (vi)		rs	-18.77	-29.48
RS-3 (viii)		rs	-18.48	-29.82
RS-3 (ix)		rs	-18.24	-29.04

			Oxgen-18 PDB	Carbon-13 PDB
Spontaneous combustion sampels				
MQ-10.2Pa	bituminous		-4.23	-0.37
MQ-10.2Pb	light, no bit., fractured		-4.81	-0.54
MQ-10.2Pc	friable altered ls ext.		-7.31	-2.35
MQ-10.3Pa	darker, bit.-free ls		-6.80	-0.83
MQ-10.3Pb	lighter rim of altered ls		-8.67	-1.80
MQ-10.3Pc	friable coating, altered ls		-9.53	-3.63
MQ-10.4P	buff, highly altered ls, soft		-7.47	-3.59
MQ-10.5Pa	darker, bit.-free ls		-5.33	-0.33
MQ-10.5Pb	lighter rim of altered ls		-6.22	-2.16
MQ-10.5Pc	friable coating, altered ls		-7.77	-4.95
MQ-10.7P	unaltered bitum. ls, free bit.		-4.82	0.72
Host altered limestone form road cut				
MQ-11.1	Altered ls (white)		-5.05	-1.33
MQ-11.2	Altered ls (red)		-5.40	-1.48
Adit A6 wall samples				
A6.1Pa	230 m Secondary crust on fracture		-17.60	-29.17
A6.1Pb	230 m Altered ls (buff)	m	-06.71	-03.23
A6.2P	210 m Bituminous ls	m	-04.41	-03.26
A6.3Pa	180 m Fracture cal., micro-cx	ff	-14.74	-24.74
A6.3Pb	180 m Fracture cal., crs-cx	fc	-14.95	-24.40
A6.3Pc	180 m Altered ls	m	-16.04	-19.67
A6.4Pa	175 m Open fracture surface	ff	-16.97	-22.61
A6.4Pc	175 m Altered ls	m	-14.33	-25.82
A6.5P	160 m Altered ls	m	-14.99	-19.16
A6.6P	120 m Altered ls	m	-14.09	-20.74
A6.8Pa	2 m Laminated white calcite	ff	-15.37	-28.75
A6.8Pb	2 m Altered host ls	m	-05.60	-01.96
A6-3a (89)	2 m Unaltered bituminous ls	m	-05.36	-00.92
KZ-10a	host red marble	kz	-12.17	-15.52
KZ-10b	pale red, along fracture	kz	-12.55	-15.23
KZ-10c	white fracture surface coating	kz	-0110.	-19.94
KZ-11a	host maroon marble	kz	-09.24	-17.30
KZ-11b	buff dusting on 11a	kz	-06.06	-09.89
KZ-11c	laminated, crs cx (recx ?)	kz	-09.00	-11.69
KZ-11d	powdery lams of calc.	kz	-07.79	-14.80
KZ-12a	red marble clast in white calcite	kz	-10.43	-1711.

			Oxgen-18 PDB	Carbon-13 PDB
KZ-12b	green clast/mottle	kz	-10.43	-15.74
KZ-12c	white calcite vug lining	kz	-08.00	-09.81
KZ-13a	dark buff/grey host ls	kz	-10.07	-14.47
KZ-13b	white crpt cx ca. fract lining		-06.75	-05.19
KZ-13c	crs cx cal. in middle of fract.		-09.88	-07.04

KHOURY

M1		-11.4895	-24.51
M2	calcite, qtz, thaumosite	-08.07485	-18.22
M3		-14.1668	-15.44
M4	calcite, thaumosite	-11.0917	-14.58
M5	calcite, thaumosite, tobermorite, wollas	-14.4966	-16.21
M6	calcite, thaumosite, apatite, wollastoni	-13.0319	-15.36
M7	calcite, thaumosite, apatite	-09.11281	-17.59
M8	thaumosite, calcite, apatite	-12.4692	-19.39
M8A	thaumosite, calcite, apatite	-10.9559	-17.85
M9		-11.1693	-15.37
M10		-10.6649	-19.22
M11	calcite, spurrite, apatite?	-14.5937	-19.11
M12	calcite thaumosite, portlandite, apatite	-13.6430	-16.89
M14	no carbonate		
M15		-13.2647	-14.00
M24	calcite, apatite, spurrite	-14.8459	-18.94
M26	calcite, portlandite, apatite	-14.0892	-18.31

A5 Ra-226 AND Rn-222 ISOTOPIC DATA

Table A5.1 Summary of Rn and Ra determinations on waters from North Jordan.

Sample number	site description	Activity (pCi l-1)	Activity (Bq l-1)
Radium-226			
MQ1 Ra-226	Small clear pool on floor of adit A6	13	0.49*
MQ2 Ra-226	Stalactite drips 5m north MQ1	27	0.99*
MQ5 Ra-226	Spring seepage Wadi Yarmouk	<11	<0.40
MQ6 Ra-226	Spring seepage Wadi Yarmouk	<11	<0.40
MQ8 Ra-226	Railway cutting	<11	<0.40
Radon-222			
MQ1 Rn-222	Small clear pool on floor of adit A6	5280	195
MQ2 Rn-222	Stalactite drips 5m north MQ1	3390	125
MQ5 Rn-222	Spring seepage Wadi Yarmouk	3420	125
MQ6 Rn-222	Spring seepage Wadi Yarmouk	5300	195
MQ8 Rn-222	Railway cutting	nm	nm

Radium-226 results are quoted with a detection limit of 0.5 Bq l^{-1} which is based on an integrated sample count one sigma above an average integrated background count of 6.4 cpm.

Radon-222 results have an avarage error of ± 6 % one sigma.

* Counting errors associated with these measurements result in an error of approximately ± 20 % 1 sigma.

nb. 1 Bq l^{-1} ^{226}Ra = 2.73 x 10^{-5} ppm ^{226}Ra

1 Bq l^{-1} ^{222}Rn = 1,76 x 10^{-10} ppm ^{222}Rn

Table A5.2 Raw Data and instrument details

SAMPLE	SITE	SAMPLE	SAMPLE	ANALYSIS	ANALYSIS	CELL	Cell Sensitivity	BACKGROUND	SAMPLE
NO		DATE	TIME (BST)	DATE	TIME (BST)	NO	(cpm/pCi)	(5 MIN COUNT)	(5 MIN COUNT)
MQ1 Rn-222	Small clear pool on floor of adit A	6-Jun-90	08:57	19-Jun-90	14:54	C	0.96	4	303
MQ2 Rn-222	Stalactite drips 5m north MQ1	6-Jun-90	09.00	19-Jun-90	14:41	B	0.92	32	216
MQ5 Rn-222	Spring seepage Wadi Yarmouk	6-Jun-90	13.20	19-Jun-90	15.33	D	0.96	2	201
MQ6 Rn-222	Spring seepage Wadi Yarmouk	6-Jun-90	13.19	19-Jun-90	15.49	E	1.02	5	332
MQ8 Rn-222	Railway cutting	6-Jun-90	08.00	nm	nm	nm	nm	nm	nm
MQ1 Ra-226	Small clear pool on floor of adit A	6-Jun-90	08.57	6-Aug-90	13.01	B	0.92	4	12
MQ2 Ra-226	Stalactite drips 5m north MQ1	6-Jun-90	09.00	6-Aug-90	13.30	A	1.03	1	19
MQ5 Ra-226	Spring seepage Wadi Yarmouk	6-Jun-90	13.20	6-Aug-90	13.42	C	0.96	10	8
MQ6 Ra-226	Spring seepage Wadi Yarmouk	6-Jun-90	13.19	6-Aug-90	13.54	D	0.96	10	9
MQ8 Ra-226	Railway cutting	6-Jun-90	08.00	6-Aug-90	14.09	E	1.02	7	12

Table A5.2 (Continued)

SAMPLE	TIME DELAY	FACTOR	CORRECTED	222Rn ACTIVITY	222Rn ACTIVITY
103 ml (CPS9	(HRS)		(CPS/l)	(pCi/l)	(Bq/l)
1.00	317.95	11.03	85	5283	195
0.61	317.68	11.00	52	3386	125
0.66	314.22	10.72	55	3418	126
1.09	314.50	10.74	90	5298	196
nm	nm	nm	nm	nm	nm
0.03	1468.07	1.00	0.21	13.35	0.49
0.06	1468.50	1.00	0.46	26.89	0.99
-0.01	1464.37	1.00	-0.05	-3.21	-0.12
0.00	1464.58	1.00	-0.03	-1.60	-0.06
0.02	1470.15	1.00	0.13	7.54	0.28

B RESULTS OF THE SOURCE TERM DIGESTIONS BY UO AND GSC

J. LOOP and G. HALL

Source Term Evaluation - Determination of the major, minor and trace element distribution between the calcite and bitumen phases of the unaltered Maqarin bituminous limestone.

Samples:

- A6 - 3A - Unaltered bituminous limestone, sampled 89-5-21 from mouth of Adit A-6. Light grey, v. hard, strong reaction to 5 % HCl.
- A6 - 2P - Unaltered bituminous limestone, collected 90-6-6 from 210 m point in Adit A-6. Very hard, dark grey, sli. bitumen smell, very strong reaction to 5 % HCl.
- A6 - 7P - Unaltered bituminous limestone, collected 90-6-6 from 105 m point in Adit A-6. Dark grey/brn, soft material.
- MQ10.1P - Bituminous limestone collected 90-6-6 from site of burning waste rock dump. Bitumen content enriched by heating and bitumen migration. Soft, loose, brown material with strong bitumen smell. Weak reaction to 5 % HCl.

Sample treatment:

1. Samples crushed and disolved in 5 % HCl for 5 days,
2. Filtered with 0.45 µm pore diameter disks. Filtrate air dried and weighed for calculation of bitumen content. Note, filtrant had in all cases a pale yellow colour, indicating mild leaching of organic material.
3. Filtrant analysed by ICP-OES and ICP-MS. Results calculated as ppm (ICP-OES) and ppb (ICP-MS, except Ni) of total rock.
4. Air dried filtrate weighed into clean, fired COORS crucibles and thermally decomposed by gradual heating to 550C. Residue weighed for calculation of non-carbonate, non-bitumen content.
5. Residue reacted in 1 ml ULTREX HNO_3 followed by 3 ml ULTREX HCl. Samples then filtered (0.45 µm) and the filtrant analysed by ICP-OES and ICP-MS. Results calculated as ppm (ICP-OES) and ppb (ICP-MS, except Ni) of total rock.
6. Filter papers were ashed at 450C and weighed to calculate the soluble fraction.

Analysis:

ICP-OES John Loop
Geochemistry Laboratory
University of Ottawa

ICP-MS Gwendy Hall
Geological Survey of Canada
Ottawa, Canada

Carb = Concentration in carbonate phase expressed as ug/g of total rock.
Bit = Concentration in bitumen phase expressed as ug/g of total rock

ICP-OES (J. Loop)

Sample	Fraction Bitumen	Fraction Non-carb Non-bit	Na		K		Ca		Mg	
			Carb	Bit	Carb	Bit	Carb	Bit	Carb	Bit
A6-3A	0.20	0.06	305	33	126	89	112493	232	1721	-0
A63Ar	0.20	0.06	299	30	125	50	156335	370	1723	-0
MQ10-1P	0.41	0.28	299	421	127	1420	176747	746	893	-16
A6-2P 210 m	0.08	0.02	389	118	334	162	243983	311	2439	-1
A6-7P 105 m	0.14	0.07	374	87	825	540	300289	658	561	1
BLANK	0	0.00	0	2	0	0	0	3	0	0

Sample	Sr		Ba		Cr		Mn		Fe	
	Carb	Bit	Carb	Bit	Carb	Bit	Carb	Bit	Carb	Bit
A6-3A	1062	5	121	5	219	0	14	-0	5575	2
A63Ar	1064	7	134	24	214	-0	15	0	5640	2
MQ10-1P	1840	-2	48	-0	351	10	22	0	2481	1
A6-2P 210 m	649	3	41	1	77	2	112	2	4951	1184
A6-7P 105 m	1259	1	83	-0	99	0	26	0	698	27
									0	1

Sample	Co		Ni		Cu		Zn		Cd		Al	
	Carb	Bit	Carb	Bit	Carb	Bit	Carb	Bit	Carb	Bit	Carb	Bit
A6-3A	1	1	75	47	30	21	276	16	2	0	13146	143
A63Ar	0	0	76	43	22	19	276	14	2	-0	12972	114
MQ10-1P	0	14	63	-24	12	22	227	50	1	-10	18778	7982
A6-2P 210 m	1	2	45	31	10	18	57	14	1	4	2445	404
A6-7P 105 m	1	0	73	-3	17	19	287	20	2	0	3050	3827
BLANK	0	0	0	0	0	0	0	0	0	-0	0	4

ICP-MS (G. Hall)

Sample	Ni (ppm)			Se (ppb)			Sn (ppb)			Pb (ppb)		
	Carb	Bitumen	+/-	Carb	Bitumen	+/-	Carb	Bitumen	+/-	Carb	Bitumen	+/-
A6-3A	2541	40	2	17098	161	33	191.7	90.1	65	2389	447	348
A63Ar	0	38	2	0	163	31	0.0	75.0	60	--	400	323
MQ10-1P	78	14	3	1413	8068	56	105.7	240.9	110	2376	2755	590
A6-2P 210 m	53	22	7	<50	2650	149	124.1	275.5	290	2982	2010	1563
A6-7P 105 m	93	45	3	5230	3264	57	53.7	134.0	111	1073	1164	596
BLANK	--	<0.1		<50	<2.0		0.0	3.9		--	21	

Sample	U (ppb)			Th (ppb)			Pd (ppt)
	Carb	Bitumen	+/-	Carb	Bitumen	+/-	
A6-3A	18356	878	83	1015	46	10	<0.2
A63Ar	--	953	77	--	54	9	<0.2
MQ10-1P	8358	450	141	115	798	17	<0.2
A6-2P 210 m	4618	3648	372	900	395	45	<0.2
A6-7P 105 m	8001	10132	142	176	681	17	<0.2
BLANK	<1	<5		<1	<0.6		

C DESCRIPTION OF THE MINERALOGY, PETROGRAPHY AND GEOCHEMISTRY OF THE MAQARIN SOURCE-TERM ROCKS AND THEIR SECONDARY ALTERATION PRODUCTS

A.E. MILODOWSKI, H.N. KHOURY, J.M. PEARCE, E.K. HYSLOP and I.D. CLARK

C 1 Introduction

This appendix is a companion to chapter 4.1 and contains the detailed description of the mineralogy, petrography and geochemistry of the Maqarin source-term rocks plus information on their secondary alteration products. Discussion is kept to the minimum as most important points are covered in chapter 4.1. Please note that any papers cited are detailed in the main reference list.

C 2 Analytical methods

C 2.1 Samples

A representative suite of samples for mineralogical and geochemical analysis was examined from unmetamorphosed host sedimentary rocks, high temperature metamorphic rocks and retrograde hydrated and leached metamorphic rock types. Most rock samples were collected from wall exposure in the dam site investigation adit A-6 (samples prefixed "A6" eg. A6.1P) together with selected samples taken from narrow diameter site investigation cores, now curated in the University of Jordan, (UJ) Amman, drilled into the metamorphic zone in adits A-6 and A-7 (samples prefixed "M" eg. M15P). In addition, contemporary travertine and carbonate deposits precipitated from active hyperalkaline discharge zones (MQ1, MQ2, MQ5, MQ6 and MQ7-9) were also analysed. A series of samples was also collected from a rock waste spoil tip left by the dam site investigations (samples prefixed "MQ10"). The spoil was found to be actively burning as a result of spontaneous combustion. Temperatures in excess of 300 C were measured within 10 cm depth and bitumen could be seen seeping out of the rock and migrating (condensing) to cooler parts of the spoil.

C 2.2 Mineralogical analysis

Detailed mineralogical and petrographic analyses of the rocks and precipitates were undertaken by BGS and augment the data obtained previously by UJ (KHOURY and NASSIR, 1982b; KHOURY unpublished data). Polished thin sections were prepared from the metamorphic and sedimentary rocks and examined by optical petrographic microscope, cathodoluminescence microscopy (CL), backscattered scanning electron

microscopy with qualitative energy-dispersive X-ray microanalysis (BSEM-EDXA) and limited wavelength-dispersive electron microprobe analysis (EMPA). Fission-track prints were prepared from the polished thin sections prior to detailed BSEM-EDXA examination. The fission-track prints were used to provide a map of the uranium distribution, to aid location of uranium-bearing species for identification under BSEM-EDXA observation and to quantify the uranium present in different mineral species. Fracture/cavity infill and coating minerals were hand separated under binocular microscope for identification by X-ray powder photography (Debye-Scherrer camera). Samples of rock and secondary precipitate were crushed and powdered to less than 125 μm size and analysed semi-quantitatively by X-ray diffraction analysis (XRD). A summary of the samples analysed is given in table C1. Details of the analytical techniques employed are given in chapter 3.

C 2.3 Geochemical analysis

Samples of unmetamorphosed rocks, metamorphosed rock, retrograde altered rocks, secondary precipitates and some hand-separated mineral phases were analysed via BGS for elemental (Li, Sr,Ba, Pb, Cd, Ag, Zn, Cu, Co, Ni, Mn, V, Ti, Cr, Mo, Sn, U, Th, Nb, Zr, Y, Sc, As, S, Se, F and Cl) geochemistry by a combination of X-ray fluorescence (XRF) spectroscopy, inductively-coupled plasma - optical emmission spectroscopy (ICP-OES) and atomic absorption spectroscopy (AAS). Rare earth analyses were carried out by ICP-OES after acid digestion and ion-exchange pre-concentration (WALSH et al., 1981). Where insufficient material was available for routine analysis (as in the case of some hand-picked mineral separates), semi-quantitative trace element analyses were performed by XRF on loosely dispersed powders.

Pd was determined on a limited number of samples by fire assay-silver collection with electrothermal atomisation-AAS finish. Further analyses were undertaken via the University of Ottawa in order to try to determine the trace element composition of both the acid-soluble "carbonate" fraction and the "bituminous" acid-insoluble fraction within the unaltered bituminous limestone. Solutions were analysed by ICP-OES and ICP-MS techniques. A summary of the geochemical analysis schedule and samples analysed is given in table C2. Further details of analytical techniques used are given below.

In addition to the analyses above, a limited number of samples were analysed for natural decay series disequilibria at the Scottish Universities Research and Reactor Centre (SURRC) and at the Environmental Radiochemistry Laboratory of the Australian Nuclear Science and Technology Organisation (ANSTO).

C 2.3.1 Detailed description of the analytical methods

Backscattered Scanning Electron Microscopy

Backscattered scanning electron microscope (BSEM) petrographic analyses were undertaken using a Cambridge Instruments Stereoscan S250 scanning electron microscope fitted with a 4-element solid-state (diode-type) backscattered electron detector (KE Developments Ltd.). Mineralogical and chemical characterisation of phases imaged under BSEM was facilitated by qualitative observation of their energy-dispersive X-ray spectra. These were recorded using a Link Systems 860 energy-dispersive X-ray microanalyser (EDXA). The EDXA system has a detection limit of approximately 0.2% (weight) for most common elements but this is probably of the order of 0.5 % (weight) for uranium, thorium and other heavy elements at typical count-times of 100 seconds at 20kV beam voltage used.

Under BSEM images are related to the composition of the material being examined. Image brightness is proportional to the average atomic number of the material, thus allowing the distribution of different minerals or phases to be determined on the basis of their chemical composition. (GOLDSTEIN et.al., 1981).

All BSEM analyses were carried out using polished thin sections. Prior to examination the sections were coated with approximately 200 Å of carbon by evaporation onto the specimen surface under vacuum. BSEM observation was conducted using a 20kV beam potential.

Cathodoluminescence microscopy

The phenomenon of the emmision of light from certain minerals during electron irradiation (cathodoluminescence) is well documented in the literature (eg.. NICKEL, 1978; MARSHALL, 1987). Cathodoluminescence (CL) has its origin in the "molecular" distortions of the crystal lattice. These structures give resonance under electron bombardment, but radiation is also controlled by the highly complex balance of valance electrons in the crystal lattice. CL is often a very useful tool for locating trace luminescent phases and for revealing the original fabric in recrystallised rocks (particularly carbonates). It is a particularly sensitive technique for identifying multiple generations of mineralisation and growth zoning within carbonate minerals.

CL analyses were conducted on polished thin-sections using a Technosyn model 8200 MkII cold cathode stage fitted to an optical microscope with long working-distance lenses. The instrument was operated at an excitation voltage of 10-20kV and a beam current between 500-700 µA. Care was taken in order to prevent the sample being damaged during electron bombardment.

Fission-Track Registration

In any comprehensive mineralogical and geochemical study of radionuclide occurrence and distribution, the location of all possible hosts by charged particle track registration techniques is an essential precursor to evaluation by identification methods such as optical and electron microscopy. In this study the precise location of all uranium sites in polished thin section was achieved by recording fission fragments derived from uranium under neutron irradiation in a reactor [(n,f) reaction]. Interference from thorium was avoided by selecting a highly thermalised neutron flux in which only ^{235}U undergoes appreciable fission. Irradiations were carried out at the Scottish Universities Research and Reactor Centre, East Kilbride (SURRC).

The method employed was based on that of KLEEMEN and LOVERING (1967). "Lexan" polycarbonate plastic was used as a detector and tracks of the induced fission fragments revealed by etching for 5 minutes at 60 C in 6 molar NaOH solution. The technique yields accurate spatial information on the location of uranium in the polished section in the form of micromaps. Quantitative estimation of the uranium content of different host minerals was achieved by the irradiation of uranium-doped standard glasses along with the sample batches and consequent track counting on an equal area basis using an optical microscope.

Electron Microprobe Analyses

Mineral compositions were determined by wavelength-dispersive electron microprobe analyses (EMPA). Analyses were made from carbon-coated polished thin sections after detailed backscattered scanning electron microscope examination. A Cameca SX50 electron microprobe was used to carry out the analyses. Points for EMPA analyses in a given polished-section were located under a petrological microscope and their coordinates programmed automatically into the microprobe via an automated stage on the microscope. Potential analyses points were re-checked once the section was placed inside the microprobe, using backscatterd electron imaging and qualitative energy-dispersive X-ray microanalyses. Corrections and changes were made as necessary to the programmed analyses points. The electron microprobe was initially operated at a beam voltage of 15kV, 200000x magnification and a specimen current set to 20nA. However, volatilisation of some elements (mainly alkalis and selenium) was suspected due to the high specimen current. Consequently, analyses were re-checked with specimen currents reduced to 10nA or 5nA where necessary.

The microprobe was pre-calibrated using in-house mineral, pure metal and oxide standards and calibration simply re-checked and "refreshed" as appropriate prior to use. Data was processed, and atomic number, X-ray absorption and X-ray fluorescence corrections taken into account, using Cameca software.

X-ray diffraction

For bulk-rock X-ray diffraction analysis, the samples were crushed in a rotary agate mortar and pestle until the sample was finer than 125 μm. A representative subsample was taken from the <125 μm powdered material and micronised for 5 minutes under acetone in a micronising mill to further reduce the grain size. The micronised material was dried overnight at 55 C before being dissaggregated in a pestle and mortar. The finely powdered material was back-loaded into a sample holder to produce a randomly oriented X-ray diffraction mount.

Prepared XRD mounts were analysed on a Phillips 1700 series automatic diffractometer using Co-Kα radiation. The X-ray generator was operated at 45kV and 40mA. Diffraction traces were processed using Phillips ADP1700 software coupled to a JCPDS database running on a DEC MicroVax 2000 computer system. Whole-rock XRD scans were completed over the range 3-50° 2 θ at a rate of 0.9° 2 θ per minute.

X-ray powder photography

X-ray powder diffraction photography (XRPD) allows a very small sample to be analysed by X-ray diffraction techniques. Small pin-head sized samples were extracted with a scalpel from rock specimens and mixed with "Durofix" cement diluted with amyl acetate to form a paste. This was then rolled out to form a spindle approximately 5 mm long and 0.1 mm diameter. The spindle was mounted in a Debye-Scherrer camera of 130 mm diameter and irradiated with a columnated beam of Cu-Kα radiation. Exposure times were made between 30-40 hours to ensure that good diffraction patterns were obtained. The resultant X-ray photograph was developed and the pattern measured manually and compared with the JCPDS index using the JCPDS Hanault Search Manual to identify the phase(s) present.

Whole rock geochemical analyses

Whole-rock geochemical analyses for major and trace elements were obtained by a combination of X-ray fluorescence and inductively-coupled plasma - optical emmission spectrometry (ICP-OES). Si, P, As, Cl, F, Se, S, Sn, Th, U and Zr were determined by XRF on pressed powder pellets (CALEB BRETT LTD). Al, Mg, Ca, Na, K, P, Fe (total as ferric iron), Ti, V, Cr, Mn, Li, Ba, Sr, Ni, Co, Cu, Zn, Ag, Zr, Nb, and Sc were determined by ICP-OES (ROYAL HOLLOWAY and BEDFORD NEW COLLEGE) after perchloric acid/hydrofluoric acid digestion. In addition, Pb, Mo and Cd were determined on the same solutions by atomic absorption spectrometry. Rare Earth Element (REE) compositions were also determined (RHBNC) by ICP-OES after ion-exchange pre-concentration using the method of WALSH et. al. (1981).

A limited number of samples were also analysed for Pd by Caleb Brett Ltd. using a modified fire-assay technique. This employed preparation as a lead button using a silver carrier, followed by dissolution in nitric acid and sulphuric acid. The resultant solution was analysed by atomic absorption spectrometry with electrothermal atomisation (ETA-AAS).

Where insufficient material was available for routine quantitative XRF material was analysed at BGS by XRF as dispersed thin-film mounts. Samples were scanned qualitatively to identify the elements present. U was semi-quantitatively estimated by comparison to standard samples prepared under similar conditions.

C 3 Mineralogy and Petrography

C 3.1 Bituminous limestone and marl

Primary and detrital mineralogy

Bulk XRD data for all the samples analysed during this study are presented in table C3. The unaltered bituminous limestone and "marl" samples examined during this study are very similar to the bituminous limestones described previously from a larger survey of the bituminous limestone of the Maqarin area (Abed and Amireh, 1983). The rocks vary in colour from light grey to brown and black and are bituminous, having a distinctive hydrocarbon odour. They comprise fine grained biomicrites containing silt-grade to fine sand-grade calcareous foraminiferal debris (10-200 μm) floating in a matrix of fine grained (<5 μm) comminuted foraminiferal and other calcareous debris and minor amounts of clay minerals (Plate 1). However, the abundance of complete tests varies considerably between samples but they appear to be particularly common in sample A6.9P. BSEM observation suggests that several different genera of foraminera and other microfossils are present, including multi-chambered tests of large forams, single chambered oblate and spherical forms, and calcareous "wheel-shaped" spicules possibly derived from sponges.

Clay mineral content is low and undetected by bulk XRD (table C3, figure C1) and although no clay fraction XRD analyses were performed, BSEM-EDXA observation indicates that the major clay mineral species appear to be kaolinite and illite. Whole-rock geochemistry (section C4) also indicates low clay mineral contents. Recalculation of the sodium, potassium and aluminium content of samples A6.7P (Na2O = 0.07%; K2O = 0.81%; Al2O3 = 2.33) and A6.9P (Na2O = 0.10%; K2O = 0.18%; Al2O3 = 2.77%) indicates an equivalent content of approximately 6% illite (assuming ideal illite composition $K(Na)_{1.5}Al_4[Si_{6.5}Al_{1.5}O_{20}](OH)_4$) and 0-1.5% kaolinite (as $Al_4(Si_4O_{10})(OH)_8$). In A6.7P the sodium and potassium content is in excess of the

aluminium required for it all to be accounted for by illite. These observations are consistent with previous analyses of limestones from Maqarin area which indicated average clay contents of 5% (ABED and AMIREH, 1983).

Authigenic mineralogy

Overall, diagenesis has had little effect on the matrix which is relatively uncompacted and microporous, and the rock appears to have suffered only minor burial compaction as evident from only slight crushing of foraminiferal tests (Plate 1). Fragmentation of the delicate microfossils appears largely to be the result of sediment transport processes. There is little evidence for wholesale recrystallisation of the sediment. The microfossil remains are well-preserved, and CL and BSEM reveal that they have retained their original microfibrous calcite fabrics similar to that seen in modern foraminifera (eg. BARBIN et al., 1991). However, BSEM-EDXA also revealed an extremely complex assemblage of authigenic phases, some of which are rare or previously unknown minerals. Most of the authigenic mineralisation is very closely associated with the infillings of foraminera tests chambers and little mineral authigenesis, other than relatively minor amounts of pyrite, occurs in the matrix. This implies that much of the mineral authigenesis within the sediment was controlled by microenvironments prevailing within microfossil cavities.

Authigenic microcrystalline apatite or gel-like collophanic material infills some microfossil chambers or replaces the microfossil walls (Plate 2). Bulk XRD shows that although dominated by calcite, apatite is a significant component of the limestones (table C3, figure C2). Complex substitutions by CO_3^{2-}, F^-, Cl^- and OH^- occur in the apatite structure (eg. McCLELLAN, 1980) making it very difficult to specify the type of apatite present from its XRD pattern. No probe data are available to resolve this. However, the diffraction patterns obtained most closely matched fluorapatite ($Ca_{10}(PO_4)_6F_2$; JCPDS 15-876), probably containing some solid-solution with francolite (carbonate-substituted apatite $Ca_{10-x-y}(Na,K)_xMg_x(PO_4)_{6-z}(CO_3)_zF_{0.4z}F_2$), and is typical of apatites from phosphorites and phosphatic chalks (eg. JARVIS, 1980).

Pyrite is particularly abundant, visually estimated to account for between 1-5% of the rock. Several morphologies and generations are present (Plates 1, 3, 4-7). Most pyrite comprises micron to submicron octahedra in spherical (framboidal) aggregates up to 20 μm diameter often in clusters. This appears to be the earliest diagenetic phase and is often included in all later minerals. The majority of the pyrite occurs within the microfossil chambers (Plate 3) but a minor amount of framboidal and dispersed fine octahedral pyrite is also locally present in the limestone matrix, usually concentrated along certain (organic-rich?) bedding planes. Pyrite can be found replacing microfossil test walls in a patchy manner, mimicking the original skeletal fabric. Some of this early framboidal pyrite has locally recrystallised to idiomorphic equant octahedral and complex (pyritohedron) crystals of similar size to the framboid aggregates. This recrystallisation is also relatively early and this recrystallised pyrite is enclosed in later

authigenic minerals. Pyrite may also occur in much coarser blocky (Plate 4) or prismatic (Plate 1) crystals up to 200 µm across, or can completely infill microfossil chambers.

A particularly abundant form of pyrite occurs as sheet-like, book-like or vermicular masses (Plates 5 and 6), or as parallel or radiating fibrous masses (Plate 7), only present within microfossil chambers (Plates 5-7). The pyrite appears to have pseudomorphed an earlier authigenic micaceous mineral (Plates 5-6). In most cases all traces of the precursor mineral have disappeared but a few examples revealed the presence of relicts of an iron-rich silicon, potassium, sodium, aluminium-bearing mineral. Calcium was also present but it was difficult to determine whether the EDXA signal was influenced by X-rays derived from adjacent calcite. Chromium and vanadium are also detectable by qualitative EDXA and are probably present at levels of 1-2% within the silicate precursor (EDXA detection limit is approximately 0.2 %). The authigenesis of the micaceous phase occurred very early during diagenesis, prior to any burial compaction. Minor to moderate compaction caused some minor crushing of forams, resulting in the deformation of the enclosed authigenic "mica" (Plate 7). The pyritised mica sometimes encloses framboidal pyrite. The morphological evidence, indicating early diagenesis prior to burial, micaceous habit and the remnant chemistry imply that this precursor to pyrite was well-crystallised glauconite ($(K,Na,Ca)_{1.2\text{-}2.0}(Fe^{3+},Al,Fe^{2+},Mg)_4[Si_{7\text{-}7.6}\ Al_{1\text{-}0.4}\ O_{20}](OH)_4.n(H_2O)$), with significant Cr and V substitution in the octahedral layer. Restricted occurrence within forams is a common feature of glauconite formation (McRea,1972). Replacements of the glauconite by pyrite in these rocks typically displays "splaying" of the pseudomorphed mica plates edges as shown in Plate 6. Some pyrite-replaced pelloids may represent reworked glauconite grains.

BSEM-EDXA shows that a number of other minor but common trace phases are spatially related to pyrite authigenesis. A zinc-sulphur mineral, probably sphalerite (ZnS) is common. This occurs as tiny 1-5 µm crystals usually closely associated with framboidal pyrite where it appears to be interstitial to the component pyrite octahedra of the framboids, or as coarser equant crystals surrounding framboids. Lead, cadmium and manganese are detectable (probably at the 1-2% level) by EDXA within the sphalerite. Similarly, copper-zinc-sulphur and nickel-iron-selenium minerals (most probably sulphides and selenides, respectively, since associated with pyrite) are also present around framboids and as inclusions within coarser pyrite crystals. The framboidal pyrite itself contains levels of selenium, arsenic, copper, lead, zinc, and nickel detectable by EDXA which implies concentrations in excess of 0.2% (EDXA detection limit). Selenium and zinc are particularly abundant and in some cases selenium must be present at levels of 5-10%. These elements are present in the coarser pyrite but the levels are generally lower, and selenium, nickel and zinc tend to be most commonly detected. A discrete phase containing only selenium was also identified in close association with pyrite. Although elements such as oxygen cannot be detected by EDXA, the association of this phase with sulphide would tend to indicate that this selenium mineral is native selenium (Se). Native selenium is seen around

framboids (Plate 3) and with coarser pyrite (Plate 1). Careful BSEM examination reveals a peculiar fabric reminiscent of heavy-metal mineralised microbial cell walls reported from sediments, rocks and soils (eg. DEGANS and VENUOPALEN, 1982; BASHAM et al., 1989; MILODOWSKI et al., 1989; 1990) or from laboratory experiments (BEVERIDGE et al., 1983). The "cell-walls" have been fragmented and mineralised by selenium (Plate 8). Similar fine pyrite-mineralised fabrics were also seen.

Calcite is abundant as a cement within intact microfossils. Possibly two generations are present: an early microscopic dog-tooth rim overgrowth on the inner surface of the microfossils, sometimes coated with fine pyrite (resolved only by BSEM); and later coarser chamber-filling sparry calcite which encloses pyrite (eg. Plates 3 and 5). CL behaviour of the carbonates varies; the walls of microfossils display bright orange-red luminescence whereas the sparry infilling calcite cement shows duller red-luminescence. The marls and limestones also contain fractures and veins mineralised by calcite and many of these display brecciation of the wall rock (eg. M2P). An early generation of luminescent calcite, identical to the calcite infilling forams, fills most of the vein breccia but CL reveals that, following this early mineralisation, the fractures were reactivated, re-brecciated and subsequently mineralised with a later generation of non-luminescent sparry calcite. Minor amounts of zinc, manganese and iron were just detectable by EDXA in the foram-mineralising calcite. Chemical analysis of pure separated vein breccia calcite (M2P) is given in table C4.

Traces of quartz were detected by XRD in some samples and this can be accounted for by minor authigenic microcrystalline quartz (chalcedony) cements infilling microfossil chambers. Similarly, minor amounts of low-birefringent gel-like amorphous or microspherulitic silica (opaline) also occur. These observations agree with previous analyses (ABED and AMIREH, 1983), indicating average quartz contents of about 6%. Many microfossils also contain a calcium-potassium-sodium-aluminium silicate mineral (Plate 1, 4 and 9). This phase is often gel-like and easily damaged by the electron beam during BSEM observation, indicating that it is probably very hydrous. It has low relief and birefringence and may be a zeolite. Silica and zeolitic materials both post-date and enclose calcite (Plate 9).

A complex series of calcium, strontium, sulphate and selenate phases fill much of the remaining porosity within forams (eg. Plate 10). They are commonly associated with pyrite altered to goethite (Plate 11), indicating a relationship to late oxidative weathering alteration. These minerals vary in morphology from low-birefringent fine grained microfibrous (Plate 10) and microbotryoidal infillings and efflorescences (Plate 11) to sparry void-fills (Plate 12). Some are clearly gypsum but vary in different microfossils from pure gypsum, strontium-rich gypsum, selenium-rich gypsum, strontium-calcium-selenium-sulphate to pure calcium selenate. Optically, it is impossible to distinguish the phases but BSEM shows that the selenium-rich phases may occasionally form discrete later syntaxial overgrowths on earlier gypsum. No natural calcium selenates or calcium-strontium selenates have previously been

reported and these therefore represent new minerals. Calcium selenate ($CaSeO_4$), calcium selenate hydrate ($CaSeO_4.2H_2O$) and calcium selenate hemihydrate ($CaSeO_4.0.5H_2O$) are known as synthetic compounds (JCPDS, 1985) and are analogous to the natural calcium sulphates: anhydrite gypsum and bassanite. Syntaxial overgrowth of the selenates on gypsum, indicates that the Maqarin selenium minerals are structurally similar to gypsum i.e. most probably calcium selenate hydrate ($CaSeO_4.2H_2O$). Bassanite has been recorded from the Maqarin area (table 4.1.2) and in fine grained secondary alteration products would probably be indistinguishable from gypsum, both optically and by BSEM-EDXA. It is therefore possible that some of the fine grained calcium selenate could represent a selenium analogue of bassanite.

All the limestone samples examined displayed some oxidation of pyrite with the production of secondary sulphates and selenates. However, precipitation of these secondary minerals is confined within foram chambers and does not affect the sediment matrix. Nor are the calcitic walls of microfossils affected by pyrite oxidation. Chromium is enriched in goethite alteration products and is easily detected by EDXA. Ettringite ($Ca_6Al_2(SO_4)_3(OH)_{12}.25H_2O$) was identified by BSEM-EDXA in fine hairline fractures in the limestone samples examined.

Uranium distribution

Fission-track prints show a generally uniform distribution of uranium in the matrix of the samples. The background content is relatively high and fission-track densities indicate levels varying between 10 to 20 ppm U, being higher in the more organic-rich limestones. These levels agree very closely with whole-rock uranium levels determined by XRF (section C4). Lower levels (5-10 ppm U) were found in wallrock of the calcite vein breccia (M2P) but this may be due to sedimentary variation since no change in uranium content is noted with respect to vein contacts.

Small higher density fission-track clusters correspond to clasts (ie foraminifera tests) and in some cases where microfossils have been mineralised with apatite or collophanic material, uranium contents up to 50 ppm are indicated. Yellow goethitic stained clasts (probably oxidised pyritised forams) may contain 50-100 ppm U. Optically discrete organic particles appear to be devoid of uranium and no uranium appears to be present in fine ettringite-filled microcracks. Fission-track registration also indicates the absence of uranium in the vein calcites and this is confirmed by semi-quantitative XRF analysis.

C 3.2 High-temperature metamorphic zone

Primary metamorphic assemblage

The primary metamorphic rocks vary in colour from dark grey, to black and red varieties often on a few centimetres scale. The black colouration is probably due to the presence or absence of graphite which has been identified previously (KHOURY and NASSIR, 1982) and red colours are probably due to very finely-dispersed primary hematite. A common feature is the presence of regular polygonal (hexagonal) columnar micro-joints on a scale of 0.5 -1.0 cm (Plate 13). Similar features are seen in the combustion-metamorphic rocks in the Daba-Siwaqa area of Jordan and can be seen in contact metamorphosed limestones (eg. Camas Mor, Isle of Muck, Scotland). The joints probably arise from contraction on rapid cooling from high temperatures in a similar manner to the development of columnar joints often seen on a larger scale in basalt flows. Table 4.1.2 summarises the primary high-temperature metamorphic minerals identified from the Maqarin metamorphic rocks (based on data from this study and from KHOURY and NASSIR, 1982).

In thin-section, the rocks are seen to possess a strongly-developed planar fabric, defined by elongated grains of calcite (Plate 14). This is unaffected by polygonal joints. Many of the calcite grains are recognisable as recrystallised former microfossils (Plate 14). Comparison with unmetamorphosed bituminous limestone indicates that the planar fabric, as defined by recrystallised calcite, represents the original sedimentary fabric. The recrystallised calcite is xenomorphic; occuring as a mosaic of uniform non-luminescent, interlocking crystals.

Minute, extremely bright blue to blue-violet and greenish luminescent grains can be seen in the calcite under CL. BSEM-EDXA shows that they are equant, rounded to equant euhedral grains of a calcium-sulphur mineral typically between 1 to 10 μm in size (Plate 15). In recrystallised microfossils these minute grains are concentrated in inclusion-trails 15-30 μm long within the margin of the calcite. These inclusions delineate the former inner surface of the microfossil tests (Plate 16). In smaller calcite "pools" the inclusions are more randomly scattered, but always well within the calcite. The phase has equant morphology, indicative of cubic symmetry, and appears to be isotropic although, because it occurs as very small grains in a highly birefringent groundmass, it is difficult to be certain about this property. Despite the small grain size, the mineral could be located under EMPA due to its strong luminescence. EMPA analyses, together with the apparent cubic symmetry, and strong CL luminescence (cf. MARSHALL, 1988), identify the mineral as oldhamite (CaS), although, most analyses gave slightly low analytical totals and slightly excess calcium due to interference from host calcite.

Assuming any excess calcium is derived from calcite and normalising the residual analysis to 100%, it is apparent that some substitution of sulphur by selenium in the

oldhamite occurs in a range of compositions from pure CaS to $CaS_{0.9}Se_{0.1}$. Oldhamite is known only from experimental studies (FINCHAM and RICHARDSON, 1954; LARIMER, 1968; HELZ and WYLLIE, 1979), meteorites (KEIL, 1968; LARIMER, 1968; BLANDER, 1971; SKINNER and LUCE, 1971; GRAHAM et al., 1977) and from blast-furnace slags (BUTLER, 1977; SCOTT et al., 1986) and this is the first record of oldhamite in terrestrial rocks. Trace amounts of potassium (0-2736 ppm), sodium (185-2625 ppm), strontium (0-1857 ppm), copper (112 ppm - 4%) and iron (1404-2092 ppm) were detected in oldhamite by EMPA.

Oldhamite appears to be very susceptible to dissolution, and sometimes the only evidence for its former presence are small equant cavities in calcite, locally filled by very fine secondary iron oxide (Plate 16). Tiny grains of copper sulphide and potassium-copper sulphide-selenide often occur included in or intergrown with oldhamite, usually concentrated at grain margins (Plate 17). However, their very small size severely limits EMPA analyses. Careful X-ray mapping (figure C3) shows that Cu, K and to some extent Se, are virtually exclusive of Ca in these composite grains. A single analysis of a copper sulphide indicated that it was probably covellite (CuS, containing traces of sodium up to 576 ppm; potassium up to 175 ppm, selenium up to 0.688 ppm). Two analyses of the copper-potassium selenide-sulphide (assuming all Ca is present as the host phase calcite and normalising to 100%) indicate an approximate composition of $Cu_{10.2}K_3Na_{0.2}Se_{7.7}S_{2.3}$. Alkali-transition metal sulphides have been synthesised but are known only very rarely from terrestrial rocks (CZAMANSKE et al, 1978; CLARKE, 1979) and from meteorites (FUCHS, 1966). None of these resembles the above phase in composition which appears to be a new mineral. In the primary metamorphic rocks alkalis appear to be present in this new mineral and to a lesser extent as traces within oldhamite and covellite.

Bulk XRD (table C3, figure C2) and BSEM-EDXA (Plate 14) show that, in addition to calcite, the largely unaltered metamorphic rocks examined during this study (M15P and M33P) are composed mainly of apatite with minor spurrite. However, these rocks are probably more phosphatic variants, and relicts of unaltered rock within largely hydrated samples suggest that, elsewhere, lithologies may be more spurrite rich (Plate 18). These contain an assemblage of calcite, porphyroblastic (often coarse radiating prisms up to 2-3 mm) spurrite ($Ca_5(CO_3)(SiO_4)_2$) in a granoblastic groundmass of fluorapatite or ellestadite ($Ca_{10}(P,Si,S)O_{24}(Cl,OH,F)_2$, larnite (a-$Ca_2SiO_4$), calcite and a calcium aluminate (Ca-Al oxide) phase. Larnite was not seen in contact with calcite. Spurrite porphyroblasts appear to have grown at the expense of ellestadite (or apatite), larnite and calcium aluminate (undefined) and often include corroded relicts of these minerals (Plates 18 and 19). Brownmillerite ($Ca_2(Al, Fe)_2O_5$) is common in the spurrite-larnite-rich relicts and appears to be the latest crystallised metamorphic mineral, developing initially along grain boundaries as a poikiloblastic replacement at the expense of ellestadite (or apatite), larnite and calcium aluminate, eventually developing as small (up to 100 µm) prismatic porhyroblasts (Plates 18 and 19). Ellestadite, larnite and spurrite are difficult to distinguish under BSEM due to similar backscatter properties (Plates 18 and 19).

In the more phosphatic rocks, spurrite appears to be relatively minor, and the groundmass comprises largely xenoblastic fluorapatite (with significant silico-sulphate apatite (ellestadite) solid-solution) containing rounded equant crystals of aluminous (<2% Fe_2O_3) brownmillerite (Plates 20 and 21) and myriad minute inclusions (<0.1 µm to 5 µm) of platy Cr, Zn, Ti, Al, Mn, Mg, Fe and Al, Cr,(Ba?) Fe phases, probably ferrites (Plates 20 and 22). The platy habit suggests that the ferrites are not cubic spinel-structured oxides. Very high BSEM magnifications indicate that even some of these minute inclusions are themselves complex intergrowths of platy ferric oxide (hematite ?) or Fe,Cr-oxide partially replaced by more complex Cr,Zn,Ti,Al,Fe oxide (Plate 23). Calcium may be present in many of these inferred ferrites but, because of their fine size and inclusion within a calcium-rich background, it is impossible to assign the calcium from EDXA with any certainty. The grains were mostly too small to locate for EMPA purposes. One discrete grain gave a composition close to calcium ferrite ($CaFe_2O_3$) but with low element totals (95%).

The phosphatic rocks were also found to contain minor but very common uranium-rich grains. These occur as small (up to 20 µm diameter), subhedral poikiloblastic crystals having very bright BSEM characteristics (Plate 24). The poikiloblastic habit indicates that it formed relatively late, at the expense of apatite. EMPA analysis was hampered by the presence of abundant apatite inclusions and by small grain size. The best analyses consistently indicated a 2:1 Ca : U composition, with low element totals of about 85% indicating the presence of carbonate, fluoride, hydroxyl or water (which cannot be determined by EMPA). Hydrous uranium minerals are normally associated with low-temperature secondary alteration and readily dehydrate and therefore hydrous uranium phases are unlikely to be present in the primary high-temperature metamorphic rocks. Assuming that the analysis deficit is due to carbonate, recalculated EMPA data suggest that this phase corresponds very closely to either $CaO.[UO_2]_2.[CaCO_3]_3$ if all the uranium is assumed to present as U^{4+}. Alternatively, the analyses can be recalculated to$[CaO]_2[UO_3]_3[CaCO_3]_4$ assuming all uranium is U^{6+}. In the combustion metamorphic zone, U^{6+} seems more probable than U^{4+}. This phase appears to be a previously unrecorded natural uranium mineral. Minor phosphate, silicate and sulphate are present in all analyses and may be intrinsic or derived from host-phase silicate-substituted fluorapatite.

Other minor phases include a common poikiloblastic Ba, Ca, sulphate-silicate (undefined) associated with apatite groundmass and a rare poikiloblastic Zr, Ba, Ca, Mo silicate sometimes in association with, or partially overprinted by, the Ca,U-oxycarbonate. Brownmillerite present in the more phosphatic rocks is aluminous and contains abundant minute inclusions (Plate 21) that appear to contain largely calcium. The inclusions appear to be unaffected by the electron beam during BSEM-EDXA and may represent excess lime (CaO) but the identification could not be refined further.

EMPA indicate the presence of strontium (c.1700-4200 ppm) in apatite and ellestadite. Chromium, aluminium, iron and zinc present in a number of analyses are almost

certainly due to the presence of unresolved fine ferrite inclusions. Spurrite may contain strontium (850-4200 ppm) and occasionally zinc (0-2500 ppm), and possibly some chromium (0-600 ppm). Spurrite analyses all indicated minor phosphate and sulphate substitution (up to 4 % P_2O_5 and 4 % SO_3). In part this may be due to apatite or ellestadite impurity but phosphate and sulphate appear to be ubiquitous in many analyses of high-temperature calcsilicates (eg.. Sabine et al., 1985). Larnite contains traces of strontium (c.850 ppm), sodium (500-1000 ppm) and minor iron, aluminium, phosphate and sulphate may also be present. Brownmillerite contains minor titanium (<0.3% TiO_2 in the more aluminous varieties to 1.5% TiO_2 in the more ferric varieties), zinc (up to 1.2 % ZnO), chromium (0-2000 ppm) as well as minor phosphate, silicate and sulphate. Calcite contains traces of magnesium (0-3780 ppm), strontium (1600-3300 ppm) and, in some analyses, barium (up to 1000 ppm).

Retrograde alteration mineralogy

Low-temperature alteration has produced a very complex assemblage of secondary minerals (see table 4.1.2) including calcite, apatite(s), ettringite, thaumasite and portlandite (see also table C3). However, locally and in some veins and dissolution cavities, gypsum, afwillite, apophyllite, vaterite, birunite and various tobermorites are the major minerals (table C4). In many cases these veins are monomineralic. The rocks are extremely variable in colour, often mottled, and the same minerals may exhibit a wide range of colours with violet, pink, orange, yellow and green as well as white the most common colours of secondary phases

Much of the alteration is very fine-grained and, because the different phases are often intimately intergrown and very hydrous, it is difficult to identifty the products with confidence by optical, BSEM-EDXA or EMPA methods. In the samples examined, the larnite-spurrite-calcite-ellestadite-brownmillerite rich rocks appear to be the most readily altered, the original fabrics being preserved only as relict phases. The more phosphatic rocks with an assemblage dominated by calcite, apatite (or silicosulphate apatite), brownmillerite and ferrite phases (red and black marble) seem to be most resistant to alteration (eg. M15P and M33P).

Larnite and spurrite are the most readily altered minerals, followed by ellestadite, then brownmillerite, with primary calcite and fluorapatite or hydroxylapatite being the least reactive. Relict fragments of unaltered primary apatite floating in a totally altered groundmass (Plate 25) are very common in altered former larnite-spurrite-rich rocks. Eventually, even primary calcite and apatite are replaced by secondary products. Calcium aluminate and aluminous brownmillerite are more reactive than iron-rich varieties. Iron-rich brownmillerite, surrounded by a hydrated iron oxide alteration rim may often be found in totally altered groundmass (Plate 26). More phosphatic rocks show pervasive alteration initially along fractures but then spreading out into the groundmass (Plate 27). Oldhamite, covellite and K-Cu sulphide-selenide are the first minerals affected b alteration and rapidly disappear towards fractures. Often these

phases leave tiny cavities in the calcite host which are subsequently filled by ettringite and/or amorphous iron oxide. The alteration along fractures appears to cause some degree of expansion and disruption, possibly causing further microfracturing and subsequent alteration (Plate 27). The polygonal cooling joints are fundamental in providing the initial pathways along which alteration occurs. Even primary calcite appears to be removed as alteration proceeds, leaving only corroded remnants of apatite and calcite in a groundmass of ettringite (Plate 28).

Secondary mineral paragenesis is complex. In all rock-types, the earliest alteration product appears to have been a calcium silcate hydrate with fibroradiate or globular gel-like morphology which appears to have lined or infilled fractures, vugs and other cavities (Plate 29), EMPA analyses identify the mineral as a very hydrous calcium silicate with Ca:Si = 0.8-0.85, indicating that this phase is a tobermorite-like mineral. The tobermorite also contains several percent of Al_2O_3. Tobermorite is almost always overgrown and at least partially replaced by ettringite (Plate 29). Ettringite is often very abundant and may dominate altered lithologies. In most fractures, ettringite is accompanied by thaumasite which encloses earlier precipitated ettringite crystals (Plate 30).

In the matrix, alteration to ettringite is usually accompanied by the nucleation of minor secondary baryte, celestite, calcian barytocelestite, chromian baryte, chromian barytocelestite and barium chromate (hashemite). Hashemite containing 77% end-member barium chromate in solid-solution with baryte has previously been recorded only from Daba in central Jordan (NASSIR and KHOURY, 1982). In contrast, the Maqarin mineral varies considerably in composition even within the same thin-section and appears to demonstrate a complete solid-solution between end-member baryte and barium chromate. There also seems to be considerable solid-solution between hashhemite and celestite. Hashemite, celestite and baryte usually form platy crystals nucleating within ettringite (Plate 31). Hashemite and baryte are often found immediately adjacent to sites of altering ferrite inclusions in apatite, particularly if it accompanies alteration of adjacent minor primary calcium-barium silcates.

In the rock matrix, most ettringite is usually fibrous but in fractures euhedral crystals and prisms are present. In many fractures, and in more severely altered rock matrix, ettringite is replaced along cleavage and parallel to the fibres by fibrous or gel-like thaumasite. Occasionally another secondary fibrous calcium fluorosilicate can be found replacing ettringite (Plate 32). This forms fibroradiate masses identified by EMPA as a hydrous phase (but less hydrous than tobermorite)with Ca:Si = 2.13-2.5 and with a significant F content (Ca:F = 1.4-2.75). X-ray powder photographs made from material from veins containing this phase allow tentative identification of afwillite (eg. M33P2, table C4). The Ca:Si ratio is close to, or in good agreement with, ideal afwillite but unlike any previously published data with the Maqarin phase appearing to have between 18-36 % of OH substituted by by F (ie fluoroafwillite). Afwillite replacement of ettringite preceeded thaumasite precipitation, as evident from veins of thaumasite cutting afwillite-ettringite fabrics (Plate 32).

Less commonly, some rocks appear to be replaced almost entirely by fluoroapophyllite and calcite. In these rocks, fluoroapophyllite fills veins and vuggy cavities. Often it is brightly coloured (eg. golden yellow) and under BSEM is seen to be strongly zoned due to the extensive strontium substitution for calcium (Plate 33). The zoned fabric of these veins (Plate 33) indicates a petrogenesis which involved an initial precipitation of moderately Sr-bearing apophyllite followed by a sharp transition before deposition of low-Sr apophyllite. A second sharp transition is seen associated with the precipitation of highly Sr enriched apophyllite, before a relatively rapid gradation back to slightly strontian apophyllite. EMPA analyses are deficient in potassium for the ideal apophyllite composition. This suggests that the apophyllite contains significant ammonium (eg. MARRINER et al, 1991) substituting for potassium. Ammonium would not be detected by EMPA. In the matrix, relict afwillite or tobermorite-like phases appear to have been overprinted by apophyllite. This suggests that apophyllite is a relatively late mineral.

Apophyllite-replaced rocks display the development of secondary apatite. XRD suggests that the apatite closely matches fluoroapatite which is consistent with its coexistence with fluoroapophyllite. The apatite initially forms as minute (<1 μm) dispersed grains within the matrix (Plate 34). Progressive development of apatite is seen until it eventually develops elongate to almost needle-like poikiloblastic crystals (Plate 35) up to 100 μm in length. Trace amounts of cadmiun sulphate and lead sulphate minerals may be found along the borders of apophyllite veins. Other trace phases common to most of the altered rocks include possible fine-grained zinc and complex zinc-copper secondaries (possibly carbonates and/or hydroxides/oxides since no other elements were detected by EDXA)

The most altered rocks are almost totally replaced by calcite and ettringite, sometimes with traces of aragonite. Apatite and thaumasite may also be detectable in bulk samples. XRD also indicates that vaterite is present as a minor mineral in the bulk rock. Vaterite is also present as monominerallic soft powdery infills of thin veins and hairline cracks in these rocks. It may also be associated with fibrous thaumasite. Vaterite is a very rare mineral but has been recorded from altered larnite nodules in contact metamorphosed chalk from Northern Ireland (McConnell, 1960). In thin section, these rocks comprise very fine grained, microporous, friable rocks. The calcite dominating the mineralogy is seen as minute equigranular particles loosely enclosed with interstitial, fine porous thaumasite. These rocks appear to be thoroughly leached, recarbonated rocks.

Late-stage veining of some parts of the altered metamorphic rocks has resulted in gypsum-mineralised fracture breccias. The gypsum veins may be 1-2 cm thick and are often brightly coloured with yellow, violet and green hues.

Although EMPA analyses of altered material were difficult, some indication of trace element composition of the major minerals can be determined. Portlandite and

secondary calcite were too finely intergrown with other phases to make reliable EMPA but observations indicate the presence of significant fluorite (up to 4000 ppm), chromium (up to 1000 ppm) and zinc (up to 1500 ppm). Tobermorite and fluoroafwillite appear to be typically devoid of trace elements except for small to moderate levels of aluminium, phosphorous and sulphate. Thaumasite was found to contain minor phosphate and probably contains significant solid-solution with ettringite. The more thaumasitic material has generally low trace element levels, although zinc may be present in some analyses (up to 1000 ppm). Ettringite contains trace amounts of chromium generally between about 50 ppm to 100 ppm Cr but some analyses contain up to 4000 ppm Cr. Strontium is also present in some ettringite analyses (up to 2500 ppm) and sodium is also often present in trace amounts (0-1500 ppm). Apophyllite contains strontium (c. 0.08-8% SrO). An analysis of a late vein gypsum (violet colour) is given in table C5 (sample MI8P) and indicates that it may contain significant strontium (643 ppm) and chromium (1468 ppm).

Qualitative XRF scans on small amounts of separated vein material indicated the presence of trace amounts of iron, nickel, titanium, vanadium, chromium, gallium, copper, zinc, selenium, strontium and arsenic or lead (the two elements interfere on XRF) in mixtures dominated by thaumasite and vaterite. Traces of chromium, iron, nickel, copper and strontium were identified by qualitative XRF scans in gypsum. Manganese, iron, nickel, copper, zinc and strontium were qualitatively detected by XRF in calcite vein fills. A vein filling tentatively identified as being a mixture of birunite and calcite was found to have qualitatively detectable levels of titanium, vanadium, chromium, iron, nickel, copper, zinc, selenium, strontium, yttrium, uranium and arsenic or lead.

Uranium distribution

In unaltered apatite-calcite-brownmillerite rich rock (M15P and M33P), fission-track prints indicate that uranium is present in two distinct locations. Background levels of 15-20 ppm U, are probably largely associated with the matrix apatite (Plates 37 and 38). Discrete dense fission-track clusters correspond to tiny discrete uranium calcium oxycarbonate (?) grains (described earlier) scattered randomly through the rock. The uranium has been completely redistributed in altered wallrock along fractures associated with secondary ettringite and thaumasite mineralisation. BSEM shows that the discrete uranium calcium oxycarbonate(?) has disappeared in the altered wallrock. Fission-track analyses indicate that the uranium is evenly redistributed (Plates 37 and 38) within secondary phases in concentrations similar to, or slightly enhanced above that of the unaltered background (c.15-20 ppm).

In more altered larnite-spurrite lithologies, uranium appears to be remobilised from discrete primary minerals and concentrated to levels up to 50 ppm U in bands close to the alteration fronts (Plates 39 and 40). However, uranium appears to be absent or at low levels (typically 5-15 ppm U) in the fine-grained calcite-portlandite-CSH-ettringite-

thaumasite matrix alteration. BSEM analysis suggests that the uranium distribution corresponds to concentrations of secondary iron oxide staining and also to hydrated alteration rims (again iron oxide gel-like material) around relict brownmillerite and ferrite grains. A few very high-density fission-track clusters were found under the BSEM to correspond to tiny (c 10 μm) grains of a uranium-calcium silicate phase (Plate 36). BSEM images show that the phase displays drying shrinkage, thereby indicating that it is probably very hydrous in the natural state.

Fission track prints show a distinct absence of uranium with ettringite, thaumasite, gypsum, vaterite and apophyllite vein and cavity infillings. Tracks indicating levels of uranium between 30-40 ppm U, were recorded along the margin of a prominent apophyllite vein in one sample (M17P) but are related to a concentration of secondary iron oxide on the vein wall.

In this case, the iron oxide was also associated with traces of fine-grained secondary cadmium and lead sulphates. A notable exception to this was an indurated laminated calcite-birunite vein coating (M4P) associated with a green vitreous phase identified as brownmillerite. This porcelainous calcite-birunite vein contained 10 ppm U (M4P2, table C5).

Fission-track prints indicate that apophyllite-calcite replaced rock generally has a maximum background level of 5 ppm U (M17P). However, uranium distribution appears to be broadly zoned, showing narrow bands or fronts in which uranium levels are very low (0-1 ppm U), separating the bulk of the rock (c.5ppm U) from regions of higher uranium (7-10 ppm U). BSEM observations shows that this distribution relates to the development of secondary apatite, which increases in concentration in the areas of higher uranium content. Discrete tiny (c.0.1-0.2 μm) grains of an uranium mineral could be found in a number of coarser secondary apatite crystals but were too small to identify. Highly porous, soft recarbonated calcite-vaterite-thaumasite rock appears to have a low, but uniform level of uranium (c.15 ppm) with no sites of specific concentration.

C 3.3 Leached or altered sedimentary rocks

Mineralogy

Close to the altered metamorphic zone, the unmetamorphosed host sediments appear to have been affected by the alkaline fluids emanating from the low-temperature alteration of the metamorphic rocks. Alteration proceeds along fine fractures in the marls and limestones. They show extensive oxidation of pyrite and veining by fine ettringite stringers (Plate 41). Locally, the matrix may be completely replaced by fibrous ettringite, with the progressive loss of all original sedimentary fabrics, including calcitic foram tests. Plate-like secondary aluminium oxide or hydroxide (probably gibbsite) is a

common component of the fine ettringite-filled fractures.

Larger fractures lined by non-luminescent dog-tooth calcite are also present (Plate 42). These veins are complex in fabric. The margins of the veins contain an early generation of zoned strontium-rich calcite (Plate 43) which has been severely corroded in places prior to the growth and partial infilling of the vein by coarser low-Sr calcite (Plate 44). Secondary strontianite is present at the junction between the two generations of calcite and appears to have formed partially by replacement of strontium-rich calcite. The later calcite has been corroded and subsequently mineralised by gibbsite (Plate 42).

Uranium distribution

Uranium appears to have been mobilised during alteration and removed from the sedimentary rocks. In the sample examined (A6.1P), the areas of unaltered rock possessed levels of uranium between 5-10 ppm. Although lower in concentration, the uranium distribution is similar to that of the other limestones and marls. However, in areas affected by ettringite-gibbsite veining, the uranium is much reduced and is locally absent where ettringite veining is very intense.

C 3.4 Modern precipitates and travertine deposits

The precipitates from the active hyperalkaline discharges were too friable to examine in thin section. However, bulk XRD analyses are given in table C3. In all the discharge areas calcite is the dominant phase, but aragonite is usually a major component. Portlandite and quartz were also detected as traces in some precipitates.

C 4 Geochemistry

Whole-sample geochemical analyses of selected rocks and some hand-separated vein minerals are given in table C5.

C 4.1 Bituminous limestone and leached sedimentary rocks

Analyses of unaltered marl and limestone (A6.7P and A6.9P) indicate the presence about 13-14 % non-carbonate material (clays, silica, quartz etc) as shown by SiO_2, Al_2O_3, Fe_2O_3 and K_2O. Much of the Al and Si can be attributed to minor detrital illite and kaolinite, and to authigenic phases such as opaline silica, zeolite and relicts of glauconite. The excess of K over Al suggests that glauconite (K-Fe rich mica), rather than illite or zeolite, is probably the major source of K in A6.7P.

Many of the trace elements (Sr, Ni, Cu, Zn, Co, Cr, V, U, F, Se) are enriched relative to average limestones and shales (WEDEPOHL, 1978). Se in particular is very high (150-250 ppm) compared both to average limestone (normally 0.05-0.08 ppm) and even black shales (c.up to 5ppm). Levels of Cu, Ni, Zn, Co, V and Cr in these rocks are more similar to those of black shales (WEDEPOHL, 1978). Uranium levels appear to be of the order of 15-20 ppm which is high for typical limestone values (1-2 ppm) but within the range of concentrations found in black shales. Sr concentrations of these rocks are very high (1700-2300 ppm) but are comparable to levels seen in European Cretaceous chalks and phosphatic chalks (eg. JARVIS, 1980).

ICP-OES and ICP-MS data for dilute HCl-soluble and HCl-insoluble fractions of the bituminous limestones are given in table C6. Analyses suggest unaltered bituminous limestones contain between 8-20% organic matter. Sample A6.3P is altered bituminous limestone with fine secondary ettringite-filled fractures. Sample MQ10.1 was taken from material in an actively combusting spoil heap which had become enriched in bitumen "sweated-out" of adjacent material. Most elements analysed are strongly associated with the acid soluble fraction. This is largely calcite but the 10% HCl used during leaching will also have dissolved water-soluble minerals including secondary oxidation products such as gypsum and the calcium selenates (identified in section C3). This would partially account for the high Se contents within acid-soluble fractions. Some of the sulphides may also have been affected by acid attack and could account for Ni, Cu, Zn and Cd in the acid soluble fraction. These elements could also have leached by HCl from secondary goethite alteration products of the sulphides. Glauconite is also readily attacked by acids (McRae, 1972) and dissolution of this phase will have accounted for the presence of high concentrations of K, Na, Al, Cr and probably Fe in the acid soluble fraction. Sr and Ba are most probably derived from the carbonate phase.

The acid-insoluble residue is largely bitumen or other organic matter. In most cases elements such as Al, Fe, Ca, K and Na are most probably associated with insoluble clay minerals or other silicates rather than the organic matter in the acid-insoluble fraction. Se, Sn, Pb, U and Th appear to be present in significant amounts in both acid-soluble and acid insoluble fractions. In the acid-soluble fraction, U and Th are probably largely derived from phosphatic material (collophane, apatite) but may also have been present in the carbonate. There is a paucity of heavy minerals such as zircon, monazite and other resistate minerals in the limestones to account for U and Th. Therefore it seems likely that a significant proportion of these elements are complexed with the acid insoluble organic material. Se, Sn, Pb, Zn, Cu, Fe and Ni in the acid insoluble fraction may in part be complexed with organic matter but are more probably contained in the abundant pyrite which is known to contain many of these elements (section C 3.1) and which is insoluble in HCl (DEER et al, 1966).

Figure C4 shows the element distributions (excluding REE) of the bituminous limestones and marls normalised with reference to marble M15P. M15P was chosen as an arbitrary local normalisation reference because of its limited retrograde alteration. This allows major differences between the sedimentary and metamorphic rocks to be

identified. Most elements show little significant differences between the marble M15P and the primary sedimentary rocks. The major variations seen are for K and Zr which are higher in the sedimentary rocks than in M15P and probably reflect initial sedimentary variations in detrital zircon and glauconite contents in the sedimentary rocks. Sample MQ10.5P shows a significantly lower Cl and Se content in comparison to M15P or the other limestones (A6.7P and A6.9P). This sample from partially combusted surface material in actively burning spoil may have lost these elements as volatiles to the atmosphere on combustion. There appears to be very little significant difference in the distribution of REE of the primary sedimentary rocks compared to the unaltered metamorphic rock M15P (figure C5).

Bituminous limestones affected by ettringite-thaumasite-gibbsite alteration resulting from contact with hyperalkaline fluids generally have very similar element distribution patterns to the unaltered bituminous limestones and primary metamorphic rocks. Both unaltered and altered bituminous limestones have lower U contents than M15P. This is most probably a reflection of variations in the primary sedimentary distribution since M15P marble appears to have been derived from a more phosphatic limestone than the unaltered limestones examined in this study. The altered limestones examined have slightly lower U contents (13-15 ppm U) than the unaltered limestones or partially combusted rock (16-19 ppm). Because of the limited number of samples analysed, it is difficult to ascertain with any statistical confidence, from the bulk geochemistry alone, whether this difference is due to primary sedimentary variation in U concentration or due to leaching of U during alteration. However, evidence from fission-track registration studies (section C 3.3) would tend to support the conclusion that there has been an overall loss of U from the altered bituminous limestones. Se concentrations are significantly lower in the altered bituminous limestones (13-15 ppm) than in either M15P marble (116 ppm) or unleached bituminous limestones (>300 ppm) and indicate that Se has been leached during alteration of the bituminous limestone. However, for most elements the alteration has not resulted in significant mobility other than a local redistribution during the formation of secondary minerals.

C 4.2 High-temperature metamorphic zone

As outlined above, there is very little significant difference in chemistry that can be determined (other than those differences likely to be related to primary sedimentary variations) between the unaltered primary marble examined (M15P) and the original bituminous limestones. A possible exception to this is Se which appears to be lower in the metamorphic rock and may have been partially lost as a volatile phase during combustion. This interpretation is supported by the apparent loss of Se in modern combusted bituminous limestone described above.

Elemental distributions (normalised to M15P) of the combustion-zone marbles are shown in figure C6. The altered marbles examined in this study (A6.4P, M3P, M28P) have lower F and Cl contents than the unaltered marble M15P but this probably reflects

the initial higher content of apatite (fluorochloroapatite) in the unaltered sample. Similarly, variations in Zr may reflect primary sedimentary variations. However, other elements do appear to have been redistributed during alteration. Se appears to be significantly reduced in altered marbles (typically <40ppm compared to 116 ppm in M15P), indicating that Se is probably being leached during alteration. U is lower in altered rocks than in M15P but this is partly a reflection of probably higher initial concentration in the more phosphatic facies. However, the most highly altered marbles (M28P and A6.4P) have relatively low uranium contents compared to either M15P or less phosphatic unaltered bituminous limestones. This taken together with fission-track registration evidence (section C 3.2) indicates that uranium is being mobilised during alteration. K appears to have been leached from the most altered marbles (M28P, A6.4P) to levels below routine XRF detection limits for major elements (>0.01%). Na similarly appears to have been leached from the altered marbles. However, for most elements it is difficult to determine any systematic variation in composition during hydration and alteration of the marbles. The altered marbles show similar REE distribution patterns to unaltered marble M15P but absolute concentrations are slightly lower. Lower concentrations in REE can be accounted for by effective dilution as a result of hydration, but no apparent fractionation or significant mobilisation of REE is discernable from the bulk rock geochemistry.

C 4.3 Modern precipitates and travertine deposits

The secondary precipitates and travertines are essentially dominated by calcium carbonate and consequently contain little other than Ca in the major element XRF data. Si is present in minor amounts in all samples and reflects the presence of quartz identified in trace amounts by XRD. Higher levels of silica are indicated in travertines from springs MQ5 and MQ6. Minor amounts of Al are also present in most analyses. High concentrations of S are present in all precipitates (up to 1.5% in precipitate from spring MQ6) and probably present as sulphates (gypsum and/or ettringite). S contents do not seem to vary systematically between the different spring sites. Sr concentrations are also very high (1300-2700 ppm) and are present in similar levels to that found in the bituminous limestones and metamorphic zone rocks. Higher Sr concentrations are found in precipitates from MQ5 and MQ6 springs. Ba, Mn, Ti and REE are similarly significantly higher in precipitates from MQ5 and MQ6 springs. Travertine from MQ6 is most strongly enriched in trace elements, particularly with respect to Cr, Ti, Mn, Ni, Zn, V, Zr, Cl, F, S, Se, and REE. The levels of Zr in MQ6 travertine are similar to that of the background sedimentary and metamorphic rocks, suggesting that Zr is significantly mobile in this system. The enrichment of trace elements in travertines from MQ5 and MQ6 reflects the higher concentrations of many of these trace elements in the groundwaters from these two sites (chapter 4.2).

REE distribution patterns of the travertine precipitates (normalised with respect to reference marble M15P) are presented in figure C7. The REE analyses for sites MQ1, MQ2, MQ7 and MQ9 are close to detection limits and give rise to "saw-tooth"

distribution patterns that appear to reflect underlying relative solar abundances which have not been "smoothed" by normalisation (HENDERSON, 1984). The REE distributions of travertines from springs MQ5 and MQ6 by comparison are quite distinct from those associated with the eastern area. They tend to show a slight positive Ce anomaly and a slight progressive depletion in heavy REE relative to the marble implying some degree of fractionation of the REE during precipitation from groundwater or leaching of the source rock.

C 5 Natural Decay Series Radionuclides

A limited number of samples of bituminous limestone, marble, altered marble and travertine deposits were submitted for uranium- and thorium-series disequilibrium determination at the Environmental Research Laboratory, Australian Nuclear Science and Technology Organisation (ANSTO) and at the Scottish Universities Research and Reactor Centre (SURRC). The data are presented in table C7. The general principle of interpretation of uranium series disequilibrium data is that if a daughter radionuclide is present at less than (radioactive) equilibrium proportions relative to its parent (the daughter/parent activity ratio is less than unity), then either recoil-aided or solution-caused mobilisation or both has occurred. Conversely, daughter/parent activity ratios greater than unity imply either preferential leaching of the parent (e.g. ^{234}U relative to ^{230}Th) or preferential precipitation of the daughter radionuclide (e.g. ^{234}U from a solution deficient in ^{238}U).

There are some significant differences between the data sets (table C7) from the two different laboratories which may, in part, be due to sample differences in this very heterogenous material. However, $^{234}U/\ ^{238}U$ activity ratios are generally in good agreement. Although largely unaltered, both bituminous limestone sample A6.7P and marble M15P from adit A6 have $^{234}U/\ ^{238}U$ activity ratios less than unity, implying that uranium has been mobilised from the sample with prefential leaching of ^{234}U. Leaching of uranium from the marble is also implied by the high $^{230}Th/\ ^{234}U$ activity ratio for M15P (SURRC data, table C7) Differences between SURRC and ANSTO data for $^{230}Th/^{234}U$ activity ratio results for M15P almost certainly result from sample inhomogeneity in this case. These observations are consistent with the fission-track registration observations which showed uranium mobilisation associated with minor alteration along fractures. This pattern is also reflected in more altered material (M3P). The travertines have $^{234}U/\ ^{238}U$ activity ratios in excess of unity which is compatible with the co-precipitation of uranium from contemporary groundwaters which have preferentially leached ^{234}U from other sources such as the metamorphic marbles or from the bituminous limestones.

It is standard practise to utilise isotopic disequilibria in the natural decay series as an indicator of the timing of rock-water interactions (eg. CHERDYNSTEV, 1955; IVANOVICH and HARMON, 1982) because, in theory at least, the period elapsed since the system was disturbed may be assessed by knowledge of the half-lives of the

nuclides involved. A disturbance of, for example, the $^{226}Ra/^{230}Th$ daughter/parent pair by removal of ^{226}Ra will be detectable for around $8x10^3$ years because the in growth of ^{226}Ra is governed by its half-life (~ 1.6×10^3 years) and is theoretically measurable for around five half-lives.

However, to date any such distrurbance using this simple method requires that the daughter/parent pair remain in a closed system since the disturbing event and also that the event itself lasted a very short time relative to the half-lives used, something which is often impossible to assess (eg. THIEL et al., 1983; ALEXANDER et al., 1990). Even more importantly, any given daughter/parent isotopic ratio can be shown to be produced by a wide variety of daughter loss and recovery scenarios if a closed system cannot be proved (SCOTT et al., 1992) as is more usually the case. Thus, although it is tempting to "convert" the disequilibrium values of table C7 into dates of alteration of the sample, this is not really justifiable without much more evidence to prove that the system has remain closed since the disequilibrium inducing event.

For some samples the decay series relationships are very complex. The highly altered marble sample M28P appears to have a $^{234}U/\ ^{238}U$ activity ratio close to equilibrium. Since uranium appears to have been mobilised in most samples with similar alteration characteristics, it may also have occurred in this sample. The high $^{230}Th/^{234}U$ activity ratio for M28P further supports the inference that uranium has been removed relative to normally less mobile thorium. Assuming that groundwater hydration of the unstable metamorphic rock occurred soon after metamorphism, this may give an indication of the lower time limit of the metamorphic event (or one of a number of such events). However, once again this inference on the timing of metamorphism must be treated cautiously as the situation is complicated by ^{230}Th which is unsupported by its parent ^{234}U. Thus either thorium has been added to the system or uranium has been mobilised without isotopic fractionation.

Comparison of the $^{230}Th//^{234}U$ activity ratio (0.76) with the $^{234}U/\ ^{238}U$_activity ratio (0.91-0.98) does tend to suggest that, in this sample at least, there has been some mobilisation of thorium. ^{230}Th appears to have been preferentially mobilised with respect to its parent ^{234}U and, as thorium is known to be mobilised by high temperatures (>600 C; LANGMUIR and HERMAN, 1980) and highly alkaline solutions (LAFLAMME and MURRAY, 1987; BATH et al., 1987) and both occur in this particular rock-water system, this is not unreasonable. The $^{234}U/\ ^{238}U$ activity ratio also indicates some degree of leaching of uranium but possibly to a lesser degree than thorium.

The isotopic data also indicate that radium is mobile in the Maqarin system. M15P marble and bituminous limestone A6.7P both show a disequilibrium between ^{226}Ra and its parent ^{230}Th indicating preferential leaching of the daughter isotope ($^{226}Ra/^{230}Th$ activity ratio <1). However, radium appears to be reprecipitated in the more altered rocks ($^{226}Ra/^{230}Th$ activity ratio >1). Radium mobility also explains the variation in $^{228}Th/^{232}Th$ activity ratios since ^{228}Ra is an intermediate daughter in the decay series from ^{232}Th to ^{228}Th.

Table C1 Schedule of mineralogical and petrological samples analysed

sample type	code	XRD	X-ray photo.	Optical	CL	BSEM	EMPA	Fission track anal.
bituminous limestone	A6.7P	*		*	*	*		*
bituminous limestone	A6.9P	*		*	*	*		*
hard, cherty black limestone	A6.2P	*						
altered marl/limestone (leached)	A6.1P	*	*	*	*	*		*
calcite veined marl/limestone (vein breccia)	M2P					*		*
marble	M3AP	*						
marble	M15P	*		*	*	*	*	*
partially altered marble	M33P		*	*	*	*	*	*
altered marble (retrograde)	M4P		*					
highly altered marble (retrograde)	M13P		*					
altered marble (retrograde)	M17P	*	*	*		*	*	*
purple gypsum vein in brecciated altered marble (retrograde)	M18P		*	*		*	*	*
highly altered marble (retrograde)	M19P		*	*	*	*		*
very altered marble (retrograde)	M21P			*		*		*
altered marble (retrograde)	M28P	*						
altered marble (retrograde)	M39P	*	*	*	*	*	*	*
altered lmstn /re-carbonated rock	A6.3P	*	*	*	*	*		*
mottled recarbonated rock	A6.4P	*	*					
soft white precipitate in drip pool (seepage MQ1 - Adit A-6)	MQ1.1P	*						
hard crust around drip pool (seepage MQ1 - Adit A-6)	MQ1.2P	*						
dripstone/flowstone precipitate (seepage MQ1 - Adit A-6)	MQ2.1P	*						
travertine crust (spring MQ5)	MQ5P	*						
green effluorescent precipitate associated with spring	MQ6.4P MQ6		*					
yellow-white flowstone (seepage MQ7, rail cutting)	MQ7.2P	*						
flowstone stalactite (seepage MQ9, rail cutting)	MQ9P	*						

Table C2 Schedule of geochemical samples analysed

sample type	code	Major	Traces	Pd	Assay	Semi-quant XRF mineral separates	Selective leaching
bituminous limestone	A6.7P	*	*		*		*
bituminous limestone	A6.9P	*	*				
hard, cherty black limestone	A6.2P	*	*		*		*
altered marl/limestone (leached)	A6.1P	*	*				
calcite veined marl/limestone (vein breccia)	M2P	incompl	incompl				*
marble	M15P	*	*		*		
altered marble	M3P	*	*				
altered marble (retrograde)	M4P		*			*	
purple gypsum vein in brecciated altered marble (retrograde)	M18P	incompl.	*			*	
altered marble (retrograde)	M28P	*	*				
altered lmstn/ re-carbonated rock	A6.3P	*	*		*	*	*
mottled recarbonated rock	A6.4P	*	*			*	
soft white precipitate in drip pool (seepage MQ1 - Adit A-6)	MQ1.1P	*	*		*		
hard crust around drip pool (seepage MQ1 - Adit A-6)	MQ1.2P	*	*		*		
dripstone/flowstone precipitate (seepage MQ1 - Adit A-6)	MQ2.1P	*	*		*		
travertine crust (spring MQ5)	MQ5P	*	*		*		
travertine crust (spring MQ6)	MQ6.2P	*	*				
yellow-white flowstone (seepage MQ7, rail cutting)	MQ7.2P	*	*		*		
flowstone stalactite (seepage MQ9, rail cutting)	MQ9P	*	*				
baked bituminous limestone from site of burning rock spoil dump	MQ10.5	*	*				
heated bituminous limestone from site of burning rock spoil. bitumen enriched by migration during heating	MQ10.1P						*

Table C3 Results of bulk X-ray diffraction analysis

Hand Specimen Description	Sample Code	Calcite	Aragonite	Apatite	Spurrite	Quartz	Portlandite	Ettringite	Thaumasite	Vaterite	Hydroxylllestadite	Afwillite	Apophylite
Bituminous limestone	A6.9P2.1	***		**									
Highly bituminous black, ?unaltered limestone	A6.7P3.2	***		**		tr.							
Hard, black cherty limestone	A6.2P3.1	***		**									
Leached marl/limestone	A6.1P1.1	***				tr.							
Marble	M3AP1	***		**	*								
Marble	M15P3.1	***		**	*		tr.						
Altered marble	M17P1	***		*									**
Altered marble	M28P1	***		**		?tr.	**	*		tr.	?*	?tr.	
Altered marble	M39P	***		*			**	*				?tr.	
Altered and recarbonated marble	A6.3P1.1	***		*					**				
Yellow phase of recarbonated material from yellow and white mottled rock	A6.4P3.1	***	*	**									
White phase from recarbonated mottled rock	A6.4P3.2.1	***		**		tr.		?*	**				
Altered material with white secondary minerals	A6.1P3.2	***		**									
Drip precipitate and flowstone	MQ2.1P1.1	***	**			?tr.	?tr.						
Travertine crust	MQ5P1	***											
Hard, white crust around pool	MQ1.2P1.1	***	**			tr.							
Yellow-white flowstone	MQ7.2P1.1	***				tr.							
Flowstone stalactite	MQ9P1.1	***	**			tr.							
Soft, white precipitate with greenish effluorescene	MQ1.1P1	***	**				tr.						

*** Dominant ** Major * Minor tr. Trace ?Possible

Table C4 X-ray powder photography results

Description	Sample Code	Calcite	Gypsum	Apatite	Portlandite	Ettringite	Thaumasite	Vaterite	Brownmillerite	Birunite	Afwillite	Apophyllite
Yellow mm thick band in banded marble	M39P1	***		**					?			
Finely banded altered marble- clear/pink mm thick band	M39P2						***					
Altered marble- Hard white phase	M4P2.1	***						?		**		?
Green vitreous vein infil in altered marble									***			
Vein filling in altered rock	M33P2	***				*		***		?	?	
Vein filling in altered rock	M33P	*					?	***				
Bright yellow vitreous crystalline vein material	M17P1											***
Altered marble - underlying translucent vein material	M17P2											***
Altered marble - cream to white vug lining adjacent to wall	M17P3	?										***
Altered marble - buff vug lining in centre of vug	M17P4											***
Altered marbel - translucent colourless millimetre thick vein infill	M17P5	***										**
Vein infill in altered marble	M19P2	***							**			
White translucent vein infilling	M2P2.3	***										
White secondary minerals	A6.1	***										
White powdery costing on altered leached metamorphosed rock	A 6.1P3.1	***										
White fracture infill in black cherty material	A6.2P1	***										
Soft white secondary mineral in recarbonated calcareous material	A6.3P3.2						**	**				
Slightly off-white secondary mineral in recarbonated rock	A6.3P2					***	**					
White fibrous vein material in leached metamorphic rock	A6.4P3.1	***										
Purple vein material in altered rock	M18P3		***									

Table C5 Whole rock and secondary precipitate chemical analyses

Element	MQ1.1P	MQ1.2P	MQ2.1P	MQ5P	MQ6.2P	MQ7.2P	MQ9P
weight %							
SiO_2	0.66	0.16	0.43	2.73	5.59	0.18	0.37
Al_2O_3	0.21	0.04	0.03	0.39	0.80	0.06	0.08
Fe_2O_3	0.07	0.01	0.01	0.18	0.36	0.02	0.03
MgO	0.05	0.00	0.00	1.68	1.82	0.02	0.03
CaO	51.34	52.52	51.26	48.05	46.54	48.46	51.93
Na_2O	0.03	0.02	0.02	0.08	0.11	0.03	0.04
K_2O	0.01	0.01	0.01	0.08	0.27	0.01	0.00
P_2O_5(XRF)	0.14	0.01	0.02	0.09	0.76	0.03	0.03
P_2O_5(ICPOES)	0.14	0.07	0.06	0.10	0.41	0.06	0.07
ppm							
Li	15	14	14	16	24	13	16
Sr	1945	2151	1378	2716	2669	1870	2412
Ba	27	21	21	349	306	26	30
Mn	5	1	2	35	64	3	5
Ti	58	34	25	212	428	52	68
Co	7	7	7	8	8	7	7
Cu	18	9	6	4	8	3	4
Ni	11	1	2	9	23	2	<1
Zn	79	58	60	19	69	25	43
Pb	<5	<5	<5	<5	<5	<5	<5
Cd	<1	<1	<1	<1	<1	<1	<1
Ag	<1	<1	<1	<1	<1	<1	<1
Mo	<25	<25	<25	<25	<25	<25	<25
Cr	21	4	4	14	111	13	52
V	11	6	6	14	26	6	8
As	<1	<1	<1	<1	<1	<1	3
Sn	<2	<2	3	<2	<2	<2	<2
Sc	2	1	1	2	2	1	1
Zr(XRF)	16	11	11	19	32	11	11
Zr(ICPOES)	<1	1	1	3	7	<1	<1
Nb	2	2	2	1	1	2	2
Th	1	<1	4	<1	<1	<1	<1
U	3	<1	<1	<1	<1	<1	<1
Cl	<6	<6	<6	9	36	<6	25
F	281	700	642	632	876	583	447
S	11299	7356	7983	5530	15763	11000	14691
Se	<2	<2	<2	<2	10	2	2

Table C5 (continued)

Element	MQ1.1P	MQ1.2P	MQ2.1P	MQ5P	MQ6.2P	MQ7.2P	MQ9P
ppm							
Y	1.40	0.10	0.10	1.40	7.90	0.20	0.20
La	0.90	0.20	0.21	1.69	4.88	0.38	0.54
Ce	2.38	1.18	0.69	4.45	6.89	1.25	2.47
Pr	0.29	0.22	0.25	0.21	1.06	0.32	0.35
Nd	1.70	1.60	1.10	3.50	4.70	1.50	2.70
Sm	0.02	0.09	0.12	0.11	0.69	0.12	0.11
Eu	0.05	0.00	0.00	0.06	0.18	0.01	0.01
Gd	0.35	0.14	0.06	0.49	0.93	0.21	0.33
Dy	0.17	0.02	0.01	0.26	0.91	0.03	0.05
Ho	0.06	0.02	0.01	0.07	0.20	0.02	0.04
Er	0.05	0.08	0.06	0.21	0.62	0.06	0.06
Yb	0.10	0.01	0.01	0.13	0.56	0.01	0.03
Lu	0.04	0.02	0.02	0.04	0.10	0.02	0.03
ppb							
Pd	<1	<1	<1	<1	nd	<1	nd

Table C5 (continued)

Element	MQ10.5P	A6.1P	A6.2P	A6.3P	A6.4P2.1	A6.4P2.2	A6.7P
weight %							
SiO_2	8.84	13.46	11.55	7.65	12.02	nd	9.53
Al_2O_3	2.72	4.29	3.32	1.53	4.02	2.99	2.33
Fe_2O_3	1.30	1.46	1.02	0.65	1.64	0.84	1.04
MgO	0.20	0.28	0.18	0.19	0.22	0.37	0.19
CaO	47.02	43.37	44.17	48.08	41.83	37.12	43.24
Na_2O	0.05	0.09	0.05	0.03	0.04	0.04	0.07
K_2O	0.14	0.58	0.17	0.00	0.01	0.00	0.81
P_2O_5(XRF)	2.80	2.45	2.49	2.11	2.38	nd	3.68
P_2O_5(ICPOES)	1.49	1.31	1.32	1.10	1.44	0.95	1.78
ppm							
Li	21	52	17	15	15	15	32
Sr	1259	2942	1320	991	914	820	2263
Ba	216	177	64	95	62	54	174
Mn	35	42	27	30	32	20	42
Ti	561	876	608	318	751	499	461
Co	10	11	9	9	10	8	9
Cu	68	47	51	63	47	33	66
Ni	154	153	122	137	136	80	159
Zn	233	311	198	160	325	178	364
Pb	<5	13	10	<5	<5	<5	12
Cd	<1	3	<1	<1	<1	<1	3
Ag	<1	<1	<1	<1	<1	<1	<1
Mo	<25	<25	<25	<25	35	33	<25
Cr	218	457	363	178	320	485	313
V	97	93	101	72	98	64	91
As	9	12	5	<1	12	nd	6
Sn	<2	<2	<2	5	3	nd	3
Sc	5	6	5	4	6	4	5
Zr(XRF)	31	34	19	24	36	nd	25
Zr(ICPOES)	15	16	13	11	17	11	12
Nb	<1	1	<1	1	<1	<1	<1
Th	<1	<1	<1	<1	1	nd	<1
U	16	15	13	15	14	5	19
Cl	36	59	46	<6	26	nd	157
F	1881	1520	1569	886	1139	nd	1988
S	73697	10826	22841	60629	94493	nd	8616
Se	23	26	40	13	17	nd	148

Table C5 (continued)

Element	MQ10.5P	A6.1P	A6.2P	A6.3P	A6.4P2.1	A6.4P2.2	A6.7P
ppm							
Y	28.70	25.10	21.80	23.20	23.80	15.20	27.60
La	13.93	15.70-	9.66	10.27	13.56	9.43	14.10
Ce	14.94	26.80	20.90	13.61	20.07	13.34	15.65
Pr	2.16	3.40	2.90	2.69	3.57	2.31	3.55
Nd	11.50	16.90	14.60	11.60	15.40	9.90	15.00
Sm	2.08	2.36	1.94	1.65	2.15	1.47	2.26
Eu	0.55	0.65	0.57	0.51	0.66	0.43	0.66
Gd	2.67	2.31	2.54	2.15	3.08	1.91	3.23
Dy	2.81	2.91	2.44	2.41	2.71	1.74	2.99
Ho	0.61	0.64	0.55	0.53	0.59	0.37	0.65
Er	2.04	1.80	1.53	1.57	1.63	0.88	1.66
Yb	1.85	1.67	1.46	1.52	1.57	1.00	1.80
Lu	0.33	0.25	0.28	0.24	0.25	0.18	0.32
ppb							
Pd	nd	nd	3	4	nd	nd	5

Table C5 (continued)

Element	A6.9P	M2P2	M3P	M4P2	M15P	M18P	M28P
weight %							
SiO_2	10.07	nd	10.27	nd	8.64	nd	10.80
Al_2O_3	2.77	0.02	1.22	0.64	2.73	0.17	1.10
Fe_2O_3	1.00	0.01	0.25	0.16	0.74	0.02	0.45
MgO	0.26	0.44	0.35	0.30	0.53	0.00	0.35
CaO	40.20	54.62	50.55	43.30	52.27	31.80	48.65
Na_2O	0.10	0.02	0.03	0.03	0.22	0.02	0.07
K_2O	0.18	0.01	0.01	0.00	0.02	0.01	0.00
P_2O_5(XRF)	2.94	nd	1.82	nd	10.60	nd	1.37
P_2O_5(ICPOES)	1.42	0.07	1.09	2.00	6.32	0.06	0.81
ppm							
Li	24	12	14	13	20	11	12
Sr	1770	293	1100	1407	1638	643	769
Ba	103	18	231	43	341	10	30
Mn	25	11	19	22	39	2	20
Ti	519	11	336	187	517	6	282
Co	9	7	8	7	8	7	9
Cu	49	3	78	202	76	5	71
Ni	133	1	168	98	188	3	220
Zn	230	4	568	2530	435	10	592
Pb	7	<5	<5	<5	5	5	23
Cd	4	<1	108	<1	<1	<1	<1
Ag	<1	<1	<1	<1	<1	<1	1
Mo	<25	<25	43	45	<25	<25	62
Cr	354	3	329	275	506	1468	231
V	105	10	618	192	227	8	309
As	7	nd	<1	nd	<1	nd	23
Sn	2	nd	<2	nd	<2	nd	4
Sc	4	1	4	3	5	1	4
Zr(XRF)	32	nd	44	nd	39	nd	35
Zr(ICPOES)	12	1	1	<1	1	2	12
Nb	<1	3	2	2	2	1	2
Th	<1	nd	<1	nd	<1	nd	1
U	17	nd	19	10	28	<1	2
Cl	698	nd	163	nd	1074	nd	230
F	1881	nd	847	nd	5227	nd	1139
S	62082	nd	21026	nd	52590	nd	85655
Se	262	nd	39	nd	116	nd	20

Table C5 (continued)

Element	A6.9P	M2P2	M3P	M4P2	M15P	M18P	M28P
ppm							
Y	26.30	0.80	25.10	18.50	67.80	0.20	24.40
La	13.16	0.50-	9.63	6.70	25.60	0.22	10.25
Ce	16.21	0.63	9.61	6.09	16.68	0.54	5.08
Pr	3.51	0.21	2.39	1.82	4.03	0.11	2.16
Nd	14.00	1.50	10.40	7.40	17.40	0.90	9.50
Sm	1.92	0.10	1.44	0.87	3.03	0.09	1.60
Eu	0.57	0.05	0.45	0.29	0.82	0.01	0.46
Gd	2.48	0.20	2.34	1.17	4.34	0.07	1.90
Dy	2.60	0.12	2.27	1.54	4.91	0.02	2.29
Ho	0.60	0.08	0.54	0.38	1.17	0.00	0.52
Er	1.70	0.13	1.61	1.36	4.00	0.05	1.63
Yb	1.61	0.10	1.57	1.26	3.64	0.01	1.58
Lu	0.31	0.02	0.25	0.21	0.57	0.01	0.25
ppb							
Pd	nd	nd	nd	nd	13	nd	nd

Table C6 ICP-OES and ICP-MS analyses of HCl soluble and HCl insoluble residue fraction from bituminous limestone and altered limestone (concentrations expressed as fraction of total rock).

Sample:	A6.3P	A6.3P (repeat)	MQ10.1P	A6.2P	A6.7P	Blank
Fraction non-HCl soluble bitumen	20%	20%	41%	8%	14%	0%
Fraction non-HCl soluble inorganics	6%	6%	28%	2%	7%	0%
Element - ppm (ICP-OES)						
Na (HCl sol)	305	299	299	389	374	0
Na (HCl insol)	33	30	421	118	87	0
K (HCl sol)	126	125	127	334	825	0
K (HCl insol)	89	50	1420	162	540	0
Ca (HCl sol)	112493	156335	176747	243983	300289	0
Ca (HCl insol)	232	370	746	311	658	3
Mg (HCl sol)	1721	1723	893	2439	561	0
Mg (HCl insol)	0	0	<16	<1	1	0
Sr (HCl sol)	1062	1064	1840	649	1259	0
Sr (HCl insol)	5	7	<2	3	1	0
Ba (HCl sol)	121	134	48	41	83	0
Ba (HCl insol)	5	24	0	1	0	0
Cr (HCl sol)	219	214	351	77	99	0
Cr (HCl insol)	0	0	10	2	0	0
Mn (HCl sol)	14	15	22	112	26	0
Mn (HCl insol)	0	0	0	2	0	0
Fe (HCl sol)	5575	5640	2481	4951	698	0
Fe (HCl insol)	2	2	1	1184	27	1
Co (HCl sol)	1	0	0	1	1	0
Co (HCl insol)	1	0	14	2	0	0
Ni (HCl sol)	75	76	63	45	73	0
Ni (HCl insol)	47	43	<24	31	<3	0
Cu (HCl sol)	30	22	12	10	17	0
Cu (HCl insol)	21	19	22	18	19	0

Table C6 (continued)

Sample:	A6.3P	A6.3P (repeat)	MQ10.1P	A6.2P	A6.7P	Blank
Element - ppm (ICP-OES)						
Zn (HCl sol)	276	276	227	57	287	0
Zn (HCl insol)	16	14	50	14	20	0
Cd (HCl sol)	2	2	1	1	2	0
Cd (HCl insol)	0	0	<10	4	0	0
Al (HCl sol)	13146	12972	18778	2445	3050	0
Al (HCl insol)	143	114	7982	404	3827	4
Element - ppb (ICP-MS)						
Se (HCl sol)	17098	nd	1413	<50	5230	<50
Se (HCl insol)	161±33	163±31	8068±56	2650±149	3264±57	<2
Sn (HCl sol)	192	nd	106	124	54	0
Sn (HCl insol)	90±65	75±60	241±110	276±290	134±111	3.9
Pb (HCl sol)	2389	nd	2376	2982	1073	nd
Pb (HCl insol)	447±348	400±323	2755±590	2010±1563	1164±596	21
U (HCl sol)	18356	nd	8358	4618	8001	<1
U (HCl insol)	878±83	953±77	450±141	3648±372	10132±142	<5
Th (HCl sol)	1015	nd	115	900	176	<1
Th (HCl insol)	46±10	54±9	798±17	395±45	681±17	<0.6

Table C7 Uranium/thorium series isotope determinations

(a) ANSTO

Sample Code	M28P	M3P	M15P	A6.7P
Rock Type	v. altered marble (leached)	altered-marble (leached)	largely unaltered marble	bituminous limestone
Isotope (Bq/kg)				
^{238}U	31.08±1.00	310.7±9.0	504.7±13.7	483.5±12.7
^{234}U	31.43±1.02	304.7±9.0	460.5±12.5	454.3±12.0
^{232}Th	5.095±0.683	4.155±0.677	6.338±0.985	6.400±0.683
^{230}Th	137.4±5.3	230.2±7.8	462.3±16.5	456.0±11.2
^{228}Th	32.33±2.35	6.458±0.937	4.157±0.877	5.278±0.700
^{226}Ra	164.9±0.184	270.8±4.5	428.5±7.7	434.8±7.83
$^{234}U/^{238}U$	1.01	0.98	0.91	0.94
$^{230}Th/^{234}U$	4.37	0.76	1.00	1.00
$^{226}Ra/^{230}Th$	1.20	1.18	0.93	0.95
$^{228}Th/^{232}Th$	6.35	1.55	0.66	0.82

Table C7 (continued)

(b) SURRC1

Sample Code	M28P	M3P	M15P	A6.7P	MQ2.1P	MQ6.2P
Rock Type	v. altered marble (leached)	altered marble (leached)	largely unaltered marble	bituminous limestone	travertine precipitate	travertine precipitate
Isotope (Bq/kg)						
^{238}U	51/50.6	44/305.9	2050/204.8	83/82.7	47	24/56.6
^{226}Ra	176/-	298/-	521/-	231/-	122	66/-
$^{234}U/^{238}U$	1.03/1.03	0.91/1.04	0.91/0.91	0.97/0.97	1.16	1.20/1.16
$^{230}Th/^{234}U$	-/3.73	-/0.87	2.9	-/3.77	-/1.52	
$^{226}Ra/^{230}Th$	-/0.90	-/1.07	0.10	-/0.76	-/1.30	
$^{210}Pb/^{226}Ra$	0.82/1.03	0.82/0.82	0.90	1.40/1.37	0.82	1.30/1.33

1 1.0/0.9 indicates duplicate analyses.

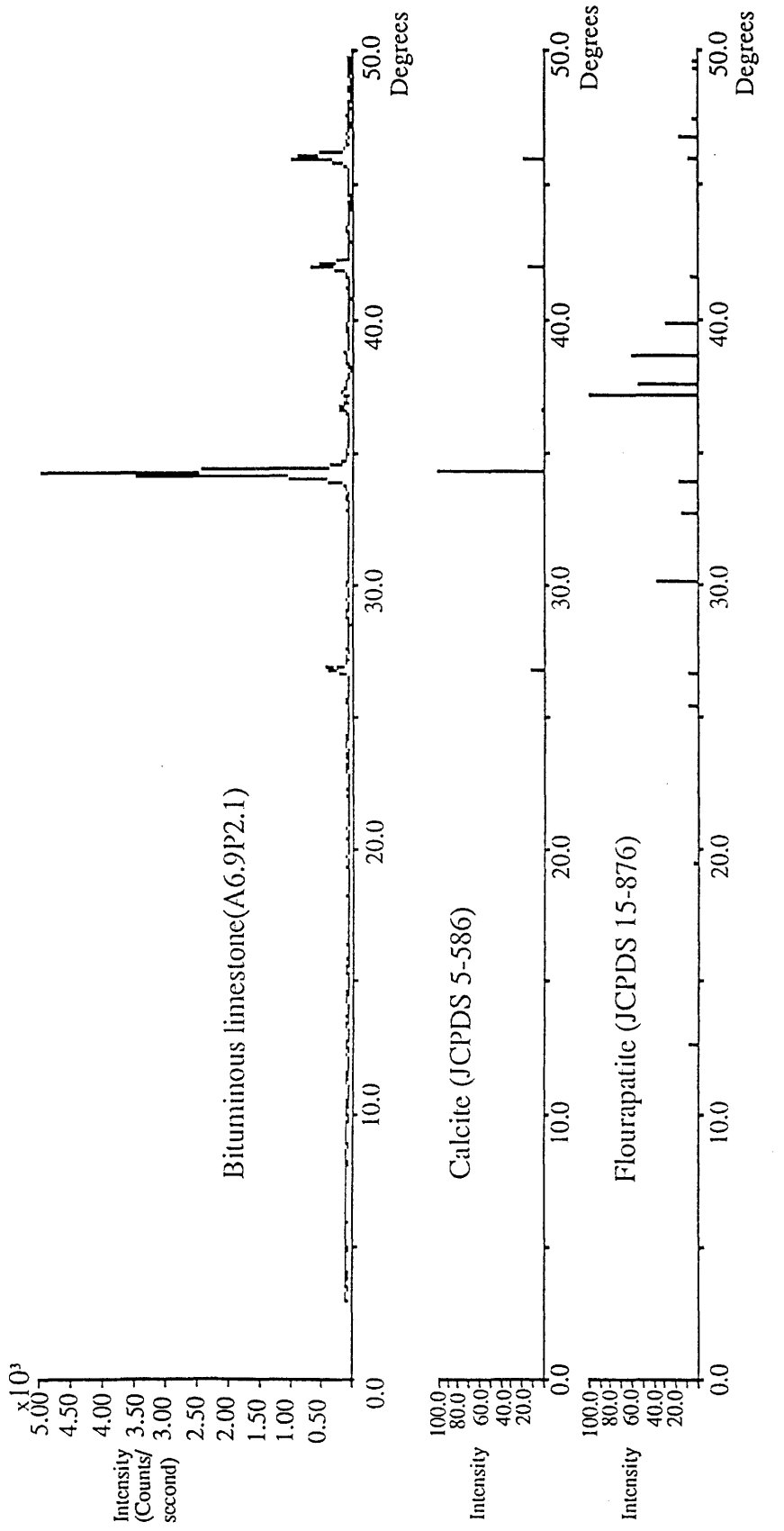

Figure C1 X-ray difraction pattern of bituminous limestone (A6.9P) compared with JCPDS stick reference patterns for calcite and fluorapatite.

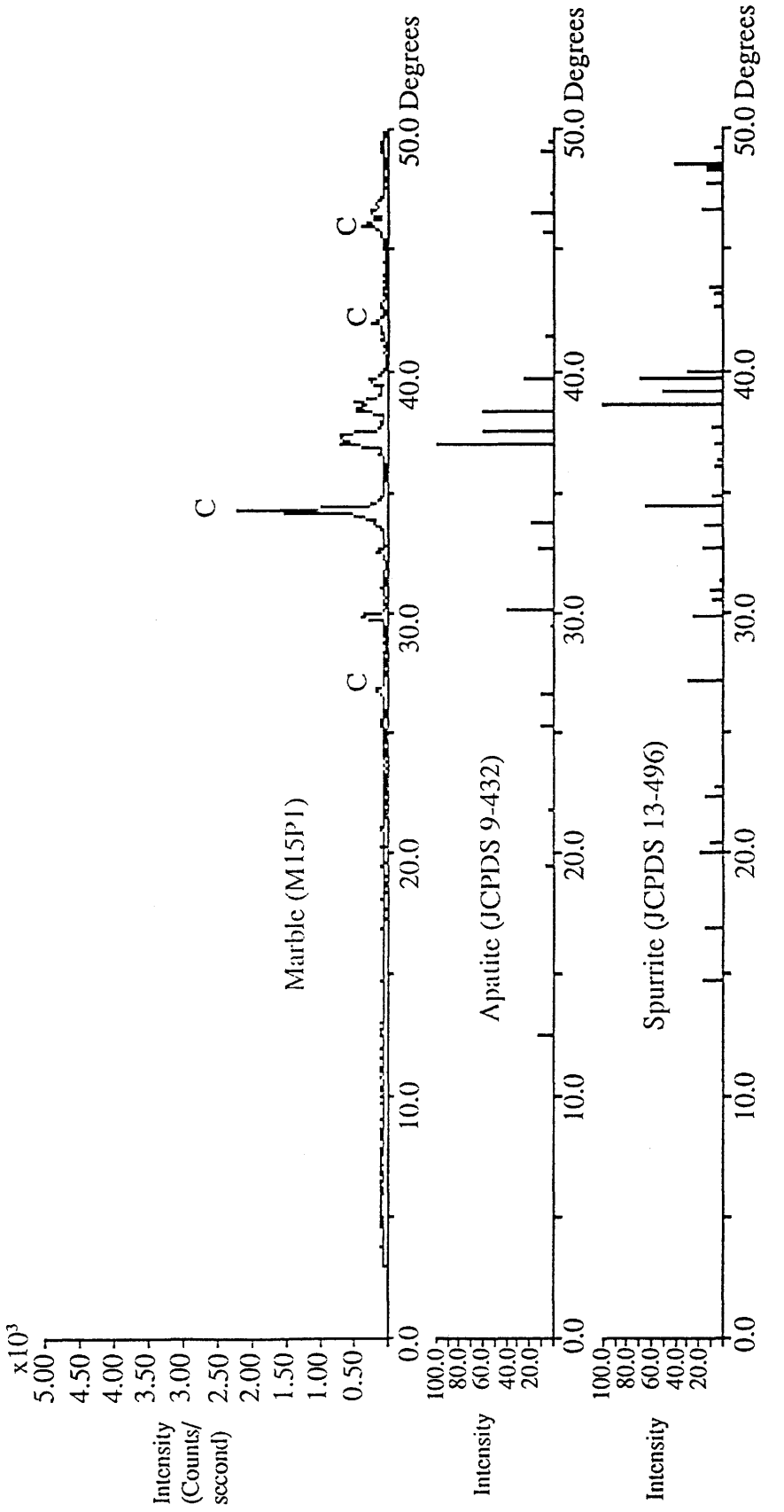

Figure C2 Comparison of JCPDS reference stick patterns with marble (M15P). C = calcite (JCPDS 5-586)

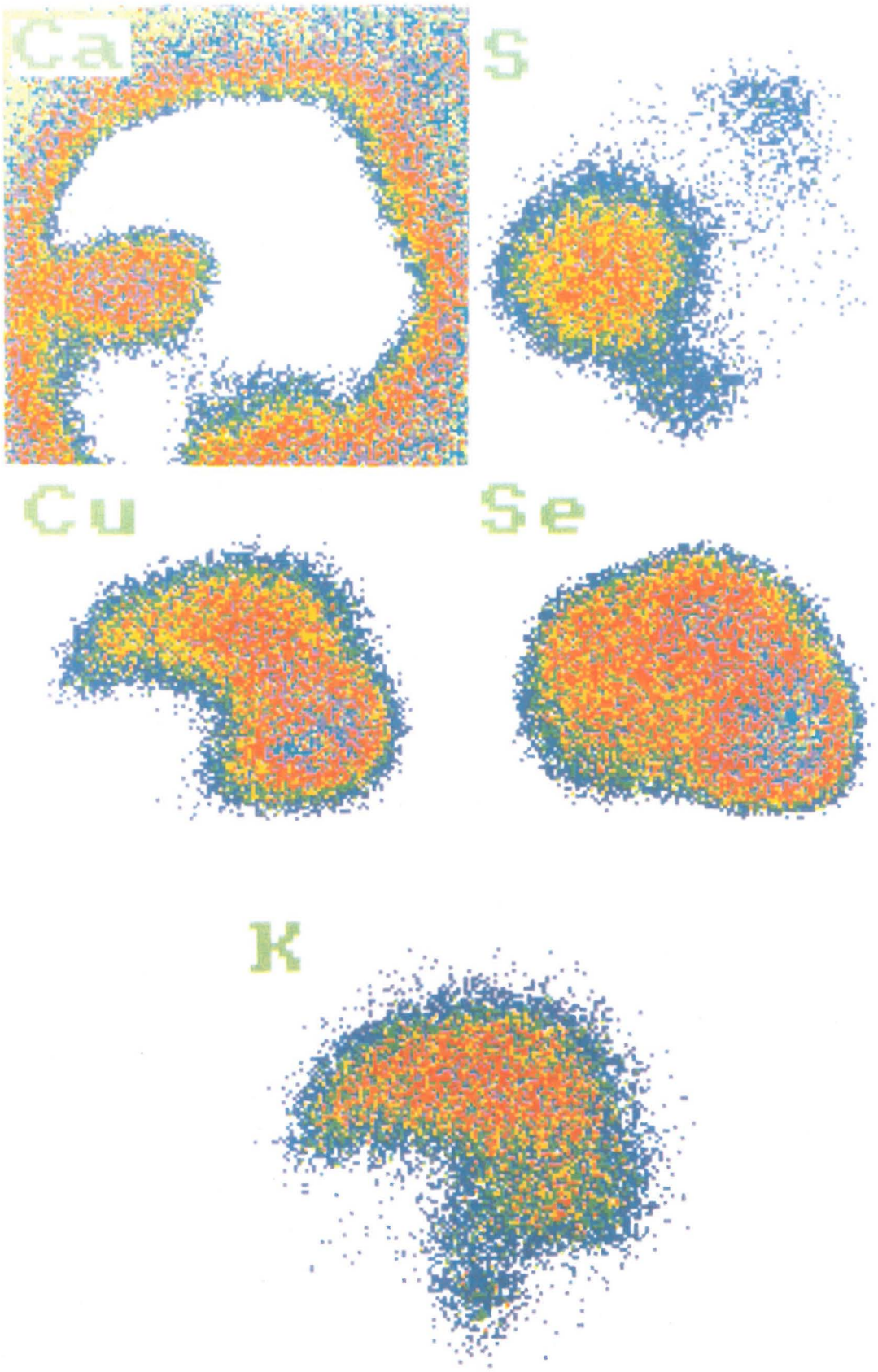

Figure C3 Electron microprobe digital X-ray map of composite oldhamite K-Cu-S-Se phase in calcite matrix within unaltered marble (M15P)

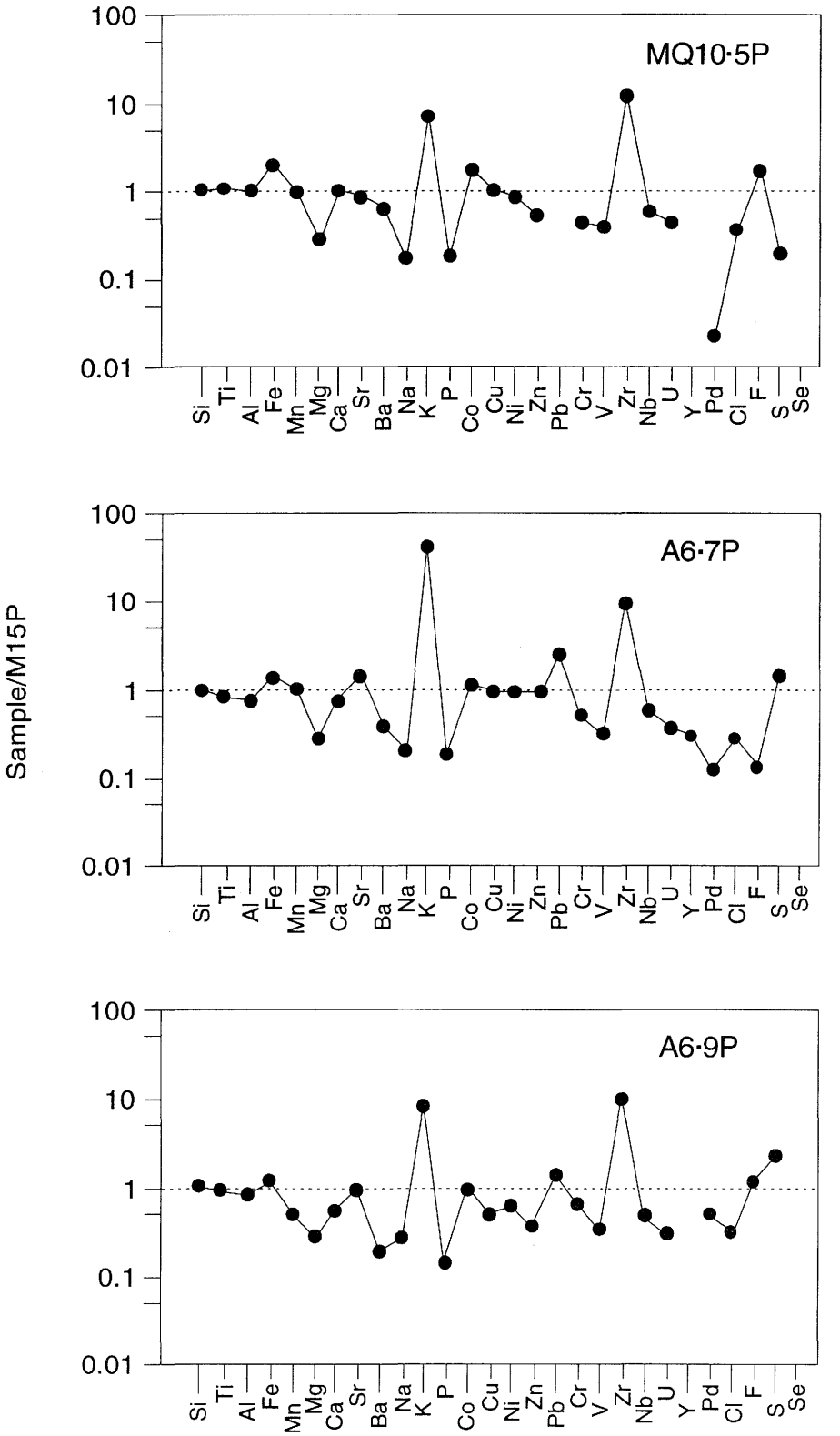

Figure C4 Major and trace element distributions of bituminous limestones (A6.7P and A6.9P) and partially combusted bituminous limestone (MQ10.5P) (normalised with reference to unaltered marble M15P).

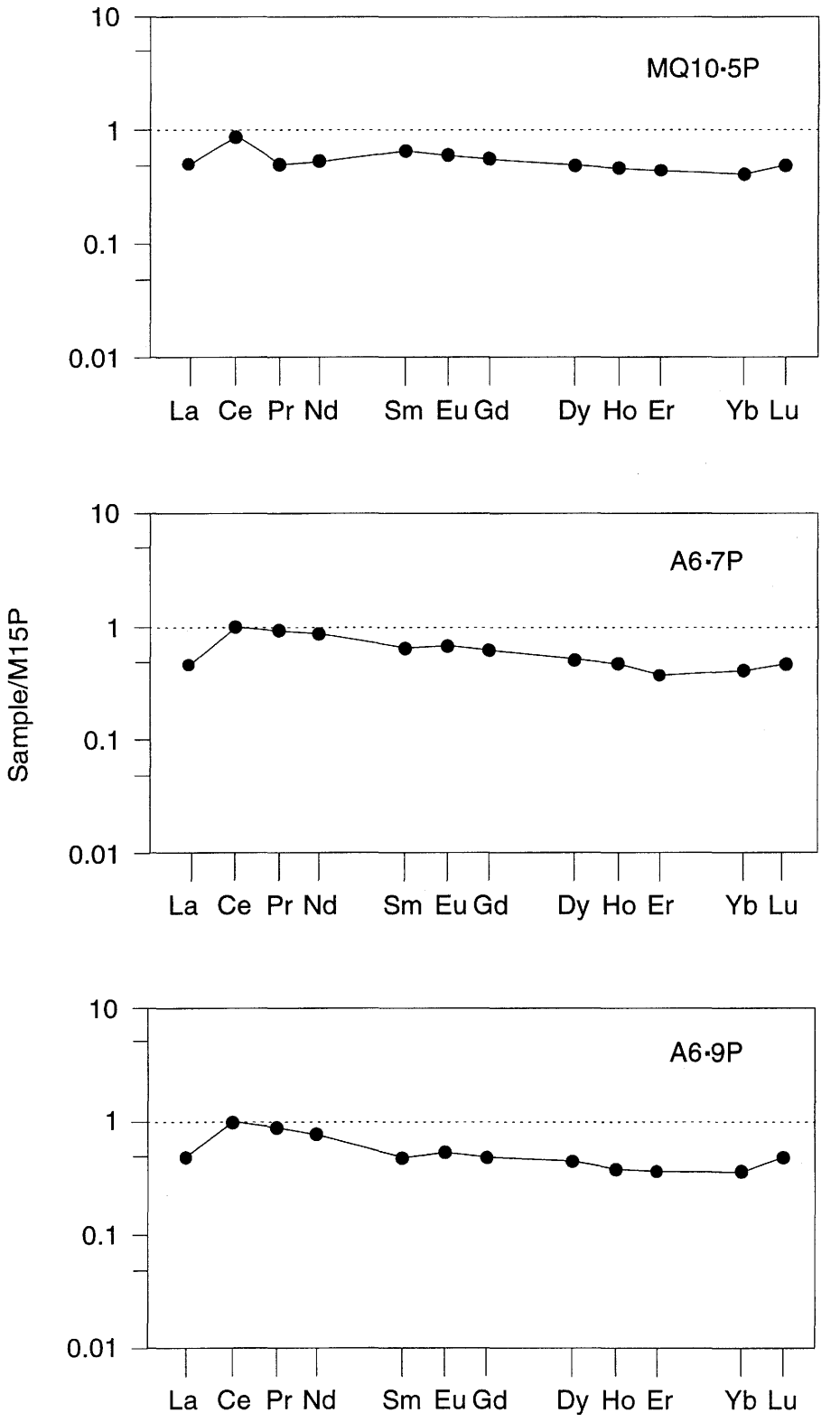

Figure C5 Rare earth element (REE) distributions of bituminous limestones (A6.7P and A6.9P) and partially combusted bituminous limestone (MQ10.5P) (normalised with reference to unaltered marble M15P).

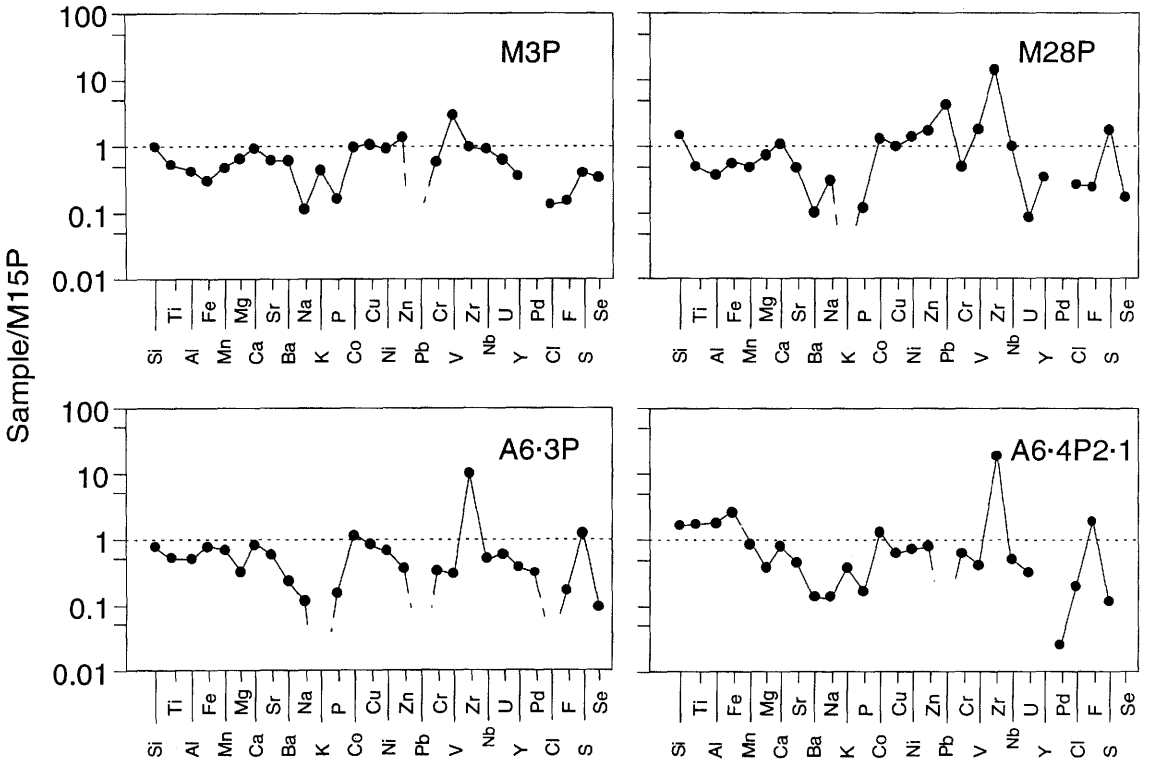

Figure C6 Major and trace element distributions of retrograde altered metamorphic rocks (normalised with reference to unaltered marble M15P).

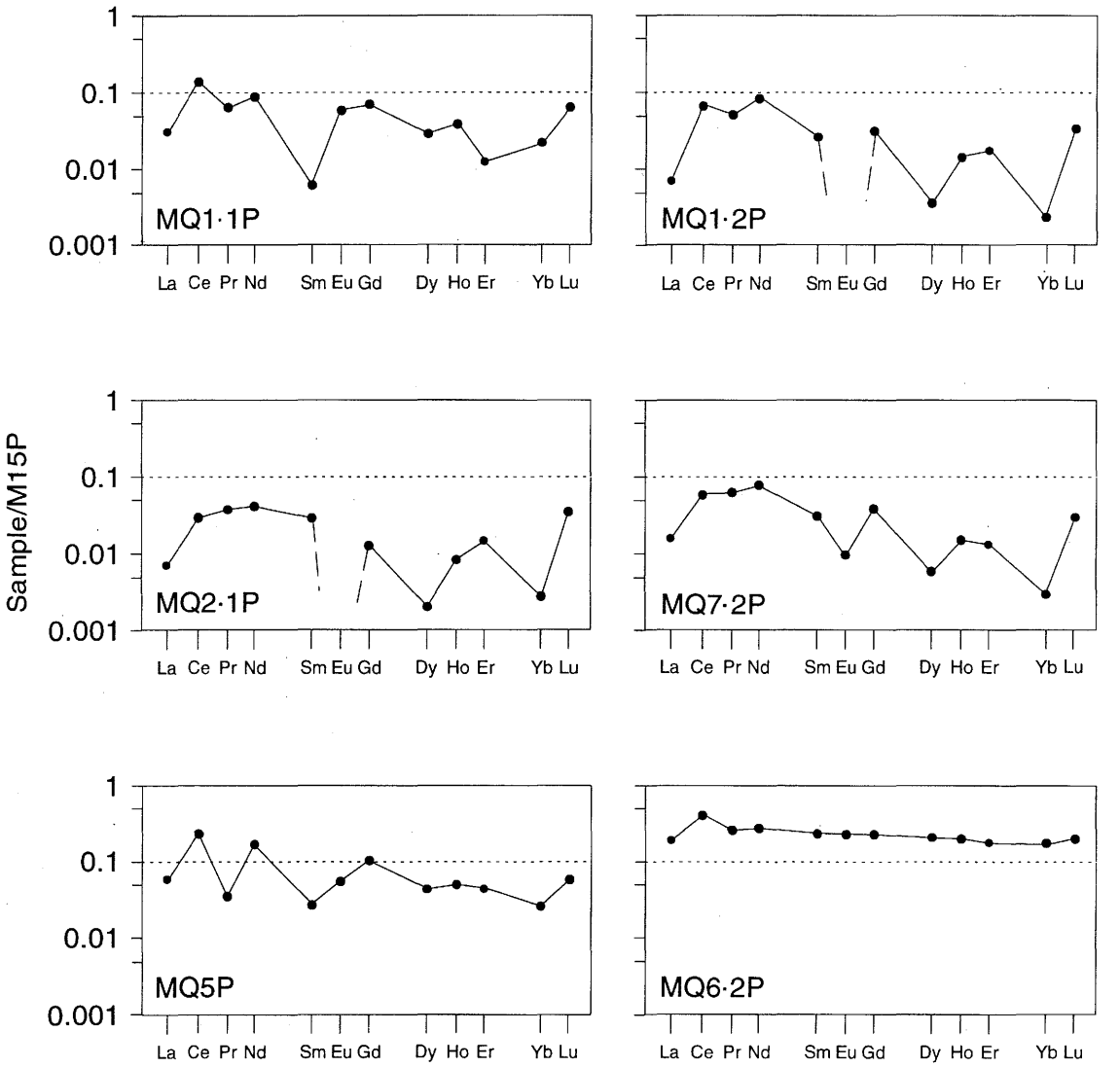

Figure C7 Rare earth element (REE) distributions of travertine precipitates associated with contemporary hyperalkaline groundwater seepage zones (normalised with reference to unaltered marble M15P).

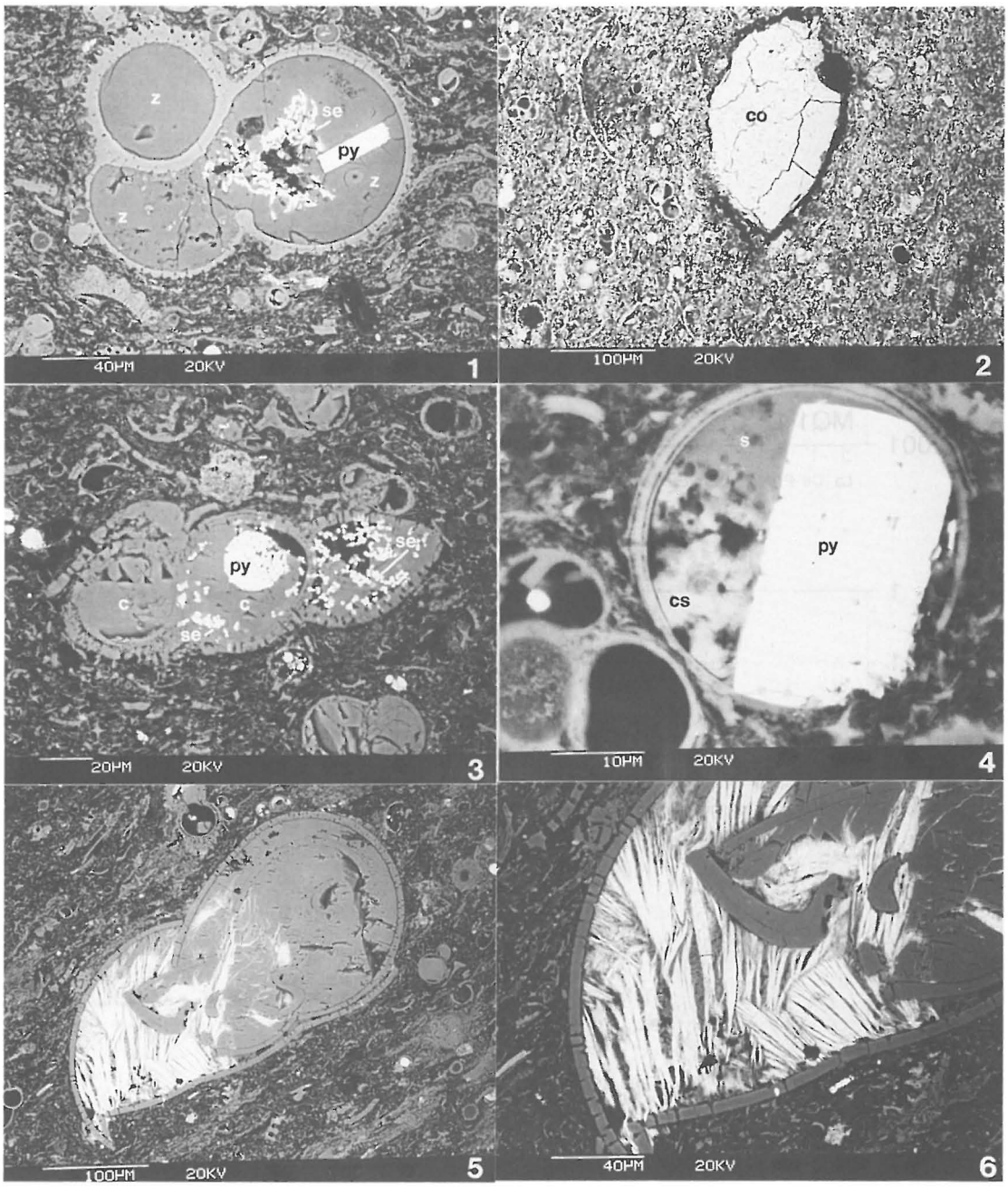

Plate 1. Well-preserved foram test in carbonate-dominated matrix of comminuted microfossil debris. Test infilled by authigenic pyrite prism (py), native selenium (Se) and zeolitic mineral (z). Bituminous limestone, A6.9P, BSEM.

Plate 2. Microfossil infilled by collophanic material (co). Bituminous limestone, A6.7P, BSEM.

Plate 3. Framboidal pyrite (py), finely dispersed selenium (Se) enclosed within later calcite cement (c) infilling foram test. Bituminous limestone, A6.9P, BSEM.

Plate 4. Coarse pyrite (py) with later silica (s) and calcium selenate (cs) in foram test. Bituminous limestone, A6.9P, BSEM.

Plate 5. Pyrite pseudomorphic replacement of early micaceous glauconite fabric (bright), enclosed in later calcite infill in foram test. Bituminous limestone, A6.9P, BSEM

Plate 6. Detail of Plate 5, showing splayed edges of pyrite pseudomorph after glauconite. Calcium selenate alteration fills between exfoliated cleavages.

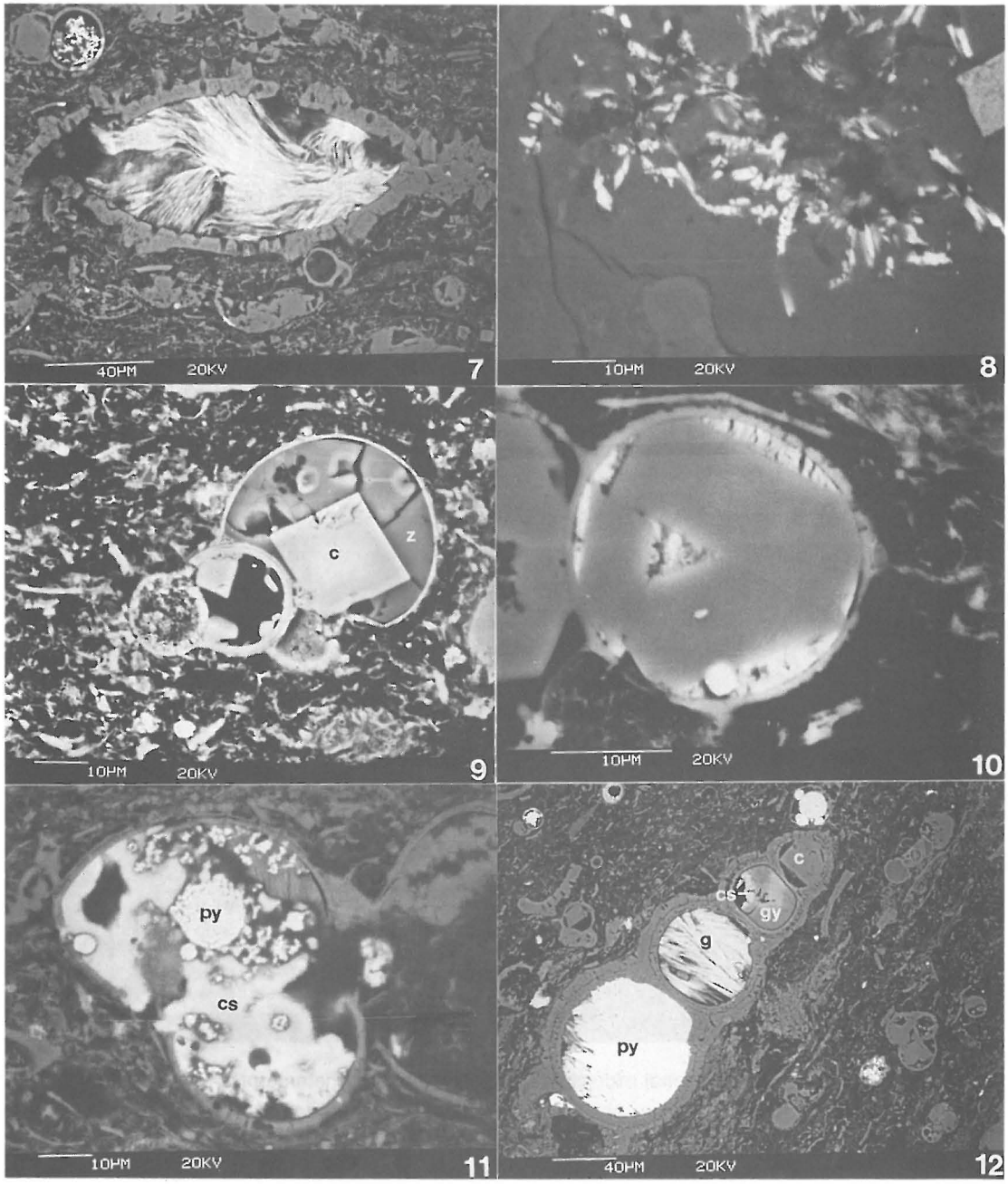

Plate 7. Micaceous to fibrous glauconite partially replaced by pyrite within microfossil. Mica and microfossil test are deformed by compaction. Bituminous limestone, A6.9P, BSEM.

Plate 8. Native selenium (bright) mineralising possible microbial cell fragments, enclosed in later (dull) zeolitic phase. Bituminous limestone, A6.9P, BSEM.

Plate 9. Mineralised foram test showing idiomorphic calcite (c) enclosed in later zeolitic mineral (z). Bituminous limestone, A6.9P, BSEM.

Plate 10. Microfibrous calcium selenate (bright) filling remaing porosity around earlier calcite cement in microfossil. Bituminous limestone, A6.9P, BSEM.

Plate 11. Microbotryoidal strontium, calcium sulphate around oxidised pyrite framboid. Bituminous limestone, A6.9P, BSEM.

Plate 12. Complex mineralised foram test showing different mineral in successive chambers: pyrite (py), goethite after pyrite (g), gypsum(g) with calcium selenate overgrowth (cs) and calcite (c). Bituminous limestone A6.9P, BSEM.

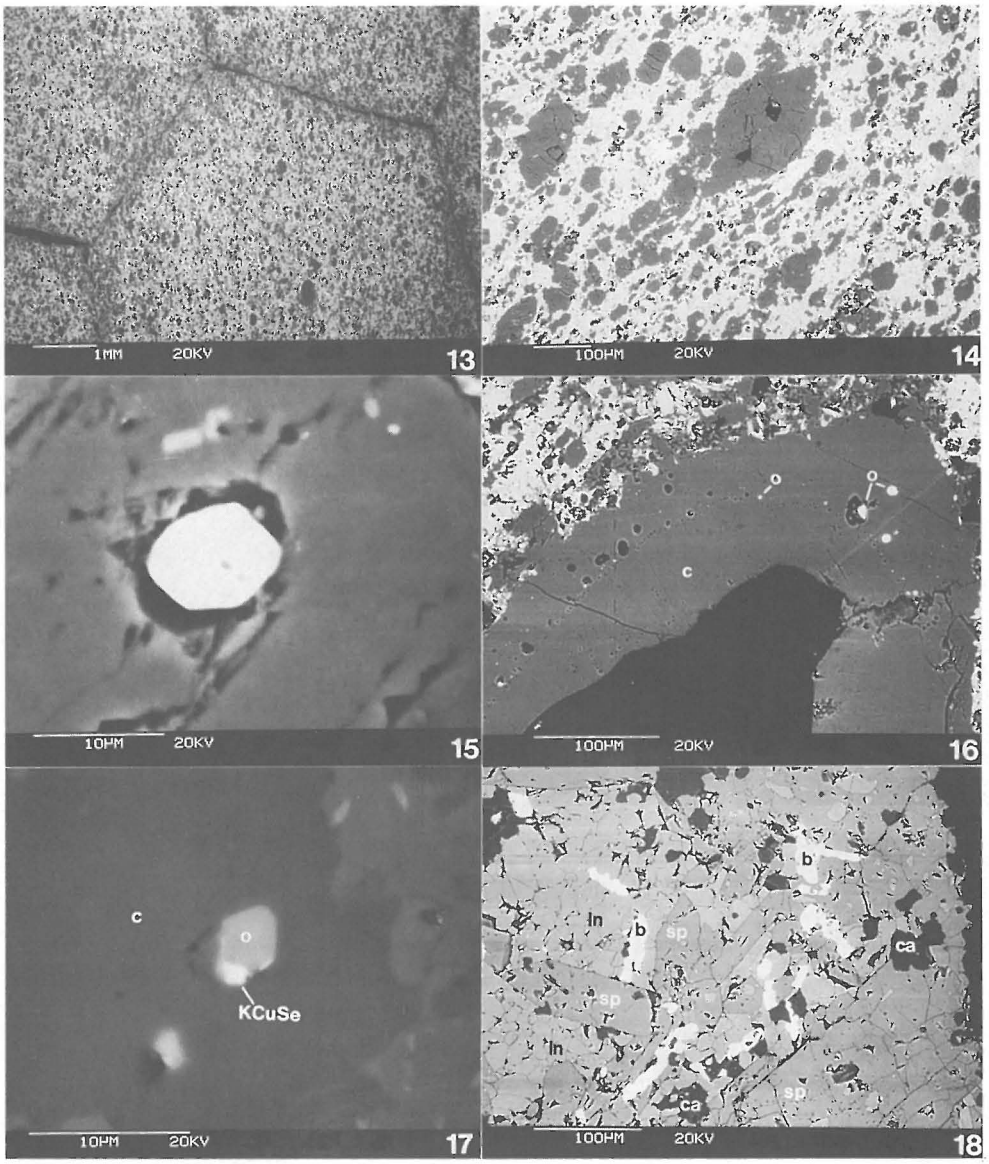

Plate 13. Polygonal hexagonal micojoints in high-temperature metamorphic rock. Incipient alteration to hydrous secondary phases (duller zones) can be seen to develop along these joints. Marble, M15P, BSEM.

Plate 14. Planar fabric defined by recrystallised calcite grains (dull grey) in ellestadite matrix. Large calcite grains recognisable as former microfossils (compare with eg. Plates 3 and 7). Marble, M15P, BSEM.

Plate 15. Equant euhedral morphology of oldhamite inclusion (bright) in recrystallised calcite grain. Marble, M15P, BSEM.

Plate 16. Recrystallised calcite microfossil (c) displaying inclusion trail of oldhamite (bright) and dissolution cavities after oldhamite which delineate the original inner surface of the microfossil test. Marble, M15P, BSEM.

Plate 17. Tiny equant inclusion of oldhamite (o) in recrystallised calcite (c) with bright copper-potassium selenide/sulphide developed around the grain boundary of oldhamite. Marble, M15P, BSEM.

Plate 18. Porphyroblastic prisms of spurrite (sp) in matrix of equigranular larnite (ln), with bright late replacive porphyroblastic needles of Fe-rich brownmillerite (b) and dull interstitial calcium aluminate (ca). Unaltered relict of larnite-spurrite-brownmillerite marble in altered marble, M39P, BSEM.

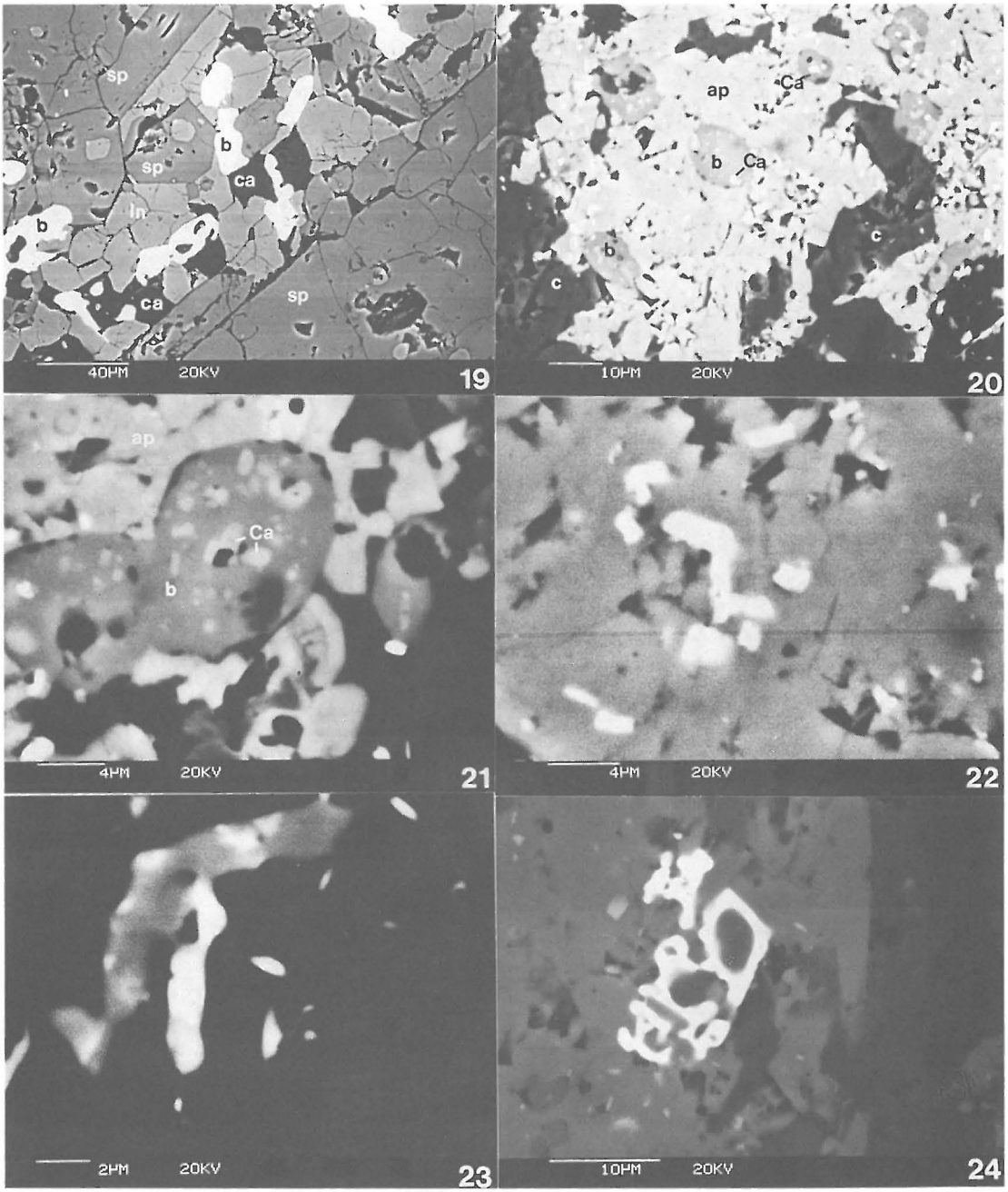

Plate 19. Detail of larnite (ln)-spurrite(sp)-brownmillerite(b)-rich marble (Plate 18) showing spurrite prisms with inclusions of larnite, equigranular larnite and calcium aluminate (ca) matrix with development of later replacive brownmillerite along grain boundaries.

Plate 20. Equant crystals of aluminous brownmillerite (b) in matrix of ellestaditic fluorapatite (ap) which contains abundant bright ferrite inclusions. Interstitial calcite (c) also present. Marble M15P, BSEM.

Plate 21. Equant aluminous brownmillerite (b) in apatite matrix (ap) containing calcium-rich inclusion (Ca) of probable lime. Marble, M15P, BSEM.

Plate 22. platy or prismatic inclusions (bright), probably ferrites in apatite groundmass. Marble M15P, BSEM.

Plate 23. Complex intergrowth of bright Fe-Cr oxide (ferrite?) partly resorbed or replaced by duller Cr,Zn,Ti,Al,Fe oxide (ferrite ?). Marble, M15P, BSEM.

Plate 24. Skeletal poikiloblastic crystal of calcium-uranium (oxycarbonate?) mineral replacing apatite along grain boundaries. Marble, M15P, BSEM.

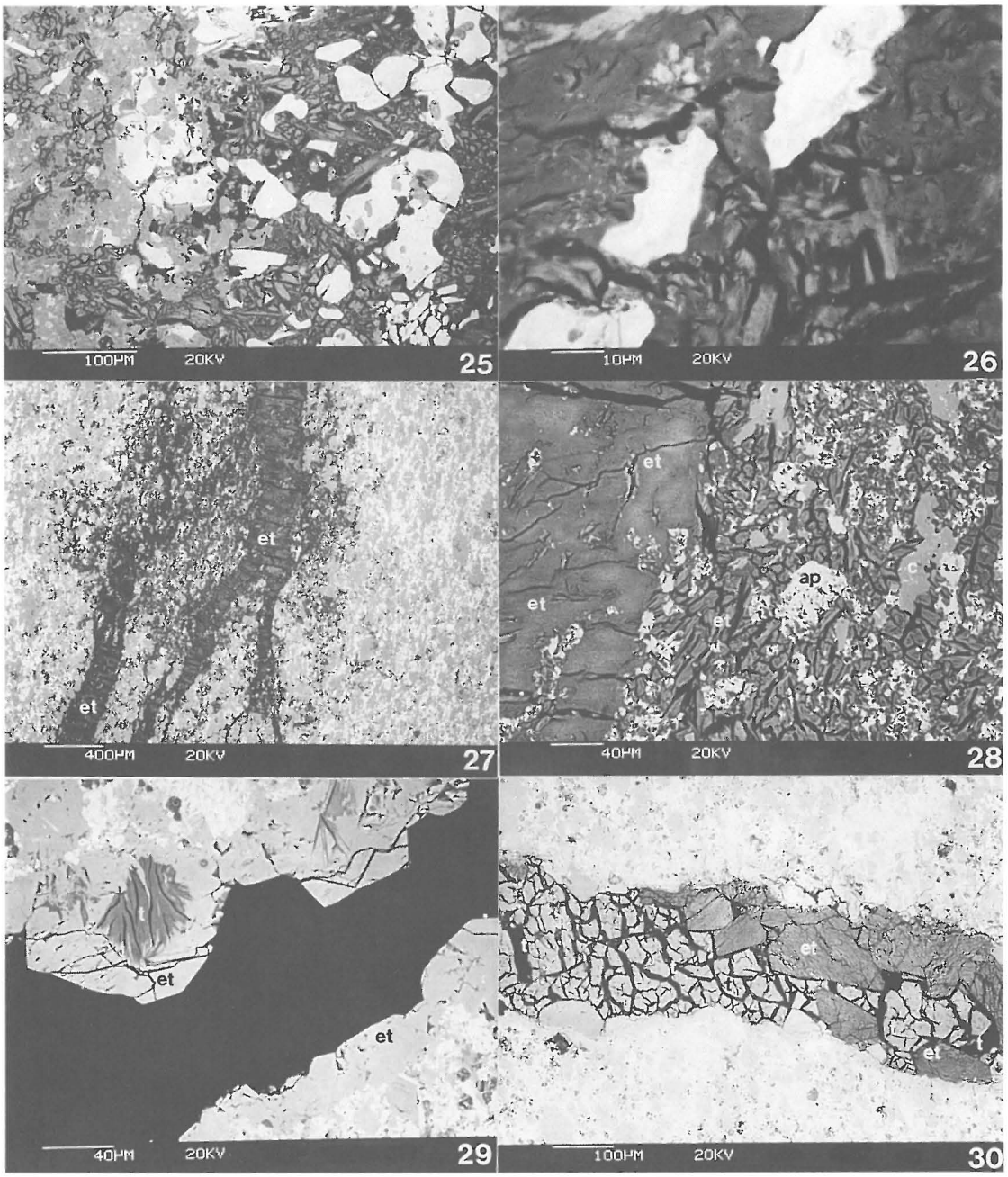

Plate 25. Relict primary metamorphic apatite in altered groundmass of secondary ettringite, portlandite vaterite and calcite. Altered marble, M39P, BSEM.

Plate 26. Altered brownmillerite showing alteration rim of ferric oxide which by fission-track registration was found to concentrate uranium. Matrix comprises secondary ettringite, calcite, portlandite and or vaterite. Altered marble, M39P, BSEM.

Plate 27. Partially altered phosphatic marble showing alteration (dull) penetrating into rock matrix along ettringite-thaumasite filled fractures (et). Marble, M33P, BSEM.

Plate 28. Altered wallrock adjacent ettringite-filled fracture (et), showing replacement of primary ellestaditic apatite and calcite by fine groundmass of secondary ettringite (et). Relicts of apatite (ap and calcite (c) still present. Marble, M33P, BSEM.

Plate 29. Fracture in marble lined by secondary aluminous tobermorite (t) partially replaced and overprinted by later ettringite (et). Marble, M15P, BSEM.

Plate 30. Fracture in marble infilled by secondary thaumasite (t) enclosing earlier euhedral crystals of ettringite (et). Marble, M15P, BSEM.

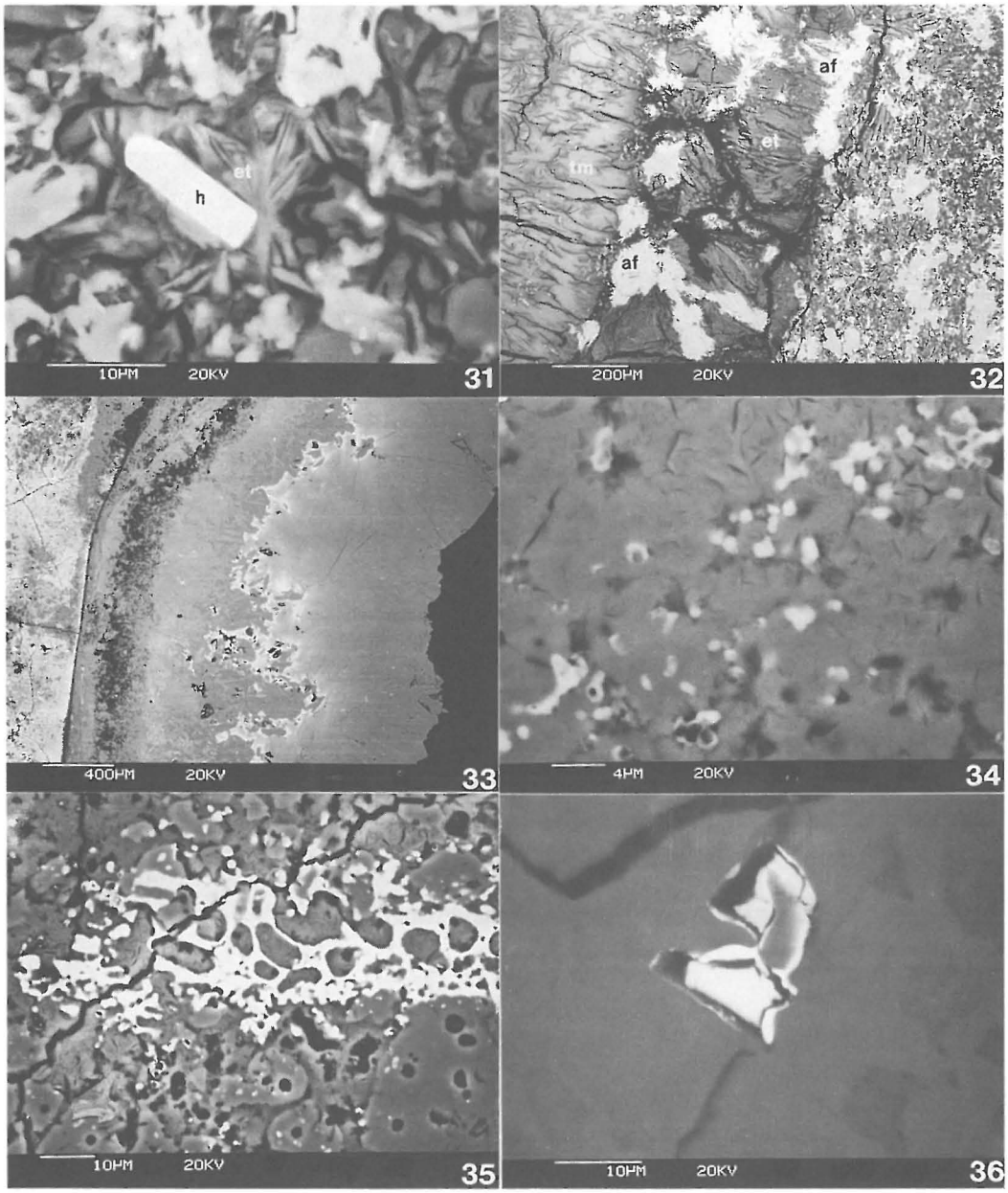

Plate 31. Platy prismatic crystal of hashemite (h) nucleating within matrix of secondary ettringite (et) forming from alteration of primary ellestadite-apatite with fine ferrite inclusions. Marble, M33P, BSEM.

Plate 32. Complex secondary vein alteration showing vein margins mineralised by early generation of fibrous ettringite (et) partially replaced by fibroradiate fluoroafwillite (af). Later thaumasite (tm) fills the vein centre and cuts across the earlier mineralised structures. Marble, M33P, BSEM.

Plate 33. Apophyllite vein filling mineralisation showing strong zoning with bright St-rich apophyllite. Altered marble, M17P, BSEM.

Plate 34. Fine-grained dispersed secondary apatite-like mineral (bright) formed in altered marble matrix comprising apopyllite and calcite. Altered marble, M17P, BSEM.

Plate 35. More advanced development of secondary apatite as poikiloblastic grains in apophyllite-calcite matrix. Altered marble, M17P, BSEM.

Plate 36. Gel-like secondary calcium-uranium silicate, showing drying shrinkage, within ettringite, calcite, portlandite alteration. Altered marble, M39P, BSEM

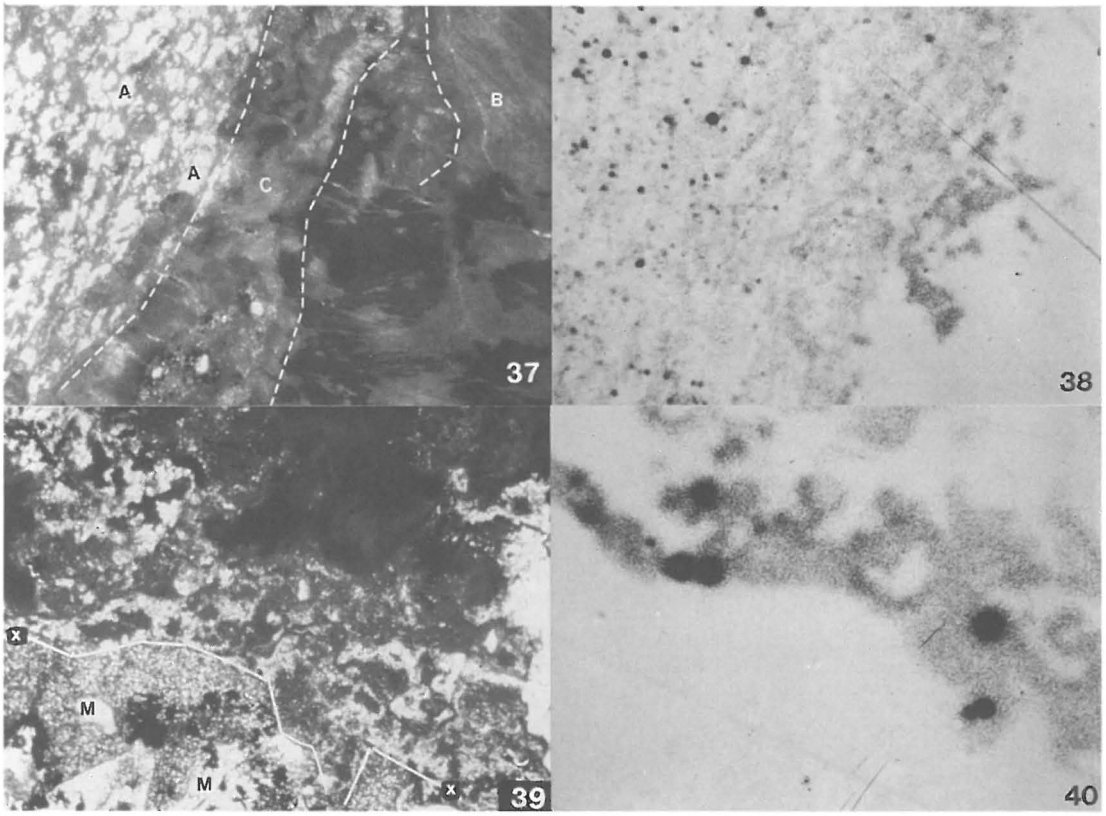

Plate 37. Primary marble largely comprising colourless calcite with interstitial apatite (region A) cut by complex ettringite-thaumasite-fluoroafwillite vein (Area B) and showing progressive alteration along vein magin (Area C). Marble, M33P, Transmitted light micrograph (plain polarised).

Plate 38. Fission-track print of same area as Plate 37 showing: high-density fission track clusters corresponding to Ca-U oxycarbonate (?); lower density fision-track distribution from areas corresponding to apatite; and very low fission-track density corresponding to primary calcite. The ñhigh-density fission-tracks disappear in the altered wallrock zone and a more uniform,and slightly higher density of fission tracks corresponds to ettringite-rich matrix alteration products. Fission-tracks are absent from the vein-filling minerals.

Plate 39. Very fine grained altered martix of former larnite-spurrite-brownmillerite rich marble containing relicts of clear calcite. Interface with relict unaltered marble (M) is identified (x-x). Altered marble, M39P, Transmitted light micrograph (plain polarised).

Plate 40. Fission-track print of same area as Plate 39 showing concentration of fission-tracks along alteration front with unaltered relict marble and scattered high-density fission-track clusters corresponding to minor secondary calcium-uranium silicate mineral.

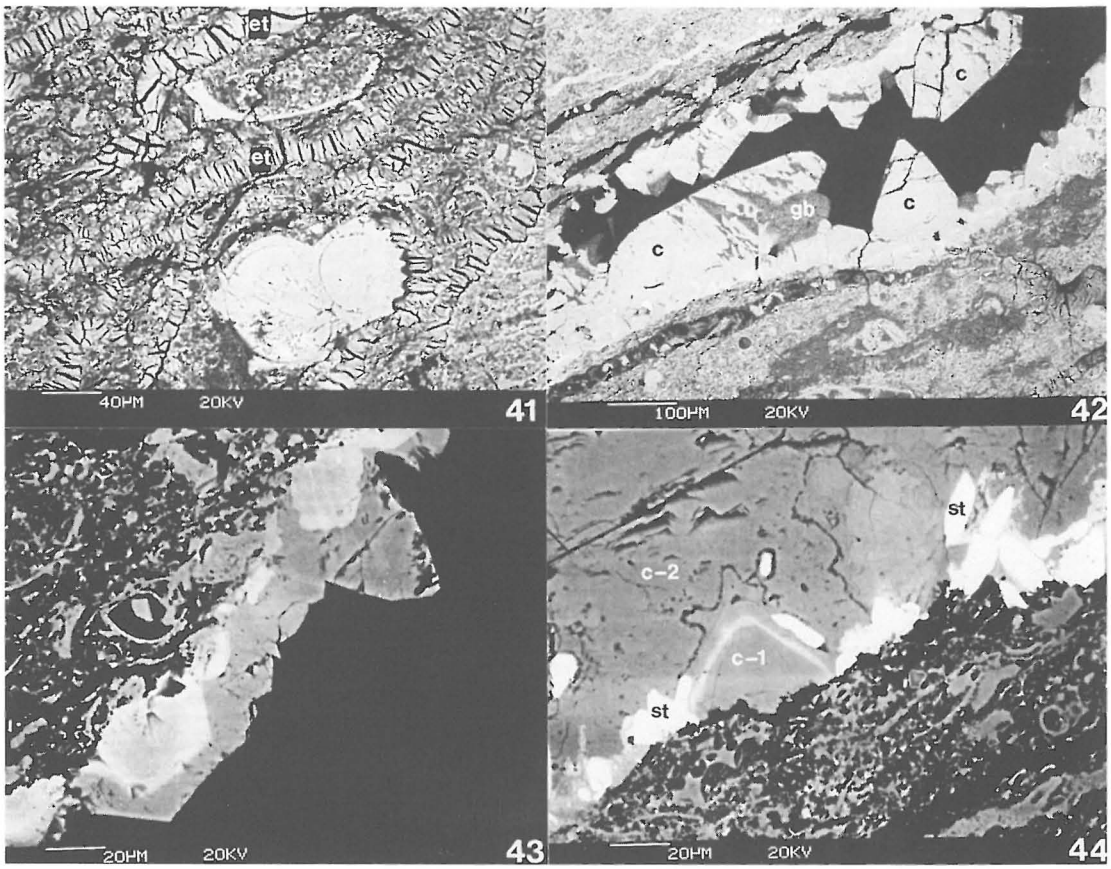

Plate 41. Highly altered matrix of bituminous limestone, cut by and partially replaced by fine anastomosing veinlets of fibrous ettringite (et). Note corrosion and replacement of calcitic microfossil debris. Bituminous limestone, A6.1P, BSEM.

Plate 42. Highly altered bituminous limestone cut by open fracture lined by euhedral calcite (c), with corrosion and replacement of the calcite by later gibbsite (gb). Bituminous limestone, A6.1P, BSEM.

Plate 43. Fracture in altered bituminous limestone lined by euhedral secondary calcite. Bright zone of partially corroded strontian calcite underlies a later overgrowth of low-strontium calcite Bituminous limestone, A6.1P, BSEM.

Plate 44. Fracture in altered bituminous limestone showing bright strontianite (st) resting on an earlier generation (now corroded) of zoned strontium-rich calcite (c-1). Later low-strontium calcite (c-2) overgrows the earlier calcite and strontianite. Bituminous limestone, A6.1P, BSEM.

D GEOCHEMICAL MODELLING OF HIGHLY MINERALIZED WATER FROM THE MAQARIN AREA: A CODE INTERCOMPARISON STUDY

J. EIKENBERG and W. HUMMEL

D 1 Introduction

The main emphasis of chapter 5 was an intercomparison of geochemical databases (for radionuclides of interest) which are currently in common usage. The study resulted in sometimes large differences of predicted solubilities and speciation of certain elements. It was stated that, although two different geochemical codes (MINEQL/PSI and PHREEQE) were utilized, no major effects were expected which were not traceable to the databases alone. This assumption is reasonable in the light of other previous geochemical code intercomparison studies carried out on weakly mineralised groundwaters (CHEMVAL PROJECT, 1989; 1990). These studies have, however, also indicated that significant deviations of calculated element speciation and solubilities can occur when highly mineralised solutions are examined because of the ionic strength correction contained in each code is calculated in a different way. Such highly mineralised groundwaters are present, for instance, within the environment of salt domes but are not of key interest for most radwaste studies. It is important, however, to note that planned L/ILW repositories will include large quantities of cementitious material and the cement pore waters in such an environment are likely to be characterised by a relatively high ionic strength of about 0.2 M (eg BERNER, 1990). Thus, it is important to investigate to which extent differences in the results of PHREEQE and MINEQL (the two codes employed by PSI in this study) calculations of cement pore waters are caused by different ionic strength corrections. The Maqarin groundwaters described in this study offer an excellent opportunity to carry out such a code intercomparison as not only are they good analogues of cement pore waters but are also rather highly mineralised (I = 0.1 M). Consequently, an identical data set has been established in this study and run at PSI with both MINEQL/PSI (WESTALL et al., 1976) and PHREEQE (PARKHURST et al., 1980) and the results are presented here.

D 2 Ionic strength correction

Geochemical codes generally use data bases which contain equilibrium constants that refer to standard conditions (i.e. $I = 0$), and thus are valid only for infinitely dilute solutions. In order to evaluate the water speciation under real conditions ($I > 0$), geochemical codes apply different types of ionic strength corrections to the standard equilibrium constants.

For example, consider the formation of a complex AB by pairing of ions A and B (charges neglected for simplicity):

$$A + B = AB \qquad (1)$$

The mass action equation of this reaction can be written in two different ways:

$$\frac{\{AB\}}{\{A\} \cdot \{B\}} = K \qquad (2a) \qquad\qquad \frac{[AB]}{[A] \cdot [B]} = K^* \qquad (2b)$$

where { } is the activity of a species, K is the equilibrium constant, [ ] is the concentration, and K^* the conditional equilibrium constant which depends on the concentration of all the species in solution. The relation between the activity {i} and the concentration [i] of a species i is given by its activity coefficient γ_i

$$\{i\} = [i] \cdot \gamma_i \qquad (3)$$

The conditional equilibrium constant K^* of reaction (1) can be calculated using equations (2a),(2b), and (3)

$$\log K^* = \log K - \log\gamma_{AB} + \log\gamma_A + \log\gamma_B \qquad (4)$$

or $$\log K^* = \log K + \log\gamma \qquad (5)$$

This conversion from K to K^* is necessary since the analytical data are available in concentration units (Eq. 2b) rather than activity (Eq. 2a). For the activity - concentration conversion different models may be used depending on the ionic strenght and the ion interactions to be expected. The geochemical codes utilised in this study, MINEQL and PHREEQE, calculate activity coefficients using the original (or variants of) extended Debye-Hückel equation. This is written:

$$\log\gamma = -z^2_i \cdot D \qquad (6)$$

where z_i is the charge of the species i and D the Debye-Hückel term which is

$$D = A \cdot \sqrt{I}/(1 + B \cdot å_i \cdot \sqrt{I}) \qquad (7)$$

Here A and B are constants which are temperature dependent, and $å_i$ is the effective diameter of i. At 25 C, A is 0.5091 and B = 0.3283 (see GRENTHE and WANNER, 1989). I is the ionic strength of the solution, which is defined as follows:

$$I = 1/2\ \Sigma z^2_i \cdot [i] \qquad (8)$$

Note that the extended Debye-Hückel equation is an option in the PHREEQE code.

An expanded version of the Debye-Hückel equation is the Davies equation:

$$\log \gamma_i = -z^2_i \cdot D + (z^2_i \cdot A \cdot c \cdot I) \qquad (9)$$

Where A = 0.5 and $B \cdot å_i = 1$, following from equations (7) and (9):

$$\log\gamma_i = -1/2 \cdot z^2_i \quad \frac{\sqrt{5}I}{1 + \sqrt{I}} - c \cdot I \qquad (10)$$

Different values of c can be utilised and, in the PSI calculations of chapter 5, c = 0.3 for PHREEQE/PSI and 0.2 for MINEQL/PSI. This compares with c = 0.3 for both HARPHREEQE and MINEQL/HARWELL which are normally used by AEA. With the Davies equation, γ can be reasonably approximated up to an ionic strength of 0.5 M (STUMM and MORGAN, 1981). In higher molar media, this equation is, however, limited because its only ion-specific parameter is the charge. At higher concentrations, short range non-electrostatic interactions also have to be taken into account and this requires additional information of sometimes rather uncertain parameters such as specific ion interaction terms. Therefore, the method of ionic strength correction preferred in the NEA Thermochemical Data Base review is the specific ion interaction theory in the form of the Bronsted- Guggenheim-Scatchard approach (abbreviated B-G-S equation here, see GRENTHE and WANNER, 1989)

$$\log\gamma_i = z^2_i \cdot D + \Sigma_j \varepsilon_{(i,j,I)} \cdot [j] \qquad (11)$$

with $B \cdot å \cdot_i = 1.5$. If the solution is dominated by a 1:1 salt NX, then the ionic strength $I \sim \Xi = N$, and in the sum of ion interaction terms $\Sigma\varepsilon$ of equation (11) only one term has to be taken into account:

$$\log\gamma_{Cation} = -z^2_{Cation} \cdot D + \varepsilon_{(Cation,\ X,\ I)} \cdot I \qquad (11a)$$

$$\log\gamma_{Anion} = -z^2_{Anion} \cdot D + \varepsilon_{(Anion,\ N,\ I)} \cdot I \qquad (11b)$$

Note that the B-G-S equation is as yet not implemented in any geochemical code. Beside the difference of the c-values in the Davies equation (10), there is another difference between MINEQL/PSI and PHREEQE/PSI because the latter code includes the activity of water. The empirical equation used by PHREEQE is taken as the following

$$\{H_2O\} = 1 - 0.017 \cdot \Sigma[i] \qquad (12)$$

where $\Sigma[i]$ is the sum of concentrations fo dissolved species.

D 3 Results

Data for two Maqarin waters, MQ2 and MQ5, were used in this study (Tab. D1). The information was first collated as a normal MINEQL/PSI data file and was then translated, by hand, into PHREEQE format (a conversion programme is currently under development at PSI). In order to minimise the data translation effort, several elements which are present at trace levels were not considered. This simplification led, however, to no change of the ionic strength, water activity or major water characteristics. The results of the calculated speciation and saturation indices for those solids probably dominating the water chemistry are given in tables D2 to D5.

According to equation (12), the calculated activity of H_2O remains close to 1 in dilute media. For the MQ2 water, with an ionic strength of 0.04 M (see Tab. D1), $\{H_2O\}$ was calculated as 0.999 and, for the more mineralised MQ5 water (I = 0.09 M), the PHREEQE output yielded a value of 0.998. Hence, for both waters, the influence of the water activity on the stability constants is negligible. Clearly, for solutions of ionic strengths greater than a few tenths molar, correction for the water activity would significantly influence the total water speciation. In such cases, however, the Davies approximation is also no longer valid and therefore the assumption of $\{H_2O = 1\}$ in the MINEQL code can be justified.

According to the data in tables D2 to D5, it is obvious that, with respect to the Maqarin groundwaters used here, the differences between the codes are insignificant. Since correction for ionic strength is strongly dependent on charge, the largest differences are expected for ion pairs composed of highly charged anions and cations. However, for complexes such as $CaSO_{4(aq)}$ or $BaSO_{4(aq)}$ these differences are within a few per cent when using identical data sets. The major differences are caused by the NAI028 (PEARSON et al., 1989) and MINEQL/PSI databases (BERNER, 1992). See, for instance, the differences of the values of $CaOH^+$ or $BaSO_{4(aq)}$ (Tables D2 and D5).

Whereas the different procedures to correct for ionic strength produce identical results for these hyperalkaline waters, it is expected that at elevated ionic strength ($I>0.1$) the calculated results will diverge. In order to test this assumption, the ionic strength of the MQ5 water was increased by "adding" NaCl to the original solution up to a maximum concentration of 2.9. 10^{-1}M NaCl. This gives a model solution with a final ionic strength of 0.4 M. As an example, the calculated concentrations of two complexes, $BaSO_{4(aq)}$ and $CaOH^+$ are plotted as functions of the Na^+ concentration (Fig. D1). As can be seen, the $CaOH^+$ concentrations remain virtually identical over the entire range of ionic strength. In the case of $BaSO_{4(aq)}$, however, the calculated concentrations diverge with increasing ionic strength. For example, in a 0.2 M solution (~0.1 M NaCl added to the MQ5 water) the concentrations of $BaSO_{4(aq)}$ calculated by MINEQL/PSI and PHREEQE/PSI differ by a factor of two.

In order to see whether the differences shown in figure D1 are significant, the activity coefficients related to the formation of these two complexes are analysed in some detail (Fig. D2). The extended Debye-Hückel functions (Eq. 6) are calculated with $å_{H}+ = 9$, $å_{Ca}2+ = 6$, $å_{Ba}2+ = 5$, $å_{CaOH}+ = 4$, $å_{SO4}-2 = 4$ (PEARSON et al.,1989).

The B-G-S functions (Eq. 11a and 11b) are calculated using $\varepsilon_{(Ca^{+2},Cl^-,I)} = 0.14$, $_{(H^+,Cl^-,I)} = 0.12$, $\varepsilon_{(CaOH^+,Cl^-,I)} = 0.14$ (estimated from the values given for Ca^{+2} and H^+), $\varepsilon_{(Ba^{+2},Cl^-,I)} = 0.07$, $\varepsilon_{(SO_4^{2-},Na^+,I)} = 0.184 + 0.139 \cdot \log(I)$ (GRENTHE and WANNER, 1989). As can be seen from equation (5), the error introduced into speciation calculations due to the uncertainty in activity coefficients resulting from different log γ equations is directly comparable to the uncertainty in log K. The uncertainty may be estimated as $\log K_{(CaOH^+)} \pm 0.1$ (BAES and MESMER, 1976; SMITH and MARTELL, 1976) and $\log K_{(BaSO4(aq))} \pm 0.2$. The latter estimation may be even too optimistic because the recommended values range between log K = 2.28 (PEARSON et al., 1989) and log K = 2.7 (SMITH and MARTELL, 1976). As can be seen from figure D2, the activity coefficients calculated using different equations diverge with increasing ionic strength and clearly cause severe problems in waters of high salinity (e.g. sea water at $I = 0.7$). Even in the present study ($I \leq 0.4$) the uncertainty in log K is larger than the largest differences in activity coefficients calculated by the B-G-S equation and the Davies equation (c = 0.3, PHREEQE option). For the cases considered here, the Davies equation with c = 0.2 (MINEQL/PSI) agrees better with B-G-S than Davies with c = 0.3. It must be emphasized that in the ionic strength region of normal groundwaters ($I < 0.1$), the largest differences in activity coefficients are one order of magnitude smaller than the uncertainties of the log K values. Even for cement pore waters with $I = 0.2$, where the ionic strength correction procedures lead to greater discrepancies, the uncertainty in log K is still the main contribution to the overall uncertainty of the speciation calculation (Fig. D2).

D 4 Summary and Conclusions

The results of geochemical speciation calculations of highly mineralised groundwaters depend to some extent on the approximation procedures used to correct for ionic strength. Since the Maqarin hyperalkaline waters exhibit a relatively high ionic strength of up to 0.1 M, speciation calculations of typical waters from this region were performed using different geochemical codes (MINEQL/PSI and PHREEQE) with an identical data set. Activity coefficients for ionic strength correction were calculated by different versions of the Davies equation. As cement pore waters are likely to attain higher ionic strengths (up to $I = 0.2$ M) than the Maqarin waters examined here, further calculations were carried out on modified waters. The ionic strength of the groundwaters was successively increased from 0.1 M to 0.4 M by the addition of NaCl. In addition, several activity coefficient functions were studied in more detail on selected examples of complex forming reactions.

The main conclusion of this study is that the influence of different ionic strength correction procedures on the results of geochemical speciation calculations is a second order effect compared to the uncertainties of the equilibrium constants. In addition:

(1) In the ionic strength region of normal groundwaters ($I < 0.1$ M) the largest differences in activity coefficients are one order of magnitude smaller than the uncertainties of the equilibrium constants. The speciation calculations result in almost identical concentrations of aqueous species and predicted solubilities of key solid phases.

(2) The differences in calculated activity coefficients increase with increasing ionic strength, but even for cement pore waters up to an ionic strength of 0.2 M these differences are much smaller than the uncertainties of the equilibrium constants. The results of speciation calculations start to diverge for some species but these numerical differences cannot be stated "significant".

(3) With further increasing ionic strength ($I > 0.4$ M), however, proper calculation of activity coefficients becomes a serious problem. Here it is suggested that the specific ion interaction theory preferred in the NEA Thermochemical Data Base review, be examined more closely. All equilibrium constants given by NEA (GRENTHE and WANNER, 1989) are extrapolated to zero ionic strength using this theory and a direct way of approximating the original experimental data at (very) high ionic strength is using the same theory in the geochemical codes. In fact, scoping calculations utilising this correction agreed well with the MINEQL/PSI results produced with the Davies equation with $c = 0.2$.

Table D1 Major element chemistry of the MQ2 and MQ5 groundwaters

Species (mol l^{-1})	MQ2	MQ5
Ca^{2+}	1.47×10^{-2}	2.62×10^{-2}
Sr^{2+}	8.13×10^{-5}	1.79×10^{-4}
K^{+}	3.00×10^{-4}	1.57×10^{-2}
Na^{+}	2.13×10^{-3}	5.74×10^{-3}
Ba^{2+}	2.55×10^{-7}	1.60×10^{-7}
SO_4^{2-}	2.89×10^{-3}	1.54×10^{-2}
CL^{-}	1.59×10^{-3}	1.44×10^{-3}
F^{-}	2.15×10^{-5}	4.90×10^{-5}
NO_3^{-}	8.23×10^{-5}	6.16×10^{-4}
pH	12.26	12.44
pe	5.2	2.1
I[mol/l]	4.14×10^{-2}	8.59×10^{-2}

Table D2 Calculated concentrations of the major species and ion pairs in the MQ2 water.

Species	PHREEQE (1) mol^{-1}	MINEQL (2) mol^{-1}	PHREEQE (3) mol^{-1}
Na+	2.12×10^{-3}	2.12×10^{-3}	2.12×10^{-3}
K+	2.97×10^{-4}	2.98×10^{-4}	2.98×10^{-4}
Ca+2	1.18×10^{-2}	1.16×10^{-2}	1.15×10^{-2}
Sr+2	7.15×10^{-5}	7.14×10^{-5}	7.14×10^{-5}
Ba+2	2.28×10^{-7}	2.04×10^{-7}	2.04×10^{-7}
$SO4^{-}_2$	1.84×10^{-3}	1.88×10^{-3}	1.86×10^{-3}
F-	2.04×10^{-5}	2.05×10^{-5}	2.04×10^{-5}
C1-	1.59×10^{-3}	1.59×10^{-3}	1.59×10^{-3}
NO^{-}_3	8.23×10^{-5}	8.23×10^{-5}	8.23×10^{-5}
OH-	2.27×10^{-2}	2.23×10^{-2}	2.25×10^{-2}
$NaSO^{-}_4$	7.60×10^{-6}	9.52×10^{-6}	9.34×10^{-6}
KSO^{-}_4	1.49×10^{-6}	1.89×10^{-6}	1.83×10^{-6}
CaOH+	1.56×10^{-3}	2.07×10^{-3}	2.17×10^{-3}
CaSO4 (aq)	1.05×10^{-3}	9.91×10^{-4}	1.01×10^{-3}
CaF+	8.72×10^{-7}	9.90×10^{-7}	1.03×10^{-6}
SrOH+	3.32×10^{-6}	3.93×10^{-6}	4.01×10^{-6}
SrSO4 (aq)	5.86×10^{-6}	5.94×10^{-6}	5.90×10^{-6}
BaOH+	7.01×10^{-9}	7.42×10^{-9}	7.58×10^{-9}
BaSO4 (aq)	1.83×10^{-8}	4.35×10^{-8}	4.34×10^{-8}
HF (aq)	1.33×10^{-14}	1.37×10^{-14}	1.36×10^{-14}

1) Calculated with the PHREEQE database NAI0289 (PEARSON et.al.,1989)

2) Calculated with the MINEQL/PSI database (BERNER, 1992)

3) Calculated with the MINEQL data translated into PHREEQE format

Table D3 Calculated concentrations of the major species and major ion pairs in MQ5 water.

Species	PHREEQE (1) mol^{-l}	MINEQL (2) mol^{-l}	PHREEQE (3) mol^{-l}
Na+	5.65×10^{-3}	5.63×10^{-3}	5.66×10^{-3}
K+	1.53×10^{-2}	1.53×10^{-2}	1.53×10^{-2}
Ca+2	1.74×10^{-2}	1.73×10^{-2}	1.70×10^{-2}
Sr+2	1.34×10^{-4}	1.33×10^{-4}	1.33×10^{-4}
Ba+2	1.26×10^{-7}	9.07×10^{-8}	9.16×10^{-8}
$SO4^{-}_2$	9.72×10^{-3}	9.88×10^{-3}	9.86×10^{-3}
F-	4.63×10^{-5}	4.63×10^{-5}	4.63×10^{-5}
Cl^{-}	1.44×10^{-3}	1.44×10^{-3}	1.44×10^{-3}
NO^{-}_3	6.18×10^{-4}	6.16×10^{-4}	6.18×10^{-4}
OH-	3.58×10^{-2}	3.51×10^{-2}	3.56×10^{-2}
$NaSO^{-}_4$	1.02×10^{-4}	1.06×10^{-4}	1.033×10^{-4}
KSO^{-}_4	3.83×10^{-4}	4.07×10^{-4}	3.88×10^{-4}
CaOH+	3.62×10^{-3}	3.85×10^{-3}	4.16×10^{-3}
CaSO4 (aq)	5.22×10^{-3}	4.97×10^{-3}	5.07×10^{-3}
CaF+	2.91×10^{-6}	2.67×10^{-6}	2.84×10^{-6}
SrOH+ (aq)	9.55×10^{-6}	9.09×10^{-6}	9.53×10^{-6}
SrSO4	3.62×10^{-5}	3.71×10^{-5}	3.67×10^{-5}
BaOH+	5.77×10^{-9}	4.11×10^{-9}	4.32×10^{-9}
BaSO4 (aq)	3.24×10^{-8}	6.51×10^{-8}	6.47×10^{-8}
HF (aq)	1.89×10^{-14}	1.98×10^{-14}	1.93×10^{-14}

1) Calculated with the PHREEQE database NAI0289 (PEARSON et.al.,1989)

2) Calculated with the MINEQL/PSI database (BERNER, 1992)

3) Calculated with the MINEQL data translated into PHREEQE format

Table D4 Calculated saturation indices (log SI) for portlandite, gypsum, celestite and baryte in the MQ2 water.

phase	chem. comp.	PHREEQE (1)	MINEQL (2)	PHREEQE (3)
portlandite	$Ca(OH)_2$	-0.35	-0.52	-0.50
gypsum	$CaSO_4$	-0.71	-0.72	-0.71
celestite	$SrSO_4$	-0.89	-0.88	-0.88
baryte	$BaSO_4$	-0.05	-0.09	-0.09

1) Calculated with the PHREEQE database NAI0289 (PEARSON et.al.,1989)

2) Calculated with the MINEQL/PSI database (BERNER, 1992)

3) Calculated with the MINEQL data translated into PHREEQE format

Table D5 Calculated saturation indices (log SI) for portlandite, gypsum, celestite and baryte in the MQ5 water.

phase	chem. comp.	PHREEQE (1)	MINEQL (2)	PHREEQE (3)
portlandite	$Ca(OH)_2$	+0.08	-0.11	-0.08
gypsum	$CaSO_4$	0.00	-0.02	-0.01
celestite	$SrSO_4$	-0.09	-0.09	-0.08
baryte	$BaSO_4$	+0.21	+0.08	+0.09

1) Calculated with the PHREEQE database NAI0289 (PEARSON et.al.,1989)

2) Calculated with the MINEQL/PSI database (BERNER, 1992)

3) Calculated with the MINEQL data translated into PHREEQE format

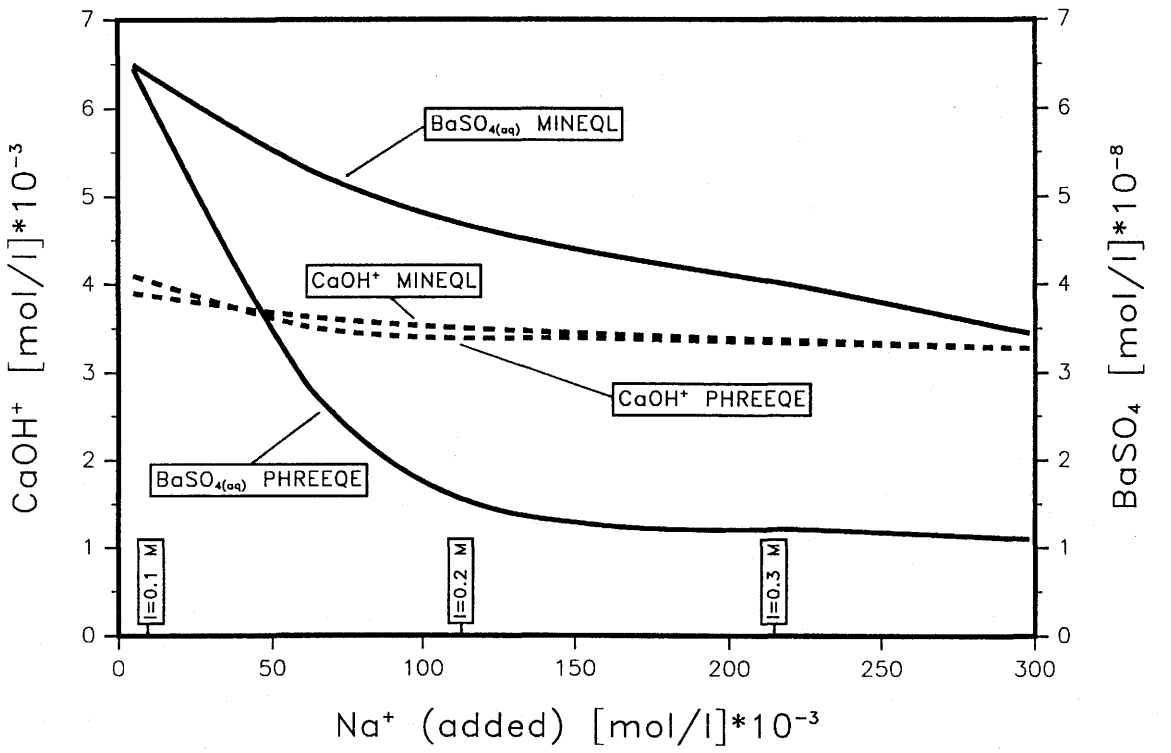

Figure D1 Concentration of $CaOH^+$ and $BaSO_4$ as a function of Na^+ added to the Maqarin groundwater.

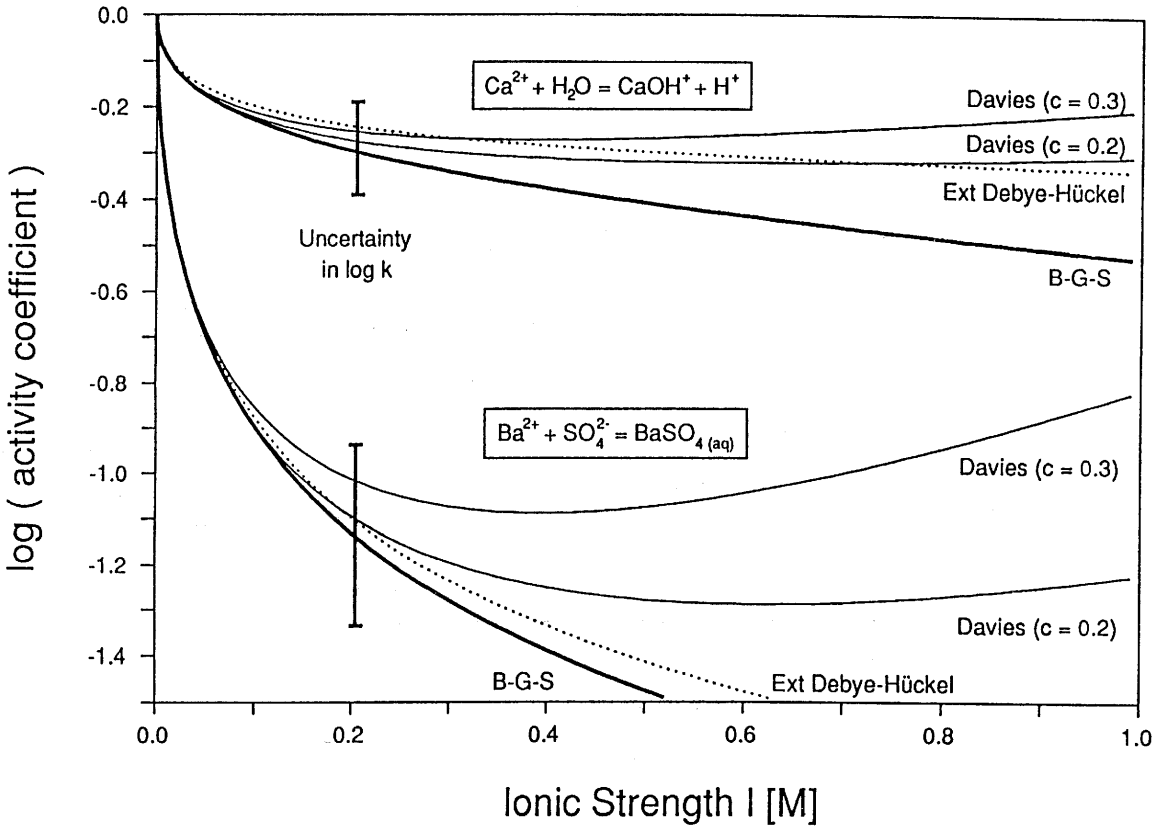

Figure D2 Variation in the calculated activity coefficients of $CaOH^+$ and $BaSO_4$ with ionic strength of the solution.

E RELEVANCE TO ^{14}C ATTENUATION IN CEMENT-BASED ENGINEERED BARRIERS

R. DAYAL and I.D. CLARK

Background to the ^{14}C Problem at Ontario Hydro

^{14}C is produced from the neutron activation of ^{17}O in the moderator heavy water as dissolved carbonate in CANDU reactor systems. It is removed from moderator water by purification systems consisting of mixed bed ion exchange resins. Over a long time period, after the short-lived radionuclides have decayed to background levels, ^{14}C accounts for more than 99 % of the bulk radioactivity in the low/intermediate level radioactive waste at Ontario Hydro. It is estimated that by the year 2005 approximately 1.6×10^6 Ci of ^{14}C will have been generated as waste associated with ion exchange resins used in the normal operations of Ontario Hydro's nuclear power plants.

Because of its long half-life and the ease with which it assimilates into biological systems, ^{14}C is known to have significant radiological impact over long time scales. This has been attributed to the relatively conservative transport behaviour of ^{14}C (present as $H^{14}CO_3^-$ anion) in the natural geologic envrionment giving rise to high rates of migration, relative to its long hazardous life (t 1/2 = 5,730 years).

In view of these considerations, a major component of Ontario Hydro's Reactor Waste Disposal Program has focussed on the assessment of cement-based engineered barriers to provide the desired containment for ^{14}C. Given the long half-life of ^{14}C and its relatively conservative migration behaviour, it is generally believed that engineered barriers would enhance the safety of the disposal system with respect to ^{14}C containment.

Ontario Hydro's Research on ^{14}C Attenuation in Cement-Based Engineered Barriers

The main objective of this research programme was to assess the effectiveness of cement-based engineered barriers, specifically a grout backfill, as a geochemical sink for ^{14}C. To date there is very little information available on the nature and extent of radiocarbon uptake by cement-based materials. Given the limited data available on the mechanistic aspects of ^{14}C attenuation in cement-based materials, laboratory experiments were conducted as part of Ontario Hydro's Reactor Waste Disposal Program to study CO_2/grout interactions and evaluate their relevance to radiocarbon attenuation in a cement-based engineered barrier.

Experiments were particularly designed to study the nature and degree of carbonation in the cement paste, emphasizing the mechanistic aspects of grout carbonation. A

considerable amount of effort was also directed at the identification of carbonation-induced changes in material characteristics affecting both the material transport properties and long-term durability of the grouts studied.

A variety of laboratory tests were performed on selected grout materials to investigate specific aspects of grout carbonation. As a starting point, powdered grout was used to induce reaction-controlled carbonation, thereby minimizing the constraints the matrix transport parameters are likely to exert in achieving the maximum carbonation. Further tests were designed to derive information on carbonation uptake kinetics, carbonation mechanisms, total carbonation capacities, as well as on the effect of water content on the rate and degree of carbonation.

In order to induce, simultaneously, radiocarbon reaction and transport processes, solid grout specimens were carbonated to investigate the effects of matrix transport parameters on the overall carbonation process. Solid grout specimens were carbonated under both batch equilibrium (diffusion-controlled) and reactant flow-through (advection-controlled) conditions. The reactant flow-through test configuration for grout carbonation provided more conducive conditions for the carbonation reaction in that the reactant can be transported through the porous matrix directly to the reaction sites. An added feature of the flow-through set-up is that information on progressive changes in material permeability, induced as a result of increasing carbonation, can be obtained.

Grout specimens used in the laboratory study were prepared using Ordinary Portland Cement, Ottawa quartz sand and deionized water with a cement/water ratio of 0.40 or 0.50. Further details of the grout formulations, curing conditions, and sample preparation for the laboratory tests are given elsewhere.

The major findings of the grout carbonation research performed as part of Ontario Hydro's Reactor Waste Disposal Program are as follows:

- Mineralogic changes associated with carbonation involve the reaction of aqueous carbon dioxide with the principal hydrated calcium-bearing compounds in grout, yielding a calcitic end product which has the potential to immobilize radiocarbon.

- The recarbonation rate of powdered grout is very fast, on the order of one day. Depending on the initial grout formulation, the maximum carbonation capacities of the various grout mixes studied range from 15 % to 19 % of the grout mass.

- Maximum carbonation capacities were not attained for soild grout samples because the rate of carbonation was much slower and limited by diffusion of the reactant through the water saturated pore network to the reaction sites.

- The geochemical modelling results indicate that the computer simulations provide a good representation of the evolution of a carbonating grout/water system. The initially stable minerals such as brucite, portlandite, and CSH phases become unstable with

progressive carbonation. Upon complete carbonation, the intermediate reaction products are transformed into stable end-products such as calcite and amorphous silica.

- Both water saturated and unsaturated grout reveal a significant reduction in permeability as a result of carbonation. This effect is even more pronounced when the grout is subjected to successive carbonation cycles.

- Besides a reduction in permeability caused by the clogging of pores with authigenic carbonate material, the other important carbonation-induced changes in grout properties include a progressive reduction in porosity and average pore size, an increase in specific surface area, with increasing degree of carbonation.

- For solid grout samples, it is the carbonation-induced changes in material transport properties, together with generation of pore water, which exert a limiting effect on the rate of transport of the reactant (aqueous CO_2) to the reaction sites.

- In a real disposal situation, the beneficial effects of carbonation would be significant improvement in the mass transport properties of the engineered barrier in that decreased permeabilities will ultimately result in diffusion-controlled mass transfer, even under advective flow conditions. Reduced water flow will impede waste leaching and subsequent transport of radionuclides escaping from the waste package.

- Carbonation of grout by inactive dissolved inorganic carbon in groundwater, prior to the release of ^{14}C from the waste package, would reduce the effectiveness of the engineered barrier as a geochemical sink for ^{14}C. In other words, the longer the time period between grout backfill emplacement and the onset of actual waste leaching, the lower will be the efficiency of the barrier for ^{14}C uptake by carbonation. At that stage, other processes such as isotopic exchange (between ^{14}C and ^{12}C) and coupled dissolution and precipitation of calcite in carbonated grout may serve to provide a certain degree of retardation of ^{14}C transport in the grout backfill.

Use of Maqarin Area System as a Natural Analogue for Grout Carbonation Studies

The unique geochemical features of the Maqarin Area system make it a potential natural analogue for evaluating grout carbonation reactions relevant to ^{14}C attenuation in cement-based engineered barriers. This is particularly important, given the strong similarities in the mineralogy and geochemistry of the laboratory and field systems.

Of particular significance to the ^{14}C problem is the observation of "retrograde carbonates" in the brecciated zone in the Maqarin Area system. The carbon and oxygen isotope data suggest that the carbonates are a product of recarbonation reactions involving decarbonated minerals in the brecciated zone following the spontaneous combustion event. Furthermore, the degree of carbonation appears to be extensive with

up to 50 % by mass of the material in the brecciated zone being calcitic, presumably a result of the reaction of recirculating DIC with portlandite and CSH-like phases. This particular component of the Maqarin Area system could serve as a natural analogue for evaluating and validiting laboratory carbonation data, based on solid grout samples. For the laboratory system, the starting mineralogy (decarbonated material), the matrix transport parameters, carbonation conditions, the availability and flux of reactant (aqueous CO_2), the rate and degree of carbonation, the intermediate and final carbonation products and resultant equilibrium water chemistries are already known.

Although the carbonation processes are similar, additional field data are needed to establish more closely the analogy between the laboratory and field systems. Specifically, the following information is needed on the retrograde altered material in the "carbonated brecciated zone" observed in the Maqarin Area:

- mineralogy of the decarbonated material and associated water chemistry
- sources and fluxes of CO_2
- degree of saturation in the brecciated zone
- potential pathways for reactant (Aqueous CO_2) to the reaction sites
- nature and degree of carbonation
- location of the carbonation front
- mineralogy of the intermediate and final carbonation products and associated water chemistries
- matrix transport properties for decarbonated and carbonated material
- CSH phase mineralogy and chemistry; C/Si ratios of CSH phases as related to degree of carbonation
- evidence for carbonation of other cement phases besides portlandite such as ettringite, tobermorite, etc.